UNIVERSIDAD AUTÓNOMA DE MADRID
DEPARTAMENTO DE BIOQUÍMICA

Genetic evaluation of a combination therapy for the treatment of KRAS mutant lung adenocarcinoma

DOCTORAL THESIS

Laura de Esteban Burgos

Madrid, 2020

DEPARTAMENTO DE BIOQUÍMICA

FACULTAD DE MEDICINA

UNIVERSIDAD AUTÓNOMA DE MADRID

Genetic evaluation of a combination therapy for the treatment of KRAS mutant lung adenocarcinoma

DOCTORAL THESIS

Laura de Esteban Burgos

Biology B.S

Molecular Biomedicine M.S

Directors:

Dr. Mariano Barbacid Montalbán

Dr. Monica Musteanu

Centro Nacional de Investigaciones Oncológicas (CNIO)

SPANISH NATIONAL CANCER RESEARCH CENTRE

Dr. Mariano Barbacid Montalbán, director of the Experimental Oncology Group at the Spanish National Cancer Research Center (CNIO)

and

Dr. Monica Musteanu, staff scientist of the Experimental Oncology Group at the Spanish National Cancer Research Center (CNIO)

Hereby certify that the Doctoral Thesis "Genetic evaluation of a combination therapy for the treatment of KRAS mutant lung adenocarcinoma", submitted by Laura de Esteban Burgos for the degree of Dr. Of Philosophy and carried out under the supervision of the undersigned in the Experimental Oncology Group at the Spanish National Cancer Research Center (CNIO), duly meets the requirements laid out by the Spanish RD 99/2011 and the Autonoma University of Madrid.

Madrid, September 30th 2019

Mariano Barbacid
PhD Thesis Director

Monica Musteanu
PhD Thesis Director

/

En primer lugar, quería agradecer a mis directores de tesis: Mariano Barbacid, por darme la oportunidad de llevar a cabo este proyecto en su laboratorio; y Monica Musteanu, gracias por ayudarme a fijar mis objetivos, a echar el freno cuando lo he necesitado y a crecer como persona y como científica.

A mis dos brújulas: a David Díaz, gracias por cruzarte en mi camino hace ya casi diez años, por contagiarme la ilusión por la ciencia y lo más importante, por encontrar mis habilidades e impulsarlas. A David Santamaría, gracias por ser el espejo en el que querer reflejarse, por enseñarme los valores que considero esenciales para la ciencia: la capacidad de desarrollar un pensamiento crítico, de ser íntegro y de mirar hacia adelante.

A todos los miembros presentes y pasados de Oncología Experimental que me han ayudado en el día a día: GRACIAS. W.Haiyun, thank you for your great input, for making easy the difficult. Lechuga, mil millones de gracias por dedicarme un hueco siempre que te lo he pedido con tu mejor sonrisa. Nuris y Alejandra, mil gracias por vuestra enorme ayuda durante el último empujón de este trabajo. A Marta e Irene, por tener ese "punch" y contagiármelo. Raski, gracias por los cafés que arreglan mundos. A Guillem y Manu por traer alegría. A Lucía por nuestros momentos caninos. Jing and Olivia, 谢谢你对我这么特别, for teaching me so many things that I didn't know. A Marina y Fer, gracias por ser tampón, por equilibraros entre vosotros, por equilibrarme a mi. Marina, gracias por ser la mente positiva, prometo aceptar todos los planes que propongas a partir de ahora. Fer, gracias por coincidir en el momento a la hora precisa, por salvarnos. Recuerda lo que vales. Y en especial, a mis Coleguitas: Carmencila, juntas desde la parrilla de salida, metimos primera, segunda, parada en boxes, cuarta, quinta y, ¡llegamos a meta! ¿Lo difícil? El camino. ¿Lo mejor? ¡Lo conseguimos! Lucía, gracias por hacer siempre la pregunta que hay detrás de cada hecho, por mantener la curiosidad en la rutina, por transmitirme tanta serenidad. Cathy, gracias por contagiar tu optimismo tan solo con tu risa. Harrichon, I don't think there is anyone who I miss every day so much but you. Thank you for being unique, for always make me laugh. A mis despachito: gracias por tocar mi fibra moral, por hacer que juntas, el zumo compense exprimir la fruta. Magdi, mi ENFP, simplemente gracias por ser como eres, por estar siempre ahí, a mi izquierda o a mi derecha, pero siempre ahí. Teresa, saber que estarás siempre cerca me tranquiliza, gracias por encontrar siempre las palabras adecuadas para sacarme una sonrisa. Patrichina, gracias por enseñarme tanto en tan poco tiempo, por cuidarme, por darme la fuerza que necesitaba, siempre estaré en deuda contigo.

Y por último a mi entorno personal,

A mis amigas, gracias por ser *casa*. Ahora si, ¿volar a dónde?

A Paloma, por luchar hasta el final.

A mi hermano, por enmascarar tu amor con llamadas para sacarme del laboratorio, por darme las herramientas para querer mejorar, por hacerme sentir alguien único.

A mis padres, gracias por ser los promotores de mis sueños, por motivarme y creer en mi, porque todo lo que soy es gracias a vosotros.

A Javi, gracias por hacer que juntos seamos más, gracias por tanto, gracias por *todo*, por ser *incondicional* porque creo que simplemente sin ti no hubiera sido posible.

A Duna, por darme alas.

“El mundo está lleno de cosas mágicas
esperando pacientemente
a que nuestros sentidos se agudicen”

William Butler Yeats

I. SUMMARY

Genetic ablation of CDK4 is known to prevent tumor development of *Kras*-driven lung adenocarcinoma (LUAD). Yet, elimination of the protein does not mimic pharmacological inhibition. We have utilized a genetically engineered mouse model (GEMM) that closely recapitulates this pharmacological treatment to evaluate the consequences of inactivating CDK4. In the present thesis, we have used two kinase dead (KD) isoforms, K35M and D140A, to eliminate the catalytic activity of CDK4. We demonstrated that the kinase function of CDK4 is not essential for mouse embryonic development. These mutant mice recapitulate most of the features of the complete elimination of CDK4 but later in time and with less penetrance. Mice expressing these CDK4 kinase dead isoforms are smaller than their wildtype counterparts and develop diabetes due to defects in the β-pancreatic cells development.

Furthermore, CDK4 inactivation impairs lung tumor initiation, although to a lesser extent than CDK4 ablation, suggesting the existence of kinase independent functions for the maintenance of cell cycle progression. Nevertheless, inactivation of CDK4 is not sufficient to eradicate aggressive *Kras*^{G12V};*Trp53*-null adenocarcinomas. Hence, combinatorial targets to improve therapeutic responses have been validated. Recently, it has been reported that elimination of RAF1 decreases lung tumor progression but unfortunately and similarly to CDK4 inactivation, it is insufficient to completely eliminate the disease in a *Trp53* deficient background. Here, we demonstrated that concomitant inhibition of CDK4 and RAF1 leads to regression of 100% of the *Kras*-driven adenocarcinomas even in the most aggressive context where the tumor suppressor *Trp53* is depleted. Of note, 24% were complete responders according to the RECIST criteria.

Still, there is a small population of remaining non-proliferative cells that survive in the absence of both targets being able to evolve and spawn new cancer growth. *In vitro* characterization of those cells confirmed the heterogenous mechanisms a cell can acquire in order to sustain tumor growth independently of CDK4 and RAF1. Both, epigenetic modifications as well as activation of alternative signaling pathways such as PI3K, are found to be responsible of CDK4 and RAF1 independent cell growth. In fact, selective treatment with 5-Azacytidine or PI3K inhibitors halts proliferation of CDK4 and RAF1 resistant cells. Further studies to understand the complex crosstalk between the cell cycle and MAP Kinase signaling will shed light on future novel treatments against KRAS mutant tumors.

La eliminación genética de CDK4 en un modelo murino de adenocarcinoma de pulmón inducido por el oncogén *Kras* impide el desarrollo tumoral. Sin embargo, la eliminación completa de la proteína no reproduce la inhibición farmacológica. Hemos utilizado un modelo de ratón genéticamente modificado que recapitula dicha inhibición farmacológica, permitiéndonos evaluar las consecuencias de la inactivación de la actividad quinasa de CDK4. En esta tesis hemos usado dos modelos, K35M y D140A, para eliminar la actividad catalítica de la proteína. Hemos demostrado que la función quinasa no es esencial para el desarrollo embrionario del ratón. Estos animales recapitulan la mayoría de las características asociadas a la eliminación completa de CDK4, pero con mayor latencia y menor penetrancia. Los ratones que expresan una forma catalíticamente inactiva de CDK4 son más pequeños que sus hermanos de camada para los que *Cdk4* está intacto y, además, desarrollan diabetes debido a un defecto en el desarrollo de las células β pancreáticas.

Por otra parte, la inactivación de CDK4 ralentiza la iniciación de los tumores de pulmón, aunque en menor medida que la eliminación completa de la proteína, sugiriendo que existen funciones catalíticamente independientes para el mantenimiento de la progresión celular. Sin embargo, la inactivación de CDK4 no es suficiente para erradicar los tumores de pulmón más agresivos dirigidos por el oncogén *Kras* donde, además, el tumor supresor *Trp53* es eliminado. Por lo tanto, hemos buscado dianas terapéuticas adicionales para ser combinadas con CDK4. Recientemente, hemos reportado que la eliminación de RAF1 disminuye la progresión de los tumores de pulmón, pero desafortunadamente como la inactivación de CDK4, es insuficiente para eliminar completamente la enfermedad en un fondo sin *Trp53*. En esta tesis hemos demostrado que la inhibición conjunta de CDK4 y RAF1 favorece la disminución del tamaño del 100% de los tumores de pulmón dirigidos por el oncogén *Kras* en un contexto donde la función de *Trp53* ha sido eliminada. Cabe destacar que el 24% de los tumores han desaparecido completamente de acuerdo a los criterios RECIST.

Aún así, hay un pequeño porcentaje de células que sobreviven en ausencia de las dos dianas terapéuticas, siendo capaces de evolucionar y promover nuevo crecimiento tumoral. La caracterización de dichas células, confirma la existencia de diversos mecanismos heterogéneos como cambios epigenéticos o la activación de vías de señalización alternativas como la vía de PI3K. De hecho, el tratamiento selectivo con 5-Azacitidina o inhibidores de PI3K impiden la progresión de las células resistentes a la inactivación de CDK4 y RAF1. Futuros estudios para entender las complejas interacciones entre el ciclo celular y la vía de MAP quinasa arrojarán luz para favorecer el desarrollo de nuevos tratamientos contra los tumores con mutaciones en KRAS.

II. Contents

III. ABBREVIATIONS

ADC: Adenocarcinoma

Adeno-Cre: Adenovirus carrying the Cre recombinase gene

Adeno-Flp: Adenovirus carrying the Flp recombinase gene

A-Loop: Activation Loop

AKT: RAC-alpha serine/threonine-protein kinase

ALK: Anaplastic Lymphoma Kinase

ASK-1: Apoptosis Signal-regulating Kinase 1

ATI: Alveolar Type I

ATII: Alveolar Type II

ATP: Adenosine Tri-Phosphate

AURKA: Aurora Kinase A

BAD: Bcl-2 Antagonist of cell Death

BAG1: Bcl-2 Associated Athanogene 1

BAK1: BCL2 Antagonist/Killer 1

BASCs: Bronchioalveolar Stem Cells

BCL-2: B-cell Lymphoma 2

BH3: Interacting-domain death agonist

BID: Twice-daily

BRAF: V-Raf Murine Sarcoma Viral Oncogene Homolog B1

BrdU: 5-bromo-2'-deoxyuridine

bp: base pair

CAK: Cdk-Activating Kinase

CC3: Cleaved Caspase 3

CDK: Cyclin-dependent kinase

CDKN2A: Cyclin-Dependent Kinase inhibitor 2A

CDC25A: Cell Division Cycle 25A

CDK4: Cyclin-Dependent Kinase 4

cDNA : Complementary DNA

CIP: CDK interacting protein

CR: Conserved Region

CRD: Cysteine-Rich Domain

CT: Computed Tomography

CTL: Cytotoxic T Lymphocyte

Ctrl: Control

CreERT2: a tamoxifen inducible Cre-estrogen receptor (ER) fusion protein

DCAFs: D-Cyclin activating features

DDR2: Discoidin Domain-containing Receptor 2

DEGs: Differentially Expressed Genes

DFG: conserved Asp-Phe-Gly (DFG) motif

DLT: Dose-limiting toxicities

DMEM: Dulbecco's Modified Eagle Medium

DNA: Deoxyribonucleic acid

DNMT1: DNA Methyltransferase 1

dNTP: Deoxynucleotide

EGFR: Epidermal Growth Factor Receptor

ERBB2: Erb-B2 Receptor Tyrosine Kinase 2

ERK: Extracellular Signal Regulated Kinase

FAS: Fas cell surface death receptor

FBS: Fetal Bovine Serum

FC: Fold Change

FDA: Food and Drug Administration

FFA: Foci Formation Assay

FGFR: Fibroblast Growth Factor Receptor

FKBP: FK506 Binding Protein

FOXM1: Forkhead Box M1

FOXO: Forkhead Box O1

GADD45G: Growth Arrest and DNA Damage Inducible Gamma

GDP: Guanosine Diphosphate

GSEA: Gene Set Enrichment Analysis

GTP: Guanosine triphosphate

GEMM: Genetically Engineered Mouse Model

HDAC: Histone Deacetylase

HER: Human Epidermal Growth Factor Receptor 2

HR: Hormone Receptor

H&E: Hematoxylin and Eosin

hUBC: Human Ubiquitin C

H4R3: H4 Arginine 3

IHC: Immunohistochemistry

INK4: INhibitors of CdK4

IP: Immunoprecipitation

JNK: Jun Nuclear Kinase

KD: Kinase Dead

KEAP: Kelch-like ECH-Associated Protein

KIP: Kinase Inhibitory Protein

KO: Knock-out

KSR: Kinase Repressor of RAS

KRAS: Kirsten Rat Sarcoma Viral Oncogene Homolog

LAST1: Loss of Large Tumor Suppressor 1

LUAD: Lung Adenocarcinoma

LSL: Lox-STOP-Lox

MAPK: Mitogen Activating Protein Kinase

MAT1: CDK-Activating Kinase Assembly Factor MAT1

MBC: Metastatic Breast Cancer

MET: Mesenchymal Epithelial Transition

MEF: Mouse Embryonic Fibroblast

MEK: Mitogen Activating Protein (MAP) Kinase

MEP50: Methylosome Protein 50

MST2: Mammalian Sterile 20-like kinases

MOCK: condition with no antibody in an immunoprecipitation

MOI: Multiplicity Of Infection

MTT: 3-[4, 5-dimethylthiazol-2-yl]-2, 5-diphenyl tetrazolium bromide

MYC: v-myc avian myelocytomatosis viral oncogene homolog

Neo: Neomycin

NES: Normalized Enrichment Score

NF1: Neurofibromin 1

NK: Natural Killer

NOTCH: Notch Homolog 1, Translocation-Associated

NRF2: Nuclear Factor erythoid 2-Related Factor 2

NSCLC: Non-Small Cell Lung Cancer

OCT: Optimum Cutting Temperature compound

ON: Overnight

PBS: Phosphate Buffered Saline

PD: Progressive Disease

PD-1: Programmed Death protein 1

PD-L1: Programmed Death Ligand 1

PDGFR: Platelet Derived Growth Factor Receptor

PFU: Plaque forming Unit

PI3K: Phosphatidylinositol-4,5-bisphosphate 3-kinase

PKC: Protein Kinase C-theta

PLK1: Polo-Like Kinase 1

PP: Protein Phosphatase

PPAR: Peroxisome Proliferator Activated Receptor

PR: Partial Response

PROTAC: Proteolysis Targeting Chimera

PO: *Per Os*, oral administration

PUMA: p53 Upregulated Modulator of Apoptosis

QD: Once-a-day

qRT-PCR: Quantitative Real Rime Polymerase Chain Reaction

RAF1: V-Raf-1 Murine Leukemia Viral Oncogene Homolog 1

RB: Retinoblastoma

RBD: Ras Binding Domain

RECIST: Response Evaluation Criteria in Solid Tumors

RIN: RNA Integrity Number

RNA: Ribonucleic Acid

ROK-α: rho-associated, coiled-coil-containing protein kinase 1.

ROS: Proto-Oncogene Tyrosine-Protein Kinase ROS

RP: Responders cells

RSK: Ribosomal S6 Kinase

RT: Resistant cells

RTK: Receptor Tyrosine Kinase

SCC: Squamous Cell Carcinoma

SCLC: Small Cell Lung Cancer

SD: Stable Disease

SDS: Sodium Dodecyl Sulfate

Sf9 cells: *Spodoptera frugiperda*

shRNA: short hairpin RNA

SOX2: SRY-box 2

SPOP: Speckle-type POZ

SQSTM1: Sequestome 1

ssGSEA: single Sample Gene Set Enrichment Analysis

STAT3: Signal transducer and activator of transcription 3

STK11: Serine/Threonine Kinase 11 or LKB1

Taq-Polymerase: *Thermus aquaticus* DNA Polymerase

TBS: Tris Buffered Saline

TCGA: The Cancer Genome Atlas

Tg: Transgenic

TGFβ: Transforming Growth Factor TNF: Tumor Necrosis Factor β

TKI: Tyrosine Kinase Inhibitors

TPM: Transcripts Per Million

Treg: Regulatory T cell

TRP53: Transformation-Related Protein 53

TSC2: Tuberous Sclerosis Complex 2

TX: Tamoxifen

VDACs: Voltage-Dependent Anion Channels

WNT: Homologous Wingless (Wg) and Int-1

X-Gal: 5-bromo-4-chloro-3-indolyl-β-D-galactopyranoside

YAP: Yes Associated Protein 1

4OHT: 4-Hydroxy-tamoxifen

INTRODUCTION

1. Lung cancer

1.1. Tumor epidemiology and risks factors

Lung cancer is the second most commonly diagnosed cancer accounting for 13% of all cancer cases diagnosed. But, is by far the leading cause of cancer death among both men and women, which means 1 out of 4 cancer deaths (Siegel et al., 2019). The 5-year survival rate is 19% and the median survival only one year. Only 16% of lung cancers are diagnosed at a localized stage increasing the 5-year survival rate to a 56% (American Cancer Society. Cancer Facts and Figures 2019). In Spain, lung cancer has an incidence of 10% among men and women and a 20% of mortality being the first cause of cancer death in our country (Bray et al., 2018).

The main risk factor that raises lung cancer incidence is cigarette smoking inducing mutations in oncogene drivers such as *KRAS* (Sun et al., 2013). In fact, smoking causes at least 81% of lung cancer deaths. Other risk factors include exposure to radon gas, certain metals, radiation, diesel exhaust or air pollution which also have a negative impact in lung tumor development (Zappa and Mousa, 2016). Besides, genetic susceptibility plays a key role increasing the risk of lung cancer. Carriers of *TP53* germline sequence variations who also smoke are more than 3 times more likely to develop lung cancer (Hwang et al., 2003). There has also been reported that people with a common variant in the nicotine acetylcholine receptor gene have increase nicotine dependence which is associated with lung cancer. People with only one copy of the gene have 30% increased risk of developing lung cancer, while people with both copies have an increased risk of 80% (Thorgeirsson et al., 2008).

1.2. Different lung cancer subtypes and frequent mutations

Lung cancer can be subdivided according to different histopathological characteristics between **small cell lung cancer** (SCLC) that accounts for 15% of all lung cancer cases and **non-small cell lung cancer** (NSCLC) that affects around 85% of the lung cancer patients. Loss of p53 and RB are thought to transform the pulmonary neuroendocrine cells (PNEC) giving rise to SCLC (Swanton and Govindan, 2016) (Figure 1). However, NSCLC is not a unique pathology but a heterogenous group of several diseases that can be subdivided in 3 main subgroups according to their histopathological features and their cells of origin.

Adenocarcinoma (ADC): it affects around 40% of all lung cancer patients. They normally have a glandular histology and develop in more distal airways (Xu et al., 2012) (Figure 1). Regarding the molecular alterations that occur during cell transformation v-Ki-ras2 Kirsten Rat Sarcoma viral

oncogene (*KRAS*-33% typical in smokers), epidermal growth factor receptor (*EGFR*-14% almost exclusively in never-smokers, females and Asian patients) and anaplastic lymphoma kinase (*ALK*-4%) genes could be identified. These 3 genetic modifications are normally mutually exclusive (Pikor et al., 2013). Other common mutated oncogenes in LUAD are *B-RAF* (in 10%), *PIK3CA* (in 7%), and *MET* (in 7%). Mutations involving loss of tumor suppressor genes include *TP53* (in 46%), *STK11* (in 17%), *KEAP* (in 17%), *NF1* (in 11%), *RB* -the first tumor suppressor found in NSCLC- (in 4%), and *CDKN2A* (in 4%) (Inamura, 2017; Swanton and Govindan, 2016).

Different cells of origin can explain the high diversity of lung tumor types. There is a hypothesis which postulates the idea that stem and progenitor cells tend to accumulate many genetic alterations responsible for tumor formation (Visvader, 2011). In line with this, BASCs a stem cell population, are considered responsible for the maintenance of the bronchiolar Clara cells (Club cells) and the alveolar epithelial type 1 and 2 (ATI and II) cells of the distal part giving rise to ADC upon cell transformation (Kim et al., 2005). More recent work from Desai and collaborators support the idea that ATI and ATII come from a bipotent alveolar progenitor and is not until birth when mature ATII cells behave as stem cells having renewal, repairing or tumor promoting properties (Desai et al., 2014). This process depends on aberrant signaling by EGFR and RAS (Swanton and Govindan, 2016). Other more extended studies support the idea that only ATII cells are capable of inducing ADC tumor formation in the alveolar space, whereas Club cells and BASCs have a limited role in giving rise to bronchiolar hyperplasias as demonstrated after targeting $KRAS^{G12D}$ and $KRAS^{G12V}$ in specific differentiated cells (Mainardi et al., 2014; Xu et al., 2012) (Figure 1).

Squamous cell carcinoma (SCC): it comprises 25-30% of all lung cancer cases. This subtype of NSCLC is strongly associated with smoking habits and chronic inflammation. It arises from squamous cells in the bronchiolar epithelium from the more central airways (Kenfield et al., 2008) (Figure 1). During this process many molecular alterations have been reported including destabilization of telomerase activity, *TP53* mutation, deregulation of cell proliferation (*CYCLIND1* and *CYCLINE*), loss of heterozygosity at different locus (D17S1) or apoptosis (*BCL2*) (Davidson et al., 2013) and recently, histone modifications (Inamura, 2017). There are recurrent alterations that include amplifications of *SOX2*, *PIK3CA*, *PDGFRA* and *FGFR1* as well as mutations in DDR2, AKT1 and NRF2 (Heist et al., 2012). Although *SOX2* and *PIK3CA* amplifications affect around 20-30% of the patients, inhibitors against those molecules are not approved in the clinic yet. Only BMK120, a drug against PIK3CA activity is currently in phase II clinical trials (Yang et al., 2019).

Large cell carcinoma: it accounts for 10-15% of the lung cancers. Large cell carcinoma tumors are strongly associated with smoking. Diagnosis is made by exclusion of the other two main subgroups when no signs of glandular or squamous histology are found. Large cell carcinomas rise in the central part of the lungs sometimes into nearby lymph nodes as well as distant airways (Zappa and Mousa, 2016) (Figure 1).

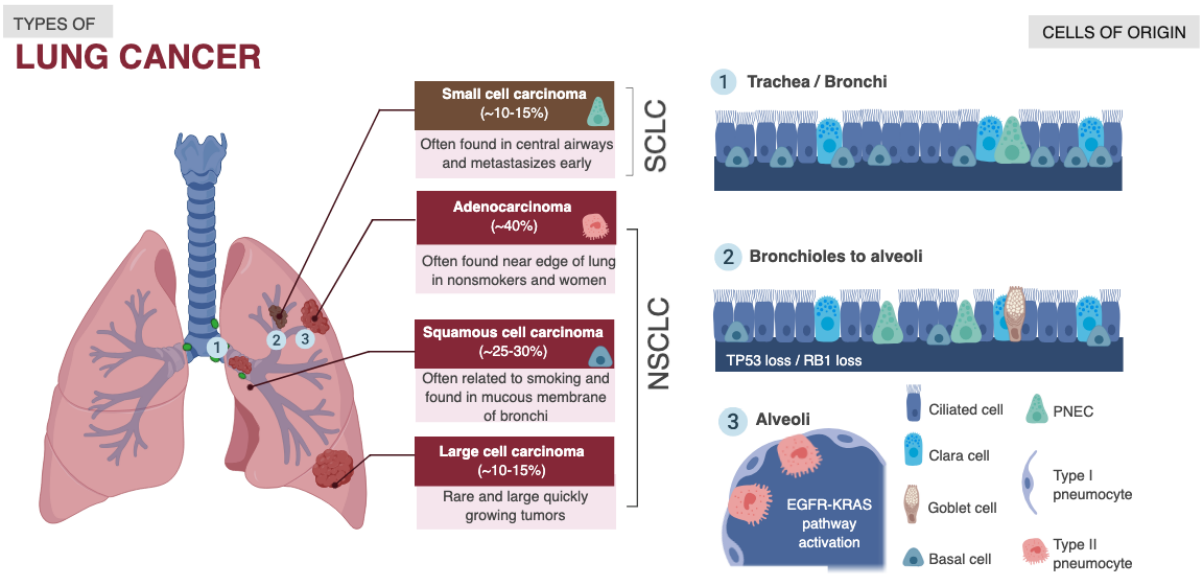

Figure 1: Classification and localization of different subtypes of lung cancer according to histopathological features and the cell of origin.

1.3. Current treatment and future directions for NSCLC

The design of current NSCLC treatments has been improved by a prognostic model that stratifies patients based on different disease variables associated with overall survival such as age, sex, respiratory comorbidity, histology, stage or mutation status (Alexander et al., 2017). Notwithstanding, the importance of early detection methods makes the difference for lung cancer treatment to succeed. Therefore, different treatments are given to patients according to early or advanced detection. For patients with early stage lung cancer (I, II or III), surgery is the recommended treatment. On top of that, an adjuvant therapy such as radiation and/or chemotherapy (using either cisplatin or carboplatin and a second drug) are given in order to prolong survival (Curran et al., 2011). The role of targeted therapies in this setting is not defined.

Unfortunately, more than 40% of the cases are stage IV with locally advanced or metastatic disease (Reck et al., 2013). For those advanced stage patients, immunotherapy may be part of the treatment strategy (Gandhi et al., 2018) but the standard first-line treatment remains platinum-based containing therapy with or without Pembrolizumab when targeted therapy does not fit as a treatment

of option (Hirsch et al., 2017; Majem et al., 2019). Target validation of the genomic aberrations found in lung cancer patients has become a challenging aim in order to understand and predict tumor response which has been demonstrated to be especially successful in young patients with adenocarcinoma, who are mostly never-smokers.

The immunotherapy phenomenon was born in the late 19th century, when the surgeon William Coley injected an inactivated bacteria into a sarcoma patient leading to tumor shrinkage (Coley, 1991). From that moment on, trying to understand how the immune system crosstalks with the tumoral cells have gained interest. Nevertheless, it was not until 2015 when Nivolumab, the first *checkpoint inhibitor*, was FDA-approved for the treatment of advance NSCLC as a second-line treatment (Table 1). The basis of these inhibitors is to activate the T cells in order to kill a cancer cell. Because, in normal conditions, immune checkpoints keep T cells inactive, until they are needed, preventing T cells from harming normal cells. Therefore, cancer cells can take advantage of these checkpoints to switch T cells off avoiding the cancer cells from being killed. Immune *checkpoint inhibitors* block either the Programmed Death Protein1 (PD-1) or the Ligand1 (PD-L1), allowing the T cells to attack (Table 1). Results from a first clinical trial in NSCLC demonstrated that smoker patients will preferentially benefit from Pembrolizumab, since genomic instability is directly induced due to tobacco habits. Moreover, 50% of the responder patients correlated with KRAS mutations (Rizvi et al., 2015). Current studies are now focused in trying to identify biomarkers to predict response to immunotherapy as a clinical option. Combination of several candidates including PD-L1 expression, tumor mutational burden (TBM) or density of tumor infiltrating lymphocytes are crucial for patient selection (Song et al., 2019).

Targeted therapy is the first-line treatment for patients with metastatic NSCLC who carry *EGFR* mutations within exons 18 to 21 which encoded for the tyrosine-kinase domain where tyrosine kinase inhibitors (TKIs) such as Erlotinib or Gefitinib bind. This last treatment, shows an overall response rate of 50% (Douillard et al., 2013). Second-generation TKIs (e.g., Afatinib) show an improvement in overall survival although they also have more toxic effects than first-generation TKIs. Necitumumab, a monoclonal antibody that targets EGFR, was approved in 2015 by the FDA for first-line treatment of metastatic SCC in combination with Gemcitabine and Cisplatin (Thatcher et al., 2015). In most of the cases tumor relapses appear due to the secondary T790M mutation in *EGFR*. Therefore, Osimertinib (AZD9291) has been approved for the treatment of NSCLC harboring this mutation showing a median progression-free survival of 9,6 months (Janne et al., 2015) (Table 1). In addition, Larotrectinib sulfate is a type of TKI used in patients whose disease has Neurotrophic receptor tyrosine kinase (NTRK) gene fusions (Scott, 2019).

Other FDA approved drugs for the treatment of *ALK*-positive rearrangements are Crizotinib, Ceritinib and Alectinib, which now constitute the backbone of treatment for these patients (Shaw et

al., 2019). Among them, Crizotinib is also approved for the treatment of *MET* amplification or *ROS1* chromosomal rearrangements (Shaw et al., 2019) (Table 1).

Everolimus, an mTOR inhibitor, was approved in 2016 for the treatment of patients with progressive, well-differentiated non-functional, neuroendocrine tumors (NET) of lung origin that are unresectable, locally advanced, or metastatic (Soria et al., 2009) (Table 1).

Although a new drug for the treatment of $KRAS^{G12C}$ mutant tumors has recently been discovered (Janes et al., 2018), the development of therapeutics to target this gene have been unsuccessfully attempted during the past thirty years. Therefore, inhibition of its downstream effectors has become the more reliable alternative approach. Patients with $B\text{-}RAF^{V600E}$ mutation and metastatic NSCLC can benefit from Dabrafenib or Vemurafenib, specific B-RAF inhibitor (Odogwu et al., 2018). MEK inhibitors, such as Trametinib or Selumetinib, were only effective as single agent in B-RAF mutated cells (Flaherty et al., 2012; Joshi et al., 2015; Sun et al., 2014) (Table 1). Nonetheless, MEK inhibitors have shown limited clinical activity as single agents for the treatment of KRAS mutant tumors (Kohler et al., 2018; Sun et al., 2014). For instance, no significant additional benefit of Selumetinib was observed in a phase II neither in a phase III clinical trial (SELECT-1) alone or in combination with docetaxel in Kras-driven NSCLC (Hainsworth et al., 2010; Janne et al., 2017). Remarkably in this phase III study, frequent adverse events were observed in the combination group compared with docetaxel alone (Janne et al., 2017). A second MEK inhibitor, Trametinib, was tested as a single agent in a phase II clinical trial in KRAS mutant tumors and again, the clinical activity was comparable to docetaxel alone. In addition, grade 4 toxicity events only occurred in the Trametinib arm (Blumenschein et al., 2015). The reasons of this modest activity in *Kras*-driven tumors are thought to be due to the early paradoxical hyperactivation of the MAPK signaling via RAF1 or the relieve of the negative feedback leading to pathway reactivation (Lavoie et al., 2013; Samatar and Poulikakos, 2014) together with its dose-limiting toxicities such as dermatological and gastrointestinal side effects (Kohler et al., 2018; Samatar and Poulikakos, 2014; Tyagi and Santiago, 2018; Welsh and Corrie, 2015).

Drug name	Target
Opdivo (NIVOLUMAB)	anti PD-1
Imfinzi (DURVALUMAB)	anti PD-L1
Keytruda (PEMBROLIZUMAB)	anti PD-L1
Tecentriq (ATEZOLIZUMAB)	anti PD-L1
Avastin (BEVACIZUMAB)	EGFR
Mvasi (BEVACIZUMAB)	EGFR
Afatinib DIMALEATE	EGFR
Gilotrif (AFATINIB DIMALEATE)	EGFR
Iressa (GEFITINIB)	EGFR
Portrazza (NECITUMUMAB)	EGFR
Tarceva (ERLOTINIB HYDROCHLORIDE)	EGFR
Vizimpro (DACOMITINIB)	EGFR
Cyramza (RAMUCIRUMAB)	EGFR or ALK
Osimertinib (MESYLATE)	EGFR T790M
Tagrisso (OSIMERTINIB MESYLATE)	EGFR T790M
Vitrakvi (Larotrectinib)	TRK
Alecensa (ALECTINIB)	ALK
Alunbrig (BRIGATINIB)	ALK
Lorbrena (LORLATINIB)	ALK
Zykadia (CERITINIB)	ALK
Xalkori (CRIZOTINIB)	ALK, MET or ROS1
Afinitor (EVEROLIMUS)	mTOR
Tafinlar (DABRAFENIB)	BRAF
Zelboraf (VEMURAFENIB)	BRAF
Mekinist (TRAMETINIB)	MEK

Table 1: List of targeted drugs approved as single agents by the Food and Drug Administration (FDA) for the treatment of NSCLC. Data from 2018, from the National Cancer Institute (NIH) and Schrank.Z et al., Cancers, 2018.

Therefore, novel genetically engineering mouse models (GEMMs) that directly or indirectly target proteins which lie downstream of KRAS such as RAF1 (Blasco et al., 2011; Sanclemente et al., 2018), or CDK4 (Puyol et al., 2010) are necessary in order to identify druggable, non-toxic therapeutic targets.

2. Cyclin-dependent kinases (CDKs) signaling pathway

2.1. How mammalian cell cycle is regulated

CDKs are serine-threonine kinases which bind to regulatory partners known as CYCLINs responsible of the kinase activity and substrate specificity. CDKs unbound to CYCLINs are normally inactive and their protein levels are constitutively maintained along the cell cycle, whereas CYCLIN levels oscillate during the different phases of the cell cycle in order to regulate its progression, hence their name (Vermeulen et al., 2003). Except for CYCLIND whose expression is not cyclical, instead it is expressed in response to proliferative signals and that is the reason why is considered a direct mitogen sensor (Ortega et al., 2002).

CDKs were first discovered in yeasts, these pioneer studies determined CDC28 in *Saccharomyces cerevisiae*, equivalent to CDK1 in mammals, as the CDK responsible of promoting cell cycle though its promiscuous interaction with multiple CYCLINs. This redundancy allows for a dynamic regulation favoring the phosphorylation of multiple substrates (Beach et al., 1982; Morgan, 1997). During evolution, CDKs have evolved to a more sophisticated scenario where more than 20 members (Malumbres et al., 2009) are able to satisfy the requirements of complex multicellular organisms (Malumbres and Barbacid, 2009). However, like its yeast ortholog, CDK1 is the only CDK essential for the promotion of the mammalian cell cycle (Santamaria et al., 2007).

According to the "classical model", cell cycle is controlled by the RB/E2F pathway (Weinberg, 1995). In normal conditions, the pocket proteins (Retinoblastoma, p107 and p103) are in a hypophosphorylated state in which E2F transcription factor is sequestered impeding cells entering in S phase (Dyson, 1998) (Figure 2). If the CDK activity gets inhibited during G1 phase and the E2F remains persistently inactive, this leads to S phase delay and apoptosis (Phillips et al., 1999). Progression throughout the G1 phase, where cells decide whether to enter into DNA synthesis (S phase) or remain quiescent, is regulated by a complex mechanism involving at least CDK6, CDK4, CDK3 and CDK2 (Malumbres and Barbacid, 2009). Upon external mitogenic stimuli such as those emitted by growth factors, D-type CYCLINs become active and preferentially bind and activate CDK4/6 kinases. The already formed complex partially phosphorylates RB at Ser^{807} and Ser^{811} and inactivates it. This partial phosphorylation consists of mono-phosphorylation (Blain, 2008) which will partially release the E2F

transcription factor allowing cells to initiate DNA synthesis by the transcriptional expression of E-type CYCLINs that bind and activate CDK2 (and, to a lesser extent, CDK1 and CDK3) (Sherr and Roberts, 1999; Ye et al., 2001) (Figure 2). Before this step, there is a fuzzy non-reversible "Restriction point" in G1 after which mitogenic signals are no longer needed in order to progress into S-phase (Pardee, 1974). Both D-type kinases and E-type kinases are able to phosphorylate RB and this phosphorylation by CDK2 requires previous phosphorylation by CDK4/6 (Figure 2). It is therefore believed that phosphorylation of RB by CDK4/6 represents the primary regulatory event that allows cells to pass through the restriction checkpoint. The subsequent induction of CYCLINA2 in S-phase, complex with CDK2 in order to phosphorylate proteins involved in DNA replication (Petersen et al., 1999). Once cells have replicated their DNA, during the G2/M transition CDK1 becomes activated by A-and B-type CYCLINs completing centrosome cycle and mitosis processes together with a set of proteins called M-phase promoting factors MPF (Riabowol et al., 1989; Sherr and Roberts, 2004) (Figure 2).

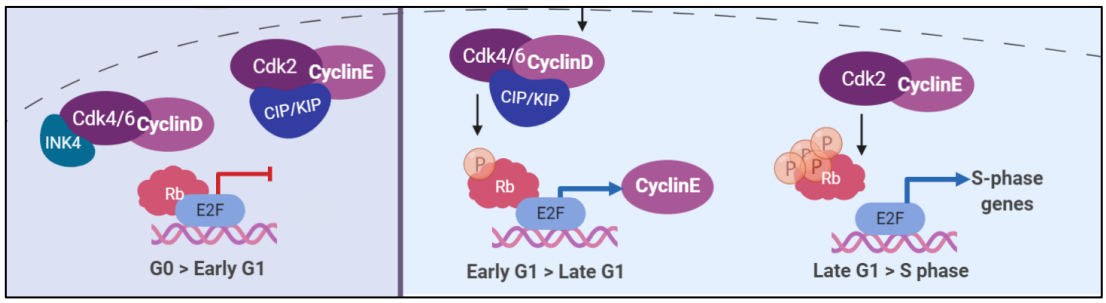

Figure 2: Illustration of the different phosphorylation status of the tumor suppressor Rb and its consequences in cell cycle entry or arrest. Adapted from Goel *et al*., Trends in Mol Biology, 2018.

2.2. Cdk4 is dispensable for cell cycle entry

The spread paradigm for the mammalian cell cycle already described is not as linear as it was thought and has considerably changed during the past years. It was originally believed that: 1) each phase of the cell cycle is driven by a unique set of CDK/CYCLIN complex, 2) CDKs must partner with CYCLINs to become active, 3) CYCLINs are mere regulatory subunits and 4) CYCLIN-dependent Kinase Inhibitors (CKIs) strictly inhibit CDK/CYCLIN complexes. Nowadays, there are enough experimental evidences that demonstrate a redundancy of CDKs making them dispensable for life (Malumbres and Barbacid, 2009). For instance, it is known that CDK4/6-CYCLIND complexes activate the transcription factor forkhead box protein M1 (FOXM1), which regulates the expression of multiple proteins that govern the G2-M transition repressing cell senescence (Anders et al., 2011). Individual subunits have functional properties, for instance, CDK6 by itself has a role in promoting angiogenesis (Kollmann et al., 2013) and CYCLIND1 prevents anoikis by repressing FOXO1 in a CDK-independent manner (Gan et al.,

2009). In addition, the CDK Interacting Protein/Kinase Inhibitory Protein -CIP/KIP proteins-, which belong to the CKIs family of inhibitors, apart from their inhibitory roles also act as positive regulators of CDK4/6-CYCLIND by stabilizing these heterodimers (Cerqueira et al., 2014).

The compensatory mechanisms among CDKs have been well characterized by genetical knock-out mouse models rising up the conclusion that even in the absence of CDK4, CDK6 or CDK2 mice are viable although showing some developmental defects that are cell-type specific. For instance, CDK4 is dispensable for MEFs (Mouse Embryonic Fibroblasts) proliferation as well as for mouse development (Tsutsui et al., 1999). Likewise, similar experiments carried out in *Drosophila melanogaster*, an organism that has a single *Cdk4/6* ortholog (*Cdc28*) yielded basically the same results observed in mice. *Cdk4 null* flies are viable and have severely reduced fertility (Meyer et al., 2000). These observations, while not excluding a role of *Cdk4* in G1-phase, raise a note of caution about the widely held hypothesis that *Cdk4* is the "primary sensor" for driving cells through the restriction checkpoint in preparation for a new round of cell division.

On the other hand, CDK4 is essential for cell cycle commitment in certain cell types *in vivo* such as the development of endocrine β-pancreatic cells and pituitary-producing lactotrophs. ***Cdk4*$^{-/-}$** mice show an insulin-deficient diabetic phenotype as well as fertility problems due to defects in the adenohypophysis (Martin et al., 2003; Moons et al., 2002; Rane et al., 1999; Tsutsui et al., 1999) (Figure 3). Re-expression of CDK4 rescues normoglycemic conditions as well as fertility, indicating a specific cell autonomous requirement of CDK4 in these cell types (Hydbring et al., 2016; Martin et al., 2003). In addition, CDK4 ablation was reported to induce abnormalities in lymphocytes differentiation and consequently in allergen response (Chow et al., 2010). On the other hand, CDK6 does have an essential role in thymocytes and hematopoietic precursors differentiation. This function in hematopoiesis was demonstrated to be kinase dependent since the expression of a CDK6 kinase inactive mutant, CDK6^{K43M}, leaded to the development of impaired thymocytes (Hu et al., 2011). Hence, ***Cdk6*$^{-/-}$** mice show mild defects such as decreased cellularity in the thymus, red blood cells and lymphocytes (Malumbres et al., 2004) (Figure 3). These limited mild defects are probably due to functional compensation by CDK4 (and possibly by CDK2) since it has been identified in combination with D-type CYCLINs.

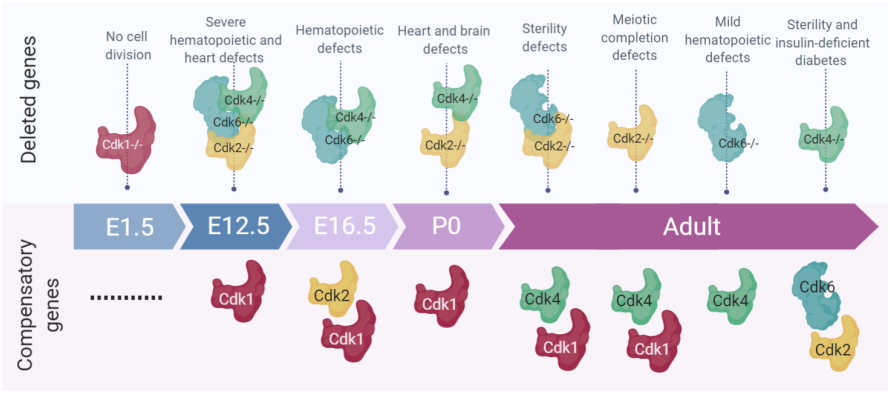

Figure 3: (Upper panel) Time line of different CDKs knock-out mouse models and (bottom panel) the gene/s that compensate for the lack of that protein. E: embryonic day. P: postnatal day. Adapted from Hydbring *et al.*, Nat Rev Mol Cell Biol, 2016.

Mice without *Cdk2,* ***Cdk2$^{-/-}$***, did not display detectable defects in mitosis but yes in meiosis (Berthet et al., 2003; Ortega et al., 2003; Tetsu and McCormick, 2003) (Figure 3). This dispensability of CDK2 during mitotic cell division is thought to be by CDK1/CYCLINA complexes compensation (Aleem et al., 2005). Later, lack of CDK2 was demonstrated to impair neural progenitor cell proliferation during postnatal development and interestingly, CDK4 but not CDK1 compensates for CDK2 deficiency until postnatal day 15 (Jablonska et al., 2007).

Likewise, ***Cdk2$^{-/-}$;Cdk6$^{-/-}$*** mice are viable and show no more obvious defects than the ones observed in the single mutants (Malumbres et al., 2004) (Figure 3). Similarly, double ***Cdk2$^{-/-}$;Cdk4$^{-/-}$*** complete embryonic development dying shortly thereafter presumably due to heart failure, demonstrating the fact that the two main interphase CDKs are exclusively indispensable for correct heart homeostasis (Barrière et al., 2007) (Figure 3). On the contrary, Berthet *et al*. showed heart defects that led to embryonic lethality at E15.5 (Berthet et al., 2006). Some years later, it was reported that these double-knock-out mice lack the intermediate zone and cortical plate of their brains, due to premature neuronal differentiation (Lim and Kaldis, 2012), supported by the idea that CDK4/CYCLIND is responsible of inhibiting neuronal differentiation by shortening basal progenitors G1 phase (Lange et al., 2009). In addition, ***Cdk4$^{-/-}$;Cdk6$^{-/-}$*** embryos die of severe anemia at late embryonic day (E16.5) (Figure 3) but later than triple *CyclinD$^{-/-}$* mice (Malumbres et al., 2004) suggesting that CDK4/CYCLIND complexes are responsible of bypassing *Cdk6$^{-/-}$* mice defects and that CDK2 and CYCLIND may also perform redundant functions. Triple knock-out embryos ***Cdk2$^{-/-}$;Cdk4$^{-/-}$;Cdk6$^{-/-}$*** die due to heart and severe hematopoietic defects (Figure 3) although MEFs are able to be immortalized as a consequence of CDK1 binding to all CYCLINs resulting in phosphorylation of RB (Santamaria et al., 2007). The only situation where no compensation has been observed is in the absence of the mitotic CDK1 (Lange et al., 2009) suggesting a scenario not so different to the one observed in yeasts where CDC28 is sufficient to induce proliferation (Beach et al., 1982).

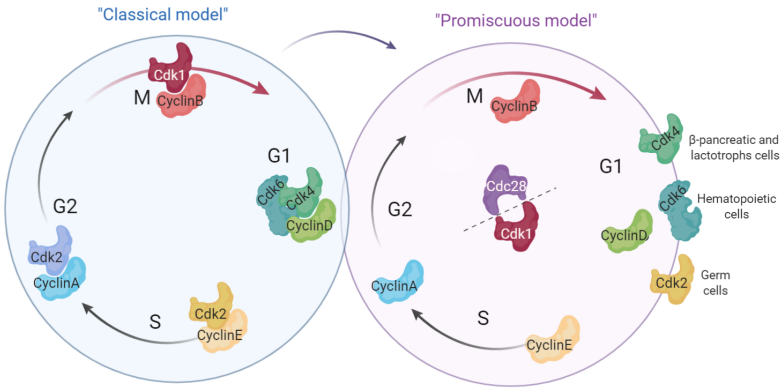

Figure 4: Illustration of the different phases of the cell cycle and the main CDKs/CYCLINs involved during this process. In the left, CDKs are located as they have been classically considered to work during specific phases. In the right, only CDK1 (CDC28 in Saccharomyces cerevisiae) is considered indispensable for cell cycle entry while CDK2,4 and 6 are only essential in tissue-specific contexts. Adapted from Malumbres and Barbacid., Nature, 2006.

All this data together leads us to change the course of how the "classical cell cycle regulation model" works and rethink about it, as a more non-canonical "promiscuous model" where alternative mechanisms to initiate and sustain the cell cycle are present (Figure 4).

2.3. Intrinsic CDK4 regulation

Inhibition of CDK4/6 is mainly dependent on the presence of inhibitory proteins called CKIs which include two families of inhibitors: the INK4 ($p16^{INK4a}$, $p15^{INK4b}$, $p18^{INK4c}$ and $p19^{INK4d}$) and the CIP/KIP ($p21^{Cip1}$, $p27^{Kip1}$ and $p57^{Kip2}$) proteins responsible of preserving genomic integrity as well as preventing neoplastic transformation (Aprelikova et al., 1995; Toyoshima and Hunter, 1994). Some of these inhibitors are induced in response to antimitogenic signals such as senescence, TGFβ or oncogenic stress (Sherr and Roberts, 1999).

When induced, INK4 inhibitors mainly bind to and inhibit the monomeric forms of CDK4 and CDK6 impeding their activation by CYCLINs. Whereas, the CIP/KIP inhibitors bind to and inhibit the CDK4/CYCLIND complexes and are also inhibitors of CDK2/CYCLINE and CDK1/CYLINB complexes blocking their kinase activity. In addition, CIP/KIP proteins seem to be involved in the stabilization and assembly of CDK4/CYCLIND-CIP/KIP ternary complexes (Cerqueira et al., 2014). These complexes sequester CIP/KIP inhibitors that are therefore maintained away from active CDK2/CYCLINE complexes. Thus, it has been proposed that CDK4 has a double function: phosphorylation of RB and sequestering of CIP/KIP inhibitors to allow for cell cycle progression (Sherr and Roberts, 1999). Since both functions result in the activation of CDK2, it is believed that the major function of CDK4 is to activate CDK2. In fact, a knock-in allele expressing *CyclinE* in the *CyclinD1* locus restores most of the defects caused by CYCLIND1 ablation, suggesting that CYCLINE is the primary downstream target of CYCLIND1 (Geng et al., 1999).

Furthermore, to fully activate CDK4 an additional step should be done followed by CYCLIND binding. CDK4 needs to be phosphorylated at the Thr^{172} residue of the activation segment (T-loop) of the CDK subunit by the CDK-Activating Kinase (CAK) (Bisteau et al., 2013). Paradoxically, this CAK in metazoans, like its substrate, is a CDK/CYCLIN complex formed by CDK7, CYCLINH and MAT1 and thus the reason why during many years CDK7 was found to have many kinase independent functions (Fisher, 2005). Nowadays, it is known that in mammals CDK7 is necessary for orchestrating CDK activation. In fact, its elimination results in CDK4 reduced kinase activity, hypophosphorylation of the T-loop and cell cycle arrest (Ganuza et al., 2012).

2.4. Non-canonical CDK4 kinase dependent and independent functions

Beyond the cell cycle, CDK4 regulates other processes such as epigenetic modifications, immune modulation, apoptosis, cell differentiation and metabolism (Lim and Kaldis, 2013).

On one hand, CDK4 complex with CYCLIND is linked to histone modifications by phosphorylating Methylosome protein 50 (MEP50) which activates the chromatin modifier PRMT5 (protein arginine N-methyltransferase 5) and demethylates the histone H3 arginine 8 (H3R8) and H4 arginine 3 (H4R3) (Aggarwal et al., 2010). This complex has also been found to have a role in DNA methylation as it has been shown to phosphorylate and activate the DNA methyltransferase 1 (DNMT1), a direct E2F target whose expression is repressed when *Rb* is activated acting as a tumor suppressor. The role of DNMT1 in complex with CDK4/CYCLIND is to prevent senescence or autophagy allowing cells to proliferate by methylation of several genes (Acevedo et al., 2016; Bourdeau and Ferbeyre, 2016). It has also been shown that upon CDK4/6 inhibition, DNMTs mRNA levels are reduced leading to an augmentation of type III interferon production and therefore enhanced antigen presentation which in turn promotes cytotoxic T cell-mediated tumor cell clearance (Deng et al., 2018; Goel et al., 2018; Schaer et al., 2018). This increase in tumor immunogenicity upon CDK4/6 inhibition is accompanied by a suppression regulatory T cells (Tregs) proliferation via $p21^{Cip1}$ demethylation which favors cell cycle arrest (Goel et al., 2018). As Tregs suppress Cytotoxic T Lymphocytes (CTLs) by promoting their exhaustion (Bauer et al., 2014), the reduction of the immunosuppressive Treg population would favor a cytotoxic antitumor response. A study by Teo and colleagues showed that although, CDK4/6 inhibition alone was not sufficient to increase anti-tumor immunity, combination of CDK4/6 together with PI3K inhibitors lead to an increase in tumor-infiltrating cytotoxic $CD8^+$ T cells and natural killer (NK) cells, and a decrease in the Treg suppressor population in triple-negative breast cancer (Teo et al., 2017). In line with this data, CDK4/6 inhibition combined with MEK inhibitors induces NK cell-mediated cytotoxicity in pancreatic and LUAD tumors (Ruscetti et al., 2018). In addition, CDK4 has a kinase-dependent role over SPOP (speckle-type POZ) protein, a cullin E3 ubiquitin ligase directly linked to PD-L1 (Zhang et al., 2018). CDK4/6 inhibitors, degrade SPOP protein, blocking PD-L1 proteasome-mediated degradation, therefore increasing PD-L1 levels. For this reason, CDK4/6 inhibitors have been recently combined with anti PD-1 antibodies, enhancing colon adenocarcinoma regression (Deng et al., 2018; Zhang et al., 2018). Thus, apart from directly affecting cancer cells, by promoting the antigenicity, suppressing the regulatory T cells or affecting the immunological features of cancer cells, tumor growth could be therapeutically modified with CDK4/6 inhibitors.

On the other hand, CDK4 may have a role in indirectly inhibiting the cell death signaling since it interacts with the apoptosis inhibitor SURVIVIN. As a result, $p21^{Cip1}$ is released from the CDK4/CYCLIND complex and interacts with the mitochondrial procaspase 3 (C3) which suppresses Fas-mediated cell

death in human hepatoma cell lines (Suzuki et al., 2000). In fact, it was recently demonstrated that MEK inhibition by Selumetinib together with CDK4/6 inhibition by Palbociclib downregulates SURVIVIN protein expression levels in *p16^{INK4a}* mutant NSCLC human commercial cell lines leading to cell death (Zhou et al., 2017).

The role of CDK4 in modulating metabolic pathways has been demonstrated to be cell-type specific. In β-pancreatic cells, CDK4/CYCLIND complexes promote insulin secretion through the expression of the potassium ATP channel. Insulin, in turn, induces the expression of D-type CYCLINs through a positive feedback loop (Annicotte et al., 2009). In adipocytes, adipogenesis is inhibited by the interaction of *CyclinD1* with the histone acetyltransferase p300, which leads to the inhibition of the transcription factor peroxisome proliferator-activated receptor γ (PPARγ), responsible of stimulating lipid uptake and new adipose tissue formation by fat cells (Fu et al., 2005). Conversely, adipogenesis is activated by CDK4/CYCLIND3-mediated PPARγ phosphorylation (Abella et al., 2005; Lagarrigue et al., 2016). Gluconeogenesis is inhibited in hepatocytes through the CDK4/CYCLIND dependent phosphorylation and activation of the acetyltransferase GCN5, which acetylates and inactivates the transcription factor PPARγ coactivator-1α (PGC1α), in this context being responsible of glucose metabolism (Lee et al., 2014). On the contrary, glycolysis is increased upon AMPKa2 phosphorylation by CDK4 in MEFs (Lopez-Mejia et al., 2017).

2.5. Cdk4 deregulation: a key player in tumor development

Loss of cell cycle regulation leading to uncontrolled proliferation, is one of the hallmarks of cancer (Hanahan and Weinberg, 2011). Not surprisingly, the CDK4/6-CYCLIND-INK4-RB pathway is altered in most human tumors (Malumbres and Barbacid, 2001), underscoring the importance of these cell cycle regulators in maintaining appropriate proliferation rates. Although mutations in the *CDK4* gene are limited, still *CYCLIND1* and *CDK4* genes rank second and fourth among the most frequently amplified loci across all human cancers respectively (Beroukhim et al., 2010). In fact, although most of the tumor-associated mutations resulting in *CDK4* deregulation occur in its regulatory subunit *CYCLIND* (Marchetti et al., 1998), genetic alteration of human *CDK4* gene has also been observed in gliomas (Schmidt et al., 1994), sarcomas (Khatib et al., 1993), breast tumors (An et al., 1999) and carcinomas of the uterine cervix (Cheung et al., 2001). A point mutation in the *CDK4* gene has also been described in spontaneous and familiar melanomas (Wolfel et al., 1995). This mutation, a substitution of Arg24 by Cys (R24C), leads to missregulation of the kinase activity by preventing binding of the INK4 family of cell cycle inhibitors without affecting the affinity of CDK4 for CYCLIND1. The generation of a knock-in mice expressing the melanoma-associated mutated form of *Cdk4*, *Cdk4^{R24C}*, shows an increase incidence of

diverse types of tumors. In addition, mice receiving carcinogen insults give rise to aggressive skin carcinomas (Rane et al., 2002; Sotillo et al., 2001).

Genetic evidences suggest that blocking CDK4 might result in some putative therapeutic benefit depending on the tissue and the oncogenic insult. For example, overexpression of a *Cdk4* transgene in astrocytes does not result in brain tumors although these transgenic mice exhibit a small increase in astrocyte number, an effect even more evident in a *Trp53-null* background (Huang et al., 2002). In addition, *Cdk4* null mice show a lower incidence of epithelial tumor development driven by *Myc* (Miliani de Marval et al., 2004). Moreover, *CyclinD1* has been observed to be essential for the development of mammary tumors expressing ERBB2 however; mice lacking CYCLIND1 displays normal mammary development, suggesting that in a non-tumor context *CyclinD1* is dispensable for normal homeostasis (Yu et al., 2006) and thus the reason why CDK4 inhibitors have been successfully approved for the treatment of ER-positive breast cancer (Finn et al., 2016). Similarly, elimination of CDK4 protein induces significant inhibition of tumor progression in *Kras-driven* NSCLC (Puyol et al., 2010).

In general, one of the main pitfalls of these studies, is the fact that most of the mouse models described above were engineered by complete ablation of the protein. We must not forget that inhibitors target the kinase activity of the protein rather than preventing its expression. Therefore, generation of inducible conditional Kinase Dead (KD) strains to allow the study of catalytic inactivation would provide more predictable information in order to asses for therapeutic benefit.

2.6. Current strategies with CDK4/6 inhibitors

Nowadays, the use of CDK4/6 inhibitors, has only received the FDA approval for the treatment of hormone receptor positive (HR^+) Human Epidermal Growth Factor Receptor 2 negative ($HER2^-$) Metastatic Breast Cancer (MBC). It is thought that the high sensitivity of HR^+ compared with the HR^- is in part RB dependent, this means that most of the HR^- subgroup is RB^- too, diminishing the possibilities to benefit from this treatment (Finn et al., 2009). Although the initial steps in this field were given broadly treating with panCDK inhibitors such as Flavopiridol or Roscovitine (Asghar et al., 2015), the efforts are now focused in identifying inhibitors for specific CDKs. Therefore, from all these efforts three orally-available inhibitors were designed against CDK4/6: Palbociclib, Ribociclib and Abemaciclib after positive results from the PALOMA-1 (Finn et al., 2015) , MONALESSA-2 (Hortobagyi et al., 2016) and MONARCH-1 (Dickler et al., 2017) clinical trials respectively . More recently, G1T28/Trilaciclib, although not yet FDA-approved, a new CDK4/6 inhibitor intravenously administered was originally developed to preserve hematopoietic stem cells from DNA-damaging agents such as those widely utilized in chemotherapy (Bisi et al., 2017) due to the CDK4/6-hematopoietic related toxicities (Malumbres et al.,

2004). Regarding the FDA approved drugs, as mentioned before, Palbociclib was the first CDK4/6 inhibitor accepted to be combined with aromatase inhibitors (Corona and Generali, 2018; Finn et al., 2015). Although Abemaciclib, was the first inhibitor approved as a monotherapy (Dickler et al., 2017), Palbociclib and Ribociclib have also demonstrated efficacy in the treatment of $ER^{+/}$ $HER2^{-}$ MBC patients (Malorni et al., 2018). In terms of chemical structure, Palbociclib and Ribociclib are more similar than Abemaciclib, this could be the reason why Abemaciclib is the only one which penetrates the brain blood barrier (Raub et al., 2015). In addition, Abemaciclib is 14-fold more specific against CDK4 than the other two inhibitors (Corona and Generali, 2018) which may be a contributing factor to its antitumor activity as monotherapy although more studies are required to clarify this. However, even though Abemaciclib is more specific than the others against CDK4 and CDK6 kinases, still the three of them have toxicity-related issues to CDK4/6 inhibition. In fact, the dose-limiting toxicities (DLT) associated to these compounds are among others bone marrow suppression and haematological adverse events (O'Leary et al., 2016) as predicted by mouse model studies due to the strict requirement for CDK4/6 and D-type CYCLINs for proper hematopoiesis. In addition to the previous mentioned adverse events, Ribociclib also induces mucositis, asymptomatic thrombocytopenia, pulmonary embolism, increased creatinine and hyponatriemia as reported in phase I clinical trials (Knudsen et al., 2017).

Nevertheless, recently documented clinical data from these trials and preclinical research are supporting evidences of resistance development upon CDK4/6 inhibition (Pandey et al., 2019). There are several mechanisms by which a cell can escape CDK4/6 inhibition. For instance, (i) an increase activity of the target: CDK4 (Cen et al., 2012) or CDK6 (Gacche and Assaraf, 2018; Kollmann et al., 2013) amplifications; (ii) loss of *Rb* and as a consequence hyperactivation of other cell cycle machinery such as *Cdk2* or *CyclinE* (Herrera-Abreu et al., 2016); (iii) an increase in DCAFs, this is "D-cyclin activating features" which compress *CyclinD1* translocations, *CyclinD2* and *CyclinD3* amplifications, mutations in the 3' UTR of *CyclinD1-3*, etc. (Gong et al., 2017), (iv) loss of INK4 or CIP/KIP inhibitors which act as tumor suppressors have demonstrated to elicit resistance (Heilmann et al., 2014); (v) epigenetic modifications which leads to $p21^{Cip1}$ inactivation and therefore, cell cycle progression as well as inhibition of proapoptotic genes in a $p21^{Cip1}$-independent manner (Acevedo et al., 2016; Guler et al., 2017; Knoechel et al., 2014); (vi) transdifferentiation of cells from the epithelial to mesenchymal (EMT) status was reported to correlate with CDK4/6 inhibition via TGFβ-Smads activation in pancreatic cancer (Liu and Korc, 2012); (vii) immune mechanisms such as a decrease in cytotoxic T cell activation by DNMT expression (Goel et al., 2017); (viii) activation of alternative oncogenic pathways such as PI3K/AKT/mTOR. In fact, combined inactivation of CDK4 and PI3K targets induces complete tumor regression by decreasing CYCLIND1 levels (Herrera-Abreu et al., 2016; Romano et al., 2018).

One of the most challenging goals for the scientific community is to deeply understand the disparate mechanisms by which these cells develop resistance as well as to identify predictive biomarkers that may help to stratify responder and resistant patients. And not least, it is mandatory to find additional therapeutic targets to be combined with CDK4/6 inhibition in order to avoid or at least delay the appearance of resistance.

3. MAP kinase signaling pathway

3.1. Development of rational targeted therapeutic combinations: crosstalk between cell cycle and mitogenic signaling pathways

The complex network established by the CDK4/CYCLIND axis draw the attention over mitogenic signaling pathways since they could be potential candidates to raise synergism with CDK4 inactivation.

One of the main interactions is the RAS-RAF-MEK-ERK signaling pathway (Figure 5) which directly controls the transcription of CYCLIND (Marshall, 1999). Ideally, inhibition of CDK4 on the one hand, together with a reduction in CYCLIND levels by MAPK inhibition on the other, will end up in an important synergistic G1 arrest. In addition, RAF1 has been described to be involved in CDC25 phosphatase activation via *c-Myc* induction, this activates CDK2/CYCLINE facilitating the G1-S transition (Galaktionov et al., 1995). In fact, RAF1 inhibition has been described to downregulate CYCLINE and to induce G1 arrest in KRAS mutant lung cancer cell lines (Takezawa et al., 2009). In line with this, RAF1 modulates the cell cycle via Aurora Kinase A (AURKA) and Polo-Like Kinase 1 (PLK1) promoting mitotic entry (Mielgo et al., 2011). Finally, both proteins, CDK4 and RAF1 have been described to have a role in phosphorylating RB. Likewise, RAF1 is translocated to the nucleus and forms complexes with RB (where it has been suggested to have a role in priming the subsequent phosphorylation of RB by CDK4 (Wang et al., 1998; Zheng and Lee, 2001). Besides, it has been demonstrated that selected inhibition of the RB-RAF1 interactions with small molecules inhibits pancreatic adenocarcinoma (Treviño et al., 2013). It was also found that lung cancer patients had increased binding of RAF1 to RB (Dasgupta et al., 2006). So, the lack of RB phosphorylation in both kinases is suggesting a potentially additive/synergistic therapeutic effect in lung ADC. It is also known that upon activation of oncogenic RAF1 the levels of $p27^{Kip1}$ are downregulated (Kerkhoff and Rapp, 1997), one possible explanation being that ERK kinases are able to phosphorylate $p27^{Kip1}$, therefore $p27^{Kip1}$ cannot bind and inhibit CDK2 complexes at the same time as the number of CDK4/CYCLIND complexes are reduced due to its scaffolding role described above. Similarly, depending on the levels of RAF1 expression cell cycle arrest or proliferation can be induced. Only when RAF1 is expressed at very high levels $p21^{Cip1}$ is induced probably by increase oncogene stress, leading to cell cycle arrest, whereas, in normal conditions RAF1 is able to induce

CYCLIND expression and promote proliferation (Sewing et al., 1997). In the opposite situation where RAF/MEK/ERK pathway is inactivated (Rasless MEFs), *Trp53* becomes activated which in turn induces $p21^{Cip1}$ expression activating *Rb* and therefore preventing cells entering cell cycle (Drosten et al., 2014). Lastly, there are evidences of alternative MAPK pathway activation upon CDK silencing, allowing cells to bypass treatment efficacies. Upon breast cancer resistance, CDK10 becomes methylated which in turns induces RAF1 transcription via ETS2 transcription factor (Iorns et al., 2008), thus suggesting the idea that combined targeting of RAF1 and CDKs, by inhibiting two distinct effectors of two "vertical signaling pathways", may synergize in order to avoid resistance mechanisms.

Another CDK4/CYCLIND connector, is the PI3K-AKT-mTOR pathway (Figure 5) since it is well defined that PI3K/AKT signaling increases CYCLIND1 levels (Albers et al., 1993; Kerkhoff and Rapp, 1997). Therefore, inactivation of this pathway has shown therapeutic benefits in combination with CDK4/6 inhibitors in several preclinical models (Bonelli et al., 2017; Goel et al., 2016; Teo et al., 2017). Interestingly, the MAPK pathway also conveys into the PI3K pathway by inactivating the tumor suppressor TSC2 which is a negative regulator of mTOR (Ma et al., 2005). When TSC2 is phosphorylated, it degrades and activates the mTOR signaling pathway. Hence, inactivation of the MAPK pathway results in suppression of PS6 kinase, a downstream effector of mTOR signaling (Hirashita et al., 2016). However, it has been shown that AKT phosphorylates RAF1 on Ser^{259} (Zimmermann and Moelling, 1999) and that inhibition of MEK leads to rapid PI3K upregulation (Wee et al., 2009), therefore combining the inhibition of MEK and PI3K in NSCLC has demonstrated to be efficient (Zimmermann and Moelling, 1999). Although not inducing durable responses (Alagesan et al., 2015). However, translating these findings into the clinic has been hampered by modest efficacy and high toxicity when MEK and PI3K/AKT inhibitors, as seen in the BATTLE-2 trial. Interestingly, present studies are suggesting that combined inhibition of cell cycle-related pathways with either the MAP Kinase or PI3K/AKT/mTOR pathways will significantly improve the efficacy of the current treatments (Figure 5).

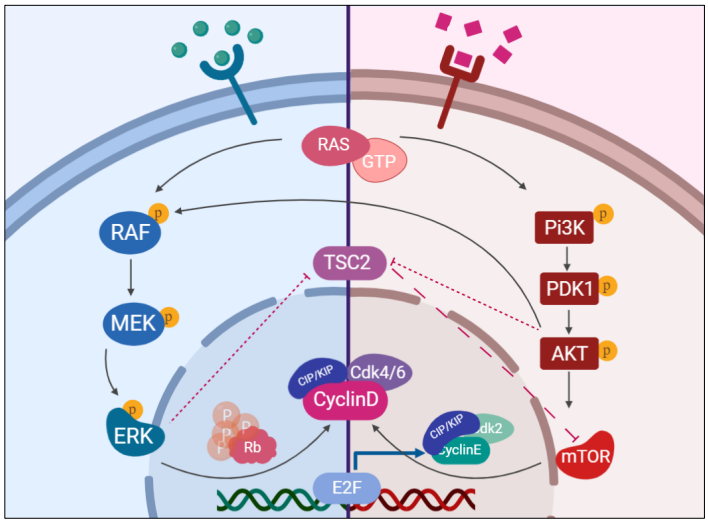

Figure 5: Illustration of the relationship between MAPK, PI3K/AKT/mTOR and cell cycle pathways.

*3.2. The Ras-Raf-*Mek-*Erk signaling regulation*

As depicted above, RAF1 serine/threonine kinase has an important role over cell cycle progression, in fact, it is mutated in 30% of all human cancers. There are three different mammalian *Raf* isoforms (A-RAF, B-RAF and C-RAF or RAF1) with high structural homology comprising three conserved regions (CR). CR1 contains elements necessary for RAS membrane recruitment (RAS binding domain, RBD) and stabilization of the Ras-Raf interaction (Cysteine-Rich Domain, CRD). CR2 is rich in inhibitory phosphorylation Ser/Thr sites which participate in the negative regulation of RAF activation. And the CR3 contains the catalytic domain of the protein, a Ser conserved residue that serves as a second binding site and a loop necessary for the activation of the RAFs proteins (Avruch et al., 2001). These three conserved regions are highly preserved from metazoans to mammals though only one RAF isoform is present in invertebrates such as *Drosophila melanogaster (D-Raf)* and *Caenorhabditis elegans (lin-45)* being more similar to the B-RAF isoform than to the other mammalian RAF kinases (Wellbrock et al., 2004) (Figure 6).

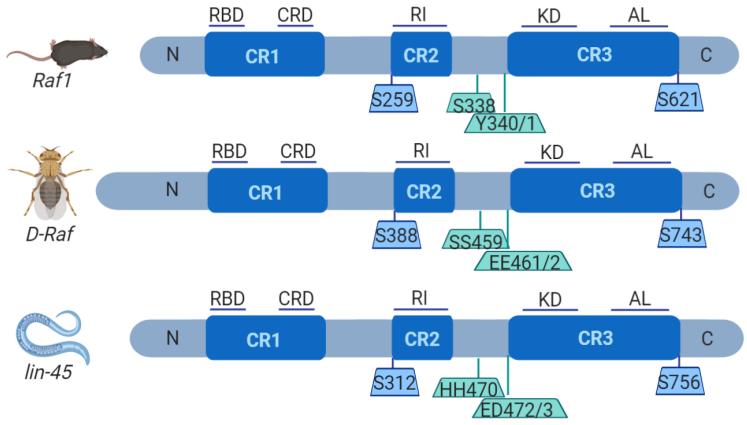

Figure 6: Illustration of RAF1 structure and its highly conserved homology with other organisms such as *Drosophila melanogaster* and *Caenorhabditis elegans*. Adapted from Wellbrock *et al.*, Nat Rev Mol Cell Bio, 2004.

In the absence of stimulation, RAF1 is maintained in a quiescent state bound to the 14-3-3 scaffold protein at RAF1 Ser^{259} (N-terminal domain) and Ser^{621} (C-terminal domain) phosphorylation sites. When a Receptor Tyrosine Kinase (RTK) ligand binds to the receptor on the cell surface, this interaction is disrupted so the RBD swaps RAS GDP for a GTP and displaces the 14-3-3 protein from RAF1 phosphorylated Ser^{259} (Avruch et al., 2001), targeting the RAF1 kinase to the plasma membrane. This enforces a conformational change yielding the N-terminal autoinhibitory domain for future interactions. Subsequently, RAF1 Ser^{338} and Y^{341} become phosphorylated to activate the Mitogen Activating Protein Kinases ($MEK_{1,2}$) which then in turn phosphorylates and activate the Extracellular Signal Regulated Kinases ($ERK_{1,2}$). These ERKs shuttle into the nucleus and induce the activity of more than hundreds of substrates (Avruch, 1998). Finally, phosphorylation made by ERK-feedback loop on RAF1 inhibitory sites renders RAF1 on its inactive form by dephosphorylating the Ser^{338} site and

phosphorylating the Ser^{259} residue again (Baccarini, 2005). Alternative mechanisms of RAF activation, independent of N-terminal phosphorylation, have been proposed by RAF homo and hetero dimerization (Rushworth et al., 2006).

3.3. Role of Raf1 in homeostasis: knock-out mouse models

Different mouse models of specific *Raf* isoforms have been developed in order to study the phenotype associated with the lack of the RAF1 protein in the mice (Hüser et al., 2001; Mikula et al., 2001; Wojnowski et al., 1998). Depending on the system used to ablate the protein and the genetic background of the animals, mice die from different stages of embryo development untill P0, furthermore, different tissues are affected such as liver, haematopoietic and neuronal organs. The first *Raf1* knock-out mouse described, showed a lethal phenotype at E10.5-E12.5 (Wojnowski et al., 1998) suggesting that until that stage, the rest of the *Raf* isoforms are able to compensate to some extent since all *Raf* isoforms are known to be required for maintaining normal embryogenesis and sustaining life (Leicht et al., 2007). The latter studies suggested the phenotype observed was due to the fact that RAF1 is neccesary to restrain apoptosis during embryogeneis (Hüser et al., 2001; Mikula et al., 2001). In common, all these models display defects in the liver and the placenta. The spongiotrophoblast of *Raf1* knock-out mice is smaller and less spongy than the wildtype litermates and the labirynth layer in the mutant mice is also smaller and less vascularized. All these data indicate that RAF1 kinase has important antiapoptotic functions.

In order to study if these effects are kinase independent specific RAF KD mouse models have been designed. A knock-in mutation in Y340F and Y341F ($Raf^{F/F}$), where the residues needed for RAF1 activation in the CR3 region have been changed to a phenylalanine, did not show a significant phenotype (Hüser et al., 2001). Although it was observed that there was no complete abolishment of the kinase activity suggesting the possibilty that some residual kinase activity could be enough to maintain normal homeostais in mice. For that reason, our laboratory (unpublished data) has developed two RAF1 KD models that are still under characterization: one mutating the ATP binding site (K375M) and the other mutating the proton aceptor (D468A) of the protein. Despite the fact that both models have impaired catalytic activity as demostrated by the lack of MEK1 phosphorylation, at least the $Raf1^{D468A}$ mutant model completes embryonic development in contrast to $Raf1^{-/-}$ mice (Wojnowski et al., 1998), indicating the presence of kinase independent functions associated to RAF1.

In all these studies either RAF1 ablation or RAF1 KD expression, ERK activation is unperturbed, indicating that MEK kinase activity of RAF1 is not essential for normal mouse development; in other

words, RAF1 antiapoptotic functions are MAPK independent (Baccarini, 2005; Hüser et al., 2001; Sanclemente et al., 2018; Takezawa et al., 2009).

3.4. Other RAF1 targets involved in programmed cell death, survival and differentiation

Nowadays, it is clear that there are other important RAF1 survival functions, apart from the accomplish by MEK1 and MEK2 effectors, independently of its kinase activity (Matallanas et al., 2011). As described above, RAF1 promotes cell survival as suggested by the fact that *Raf1*$^{-/-}$ is embryonic lethal due to an extense apoptosis in the liver and the placenta (Hüser et al., 2001; Mikula et al., 2001; Wojnowski et al., 1998). The ERK pathway restricts apoptosis by the expression of caspase inhibitors or the blockage of proapoptotic molecules such as BCL2 (Matallanas et al., 2011). Likewise, the work of Wang HG and collaborators demonstrated that RAF1 can be accumulated in the mitochondrial membrane via BCL2 and/or BAG1 (Bcl2-associated anthanogene-1) interaction where it can phosphorylate and inactivate BAD (Bcl2 associated death) proteins suppressing apoptosis (Wang et al., 1998; Wellbrock et al., 2004) (being the only kinase dependent function of RAF1 of the here-mention ones). It was then discovered that RAF1 serves as a scaffold to recruit PKC (protein kinase C-theta) and phosphorylate BAD (Hindley and Kolch, 2007). Another mechanism related to the damage of the mitochondria, is the capacity of RAF1 to suppress the releasing of the cytochrome C modifying the voltage-dependent anion channels (VDACs) thereby impeding cell death (Le Mellay et al., 2002). Moreover, RAF1 was found to directly interact with ASK1 (apoptosis signal-regulating kinase-1) inhibiting apoptosis (Chen et al., 2001). Likewise, it was demonstrated that RAF1 ablation induced apoptosis in cardiomyocytes via *p38* and JNK which are direct downstream effectors of ASK1 (Yamaguchi et al., 2004).

Similarly, RAF1-induced ROK-α inhibition allows the phosphorylation of STAT3 and MYC expression. Consequently, in skin tumors where RAF1 is depleted ROK-α becomes hyperactivated and subsequently its downstream effectors, such as COFILIN, become phosphorylated, increasing differentiation and inhibiting tumor growth (Ehrenreiter et al., 2009). A similar phenotype occurred in *Kras-driven* LUAD since phospho-COFILIN levels are increased upon RAF1 tumor ablation (Sanclemente et al., 2018). In *Raf1*$^{-/-}$ cells, ROK-α is found hyperactivated impeding the internalization of the FAS death receptor producing an accumulation of the receptor in the plasma membrane, therefore increasing the chances to become activated. In fact, genetically reducing FAS expression counteracts fetal liver apoptosis, embryonic lethality, and the apoptotic defects of embryonic fibroblasts found upon RAF1 ablation (Piazzolla et al., 2005). ROK-α hyperactivation also induces failure in migration of keratinocytes and fibroblast *in vitro* (Ehrenreiter et al., 2005).

The other proapoptotic kinase called MST2 (mammalian sterile 20-like kinases) which homologue in *Drosophila melanogaster* is *Hippo*, was also found hyperactivated in *Raf1*$^{-/-}$ cells (O'Neill and Kolch, 2005). MST2 specifically binds to the CR2 that is unique for RAF1, indicating that MST2 is an exclusive RAF1 target. RAF1 prevents MST2 homodimerization which is the active form of the kinase. In addition, RAF1 recruits the phosphatase in charge of dephosphorylating and inactivating MST2, preventing by a secondary mechanism its activation and consequently its apoptotic functions (O'Neill and Kolch, 2005). Expression of a RAF1 KD isoform has the same properties in impeding MST2 dimer formation therefore, indicating that its prosurvival function is independent of its kinase activity (Matallanas et al., 2011). Finally, in the absence of RAF1, FAS stimulation or RASSF1A expression causes the dimerization and activation of MST2, which contributes to the increased apoptosis observed in *Raf1*$^{-/-}$cells. When this happens a cascade that consists of MST2 - LASTS1 - YAP - p73 activation is initiated leading to the expression of the proapoptotic gene, *Puma* (Matallanas et al., 2007). By the inhibition of all these pro-apoptotic mechanisms, RAF1 reinforces the MAP Kinase proliferative signal, impeding the apoptotic machinery to become activated.

3.5. Role of Raf1 as an oncogene

The role of *Raf1* in mediating RAS-transformation was previously demonstrated by various works (Karreth et al., 2011; McFarlin and Gould, 2003). It was shown that *Raf1* cooperates with other oncogenes and negatively regulates tumor suppressors such as *Rb* in order to prompt cellular transformation (Wang et al., 1998). In the same line, a dominant negative form of RAF1 prevented transformation (Qureshi et al., 1993). Finally, there are studies that claim that RAF1 heterodimerization with B-RAF favors transformation due to an increase in the kinase activity (Rushworth et al., 2006). Although RAF1 was the first RAF isoform identified as a potential oncogene, there are not so many oncogenic mutations of *Raf1*. However, there is a family of syndromes caused by germline mutations in the RAS-MAPK pathway called “RASopathies” which include rare diseases such as Noonan Syndrome or Leopard Syndrome (Niihori et al., 2019). Nevertheless, overexpression of RAF1 protein is a more common event which correlated with early progression in NSCLC (Cekanova et al., 2007).

Nevertheless, the above-mentioned evident roles in cell cycle progression, survival and transformation shed light on RAF1 as a putative therapeutic target. In fact, knock-out models showed that elimination of both kinases ERK1/ERK2 or MEK1/MEK2, although efficiently block LUAD progression it is extremely toxic, inducing multi-organ failures being incompatible with adult life (Blasco et al., 2011). Surprisingly, RAF1 protein elimination completely prevented lung tumor development even in the presence of normal levels of expression of A-RAF and B-RAF in *Kras-driven* tumors (Blasco

et al., 2011; Cekanova et al., 2007; Karreth et al., 2011). Likewise, *Raf1* knock-out impairs skin tumor initiation and development via *Rok-α* (Ehrenreiter et al., 2009). In addition, ablation of RAF1 protein reduces already established *Kras-driven* LUAD via increased apoptosis (Sanclemente et al., 2018). Finally, RAF1 and EGFR concomitant elimination was recently demonstrated to induce complete regression of pancreatic ductal adenocarcinoma (Blasco et al., 2019).

Regarding the genetic validation, the main problem the scientific community faces, is that genetic ablation is by far more efficient than drug-mediated inhibition due to its high target specificity which is translated in none off-target secondary effects. In fact, there are ATP-competitive panRAF inhibitors which have been shown to unexpectedly reactivate the MAPK pathway by inducing a B-RAF-dependent paradoxical effect (Hatzivassiliou et al., 2010; Heidorn et al., 2010). In fact, Barbacid's laboratory also demonstrated that the expression of a catalytic inactive B-RAF mutant, D631, prompts lung tumor initiation and accelerates tumor progression via RAF1 heterodimerization when a wildtype B-RAF allele is still present (Nieto et al., 2017). This data raised attention for the risk of treating KRAS mutant, B-RAF wildtype patients with panRAF inhibitors, pointing out B-RAF mutant patients as putative responders to reach treatment efficacy underscoring the need for the development of selective RAF1 inhibitors in this set of patients.

Taking into account all these precedents, further research is required to identify novel targets for the treatment of KRAS mutant LUAD.

OBJECTIVES

Therapeutic intervention of RAS proteins in the clinic is not available yet due to recurrent unsuccessful attempts. However, given the prevalence of *KRAS* mutations in LUAD, around 30% of the cases, an urgent search for selective therapies against its downstream effectors had resulted in significant translational research in this field during the past years. Evidences of CDK4 and RAF1 as good therapeutic options for LUAD treatment came out from Barbacid's laboratory as well as others. Still, the lack of suitable mouse models that closely recapitulate a pharmacological treatment, raised the importance for the study of CDK4 catalytic inactive mutants that mimic ATP-competitive inhibitors. In addition, it is needed to discover effective and tolerable combinatory therapies for the treatment of *Kras*-driven lung cancer.

Hence the objectives of this thesis are the following:

1. Phenotypic characterization of mice expressing a CDK4 kinase inactive form.

2. Unveil the role of CDK4 catalytic inactivation in $Kras^{G12V}$-driven LUAD initiation and progression.

3. Study the effect of concomitant CDK4 and RAF1 inactivation as a therapeutic strategy for established $Kras^{G12V}$-driven LUAD.

MATERIALS AND METHODS

1. Mouse models:

1.1. Source of genetically engineered mouse models used in this work

The following lines were used for this study: $Kras^{+/LSLG12V}$ (Guerra et al., 2003), $Kras^{+/FSFG12V}$ (Sanclemente et al., 2018), $Cdk4^{-/-}$ (Rane et al., 1999), $Cdk4^{FlexK35M}$ and $Cdk4^{LmL140A}$ (unpublished), EIIa-Cre^{T} (Lakso et al., 1996), $Cdk4^{L}$ (Lagarrigue et al., 2016), $Raf1^{L}$ (Jesenberger et al., 2001), $Trp53^{F/F}$ (Lee et al., 2012) and *hUBC-CreERT2* (Ruzankina et al., 2007). By crossing the different mouse strains, we generated the compound genotypes used in this work.

1.2. Maintenance of mice

All mice used in this project were housed in the Animal Facility of the Spanish National Cancer Research Centre (CNIO) in accordance with the Federation of European Laboratory Animal Science Association (FELASA) recommendations and following European Union legislation. All experiments described in this thesis have been approved by the Ethical Committees of the Spanish National Cancer Research Centre (CNIO), the Carlos III Health Institute, and the Autonomous University Community of Madrid (PROEX 81/16) in accordance with the guidelines stated in the International Guiding Principles for Biomedical Research Involving Animals, developed by the Council for International Organizations of Medical Sciences (CIOMS). Mice were housed in specific-pathogen-free conditions at CNIO´s Animal Facility (AAALAC, JRS:dpR 001659). Female and male mice were used for the experiments.

1.3. Conditional CDK4 kinase inactive alleles

To inactivate the catalytic activity of CDK4 two strategies were followed: one mutating the ATP-binding site and other mutating the proton acceptor residue -in the HDR domain of the CDK4 protein- (unpublished data).

Both models were already generated at the beginning of this thesis, however the experimental design will be described as follows. For the first model, the ATP-binding site was mutated (substitution of a lysine in position 35 by a methionine). This K35M mutation has been demonstrated to eliminate the catalytic activity of the kinase (Kato et al., 1993). The mutation was then incorporated by homologous recombination into the endogenous *Cdk4* allele taking advantage of the Flex vector (Schnutgen et al., 2003). This system utilizes a combination of 4 loxP sites: 2 wildtype loxP sites and 2 mutated loxP sites (Figure 7). When the Cre recombinase is activated, it mediates the inversion of the sequence where the loxP sites are in opposing orientations which turns on the switch and then, it allows

for subsequent excision of the sequence between loxP sites in the same orientation, which eliminates one of the loxP partners to prevent re-inversion. This complex process allows the substitution of the wildtype exon 2 in *Cdk4* by an alternative sequence containing the K35M mutation, thereby inactivating its kinase activity in an inducible manner by Cre-mediated recombination (Figure 7).

In the second model, a cDNA so-called "minigene" expressing the wildtype *Cdk4*, from exons 2-8, was inserted within intron 1 of the endogenous *Cdk4* locus while simultaneously introducing in the exon 4 the **D140A** mutation (substitution of the aspartic acid in position 140 by an alanine) into the endogenous locus. This *Cdk4*^{LmLD140A} construct included the endogenous splicing acceptor to facilitate the expression of the wildtype *Cdk4* cDNA and a stop cassette to prevent transcription read-through into the mutant allele. Cre-mediated recombination of the *Cdk4*^{LmLD140A} allele would excise the entire cassette allowing the constitutive expression of the *Cdk4*^{D140A} KD isoform from the endogenous *Cdk4* promoter. This strategy has been successfully used for targeting other kinases (Dankort et al., 2007) (Figure 7).

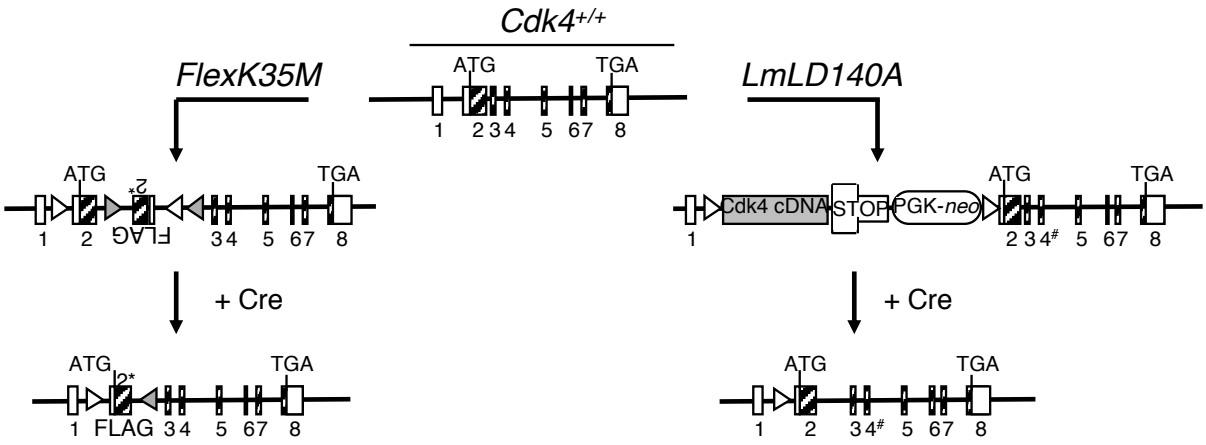

Figure 7: Schematic representation of the Cdk4^{FlexK35M} and Cdk4^{LmLD140A} alleles and their modification following Cre-mediated recombination. Exons (boxes), wildtype loxP sites (white triangles), mutated loxP sites (grey triangles), minigene (cDNA), from exon 2 to 8, Neomycin resistance cassette gene (Neo) and transcriptional Stop cassette (STOP) are depicted. The modified exons 2 or 4 encoding for the K35M and D140A mutations respectively are indicated (* or #).

To characterize the effect of the constitutive expression of two different catalytic CDK4 inactive forms, mice carrying either the *Cdk4*$^{+/FlexK35M}$ or *Cdk4*$^{+/LmLD140A}$ alleles were crossed with mice carrying the *EIIa-Cre*^{T} transgene. In these mice, the Cre recombinase is controlled by the *EIIa* promoter which is expressed from the very early stage embryos, including germ cells. Therefore, recombination happens in these cells allowing the mutations to be transmitted to the progeny (*Cdk4*$^{+/K35M}$ or *Cdk4*$^{+/D140A}$). Later, the pups were crossed with C57BL/6 mice in order to remove the *EIIa-Cre* transgene. Finally, crosses between heterozygous were set up to generate *Cdk4*$^{K35M/K35M}$ and *Cdk4*$^{D140A/D140A}$ compound strains.

1.4. Lung cancer Tumor Initiation model

To study the role of CDK4 catalytic inactivation in the initiation of *Kras-driven* LUAD, the KD alleles expressed in the germline were crossed with an inducible knock-in for *Kras*^{LSLG12V} (Guerra et al., 2003). In addition, *Cdk4* knock-out strain (*Cdk4*$^{-/-}$) was included in order to compare with the effect of CDK4 complete protein elimination (Puyol et al., 2010). The compound strains generated were the following:

Kras$^{+/LSLG12V}$;*Cdk4*$^{+/+}$,

Kras$^{+/LSLG12V}$;*Cdk4*$^{-/-}$,

Kras$^{+/LSLG12V}$;*Cdk4*$^{K35M/K35M}$,

Kras$^{+/LSLG12V}$;*Cdk4*$^{D140A/D140A}$.

This *Kras*^{LSLG12V} allele contains a lox-STOP-lox (LSL) cassette in order to prevent the expression of the mutant allele. However, upon the expression of the Cre recombinase by adenovirus instillation (codified in adeno viruses, AdCre), the STOP element is removed and the mutant version of the oncogene is expressed. Hence, inducing adenomas and adenocarcinomas specifically in the lung (*Tumor Initiation Model*, henceforth). The main disadvantage of this study is that it only allows for the study of CDK4 inactivation during the initiation events of *Kras* lung transformation, since the protein is inactivated from the germline before the oncogenic event happens (Figure 8).

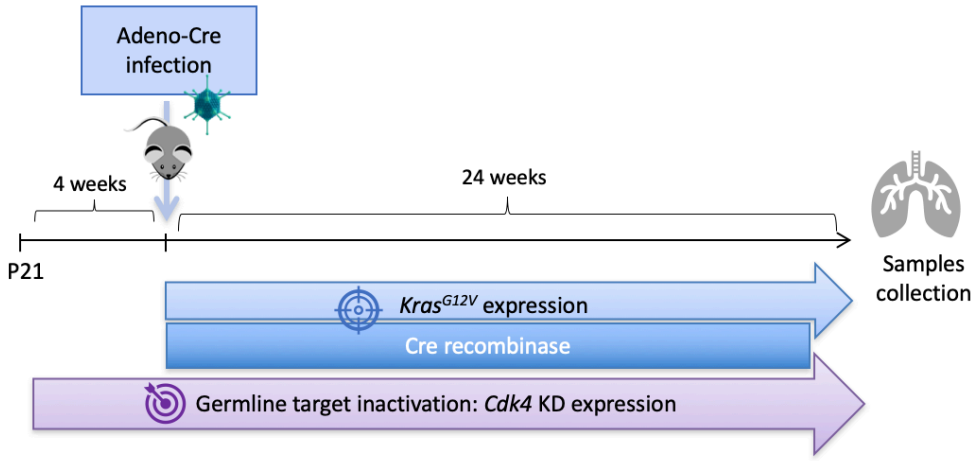

Figure 8: Schematic representation of Tumor Initiation protocol

1.5. Lung cancer Therapeutic model

In order to spatially and temporally separate the activation of the *Kras* oncogene together with and without the *Trp53* tumor suppressor from target inactivation, a dual recombinase system was used in this work. Compound strains were generated:

Kras$^{+/FSFG12V}$;*hUBC-CreERT2*$^{+/T}$,

Kras$^{+/FSFG12V}$;*Cdk4*$^{FlexK35M/L}$;*hUBC-CreERT2*$^{+/T}$,

Kras$^{+/FSFG12V}$;*Raf1*$^{L/L}$;*hUBC-CreERT2*$^{+/T}$,

Kras$^{+/FSFG12V}$;*Cdk4*$^{FlexK35M /L}$;*Raf1*$^{L/L}$;*hUBC-CreERT2*$^{+/T}$

Kras$^{+/FSFG12V}$;*Trp53*$^{F/F}$;*hUBC-CreERT2*$^{+/T}$, (henceforth: *Cdk4*$^{+/+}$;*Raf1*$^{+/+}$)

Kras$^{+/FSFG12V}$;*Trp53*$^{F/F}$;*Cdk4*$^{FlexK35M/L}$;*hUBC-CreERT2*$^{+/T}$, (henceforth: *Cdk4*$^{K35M/L}$)

Kras$^{+/FSFG12V}$;*Trp53*$^{F/F}$;*Raf1*$^{L/L}$;*hUBC-CreERT2*$^{+/T}$, (henceforth: *Raf1*$^{L/L}$)

Kras$^{+/FSFG12V}$;*Trp53*$^{F/F}$;*Cdk4* $^{FlexK35M/L}$;*Raf1*$^{L/L}$;*hUBC-CreERT2*$^{+/T}$, (henceforth: *Cdk4*$^{K35M/L}$;*Raf1*$^{L/L}$)

When the Flp recombinase (codified in adeno viruses, AdFlp) recognizes a pair of Flp recombinase target sequences (FRT sites) in the *Kras* ^{FSFG12V} locus it allows the expression of the resident *Kras*^{G12V} oncogene. FRT sites are also flanking the *Trp53* gene. Therefore, upon activation of the Flp-mediated recombination *Trp53* function is abolished. Once tumors have been developed and detected by CT, tamoxifen diet is given to the mice in order to induce the activity of the modified CreERT2-recombinase (tamoxifen inducible Cre-Estrogen Receptor (ER) fusion protein expressed from the transgene *Tg.hUBC-CreERT2*$^{+/T}$). Tamoxifen allows for the CreERT2 enzyme to translocate to the nucleus to achieve target deletion/inactivation of floxed alleles ubiquitously. This model allows the study of CDK4 and/or RAF1 inactivation once the tumors are already established, mimicking a therapeutic intervention in the patients (*Therapeutic Model*, henceforth) (Figure 9).

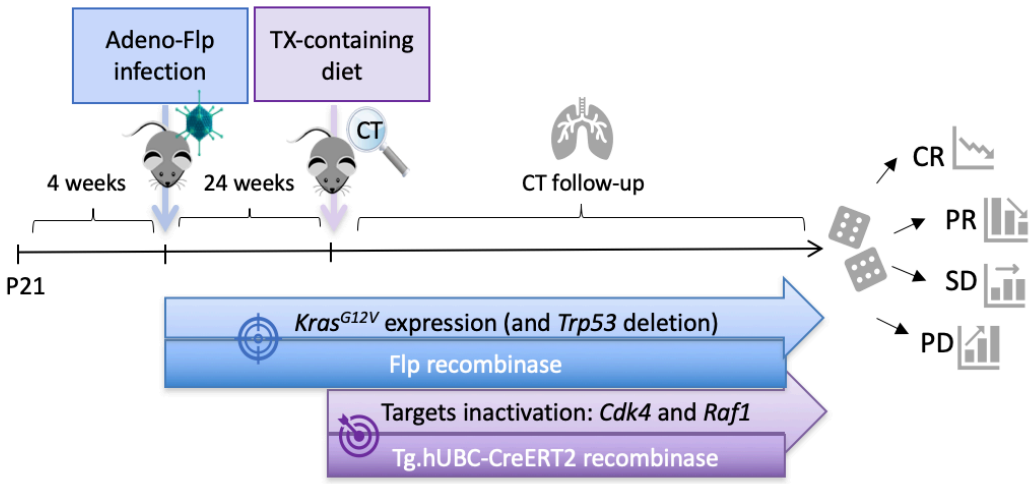

Figure 9: Schematic representation of *Therapeutic* protocol. CT: Computed-Tomography; CR: Complete Response; PR: Partial Response; SD: Stable Disease; PD: Progression Disease.

2. *In vivo* procedures

2.1. Body weight and blood glucose levels measurements

Body weight and glucose levels were measured every month during one year. For blood sampling, 1-2 mm incision in the tail with a scalpel is done, then blood is obtained by direct flow and collected in a capillary. Males are considered hyperglycemic over 180 mg/dl whereas females they are considered hyperglycemic over 160 mg/dl.

2.2. Lung tumor induction and tamoxifen exposure

Induction of LUADs was carried out in anesthetized 8-week-old mice (i.p. injection of: ketamine 75mg/kg, (Imalgene); xylacine 12mg/kg, (Rompun)). Then, AdCre (10^8pfu/mouse) or AdFlp (10^6pfu/mouse) were used to deliver transient Cre or Flp recombinase expression respectively to the lung in order to activate either the *Kras* oncogene (*Kras*^{LSLG12V}; *Kras*^{FSFG12V}), to deplete the tumor suppressor *Trp53* (*Trp53*$^{F/F}$) or inhibit the targets of interest (*Cdk4*$^{FlexK35M/L}$; *Raf1*$^{L/L}$). Viruses were administered dropwise by intranasal instillation into one nostril until the virus is completely inhaled. A final volume of 60 µl of viruses diluted in PBS was used per mouse. All the adenoviral preparations were purchased from Iowa University (Iowa City, USA).

2.3. Computed-tomography analysis: CT imaging

Image studies were done by the Molecular Imaging Core Unit at CNIO. Mice were anesthetized with a continuous flow of 1% isoflurane / 3% oxygen mixture (0.5 L/min) and the chest area was imaged by three-dimensional microcomputed tomography performed with a CompaCT scanner (SEDECAL Madrid SpainGE). Data were acquired with 720 projections by 360-degree scan, integration time of 100 ms with three frames, photon energy of 50 KeV, and current of 100 µA. Tumor measurements were obtained with the GE MicroView software v2.2. Tumor volume was calculated as follows: short axis x short axis x long axis /2.

2.4. Schedule of tamoxifen diet administration

Once mice were considered to have a detectable tumor by CT, activation of the inducible CreERT2 recombinase encoded by the *hUBC-CreERT2* transgene was carried out by feeding the mice with Teklad CRD Tam^{400}/CreER (Harlan) tamoxifen containing diet *ad libitum* (henceforth TX). Tamoxifen

is hydroxylated in the mouse liver into 4-Hydroxytamoxifen (4-OHT), the active metabolite of tamoxifen. After two weeks of tamoxifen diet a transition diet (2919S, Teklad) specially designed to support growth of rodents, was given during one week every three weeks in order to avoid excessive weight loss of mice. This diet, is formulated excluding soybean, thus minimizing the presence of isoflavones, the primary type of phytoestrogen.

2.5. Tail vein injection of cells in immunodeficient mice

A 10^6 suspension of cells diluted in PBS in a final volume of 100 µl was injected into the lateral tail vein of immunodeficient Foxn1$^{nu/nu}$ mice. Mice were sacrificed at humane end point and lung tissue analyzed.

2.6. Subcutaneous injection in immunodeficient mice and pharmacological treatments

A 2.5 x 10^4 suspension of cells diluted 1:1 PBS: Matrigel (Corning, 354234) in a final volume of 100 µl/each flank was injected into immunodeficient Foxn1$^{nu/nu}$ nude mice.

Once the tumor reached 100 mm^3 size as determined by caliper measurements, mice were treated with either 5-Azacytidine (QD 6mg/kg, IP) or CNIO-PI3Ki (QD 15mg/kg, PO). A minimum of 8 tumors/group were followed-up and tumor measurements were performed every 3 days during 21 days. Tumor growth over 1200 mm^3 was considered Humane Endpoint criteria.

2.7. Pharmacological treatment in GEMM

Kras$^{+/G12V}$;*Trp53*$^{F/F}$; *Raf1*$^{L/L}$;h*UBC-CreERT2*$^{+/T}$ and *Kras*$^{+/G12V}$;*Trp53*$^{F/F}$ mice were infected with 10^6 pfu of AdCre. Once tumors were detected by CT measurements mice harboring at least one tumor bigger than 3 mm^3 were enrolled in the different treatment groups. Abemaciclib was dosed at 50mg/kg QD (in combination) for 4 weeks, panRAF inhibitor was dosed at 20mg/kg BID for 4 weeks as single agent and at 20mg/kg QD for 4 weeks in combination with Abemaciclib 50mg/kg QD for 4 weeks. Drug efficacy was monitored by CT measurements.

In order to validate CDK4/RAF1 resistance mechanisms, RT1-2 and RT4-5 and their respective control cells harboring *Cdk4/Raf1* wildtype alleles, were subcutaneously implanted in immunodeficient Foxn1$^{nu/nu}$ nude mice. Once the tumor reached 100 mm^3 size, mice were treated with either 5-Azacytidine (QD 6mg/kg, IP) / vehicle (QD, IP) or CNIO-PI3K (QD 15mg/kg, oral gavage) / vehicle (QD, oral gavage). A minimum of 8 tumors/group were followed-up and tumor measurements were

performed every 3 days during 21 days. Tumor growth over 1500 mm^3, hunchback position or body weight loss above 20% after tumor implantation were considered Endpoint criteria.

2.8. Skin tumor promotion

Tumors were generated following the protocol of Rodriguez-Puebla's laboratory (Rodríguez-Puebla, 2002). Tumors were initiated with a single dose of 200 nmol of DMBA (7,12-dimethyl-benzanthracene) (Sigma Chemical Co., St. Louis, MO) topically applied on the shaved dorsal skin. Two weeks later, tumor growth was promoted by applying 2 μg of TPA (12-*O*- tetradecanoylphorbol-13-acetate) (Sigma Chemical Co.) twice a week for 14 weeks on the dorsal skin. Mice were observed daily. Following this protocol, papillomas appeared after 6 to 7 weeks of continuous TPA treatment. Follow-up was performed weekly for 14 weeks.

3. Processing of mouse tissues

3.1. Histopathology, immunohistochemistry and quantifications

Tissues were dissected during necropsy, fixed in 10% formalin and embedded in paraffin for immunohistochemistry analysis or introduced in Optimal Cutting Temperature Compound (OCT) and frozen at -80ºC for X-Gal staining. Then, 4 or 10 μm thick sections were cut using a microtome or a cryostat respectively. For biochemical analysis samples were frozen in 2-methylbutane embedded in dry ice reaching temperatures of -80ºC instantaneously. Embryos were extracted from the uterus of the mother at different time points: E13.5 and E18.5, fixed in 10% formalin and embedded in paraffin.

Tumors were stained with a hematoxylin and eosin (H&E), counted and classified according to standard histopathological grading discriminating between benign (adenoma) and malignant (adenocarcinoma) tumors. Tumor grading (stage II to V) was determined as previously described (Jackson et al., 2005). The list of antibodies used is described below. Immune-stained tissue slides were scanned using AxioScan Z1 scanner (Zeiss) and photos were exported and quantified using the Zen Lite software (Zeiss).

ANTIBODY	CONCETRATION	SOURCE	IDENTIFIER
Primary Antibodies			
CD3e (M-20)	1/250	Santa Cruz	sc-1127
CD4 (D7D2Z)	1/200	Cell Signalling	25229
CD8a (94A)	1/200	CNIO's Monoclonal Antobody Unit	AM (OTO94A)
CD8-Granzyme B (D6E9W)	1/200	Cell Signalling	46890
F4/80 (CI:A3-1)	1/50	ABD Serotec	MCA497
Ki-67 (D3B5)	1/50	Cell Signalling	12202
C3 Cleaved Caspase-3 (Asp175)	1/300	Cell Signalling	9661

Table 2: Antibodies used for immunohistochemistry

4. Genotyping

4.1. DNA isolation and mice genotyping

Mouse genotyping was performed by the Genomics Unit core facility (CNIO). Genomic DNA from tail clips of mice at weaning was extracted according to Truett et al. (Truett et al., 2000). Genotyping was performed by real-time quantitative polymerase chain reaction (qPCR) with fluorescent reporter-quencher custom probes. Table 3 lists the oligonucleotides used for the different genotypes. Oligonucleotides were purchased from IDT. Every reaction contained primers and differently labeled probes to amplify and interrogate two alleles from the same locus, wt (wildtype) and mutant. PerfeCTa qPCR ToughMix (QuantaBio) was combined under recommended conditions with both DNA extract and corresponding oligonucleotides, and assayed for 40 cycles in a CFX384 qPCR instrument (BioRad) with an annealing temperature of 60º. Variants were assigned after allelic discrimination analysis by the Bio-Rad CFX Maestro software.

4.2. Laser capture microdissection (LCM) for tumors genotyping and recombined allele abundance estimation

When tumors were too small to perform biochemical analysis to check for target excision cells were laser capture microdissected (LCM). Approximately 10,000 cells were obtained by LCM using a PALM microbeam Zeiss Axio Observer (Carls Zeiss) from 4µm thickness paraffin sections. DNA was isolated from captured samples by resuspending in 25 µl of lysis buffer (1x Taq Platinum Buffer supplemented with both 1% Tx 100 and 5 mg/ml of proteinase K dissolved in 1mM $CaCl_2$. Samples were incubated overnight at 55ºC shaking in a thermomixer (Eppendorf) at 750 rpm. Next day, samples were boiled at 95ºC for 10 min to inactivate the proteinase K.

A semiquantitative genotyping was performed using a nested PCR. This PCR contains each locus-specific primer needed to simultaneously detect every putative variant: wt-wildtype, KI/Lox-conditional and Del-excised (Table 3). For the second qPCR, first PCR products were diluted 1:20 in water and used as a 5x stock. This qPCR was prepared as described above with the only exception that primers and probes were added to address three alleles instead of two (Table 3). Both first PCR and genotyping reactions were performed by triplicate. Results were analyzed with the CFX Maestro Software (BioRad). Firstly, thresholds are separately set for each fluorophore channel, in such a way that they lie above their respective general noise, but below the amplification curves' plateau. In order to compare signals among channels, and extract relative allele frequencies, the three thresholds -one per channel- need to be taken to the same consensus value within their range.

The following operations are done for every sample separately. The cycle number where its amplification curves cross the common threshold (Cq as determined in "single threshold" mode) is taken, and used to estimate allele frequencies. Cq values for both KI/lox and Del alleles are averaged among sample replicates, and these two averages are subtracted from one another. The absolute value of this resulting delta Cq is used to estimate corresponding fold differences between alleles KI/Lox and Excised in the sample. For that purpose, 1.8 (a base of 2 represents a perfect doubling efficiency per cycle) is raised to the absolute delta Cq.

Kras^{LSLG12V} & *Kras^{FSFG12V}*	Sequence (5' -> 3')	Allele specificity	Function
Kras:F_11E04	GGCCTGCTGAAAATGACT	wt, KI	Fw primer
Kras:R_11E06	GTGATTCTGAATTAGCTGTATCG	wt, KI	Rev primer
KrasG12V:S_11E08	Hex-TACGCCACCAGCTCCA-IowaBlack	wt	probe
KrasG12V:S_11E07	Fam-CTACGCCTACAGCTCCAA-IowaBlack	KI	probe
Trp53^{FRT}			
Trp53-com:F_20F15	GTGACCATCGAGACAGATGA	wt, frt	Fw primer
Trp53-com:R_10F16	ATTCACTTGTGTGTAGAACAATCAAGT	wt, frt	Rev primer
Trp53-wt:S_20F17	Hex-AGCCCATATGGAAAGGTTTC-IowaBlack	wt	probe
Trp53-frt:S_33F17	Fam-AAAGTATAGGAACTTCTATGGAAAGGTTT-IowaBlack	frt	probe
hUBC-CreERT2			
Ndor1-com:F_29F13	CTTTCAGGATGTTCGGCTGA	wt, T	Fw primer
Ndor1-com:R_29F14	TGACCACATCAGCTTCCTAG	wt	Rev primer
HFUW_29F15	TGTCTTGAGTGCTTCAAGTAGT	T	Rev primer
Ndor1-wt:S_29F16	Hex-CCAAGCTCTCAGGCAGTCAG-IowaBlack	wt	probe
HFUW:S_29F17	Fam-CTAGTTACCAGAGTCACACAACAGA-IowaBlack	T	probe
Cdk4^{K35M}			
Cdk4K35M-wt:F_24F03	TTGAACATCCCAATGTTGTACG	wt, del	Fw primer(*)
Cdk4K35M-KI:F_24F04	GGAACTCCTGCACAAGGT	KI	Fw primer(*)
Cdk4K35M-com:R_16F18	CAGACATCCATCAGCCTGA	wt, KI	Rev primer(*)
Cdk4K35M-wt:F_16F16	GGTGGAGAGGACAATAGGAC	wt, del	Fw primer
Cdk4K35M-KI:F_16F15	AAACGCTAGTGAGCTCGA	KI	Fw primer
Cdk4K35M-com:R_16F17	GAACAAATGATCACCAGCTAGTC	wt, KI, del	Rev primer
Cdk4K35M-wt:S_16F19	Hex-TCCCCTTTGTCTCAACGTG-IowaBlack	wt	probe
Cdk4K35M-KI:S_16F20	Fam-CGGATCCATCGACCCATAACTT-IowaBlack	KI	probe
Cdk4K35M-e2D:S_25F12(*)	Cy5/Fam-CGTTGAGGATCTTCTAGAGCTTATAA-IowaBlack	del	probe
Cdk4^{lox}			
Cdk4-com:F_28F08	TGCTCTTAGCTGCTGAGC	wt, lox	Fw primer(*)
Cdk4-com:F_16F09	GCCATCTCTCCAGTCCTGTA	wt, lox	Fw primer
Cdk4F_28F01	GAGCGTAAGGTGAGTGCA	del	Fw primer(*)

Cdk4:F_28F02	GCAGTCTCATCCAGGATCG	del	Fw primer
Cdk4R_28F03	GCCTTCCATCTCATTGGAGAC	wt, lox, del	Fw primer(*)
Cdk4-wt:R_16F10	ACTCTGTCAGCGCTGTATTAC	wt, del	Rev primer
Cdk4-lox:R_16F11	GTTATATTATGTACCGAAGTTCCTATACT	lox	Rev primer
Cdk4-wt:S_16F12	Hex-ATCTCGCCCCGAGTGG-IowaBlack	wt	probe
Cdk4-lox:S_16F13	Fam-ATCGAATTCCGAAGTTCCTATTCTC-IowaBlack	lox	probe
Cdk4-del:S_34F06(*)	Cy5/Fam-CCGCATTCTGGTACCAGGGC-IowaBlack	del	probe
Cdk4^{D140A}			
Cdk4D140A-com:F_17F02	TGTGCCTAGTGCGATGTC	wt, KI, del	Fw primer(*)
Cdk4D140A-com:R_31F10	TCCTGTACAAGACCTCGC	wt, KI, del	Rev primer(*)
Cdk4D140A-com:F_31F09	GGAGGGTTTGATGGGAGTCTT	wt, KI, del	Fw primer
Cdk4D140A-com:R_17F03	CAACGCGATCAGCAACATC	wt, KI, del	Rev primer
Cdk4D140A-wt:S_17F04	Hex-CGCCTTAGGTAACACAAAGAC-IowaBlack	wt	probe
Cdk4D140A-e1D:S_17F05	Fam-CCCTTTAGTGAGGGTTAATTAAGC-IowaBlack	KI	probe
Cdk4D140A-KI:S_17F06	Cy5-CGCCTTAGGTATAACTTCGTATAG-Tao-IowaBlack	del	probe
Raf1^{lox}			
Raf1:F_32B09	CTGATTGCCCAACTGCCATAA	wt, lox	Fw primer(*)
Raf1:F_32B08	CACGATGCATGTAACCTGTGT	del	Fw primer(*)
Raf1-com:F_15F02	AGACATCCAGAGACAGGCA	wt, lox	Fw primer
Raf1:F_28F14	CTTGGATCCACTAGTTCTAGAGC	del	Fw primer
Raf1:R_33B01	ACTGATCTGGAGCACAGCAAT	wt, lox, del	Rev primer(*)
Raf1-wt:R_15F03'	CAGCAGTTAGGTAAGCAGGC	wt, lox, del	Rev primer
Raf1-wt:S_15F05	Hex-TCCCTGAAGCTTGCTGG-IowaBlack	wt	probe
Raf1-lox:S_15F06	Fam-AGCTCTGCAGATAACTTCGT-IowaBlack	lox	probe
Raf1:S_28F15(*)	Cy5/Fam-TAGACTCGAGGAATTCCGATCATA-IowaBlack	del	probe

Table 3. Oligonucleotides used for sample genotyping.
Primers and probes were combined as appropriate to interrogate the desired alleles. Semiquantitative genotyping of LCM samples employed separate primer sets for their first PCR (tagged with (*) in column "function").

5. Baculovirus expression system: Kinase Assay

5.1. Kinase Dead (KD) Isoform cloning into pFASTBac plasmid:

Wildtype (WT), mutant forms of CDK4 (from vectors pBABE-CDK4^{WT}, pBABE-CDK4^{K35M} and pBABE-CDK4^{D140A}) and CYCLIND1 (from vector pBABE-CYCLIND1) were subcloned into pFASTBac HT plasmids (Invitrogen), which contain a strong polyhedrin promoter

for driving protein expression tagged with an N-terminal 6xHis-tag for purification of recombinant fusion proteins (Polayes et al.,1996). To do so, first the pBABE-CDK4 plasmids were digested with BamHI/EcoRI and gel extracted. Same way, the pFASTBac was digested with the same enzymes and

then gel purified. Ligation using a molar ratio 1:5 vector to insert was carried out with 0.5 µl of T4 DNA ligase (New England Biolabs) and 1X Ligase buffer (Biolabs) in a 10-µl reaction. The ligation mixture was then transformed into *E. coli* DH5α strain and plated in Luria-Bertani (LB) agar plates containing 100 µg/mL ampicillin. 10 transformants were picked and cultured overnight (ON) in LB media with 100 µg/mL ampicillin. Next day, plasmid DNA was isolated using the Gen Jet Plasmid miniprep Kit (Thermo Scientific). To further confirm the correct insertion and orientation (in frame with the N-terminal tag) of the insert into the plasmid, restriction enzyme digestion analysis was performed. Once the right clones were identified a glycerol stock was made for long-term storage according to the normal procedures (Figure 10).

5.2. Generation recombinant bacmid DNA

Once the pFASTBac-derived recombinant baculovirus transfer vector was generated, the purified plasmid DNA was transformed into the E. coli DH10Bac (Invitrogen) strain where transposition occurs. DH10Bac cells contain a baculovirus shuttle vector (bacmid) with a mini-*att*Tn7 target site and a helper plasmid which provides the Tn7 transposition functions. Transposition takes place between the mini-Tn7 element on the recombinant pFASTBac vector and the mini-*att*Tn7 target site on the bacmid to generate the recombinant bacmid. Chemically competent DH10Bac cells were transformed with 1 ng of each recombinant transfer plasmid according to the Bac-To-Bac manual instructions. LB agar plates containing 50 µg/mL kanamycin, 7 µg/mL gentamicin, 10 µg/mL tetracycline, 300 µg/mL Blue-gal, and 40 µg/mL IPTG were used to select for positive DH10Bac transformants. Plates were incubated 48h at 37°C. Insertions of the mini-Tn7 into the mini-*att*Tn7 attachment site on the bacmid disrupts the expression of the LacZα peptide, so colonies containing the recombinant bacmid are white in a background of blue colonies that harbor the unaltered bacmid. Single white colonies (3-4) were inoculated into LB medium containing 50 µg/mL kanamycin, 7 µg/mL gentamicin and 10 µg/mL tetracycline. DNA isolation of the recombinant bacmid was performed using standard methods. Then, analysis of the recombinant bacmid to verify successful transposition to the bacmid was done by PCR. Combinations of oligos targeting the vector DNA flanking the insert, pUC/M13 forward (5′-CCCAGTCACGACGTTGTAAAACG-3′) and pUC/M13 reverse (5′-AGCGGATAACAATTTCACACAGG-3′), and specific for the *Cdk4* gene (BamHICDK4-5′(5′-GATCGGATCCATGGCTGCCACTCGATATGAAC-3′) and CDK4EcoRI-3′ (5′-GATCGAATTCTCACTCTGCGTCGCTTTCCTCCTTG-3′) or for the *CyclinD1* gene (BamHICycD1-5′ (5′ GATCGGATCCATGGAACACCAGCTCCTGTGCTGCG-3′) and CycD1EcoRI-3′ (GATCGAATTCTCAGATGTCCACATCTCGCACGTCGGTG-3′) primers were used. Each reaction contained: 1 µl of recombinant bacmid DNA (100ng), 1.5 µl MgCl2 (50mM), 5 µl 10X PCR Buffer, 1 µl dNTPs

(10mM), 0.5 µl Taq-Platinum (5 units/µl, Thermo Fisher), 2.5µl of each of the primers (10µM, Sigma), and up to 50 µl of milli-q H2O. The length of the amplified fragments was assessed by 2% agarose gel electrophoresis and the expected band sizes were 300 bp for the bacmid alone and 2300 bp when the bacmid is transposed + 300 bp of the insert (Figure 10).

5.3. Transfection of the recombinant baculovirus DNA into insect cells.

Insect cells were transfected to generate the recombinant baculoviruses. *Sf9* insect cells were culture in Grace's Insect Medium (Gibco) containing 5% FBS (Gibco), 0.1% Pluronic™ F-68 (Gibco) and 10 µg/ml Gentamycin (Gibco). Cells should be on the log phase (0.5-1.5 × 10^6 cells/mL) with greater than 95% viability prior to the transfection. 1.5 x 10^6 cells were seeded in complete Grace's Insect Medium in p25 flasks. After 2 hours, when the cells were attached, transfection was performed as follows: for each transfection sample 6 µl of Cellfectin® II (Thermo Fisher), a cationic lipid which confers high transfection efficiencies, was diluted in 94 µl of Grace's Insect Medium (without antibiotics, additives and serum). In parallel, 10 µl of the corresponding recombinant bacmid were diluted in 90 µl of Grace's Insect Medium (without antibiotics and serum). Later, both mixtures were combined and incubated for 30 min at Room Temperature. The DNA-lipid mixture was added dropwise onto the Sf9 cells, previously washed with 10 ml of unsupplemented Grace's Insect Medium as the proteins in the FBS may interfere with the Cellfectin® II Reagent, followed by an incubation of 5h at 27ºC. Then, transfection medium was replaced with 5 mL of Grace's Insect Medium containing 5% FBS and cells were incubated at 27ºC for 5 days or until signs of viral infection appeared (increased cell diameter and nuclei size, granular appearance, detachment and finally cell lysis). Finally, the culture was harvested, centrifuged at 3000 rpm for 5 min and the supernatant (P1 viral stock) was collected, and kept at 4ºC, protected from light before being used. In order to increase the titer of the viral stock, Sf9 cells were used again to generate a high-titer P2 viral stock scaling the previous procedure to bigger amounts (250 ml culture). Titers of viral stock was determined by plaque assay. Briefly, 1.5x10^6 Sf9 cells in 35-mm dishes were infected with virus stock serially diluted in complete Grace's Insect Medium, at a range of 10^{-2} to 10^{-7}. An 1% low-melting point agarose (SeaPlaque GTG Agarose, Lonza) overlay in complete Grace's Insect Medium was applied to the plates after infecting the monolayers with the corresponding diluted virus for 1 hour. Plates were incubated for 3 days at 27ºC and stained with 50 µg/m neutral red (Sigma) overnight at 27ºC before counting. Neutral red will stain healthy cells and the infected plaques will appear as clear areas (Figure 10).

5.4. Co-infection of insect cells with the CDK4 isoforms and CYCLIND1

The high-titer P2 viral stock was used to infect insect cells for large-scale expression of the recombinant protein. $5x10^8$ Sf9 cells in spinner flasks were doubly infected with $AcCDK4^{WT}$, $AcCDK4^{K35M}$ or $AcCDK4^{D140A}$ and AcCYCLIND1 at a multiplicity of infection (MOI) of 1 for each baculovirus. After 72h at 27ºC, cells were lysed in 50 mL of lysis buffer (20mM phosphate pH:7.4; 0,5M NaCl; 10% glycerol; 1% Triton X-100), sonicated (-cycles of 3'' ON, 1'' OFF for 2 min with an amplitude of about 10%) and centrifuged for 10 min at 18000 rpm in a JA25.50 rotor for 10 min at 4ºC to separate soluble and insoluble proteins. Samples from total extracts (TE), soluble fractions (SF) and insoluble fractions (IF) of each condition were analyzed by SDS-PAGE and Coomassie staining for protein expression and solubility (Figure 10).

5.5. Affinity protein purification and dialysis

HisTrap FF crude columns (GE Healthcare) are precharged Ni^{2+} Sepharose columns. In general, Ni^{2+} is the preferred metal ion for purification of recombinant histidine-tagged proteins. 5-ml HisTrap columns, connected to an ÄKTA Prime Plus (GE Healthcare) chromatography system, were pre-equilibrated with binding buffer (20mM phosphate pH:7.4; 0,5M NaCl; 10% glycerol; 50mM of imidazole; to minimize inespecific binding) prior to loading the filtered soluble fraction using a syringe. Flow rate was set at 5 mL/min. The column was then washed with binding buffer until UV 280 nm absorbance (A280nm) became stable at baseline. The his-tagged recombinant proteins were eluted in a two-step gradient with 10% and 100% of elution buffer (20mM phosphate pH:7.4; 0,5M NaCl; 10% glycerol; 500mM of imidazole). Protein fractions were collected in 2 mL each, and analyzed by SDS-PAGE. Fractions containing the recombinant proteins were dialyzed in order to remove the imidazole. Dialysis cassettes (Thermo Fisher 7000MWCO), which facilitate removal of buffer salts from the proteins that are larger than 7000 Daltons, were used. The dialysis buffer was the elution buffer without imidazole (20mM phosphate pH:7.4; 0,5M NaCl; 10% glycerol). Finally, dialyzed proteins were centrifuged (3000 rpm x 10 min, 4ºC) to remove precipitated material, concentrated by using Vivaspin concentrators with a cut-off value of 10 kDa (Vivascience) and analyzed by Western blot (Figure 10).

5.6. Kinase assay

Purified baculovirally expressed $CDK4^{WT}$, $CDK4^{K35M}$ and $CDK4^{D140A}$ proteins complexed with CYCLIND1, previously quantified by nanodrop and normalized by western blot, were assayed in kinase assay buffer (Matshushime 1999) (50mM Hepes pH: 7.5; 5mM $MgCl_2$; 2.5mM $MnCl_2$; 1mM DTT;

150mM NaCl; 1mM EDTA; 2.5mM EGTA; 01% Tween; 10% glycerol; supplemented with a cocktail of protease and phosphatase inhibitors (cOmplete Mini, Roche; Phosphatase Inhibitor Cocktail 2, Sigma; Phosphatase Inhibitor Cocktail 3, Sigma)), containing 1mM ATP, 10 µCi [γ-^{32}P]ATP and 2 µg of RB recombinant protein (Millipore) for 30 min at 30°C. The reactions were stopped by adding 4X loading buffer and 10X reducing agent (Nupage, Invitrogen) and by boiling at 100°C for 5 min. Proteins were electrophoresed and checked for incorporated radioactive ATP before being transferred to nitrocellulose membranes. Anti-CDK4 (Sta Cruz) and Anti-CYCLIND1 (Neomarkers) antibodies (1:500 dilution) were revealed with HRP-conjugated rabbit anti-mouse antibody (Dako) and rabbit anti-goat antibody (Dako) respectively in order to checked for CDK4 and CYCLIND1 equal loading of recombinant proteins (Figure 10).

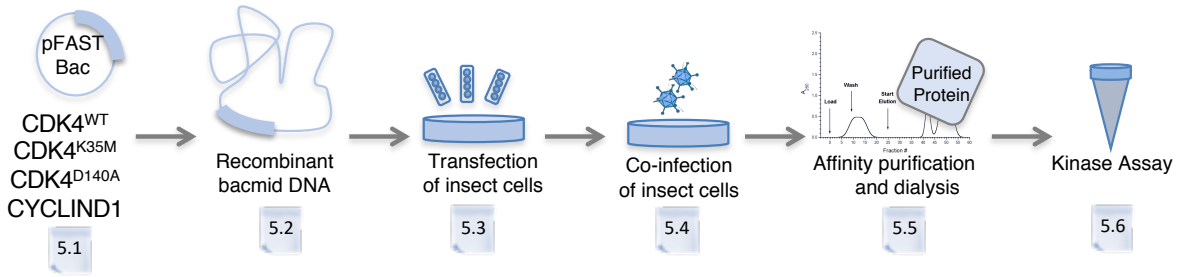

Figure 10: Schematic representation of the process followed for the generation of CDK4 proteins in a baculovirus expression system in order to check for the kinase activity of the protein.

6. *In vitro* procedures

6.1. Immunoprecipitation

Cell or embryo E.18.5 lysates were lysed in modified-homemade Ripa Lysis Buffer (150mM NaCl; 50mM Tris pH7.5; 1% NP40; 0.25% Na deoxycholate; 1mM EDTA) supplemented with a cocktail of protease and phosphatase inhibitors (cOmplete Mini, Roche; Phosphatase Inhibitor Cocktail 2, Sigma; Phosphatase Inhibitor Cocktail 3, Sigma). For tissue samples zirconium oxide beads of 2.8 mm (Precellys) were used to mechanically breakdown the sample and maximize lysis efficiency. Samples were kept on ice for 30 min, vortexing every 10min. Protein extracts were then centrifuge (13000 rpm for 15min at 4ºC) to remove the undigested membranes. In order to quantify the amount of proteins the Bradford method (2 µl of the protein extract in 1 ml of 1X Bradford reagent (Biorad)) was used. A BSA standard curve was used for quantification. Once the samples were ready to use a preclearing step was done in order to reduce non-specific binding and reduce background. Rabbit true Blot Beads (Rockland) were rinsed twice in Phosphate Buffer Saline (PBS, Lonza) prior to use and then 3 times more

in lysis buffer until a slurry was reached. 50 µl of slurry True Blot Beads were added to 1 mg of protein extract. Incubation for 2h at 4ºC was followed with gentle agitation. Then, after centrifuging (14000 rpm for 10 min at 4ºC), the supernatant was passed into a new low binding tube (Sigma Aldrich) and the bead pellet was discarded. Afterwards, 2 µg of CDK4 antibody were added to the supernatant together with 70 µl of slurry beads (IP condition), followed by an overnight (ON) incubation at 4ºC. Another tube, with protein extract but not antibody (MOCK condition) was added as a negative control. Finally, in order to compare the amount of immunoprecipitated protein an INPUT (10% of the total extract) was used. After ON incubation, 5 washes with lysis buffer of 10 min each at 4ºC were performed. CDK4, CDK2, $p21^{Cip1}$ and $p27^{Kip1}$ proteins were analyzed by electrophoresesis. In the case of embryo lysates, they were used to perform a kinase assay.

6.2. Mouse Embryonic Fibroblasts (MEFs) extraction

Primary MEFS ($Cdk4^{+/+}$; $Cdk4^{K35M/K35M}$; $Cdk4^{D140A/D140A}$; $Cdk4^{-/-}$) were isolated from 13.5 days old embryos. Each embryo was carefully separated and extracted making an excision in the uterine tissue where the placenta is located. Then, the yolk sac was gently removed, and the red tissue (liver and heart) was teared out. The head was cut for genotyping purposes. Then, the rest of the embryo was placed into a single 6 cm dish with 3 ml of 0.05% trypsin-EDTA (Gibco). After chopping up the embryos, tissues were located in a 37ºC / 5% CO_2 incubator for 5 min. Then, pieces were pipeted up and down several times and introduced again in the incubator for another 5 min. This procedure was repeated 3 times until the tissue was completely disaggregated. After that, the cell suspension was transferred to a 150 cm dish filled with 20 ml of Dulbecco's Modified Eagle's Medium (DMEM) containing 4.5 g/L D-glucose (Gibco) supplemented with 10% of Fetal Bovine Serum (FBS) (Gibco) and 1% of antibiotic/antimycotic penicillin-streptomycin solution (P/S, Gibco): complete DMEM (henceforth, DMEM/10%FBS). When confluent, usually after 48h, MEFS were frozen using standard methods for mammalian cell cryopreservation.

6.3. Immortalization of MEFs

Immortalization from the same set of primary MEFs was followed using the classical 3T3 protocol from Todaro and Green (Todaro and Green, 1963). It consists of re-plating 10^6 cells every week in fresh DMEM/10%FBS. After 5-6 passages, cells reached the crisis phase where they are not able to properly proliferate during passages. Several passages later, (on average 10-12), cells were capable to

bypass the critical phase doubling the number of cells seeded. At that point they were considered immortalized and frozen.

6.4. Packaging of lentiviruses for cell infection

Lentiviral supernatants were produced in HEK293T cells (70-80% confluence). Packaging plasmids pLP1 (1.9 µg), pLP2 (1.3 µg), pLP/VSVG (1.64 µg) (Invitrogen) and the lentiviral construct (5 µg) were mixed and added to 40 µl of Polyethylenimine (1 mg/ml) and 500 µl serum free DMEM. The mixture was vortexed for 5 seconds and incubated at Room Temperature for 15 minutes then, added dropwise to the media of HEK293T cells. Transfected cells were incubated in a 37ºC / 5% CO_2 incubator ON followed by a 48h incubation at 32ºC / 5% CO_2. Lentiviral supernatant was collected and filtered with 0.45 µm pore size filters. For cell infection lentiviral supernatants together with polybrene at a concentration of 8 µg/ml were added to the cells and incubated at 32ºC for 24h. Next day, plates were moved to a 37ºC incubator and 24h later antibiotic selection was added depending on the selection marker of each construct.

6.5. Foci Formation Assay (FFA) and staining

Focus formation assays were performed as described (Clark GJ et al; 1995). 10^5 primary MEFs (*Cdk4*$^{+/+}$; *Cdk4*$^{K35M/K35M}$; *Cdk4*$^{D140A/D140A}$; *Cdk4*$^{-/-}$; n=3/genotype) were seeded into a 6 cm dish supplemented with DMEM/10%FBS. Virus from a retroviral plasmid which contains a dominant negative version of *Trp53* isoform as well as the activated form of the *H-Ras* oncogene (*Hras*^{G12V}*/DNTrp53)* plasmid, kindly provided by L. LeCam, Montpellier) were generated in HEK293T. As control, a plasmid containing *Hras* alone, not able to induce malignant transformation, was used. Coinfection of primary MEFs with either *Hras* alone or *Hras*^{G12V}*/DNTrp53* allows for quantification of transformed cells that can grow in multiple layers by the FFA. After 15 days, replacing the medium twice weekly, "foci" were stained with crystal violet as follows: first, media was removed from the plates and washed with PBS. Cells were fixed 5-10 minutes with glutaraldehyde 1%. Then, they were rinsed with crystal violet 0.5% ON. Next day, plates were washed with water and dried at RT. Finally, number of foci was calculated visualizing against the background of non-transformed monolayer cultures.

6.6. Tumor cell line isolation from mouse LUAD

Conditional lung tumors that developed in mice were collected in 1:1 PBS + Penicillin/Streptomycin (P/S) solution during necropsy. The following genotypes were isolated: *Kras*$^{+/G12V}$;*Trp53*$^{-/-}$;*hUBC-CreERT2*$^{+/T}$;*Cdk4*$^{+/+}$;*Raf1*$^{+/+}$,

Kras$^{+/G12V}$;*Trp53*$^{-/-}$;*hUBC-CreERT2*$^{+/T}$;*Cdk4*$^{FlexK35M/L}$,

Kras$^{+/G12V}$;*Trp53*$^{-/-}$;*hUBC-CreERT2*$^{+/T}$;*Raf1*$^{L/L}$,

Kras$^{+/G12V}$;*Trp53*$^{-/-}$;*hUBC-CreERT2*$^{+/T}$;*Cdk4*$^{FlexK35M/L}$;*Raf1*$^{L/L}$

The piece of tumor was squashed against a tissue culture plate. Cells were cultured in DMEM/10%FBS at 37ºC in a humidified atmosphere of 5% CO_2 changing media every 3 days until they reach the adequate confluency to be frozen by standard methods for mammalian cell cryopreservation.

6.7. Infection of cells with adenoviruses encoding for the Cre recombinase

Conditional lung tumor derived cells, were seeded at equal densities (4 x 10^5cells/10 cm dish). Next day, cells were infected with 10 MOI (Multiplicity of Infection) of AdCre or AdGFP as control. Moreover, 4-Hydroxy-tamoxifen was added in the plates infected with AdCre in order to better excise the targets. Two days post-infection cells were seeded for proliferation and/or colony formation assays.

6.8. Senescence associated β-galactosidase (SA-β-gal) detection

2 x $10^{5.}$ tumor cells from the aforementioned genotypes were seeded in triplicates in 6 cm dishes containing DMEM/10%FBS. 4-Hydroxy-tamoxifen (4-OHT, 600nM) (Sigma, H70904) was added to the plates in order to activate the Cre recombinase and allow for the excision of the conditional targets. After 72h, cells were rinsed twice in PBS and then fixed during 5 min at RT with 2% Formaldehyde / 0.2% glutaraldehyde solution (Sigma Aldrich). After fixation, cells were rinsed twice in PBS and then incubated at 37ºC in X-Gal staining solution (1X Citric acid/sodium phosphate buffer pH6.0; 500mM Potassium ferricyanide (Prolab); 500mM Potassium ferrocyanide (Prolab); 150mM NaCl; 2mM $MgCl_2$; 1mg/ml of the substrate 5-bromo-4-chloro-3-indolyl β D-galactopyranoside (X-Gal, Applichem) dissolved in N-N-dimethylformamide). After 72h cells were washed in PBS and representative pictures of each triplicate were taken under bright-field microscopy. SA-β-gal positive cells were quantified as percentage of the total cell numbers (Zen Lite Software, Carl Zeiss). For tissue samples the same procedure was followed right after fresh lung tissues were cut in the cryostat.

6.9. Proliferation curves: MTT assay

For proliferation assays, 500 cells were seeded in 96-well plates in triplicates supplemented with DMEM/10%FBS for 10 days. Proliferation rate was inferred by the enzymatic reduction of the 3-(4,5-dimethylthiazol-2-yl)-2,5-di-phenyltetrazolium bromide (MTT, Roche, 11465007001) into formazan. MTT is diluted in PBS (5mg/ml) and filtered through a sterile 0,22 µm pore size filter. 100 µl of a 1:5 MTT/DMEM dilution were added to each plate. After 3 hours, 100 µl of 10% SDS; 0.01M HCl solution was added to solubilize the formazan. The resulting absorbance was measured with a microplate reader at 544 nm (EnVision 2104 Multilabel Reader, Perkin Elmer, Waltham, MA).

6.10. Colony formation assay

Cultivating cells at low densities is a process used to determine the proliferative potential of a cell in very restricted conditions. 5000 cells were seeded in 10 cm dishes in DMEM/10%FBS for 12 days. After this time, cells are able to form defined and separated clusters or colonies. Cells were washed with PBS, fixed during 5 min at Room Temperature in 1% glutaraldehyde and stained with 0.2% Crystal Violet ON. The next day, cells were washed and dried at Room Temperature.

6.11 Isolation of resistant cells: subcloning

Clusters of cells from the colony formation assay were individually harvested using small glass cylinders (Sigma) attached to the dish with Dow Corning® high-vacuum silicone grease (Sigma). 50 µl of 0.05% trypsin-EDTA was used to detach the cells. Then, 150 µl of DMEM/10%FBS were added on top to stop the reaction. The final volume was passed to a 96 well plate. Single cell subclones were expanded until they reached enough confluency to be frozen or used as a conventional cell line.

6.12. Ic50 determination and drug treatments in cell lines

Lung cancer cell lines were plated at 3,000 cells per well in triplicates in 96-well plates and grown for 24 hours. Doses were separated by 3 folds and spanned 1 nM to 20 µM. Control cells were incubated with media containing DMSO. To calculate the IC_{50}, values were plotted against the inhibitor concentrations and fit to a sigmoid dose-response curve using GraphPad Software. For the compound screening a library of 114 drugs from CNIO's Experimental Therapeutic Unit was used at a unique 5 µM dose during 72h. For proliferation curves 500 cells per well were seeded in 96-well plates. 5-Azacytidine (Sigma, A2385) was added at 2 µM dose on days 0, 1, 2, 3, 6 and 9 of the experiment and CNIO-PI3K

(ETP-46444) was added at 1 µM dose on days 0,3,6 and 9 of the experiment. Cell viability was assessed with Cell Titer Glo® Luminescent Cell Viability Kit (Promega, G7571) at the end of the experiment. Luminescence counts were read in a Victor Plate Reader Instrument (Perkin Elmer) with the recommended settings.

6.13. 3D cultures: spheroid formation and Topro-3/Hoechst assay

Optimal densities for each cell line (between 1000-2000cells/well) were dispensed in ULA 96-well round-bottomed plates (Costar). After seeding, plates were centrifuged (1600 rpm x 10 min) and then incubated for 4 days at 37°C, 5% CO2, until spheroids reach 380-400 µm of diameter. Once the spheroids were formed, Topro-3 staining for death cells was added at a final concentration of 1 µM and Hoechst staining for all cells was added to a final concentration of 0.1 µM. Images were obtained using a confocal ultraspectral microscope (Leica TCS-SP5) or the Opera High Content Screening (HCS) system (Perkin Elmer). Quantifications were performed with Image J software with the help of Confocal Microscopy Unit at CNIO.

7. Western blot

7.1. Protein extraction

Already described in the immunoprecipitation section (Section 6.1).

7.2. Electrophoresis, transfer and blocking

Electrophoresis was performed using the NuPAGE™ 4-12% Bis-Tris Midi gels (Invitrogen) in NuPAGE™ MES SDS running buffer (Invitrogen). First, samples were boiled for 5 minutes at 95°C, spun and loaded into the gel. In addition, 10 µl of the Thermo Scientific Spectra Multicolor Broad Range Protein Ladder were loaded as well. The gel was run with a 120V constant voltage. Wet transfer was performed as described: a piece of nitrocellulose membrane (GE Healthcare) was cut as well as six pieces of Whatman paper. The membrane, the papers and the gel were dipped in transfer buffer (pH 8.3, 26 mM Tris, 192 mM glycine, 20% methanol). As proteins migrate from the negative to the positive pol the stack is prepared as follows: +ve → sponge → whatman paper → membrane → gel → whatman paper → sponge → -ve. The gel was transferred for 70 minutes at 400 mA constant current. Afterwards, staining with Ponceau S solution (Sigma) was performed to check the efficiency of protein transfer,

followed by blocking in 5% non-fat milk or BSA diluted in TBS-T buffer (0.1 M Tris base pH 7.4, 1.5 M NaCl, 0.1% Tween-20) for 1h at Room Temperature.

7.3. Antibodies used for protein detection

All incubations with the primary antibodies were performed ON at 4ºC on a rotating platform. The next day, the membranes were washed three times with TBS-T during 10 minutes. Afterwards, they were incubated for 1 h with the secondary antibodies Horseradish peroxidase-conjugated (HRP) or fluorescently labeled. For HRP secondary antibodies, protein visualization was carried out using the Enhanced ChemiLuminiscence (ECL) detection reagent (GE Healthcare) or with SuperSignal™ West Femto (Thermo Fisher Scientific). The chemiluminescent signal was captured with AGFA® Medical X-Ray Film Blue. Fluorophore-conjugated secondary antibodies were detected using the Odyssey® CLx Imager (LI-COR Biosciences) (Table 4).

ANTIBODY	M. WEIGHT (kDa)	SOURCE	IDENTIFIER
Primary Antibodies			
CDK4	34	Santa Cruz	Sc-260
CYCLIND1	36	Neomarkers	MS-210-P1
RB	110	Santa Cruz	Sc-50
pRB (Ser 807-811)	110	Cell Signaling	Cat#9308
CDK6	36	Neomarkers	MS-451-P1
pCDK2 (Thr160)	32	Cell Signaling	Cat#2561
CDK2	32	Abcam	Ab32147
CYCLINE2	34	Santa Cruz	Sc-28351
P27	27	BD Biosciences	Cat#610242
P21	21	Santa Cruz	Sc-397
RAF1	72	BD Biosciences	Cat#610151
pAKT (Ser473)	62	Cell Signaling	Cat#9271
AKT	60	Cell Signaling	Cat#9272
pERK1 ,2	42-44	Cell Signaling	Cat#9101
ERK 1	42	BD Pharmingen	554100
ERK 2	44	BD Pharmingen	610103
CASPASE 3	36	Cell Signaling	Cat#9662
CLEAVED CASPASE 3 (Asp 175)	17	Cell Signaling	Cat#9661
βACTIN	45	Sigma	A5441
Secondary antibodies			
Goat polyclonal anti-Mouse Ig/HRP		Dako	P0447
Goat polyclonal anti-Rabbit Ig/HRP		Dako	P0448
Goat polyclonal anti-Rabbit IG H&L (Alexa Fluor 680)		Abcam	Ab175773
Goat polyclonal anti-Mouse IG H&L (Alexa Fluor 680)		Abcam	Ab175775

Table 4: Antibodies used for Western blot

8. RNA sequencing

8.1. RNA extraction and library generation

Total RNA was extracted from cells using RNeasy Micro Kit (Qiagen) according to manufacturer's protocol.

RNA integrity from the different samples was assessed with the Agilent 2100 BioAnalyzer (Agilent Technologies). Only samples with an RNA Integrity Number (RIN) value higher than 9 were used for RNA-Sequencing. 1 µg of total RNA samples was used to generate the libraries (Genomic Unit, CNIO). The PolyA+ fraction was purified and randomly fragmented, converted to double stranded cDNA and processed through subsequent enzymatic treatments of end-repair, dA-tailing, and ligation to adapters as in Illumina's "TruSeq Stranded mRNA Sample Preparation Part # 15031047 Rev. D" kit (this kit incorporates dUTP during the second strand cDNA synthesis, which implies that only the cDNA strand generated during first strand synthesis is eventually sequenced). Adapter-ligated library was completed by PCR with Illumina PE primers. The resulting purified cDNA library was applied to an Illumina flow cell for cluster generation and sequenced on an Illumina instrument by following the manufacturer's protocols. Single-end sequencing was performed.

Image analysis, per-cycle base calling and quality score assignment was performed with Illumina Real Time Analysis software. Conversion of BCL files to FastQ format was performed with the bcl2Fastq Software (Illumina).

8.3. Bioinformatic analysis and data representation

The quality of the reads was evaluated with FastQC (Andrews et al., 2010). The RNA-seq reads were then mapped onto the reference genome mouse GRCm38/mm10 using STAR (v2.4.0j) (Dobin et al., 2013). The abundance of each gene was quantified as TPM (Transcripts per million) value, which was evaluated by a statistical method RSEM (RNA-Seq by Expectation Maximization). RSEM uses a generative model of RNA-seq reads and the EM algorithm, taking read mapping uncertainty into account and achieving the most accurate abundance estimates (Li and Dewey, 2011). Deseq2 analysis was used to call the differentially expressed genes (DEGs) between two conditions compared (Love et al., 2014). The DEGs were called using adjusted P-value <0.05 as the cutoff. We formed the following comparisons: RP vs. CtrlRP (i), RT vs. CtrlRT (ii) and RT vs. RP (iii). To identify the heterogeneity of the different resistant clones, we also formed the comparisons RT vs. CtrlRT and RT vs. RP for each parental cell line respectively (iv; pairwise). The information of samples and comparisons used is in the following diagram.

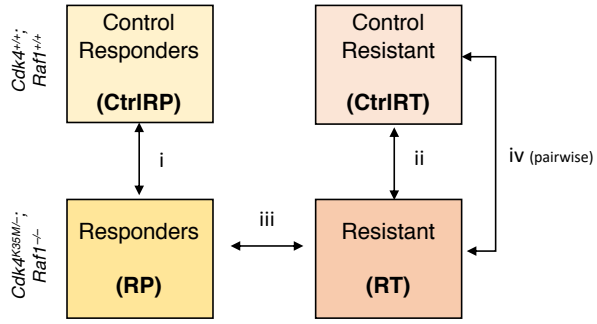

Gene set enrichment analysis (GSEA) (Subramanian et al., 2005) was employed to determine the gene sets, including KEGG, Gene Ontology, Cancer hallmarks and CGP (chemical and genetic perturbations) databases, enriched by a pre-ranked list of all genes, which were sorted by the statistical significance of differential expression defined by DESeq2 analysis. CGP database includes 3433 gene sets, representing expression signatures of genetic and chemical perturbations. Since GSEA gene sets are annotated with human, we converted the mouse genes to their orthologs in human for this analysis. Single sample gene set enrichment analysis (ssGSEA) (Barbie et al., 2009)was used to generate an activity profile of pathways that were significant enriched by DEGs (FDR adjusted P-value < 0.05).

9. Statistics

The Graph-Pad Prism software was used in this work to analyze statistics. The method used depended on the following criteria:

Normality test: is the data set well-modeled by a normal distribution?

1.. YES → PARAMETRIC tests were used

1.1. For 1 sample → T TEST

1.2. For 2 samples → Check for Homoscedasticity: has the error the same variance?

YES → T TEST

NO → WELCH TEST

1.3. For more than 2 samples → ANOVA TEST

- Corrections to compare samples (e.g. K35M, D140A, KO) with a Control (WT) → DUNNET TEST

2. NO → NO PARAMETRIC tests were used

2.1. For 1 sample → WILCOX TEST

2.2. For 2 samples → WILCOXON MANN-WHITNEY TEST

2.3. For more than 2 samples → ANOVA TEST

-Corrections to compare samples (e.g. K35M, D140A, KO) with a Control (WT) → DUNN's TEST

If the p value is: ****p<0.0001, ***p < 0.001, **p < 0.01, *p < 0.05, n.s, not significant

RESULTS

1. Study of two *Cdk4* Kinase Dead GEMMs: *Cdk4*^{K35M} and *Cdk4*^{D140A}

Previous work from our laboratory demonstrated that *Cdk4* is the only interphase *Cdk* strictly required for the initiation of LUAD triggered by an endogenous *Kras*^{G12V} oncogene (Puyol et al., 2010). However, protein elimination is still a big challenge for the clinic and most of the inhibitors are designed against the kinase core. Therefore, in order to evaluate whether its oncogenic contribution in lung is entirely dependent on its catalytic activity, two *Cdk4* "dead" kinase models have been used. One mutating the Lys (K) of the ATP-binding site by a Methionine (M), K35M, and another mutating the Aspartic acid (D) by an Alanine (A) in the proton acceptor, D140A of the CDK4 protein (See Materials and Methods, Section 1.3).

1.1. CDK4^{K35M} *and CDK4*^{D140A} *proteins have impaired kinase activity*

The baculovirus expression system is a useful tool for analyzing CDK4 kinase activity *in vitro*, since activation of CDKs is regulated by post-transcriptional modification systems that are active in the insect host cells (Harashima and Sekine, 2011). With the aim of studying the catalytic properties of CDK4, the entire CDK4 protein harboring both mutations, either K35M or D140A, was expressed in a baculovirus system (See Materials and Methods, Section 5 and Figure 10). After the recombinant histidine tag bacmids with the gene of interest (Ac-CDK4^{WT} -as control, Ac-CDK4^{K35M} and Ac-CDK4^{D140A}) were inserted in the genome of the baculovirus, Sf9 insect cells were co-infected with bacmids

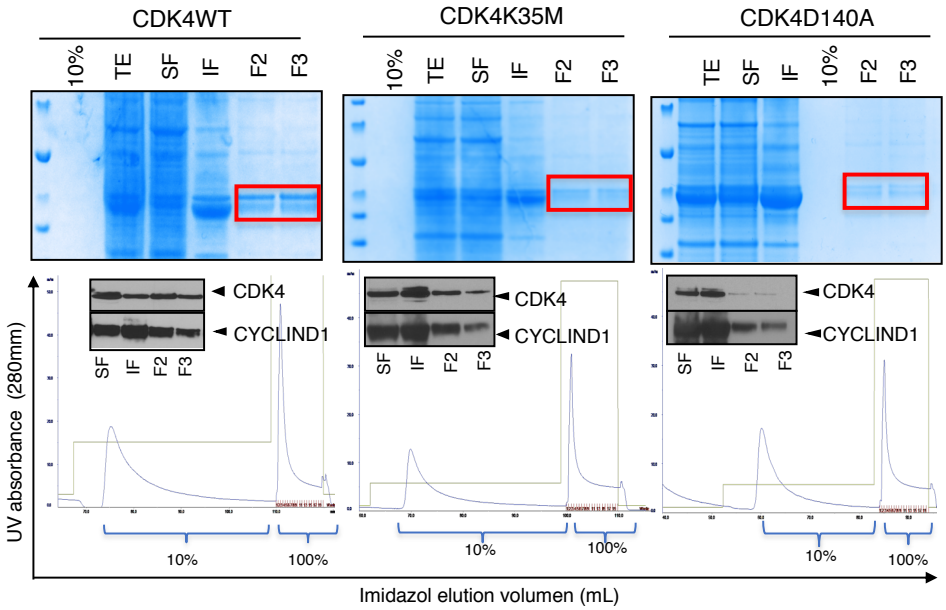

Figure 11: Protein expression and affinity purification processes.
Coomassie staining, size exclusion chromatography traces and analysis of CDK4 and CYCLIND1 proteins from total extracts (TE), soluble fraction (SF), insoluble fraction (IF), fraction from the 10% imidazole injection (10%) and fractions collected from the 100% imidazole elution process (F2 and F3) from each condition.

expressing Ac-CYCLIND1. Purified protein complexes using nickel columns that recognize the histidine tag of the bacmid were checked by Coomassie staining and Western blot. Highly pure 34 and 36 kDa proteins were detected, consistent with the molecular weight of the expected CDK4 and CYCLIND1 proteins respectively (Figure 11).

The activity of purified CDK4^{WT}, CDK4^{K35M} and CDK4^{D140A} proteins was determined by *in vitro* kinase assay which demonstrated that none of the purified mutant complexes were able to phosphorylate the main CDK4 substrate: RB (Figure 12A). In addition, normal levels of CDK4 and CYCLIND1 proteins were observed after CDK4 immunoprecipitation. In order to confirm this data and to study the catalytic activity of CDK4 in a more physiological context where all interphase CDKs are present, a kinase assay using embryo lysates at E18.5, where CDK4^{K35M} and CDK4^{D140A} were constitutively expressed, was performed. The results allowed us to confirm that neither CDK4$^{K35M/K35M}$ nor CDK4$^{D140A/D140A}$ could phosphorylate RB (Figure 12B).

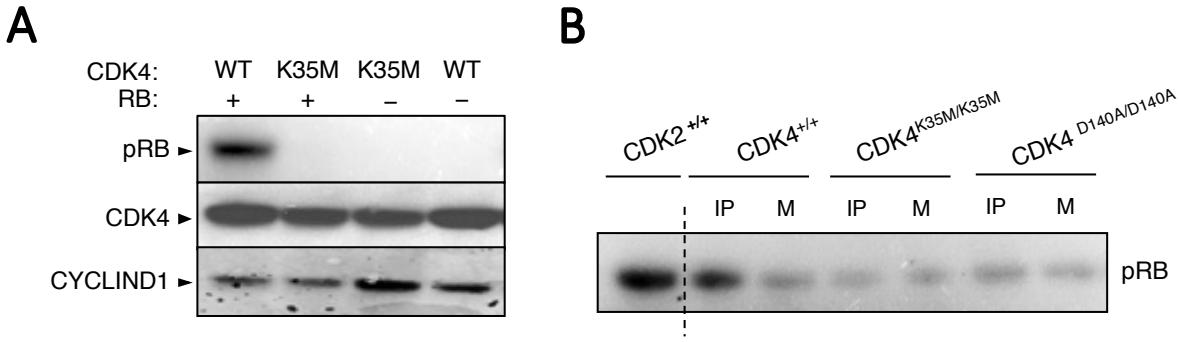

Figure 12: Catalytic activity of CDK4^{K35M} and CDK4^{D140A}
A) *In vitro* kinase activity associated with the indicated CDK4 baculoviral recombinant proteins co-expressed with murine CYCLIND1 in Sf9 cells. Recombinant RB was used as a substrate. Western blot analysis for phospho-RB, CDK4 and CYCLIND1. **B)** *In vitro* kinase activity of the indicated E18.5 embryo lysates after CDK4 immunoprecipitation. WT: wildtype; IP: Immunoprecipitation; M: Mock.

In conclusion, mutations of Lys35 to Methionine (K35M) as well as Asp140 to Alanine (D140A) inactivated the kinase activity of the CDK4 protein allowing us to further study if the effect observed upon CDK4 protein elimination in *Kras^{G12V}*-driven tumors relies on CDK4 kinase activity.

1.2. CDK4 kinase inactivation bypasses the perinatal lethality associated to CDK4 deficiency

In order to characterize the role associated to the lack of CDK4 kinase activity in normal homeostasis, we set up matings between *Cdk4*$^{FlexK35M/+}$ as well as between *Cdk4*$^{LmLD140A/+}$ and from these strains, we obtained mouse embryonic fibroblasts (MEFs) at E13.5. Unexpectedly, no CDK4 protein could be detected in extracts from homozygous *Cdk4*$^{FlexK35M/FlexK35M}$ nor from *Cdk4*$^{LmLD140A/LmLD140A}$ MEFs

(Figure 13). Infection of these MEFs with Adenoviruses encoding the Cre recombinase (AdCre) to induce the expression of both mutations, K35M and D140A, restored the function of the locus resulting in the expression of CDK4K35M and CDK4D140A respectively (Figure 13). This unfortunate result suggests that modifications performed on the *Cdk4* locus may interfere with its correct expression thus making the *Cdk4*^{FlexK35M} and *Cdk4*^{LmLD140A} functional null alleles.

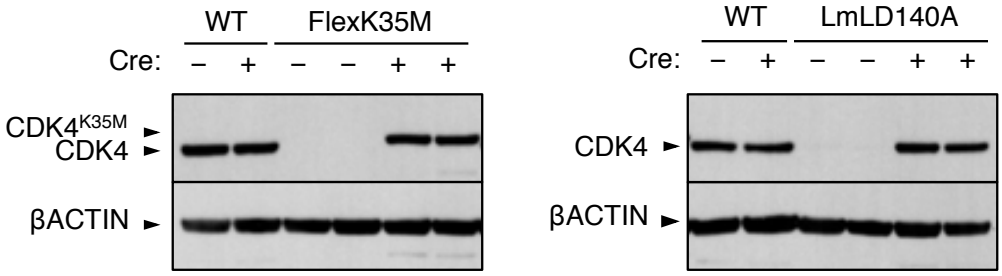

Figure 13: Protein expression of CDK4^{K35M} and CDK4^{D140A} in MEFs.
Western blot analysis of the CDK4 expression levels in whole cell extracts obtained from homozygous **(left)** *Cdk4*$^{FlexK35M/FlexK35M}$ and **(right)** *Cdk4*$^{LmLD140/LmLD140A}$ MEFs before and after exposure to AdCre. Of note, expression of the K35M mutation upon the Cre recombinase is activated leads to a slower electrophoretic migration as a consequence of the FLAG tag that was inserted after the ATG in the inverted exon. Extracts from two independent MEFs per genotype are shown. *Cdk4*$^{+/+}$ MEFs lysates are included for comparative purposes. Notice that CDK4^{D140A} is not tagged. WT: Wildtype.

However, these technical difficulties did not preclude us from exploring the consequences of expressing the kinase inactive forms of CDK4 in mouse homeostasis. To this end, we crossed mice carrying either the *Cdk4*^{FlexK35M} or *Cdk4*^{LmLD140A} alleles to the EIIa-Cre^{T} strain. The EIIa promoter targets the expression of the Cre recombinase to the early mouse embryo ensuing Cre-mediated recombination in all tissues. Subsequent backcrosses to C57BL/6J wildtype mice indicated that heterozygous *Cdk4*$^{+/K35M}$ as well as *Cdk4*$^{+/D140A}$ mice were born at the expected ratios (Table 5). Mouse colonies of *Cdk4*$^{+/K35M}$, *Cdk4*$^{+/D140A}$ together with *Cdk4*$^{+/-}$ mice were generated in a pure C57BL/6J genetic background to facilitate the comparison of their respective phenotypes when in homozygosity. Surprisingly, *Cdk4*$^{-/-}$ mice were born at a frequency (1.2%) significantly lower than the expected ratio (25%) (Table 5). Some degree of perinatal lethality associated to CDK4 deficiency has been previously reported although not to that extent (Tsutsui 1999, Padmakumar 2009; our own unpublished data). Our data suggests that this pronounced lethal phenotype might be enhanced in a pure C57BL/6J strain. Histopathological examination of E13.5, E18,5 embryos and P1 newborns failed to unveil major defects that could account for the lethality.

Since the lethality associated to CDK4 deficiency is lower in mixed genetic backgrounds we crossed the C57BL/6J strains carrying null, K35M and D140A *Cdk4* alleles to wildtype 129/Sv mice. Matings among these F1 heterozygotes restored the viability of *Cdk4*$^{-/-}$ mice almost to Mendelian ratios

(Table 5) and allowed the phenotypic comparison with *Cdk4*$^{K35M/K35M}$ and *Cdk4*$^{D140A/D140A}$ cohorts in the same C57BL/6:129/SvF2 controlled genetic background.

Table 5: Summary of the observed offspring from different genetic backgrounds

C57BL/6J genetic background

Stage	n	*Cdk4*$^{+/+}$	*Cdk4*$^{+/-}$	*Cdk4*$^{-/-}$
E13.5	47	7 (14,9%)	30 (63,8%)	10 (21,3%)
E18.5	16	3 (18,8%)	10 (62,5%)	3 (18,8%)
P0	601	238 (39,6%)	356 (59,2%)	7 (1,2%)
Stage	**n**	***Cdk4*$^{+/+}$**	***Cdk4*$^{+/K35M}$**	***Cdk4*$^{K35M/K35M}$**
P0	35	11 (31,4%)	14 (40%)	10 (28,6%)
Stage	**n**	***Cdk4*$^{+/+}$**	***Cdk4*$^{+/D140A}$**	***Cdk4*$^{D140A/D140A}$**
P0	110	28 (25,5%)	49 (44,5%)	33 (30%)

C57BL/6:129/SvF2 genetic background

Stage	n	*Cdk4*$^{+/+}$	*Cdk4*$^{+/-}$	*Cdk4*$^{-/-}$
P0	78	31 (39,7%)	34 (43,6%)	13 (16,7%)

1.3. Defects in CDK4$^{K35M/K35M}$ *and CDK4*$^{D140A/D140A}$ *mice physiology are milder than in Cdk4*$^{-/-}$ *mice.*

Previous studies have described that *Cdk4*$^{-/-}$ mice were infertile, displayed reduced body weight as well as insulin-deficient diabetes (Martin et al., 2003; Moons et al., 2002; Rane et al., 1999; Tsutsui et al., 1999). In the current study, *Cdk4*$^{-/-}$ mice in the C57BL/6:129/SvF2 background recapitulated all the previously described phenotypes. As previously reported, knock-out mice were smaller, with an average 35% decrease when compared to wildtype controls. None of the homozygous mice reached the size of the wildtype counterparts. Remarkably, both CDK4 KD strains in the same C57BL/6:129/SvF2 genetic background displayed an average reduction in body weight of 20% when compared to wildtype controls (Figure 14).

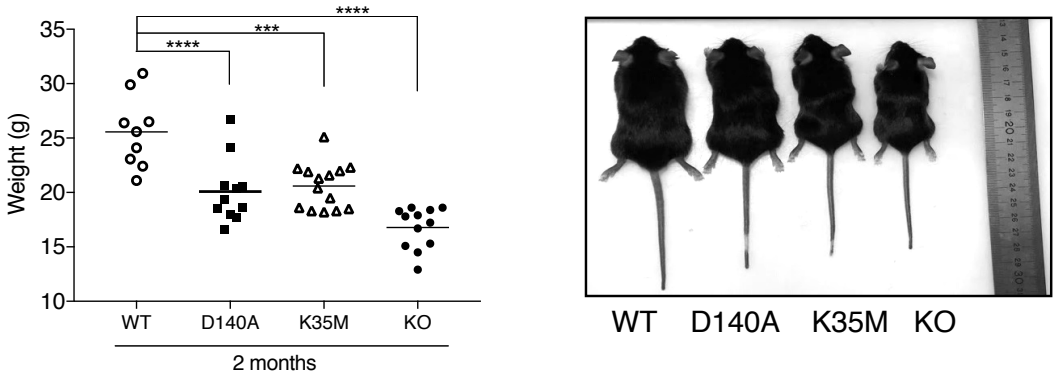

Figure 14: *Cdk4*$^{K35M/K35M}$ and *Cdk4*$^{D140A/D140A}$ mice have smaller body weight and size than *Cdk4*$^{+/+}$ mice. **(Left)** Body weight of 2-month old males from the *Cdk4*$^{+/+}$ (empty circles, n=7), *Cdk4*$^{D140A/D140A}$ (squares, n=10), *Cdk4*$^{K35M/K35M}$ (triangles, n=14) and *Cdk4*$^{-/-}$ (solid circles, n=10) expressing strains. ****p<0.0001, ***p < 0.001, ANOVA test. Data are shown as means ± SEM. **(Right)** Representative mouse pictures of the indicated genotypes. WT: wildtype; KO: Knock-out.

Furthermore, the endocrine defects were also milder in both CDK4 KD strains when compared to the CDK4 deficient cohort. Whereas all knock-out animals became hyperglycemic (>160mg/dl for females and 180 mg/dl for males) by 2 months of age due to abnormal development of pancreatic β-islet cells, the onset of the diabetic phenotype was delayed in CDK4^{K35M} and CDK4^{D140A} expressing mice with less penetrance, 8 months after birth (Figure 15A). This milder phenotype is in correlation with the degeneration of the Langerhans islets in the different genotypes, with *Cdk4*$^{-/-}$ mice displaying a more profound decrease in the size of the islets. This was estimated both as the area of islets referred to the total pancreas as well as in the total number of islets per mouse when compared to the wildtype controls (Figure 15B and 14C). The milder diabetic phenotype of both KD models correlated with a significantly extended survival when compared to CDK4 deficient mice. The latter, showed a maximal lifespan of 8 months in this genetic background whereas mice expressing the CDK4 KD reached survival rates over 12 months (Figure 15D).

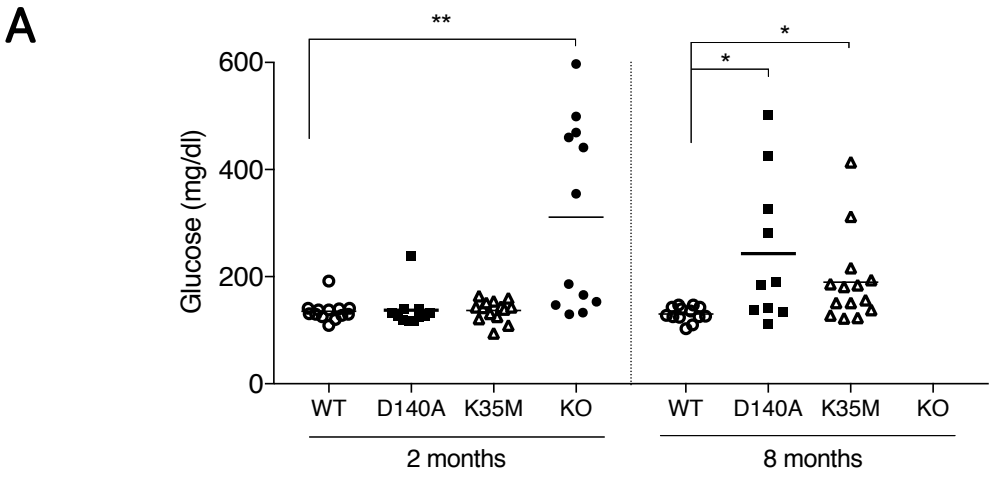

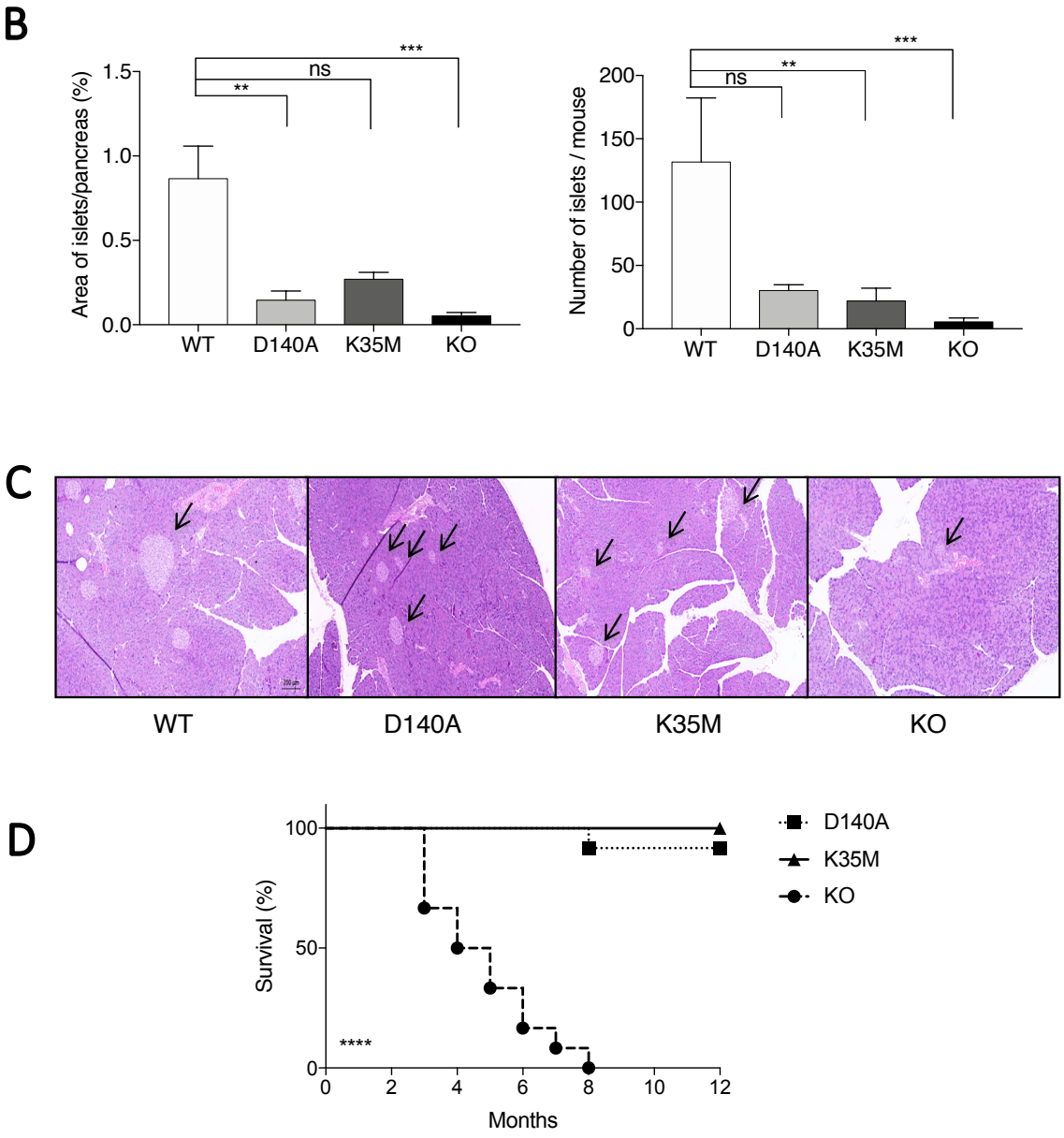

Figure 15: *Cdk4*$^{K35M/K35M}$ and *Cdk4*$^{D140A/D140A}$ expressing mice show a delay in the appearance of diabetes associated to a prolonged life span.

A) Glucose levels in blood from 2- and 8-month old males from *Cdk4*$^{+/+}$ (empty circles, n=13), *Cdk4*$^{D140A/D140A}$ (squares, n=11), *Cdk4*$^{K35M/K35M}$ (triangles, n=14) and *Cdk4*$^{-/-}$ (solid circles, n=12) mice. Note that no *Cdk4*$^{-/-}$ mice were alive at the 8-month time point. **p < 0.01, *p < 0.05, ANOVA test. Data are shown as means ± SEM. **B) (Left)** Quantification of the area of the Langerhans islets. **(Right)** Number of islets per mouse. *Cdk4*$^{+/+}$ (WT, n=7 mice), *Cdk4*$^{D140A/D140A}$ (n=8 mice), *Cdk4*$^{K35M/K35M}$ (n=11 mice) and *Cdk4*$^{-/-}$ (KO, n=4 mice) strains were analyzed. ***p < 0.001, **p < 0.01, *p < 0.05, n.s, not significant, ANOVA test. Data are shown as means ± SEM. Scale bar: 0.2mm. **C)** Representative pictures of the Langerhans islets from the indicated genotypes. **D)** One-year survival curve of *Cdk4*$^{D140A/D140A}$ (squares, n=11 mice), *Cdk4*$^{K35M/K35M}$ (triangles, n=14 mice) and *Cdk4*$^{-/-}$ (circles, n=12 mice) mice. ****p < 0.0001, log-rank test (Mantel-Cox).

Finally, both *Cdk4*$^{-/-}$ males and females were infertile. Testes of adult (>P120) of *Cdk4*$^{-/-}$ mice were small and atrophic according to histopathological evaluation. Sections of the seminiferous tubules and the epididymis showed dysplastic defects with fewer spermatocytes and no spermatids or spermatozoa at all. In the case of both K35M and D140A homozygous mice, they seemed to have slightly less spermatozoa in the seminiferous tubules but their epididymis was full or partially full of them, which suggests that they could mature in the epididymis and acquire motility properties and the capability to fecundate the ovule (Figure 16A). In fact, unlike *Cdk4*$^{-/-}$ mice, both KD male animals were fertile. In the case of the *Cdk4*$^{-/-}$ female mice, infertility was caused by pronounced defects in the hypothalamic-pituitary axis promoting a severe reduction in prolactin-producing pituitary lactotrophs (Martin et al., 2003; Moons et al., 2002). In contrast, females from both CDK4 KD homozygous strains were fertile and showed no statistically significant reduction in prolactin positive cells stained in pituitary paraffin sections from each genotype (Figure 16B).

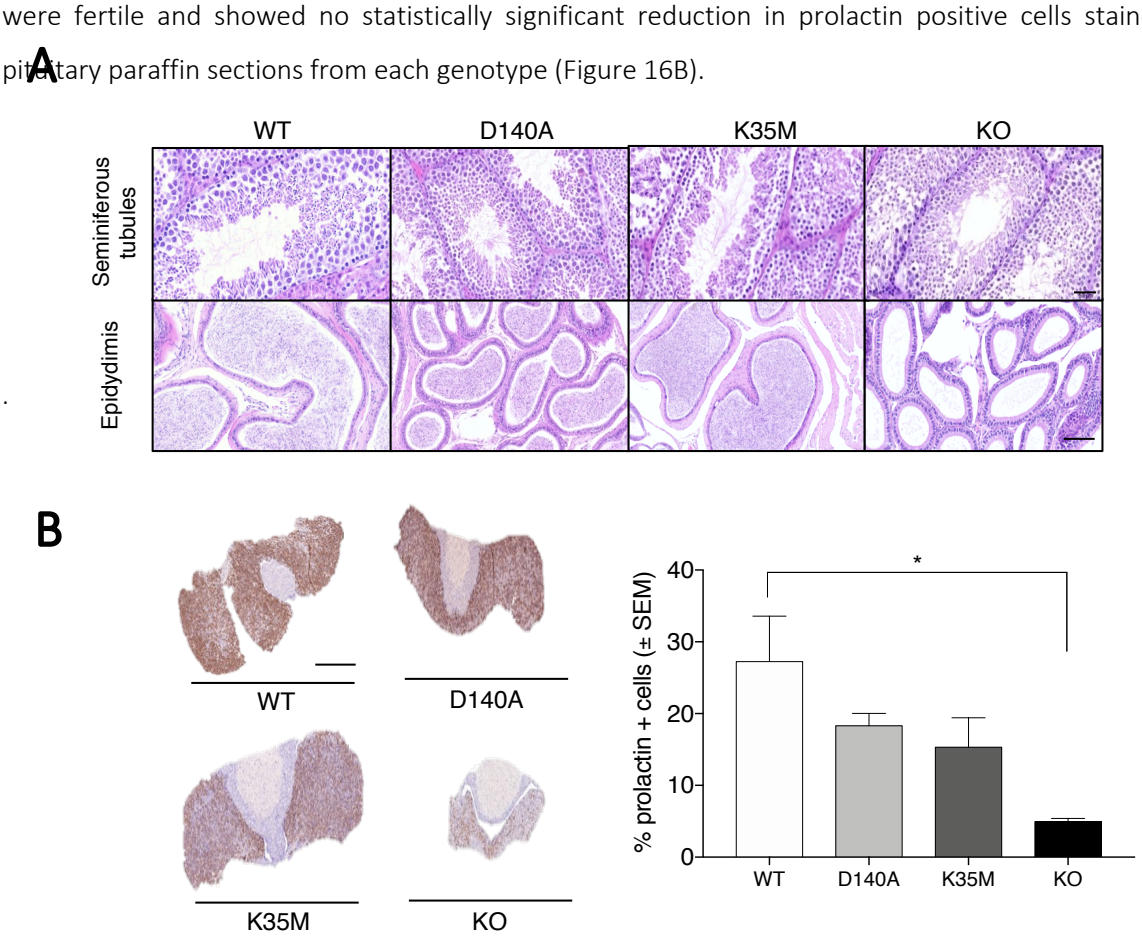

Figure 16: Cdk4$^{K35M/K35M}$ and Cdk4$^{D140A/D140A}$ males and females are fertile
A) Representative pictures of the **(upper panel)** seminiferous tubules and **(bottom panel)** epididymis of males' testes. Scale bar: 0.05 and 0.1 mm for the seminiferous tubules and epididymis respectively. **B) (Left)** Prolactin representative staining is shown for illustrative purposes. Scale bar: 0.5mm. **(Right)** Quantification of adenohypophysis positive cells for immunostaining with specific antibodies against prolactin in pituitary sections from *Cdk4*$^{+/+}$ (WT, n=4 mice), *Cdk4*$^{D140A/D140A}$ (n=7 mice), *Cdk4*$^{K35M/K35M}$ (n=6 mice) and *Cdk4*$^{-/-}$ (KO, n=3 mice) mice. *p < 0.05, ANOVA test. Data are shown as means ± SEM.

In summary, mice expressing kinase inactive *Cdk4* alleles developed a milder phenotype when compared to the full CDK4 knock-out strain suggesting the existence of relevant kinase independent CDK4 functions in homeostasis.

1.4. In vitro proliferation rate upon Cdk4^{K35M} and Cdk4^{D140A} expression

As defects in the development of mice carrying *Cdk4$^{-/-}$* alleles suggested that cell cycle progression may also be affected, we established mouse embryonic fibroblast (MEFs) from each genotype (*Cdk4$^{+/+}$;Cdk4$^{K35M/K35M}$;Cdk4$^{D140A/140A}$;Cdk4$^{-/-}$*) at E13.5 from the C57BL/6:129/SvF2 controlled-mixed genetic background. The growth curves in the presence 10% Fetal Bovine Serum (FBS) revealed a proliferation delay of *Cdk4$^{-/-}$* cultures compared to their wildtype littermates. However, the proliferation rates of both CDK4 KD MEFs did not significantly differ from those of *Cdk4$^{+/+}$* controls (Figure 17A).

Next, we determined the impact of CDK4 KD expression on spontaneous immortalization following a 3T3 protocol. Growth curves in Figure 17B indicate that CDK4 inactivation has an intermediate effect on the immortalization process compared to the wildtype control cells. The more evident difference appeared to be in the case of eliminating CDK4 resulting in a prolonged crisis-phase before they became immortal.

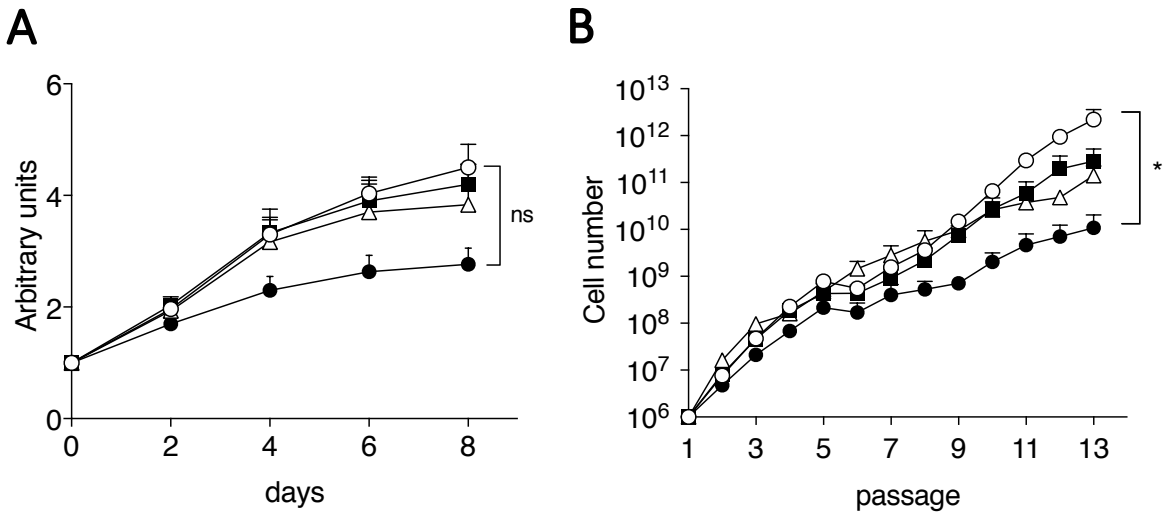

Figure 17: Proliferation of MEFs expressing CDK4^{K35M} and CDK4^{D140A} isoforms
A) Proliferation assessed by MTT assay of primary E13.5 MEFs derived from *Cdk4$^{+/+}$* (empty circles), *Cdk4$^{D140A/D140A}$* (squares), *Cdk4$^{K35M/K35M}$* (triangles) and *Cdk4$^{-/-}$* (solid circles) embryos. **B)** Immortalization of the same set of primary MEFs following a classical 3T3 protocol. Cells were cultivated in DMEM supplemented with 10% FBS. **p < 0.01; ns: not significant, ANOVA test. Data are shown as means ± SEM.

1.5. Susceptibility of MEFs for oncogenic transformation upon CDK4^{K35M} and CDK4^{D140A} expression

CDK4-CYCLIND complexes are direct targets of many oncogenic pathways and their function is required for cancer cell growth in various tumour types (Malumbres and Barbacid, 2001). We next evaluated whether the contribution of CDK4 to oncogenic transformation could also rely in part on kinase independent properties. To this end, we generated MEFs harboring the following alleles *Kras*$^{+/LSLG12V}$;*Cdk4*$^{+/+}$, *Kras*$^{+/LSLG12V}$;*Cdk4*$^{K35M/K35M}$, *Kras*$^{+/LSLG12V}$;*Cdk4*$^{D140A/D140A}$ and *Kras*$^{+/LSLG12V}$;*Cdk4*$^{-/-}$. First, cells were infected with AdCre particles inducing the expression of the endogenous mutant *Kras*^{G12V} allele. Then, cells were seeded and analyzed for their proliferation rates. Surprisingly, 8 days after seeding, cells expressing the K35M mutation stopped proliferating as the ones that lack CDK4. Yet, D140A expressing cells were more heterogenous and showed an intermediate growth rate compared to the wildtype controls (Figure 18A).

Ras signaling pathway is known to trigger transformation and loss of contact inhibition processes. The Foci Formation Assay (FFA) was used to analyze the potential oncogenic capacity of CDK4 deficient cells versus CDK4 KD. To do so, *Cdk4*$^{+/+}$; *Cdk4*$^{K35M/K35M}$; *Cdk4*$^{D140A/D140A}$; *Cdk4*$^{-/-}$ MEFs were co-infected with a plasmid containing a dominant negative version of the *Trp53* isoform as well as the activated form of the *Hras* oncogene known to transform MEFs (*Hras*^{G12V}/DN*Trp53*). After 15 days, multilayer foci were quantified. As previously reported, the capability of *Hras*^{G12V} to induce malignant transformation was significantly reduced in *Cdk4*$^{-/-}$ MEFs (Zou et al., 2002), whereas expression of both KD proteins induced an intermediate phenotype when compared to the wildtype MEFs (Figure 18B).

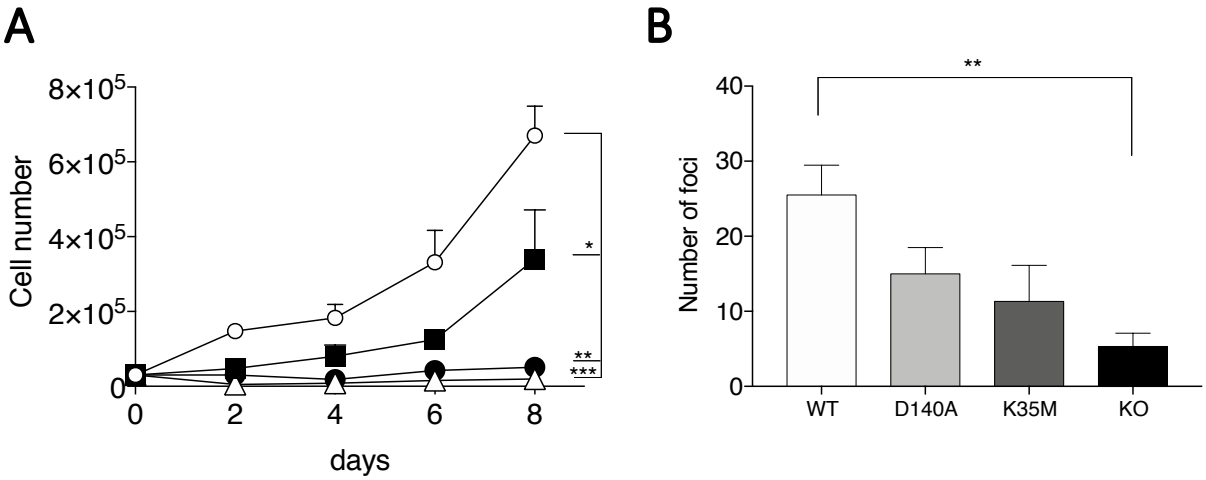

Figure 18: *In vitro* oncogenic susceptibility upon CDK4^{K35M} and CDK4^{D140A} expression
A) Proliferation of primary MEFs derived from *Kras*$^{+/LSLG12V}$;*Cdk4*$^{+/+}$ (empty circles), *Kras*$^{+/LSLG12V}$;*Cdk4*$^{D140A/D140A}$ (squares), *Kras*$^{+/LSLG12V}$;*Cdk4*$^{K35M/K35M}$ (triangles) and *Kras*$^{+/LSLG12V}$;*Cdk4*$^{-/-}$ (solid circles) embryos expressing Kras^{G12V} oncogene upon Cre mediated recombination. **B)** Quantification of the number of foci expressing *Hras*^{G12V}/DN*Trp53* of *Cdk4*$^{+/+}$ (white), *Cdk4*$^{D140A/D140A}$ (clear grey), *Cdk4*$^{K35M/K35M}$ (dark grey) and *Cdk4*$^{-/-}$ (black) primary MEFs. **p < 0.01, ANOVA test. Data are shown as mean ± SEM.

1.6. CDK4^{K35M} and CDK4^{D140A} kinase activity limit lung tumor initiation

It was demonstrated that complete CDK4 protein ablation impaired *Kras^{G12V}*-driven adenocarcinoma tumor formation (Puyol et al., 2010). Since, as discussed above, pharmacological inhibition targets the kinase activity of the protein, one of the objectives of the present thesis was to elucidate to what extent the expression of a KD isoform of CDK4 recapitulates the phenotype obtained when ablating the whole protein. Our hypothesis is that this approach targeting the kinase activity of the protein would mimic the effect of pharmacological inhibition being a better predictor of the phenotypic consequences of protein inhibition than the classical protein deletion model.

To that end, we took advantage of the *Kras^{LSLG12V}* allele (Guerra et al., 2003) and followed the *Tumor Initiation* protocol (See Material and Methods, Section: 1.4). We generated compound strains carrying the following alleles: *Kras$^{+/LSLG12V}$;Cdk4$^{+/+}$*, *Kras$^{+/LSLG12V}$;Cdk4$^{K35M/K35M}$* and *Kras$^{+/LSLG12V}$;Cdk4$^{D140A/D140A}$*. Briefly, this system allows for specific tumor induction in the lung tissue upon Cre-mediated recombination that allows for the expression of the *Kras^{G12V}* oncogene. However, once tumor induction takes place, these mice constitutively express the CDK4 KD isoforms, therefore this protocol only allow us to study the capability of the selected targets to impair or delay *Kras^{G12V}*-driven lung tumor formation rather than a therapeutic validation. A few *Kras$^{+/LSLG12V}$;Cdk4$^{-/-}$* were generated, for comparison purposes with the historical data of the laboratory.

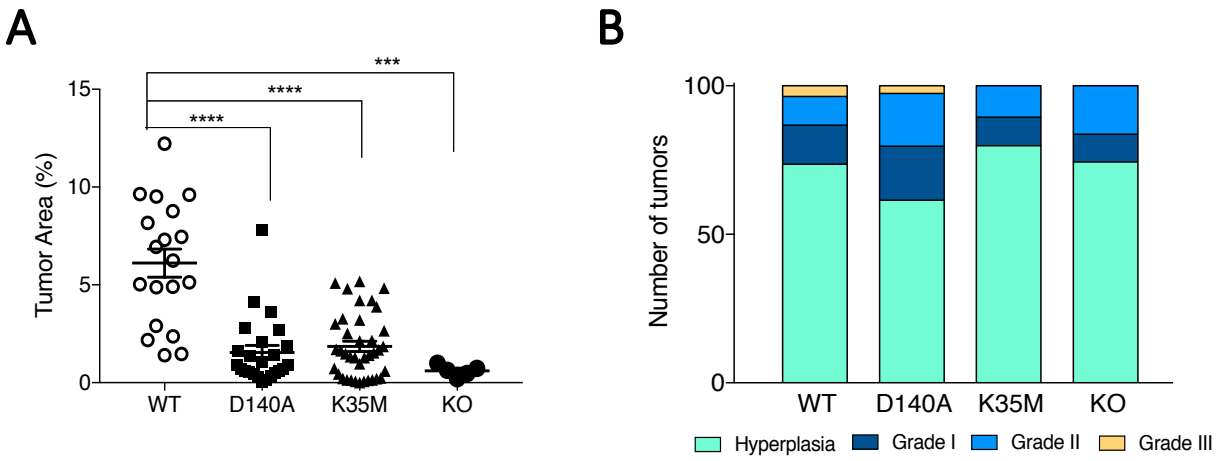

Figure 19: CDK4^{K35M} and CDK4^{D140A} impair lung tumor formation.
A) Quantification of the tumor burden of *Kras$^{+/LSLG12V}$;Cdk4$^{+/+}$* (open circles; n=12 mice), and *Kras$^{+/LSLG12V}$;Cdk4$^{D140A/D140A}$* (squares; n=16 mice), *Kras$^{+/LSLG12V}$;Cdk4$^{K35M/K35M}$* (triangles; n=21 mice), *Kras$^{+/LSLG12V}$;Cdk4$^{-/-}$* (solid circles; n=5 mice) mice. ****p < 0.0001, ***p < 0.001, ANOVA test. Data are shown as mean ± SEM. **B)** Tumor grading according to Jackson *et al.*, Cancer Research 2005.

Nevertheless, the results show that both KD models, CDK4^{K35M} and CDK4^{D140A} expression, significantly reduce tumor formation compared to the controls as measured by the percentage of tumoral area (WT: 6.1%±0.5, D140A:1.6%±0.4, K35M: 1.8%±0.3) although this effect was not as robust

as when eliminating the whole CDK4 protein, where almost complete abolishment of tumor formation was observed (KO: 0.61%±0.13) (Figure 19A), suggesting the existence of CDK4 kinase independent functions. In addition, the residual lesions analyzed 6 months after tumor induction show that CDK4 inactivation reduces tumors aggressiveness, especially when mutating the ATP binding site of the CDK4 protein ($CDK4^{K35M}$). In this group, lesions are merely of benign nature being small hyperplasias rather than adenomas (grade I and II) or adenocarcinomas (grade III and IV); in fact, no adenocarcinomas were observed upon $CDK4^{K35M}$ inactivation (Figure 19B).

1.7. CDK4 catalytic activity has a role in skin tumor development

CDK4 overexpression in epithelial tissues demonstrated that this kinase induces epidermal hyperproliferation, hypertrophy and increased malignant conversion, independently of the levels of D-type CYCLINs (Rodríguez-Puebla, 2002).

In order to further elucidate the differences between K35M and D140A expressing mutations in a *Ras* mutant epithelial model, a two-step carcinogen protocol was performed. We recapitulated the phenotype associated to CDK4 elimination described by Rodriguez-Puebla's group showing complete abrogation of skin tumor development. However, even though both KD models are able to promote papilloma development, expression of $CDK4^{K35M}$ mutation reduced more the amount and the number

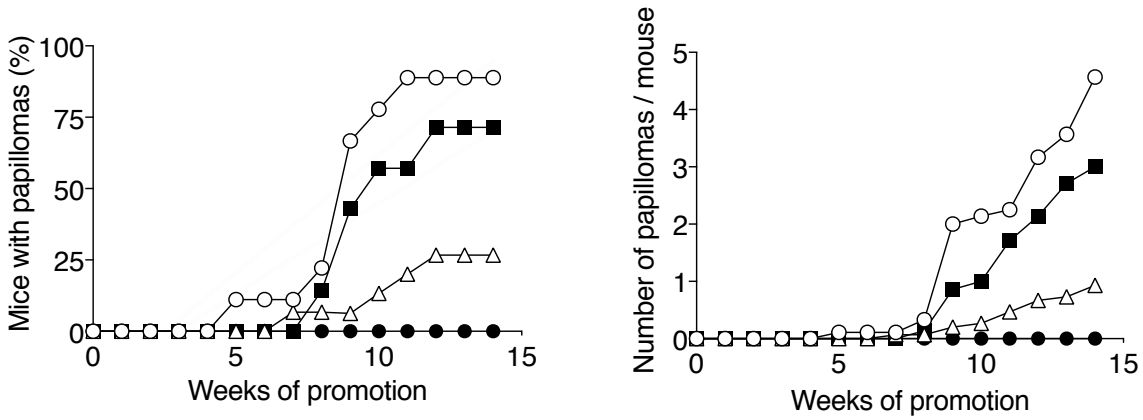

of papillomas than the expression of $CDK4^{D140A}$ mutant (Figure 20).

Figure 20: Mouse skin tumor development in $CDK4^{K35M}$ and $CDK4^{D140A}$ expressing mutants.
(Left) Incidence of papilloma development (percentage of mice which developed papillomas) and **(right)** papilloma multiplicity (average number of papillomas per mouse) in $Cdk4^{+/+}$ (empty circles; n=9 mice), $Cdk4^{K35M/K35M}$ (triangles; n=15 mice), $Cdk4^{D140A/D140A}$ (squares; n=7 mice), $Cdk4^{-/-}$ (solid circles; n=3 mice) mice during 14 weeks of DMBA/TPA treatment .

These results suggest that the increased keratinocyte proliferation is at least in part reliant on CDK4 catalytic independent functions.

1.8. Catalytic independent functions of CDK4 protein kinase may be related to CDK2

All the previous data together pointed to the fact that there are kinase independent functions for CDK4 that have to be determined. One possible explanation of the intermediate behavior of the KD models compared to the *Cdk4* deficient mice is the putative compensatory mechanisms that CDK2 could be mediating via CIP/KIP inhibitors. The dual role of $p21^{Cip1}$ and $p27^{Kip1}$ as either inhibitors (Peter M, 1994) or stabilizers of the CDK4/6-CYCLIND complexes (Cerqueira et al., 2014) is well defined. Our working hypothesis was that CDK4 KD alleles may still be able to bind to and titrate CIP/KIP away from CDK2. We were unable to validate this hypothesis in tumor samples due to the lack of LUAD development in the absence of CDK4. As an alternative, we immunoprecipitated CDK2 in *Kras*-driven MEFs carrying either $Cdk4^{+/+}$; $Cdk4^{K35M/K35M}$; $Cdk4^{D140A/D140A}$ or $Cdk4^{-/-}$ alleles and analyzed the levels of CDK2-bound $p21^{Cip1}$ and $p27^{Kip1}$ by Western blot (Figure 21A). In $Cdk4^{-/-}$ MEFs, CDK2 is highly bound to the CIP/KIP inhibitors (3,4-fold for $p27^{Kip}$ and 1,8-fold for $p21^{Cip1}$ compared to $Cdk4^{+/+}$ cells) suggesting that upon CDK4 ablation, $p21^{Cip1}$ and $p27^{Kip1}$ are inhibiting CDK2 and therefore these cells are not able to proliferate. This could be one of the reasons of the defects in proliferation associated to the $Cdk4^{-/-}$ mice (Tsutsui et al., 1999). Furthermore, in $CDK4^{K35M}$ and $CDK4^{D140A}$ KD expressing models, CDK2 is less bound to $p27^{Kip1}$ and $p21^{Cip1}$ than under conditions where the CDK4 protein is completely abolished although still, CDK2 co-immunoprecipitated 2,1-fold with $p27^{Kip1}$ and 1,5-folds with $p21^{Cip1}$ for the K35M and D140A mutations respectively compared to the $CDK4^{WT}$ (Figure 21B). This suggests that when CDK4 expresses a KD isoform, CDK4 is sequestering less $p27^{Kip1}$ and $p21^{Cip1}$ than $Cdk4^{-/-}$ cells, allowing some cells to enter in S phase by indirect CDK2 compensatory mechanisms.

A

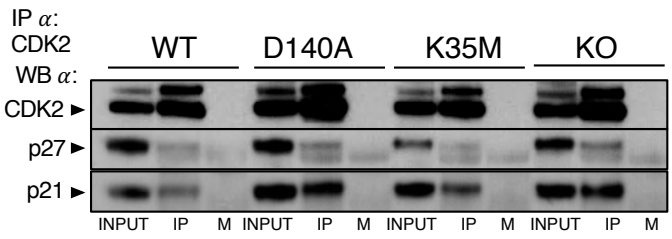

B

		WT	D140A	K35M	KO
p27/ CDK2	Ratio	0,1	0,14	0,21	0,34
	FC		1,4	2,1	3,4
p21/ CDK2	Ratio	0,7	1	0,7	1,2
	FC		1,5	1,05	1,8

Figure 21: Kinase independent functions of CDK4.
A) Western blot analysis of CDK2, p27 and p21 expression in MEFs containing $Kras^{+/LSLG12V}$;$Cdk4^{+/+}$ (WT), $Kras^{+/LSLG12V}$;$Cdk4^{D140A/D140A}$ (D140A), $Kras^{+/LSLG12V}$;$Cdk4^{K35M/K35M}$ (K35M) and $Kras^{+/LSLG12V}$;$Cdk4^{-/-}$ (KO) immunoprecipitated with CDK2 antibodies. **B)** Quantification of the p27/CDK2 and p21/CDK2 protein level ratios and FCs compared to the WT sample using ImageJ software. WT: wild type; KO: Knock-out; IP: Immunoprecipitation; INPUT: 10% of the whole lysate extract; M: Mock; FC: Fold Change.

Therapeutic evaluation of concomitant CDK4 and RAF1 target inactivation

2.1. Genetic inactivation of CDK4 kinase activity in established mutant Kras^{G12V}-driven tumors induce a minimal tumor regression

In order to mimic CDK4 pharmacological scenario we decided to study its potential role as a putative therapeutic target in established *Kras^{G12V}*-driven LUADs using a CDK4 KD model. Although the differences between both mutations, K35M and D140A, were no so evident, there was a tendency of CDK4^{K35M} expression being more similar to the lack of CDK4 protein: less *in vitro* proliferation rate, less capability to initiate lung tumors with a less aggressive phenotype and less potential to induce skin carcinogenesis, than the D140A mutation. While the molecular basis underlying these differences observed between the two KD models remains to be elucidated, we decided to utilize the *Cdk4^{K35M}* allele for the rest of the study.

We took advantage of a mouse model already used in the laboratory which recapitulates most of the features of a human lung tumor: *Kras$^{+/G12V}$;Trp53$^{F/F}$*. It consists of two independent recombinase systems to temporally and spatially separate tumor induction from target inactivation (Sanclemente et al., 2018). In LUAD patients the therapeutic treatment is administered upon diagnosis. Likewise, in our model tumor induction occurs first, followed by the systemic target inactivation. Briefly, *Kras^{G12V}* oncogene expression is induced specifically in lung tissue by intranasal instillation of adenoviruses encoding for the Flp recombinase (AdFlp) which recognizes the frt (F) sequences of the conditional alleles. Then, after tumor development is confirmed by Computed Tomography (CT) image analysis, mice harboring at least one CT detectable tumor, are fed *ad libitum* with a Tamoxifen (TX)-containing diet which will translocate the Cre recombinase to the nucleus in order to inactivate the conditional target/s. Tumors are subsequently evaluated by consecutive CT measurements every 3 weeks and anti-tumor efficacy upon target inactivation is analyzed using the Response Evaluation Criteria in Solid Tumors (RECIST) (Table 6).

Table 6: Tumor classification according to the RECIST

Category	RECIST
CR	Disappearance of all tumoral lesions
PR	Reduction of > 30% of the initial tumor size
SD	Reduction of < 30% of the initial tumor size
PD	Growth in total tumor size

RECIST: Response Evaluation Criteria in Solid Tumors; CR: Complete Response; PR: Partial Response; SD: Stable Disease; PD: Progression Disease.
The SD category has been modified from the original RECIST criteria and included in the PD category when tumors grow >20%.
Adapted from Gruber-Rouh T; World J Clin Oncol. 2017.

The hypomorphic nature of the conditional CDK4^{K35M} allele (Results Section 1.2) prevented us from using homozygous animals. In order to mimic pharmacological inhibition we used double heterozygous mice carrying a standard *Cdk4* floxed allele (kindly provided by Lluis Fajas, Lausanne and published in (Lagarrigue et al., 2016)) together with the *Cdk4*^{FlexK35M} allele. With this allelic combination, Cre-mediated recombination of the conditional *Cdk4*$^{FlexK35M/L}$ strain stops expressing the wildtype CDK4 protein from the floxed allele inducing at the same time the expression of the CDK4^{K35M} KD isoform from the targeted Flex allele (Figure 22).

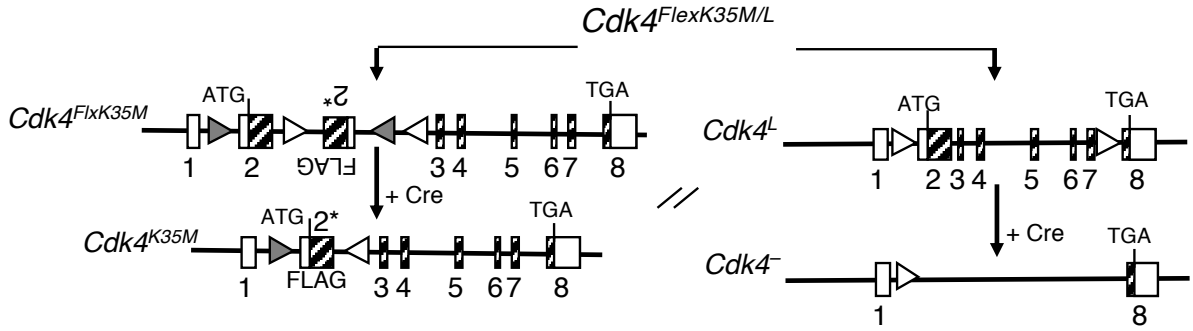

Figure 22: Schematic representation of the *Cdk4*^{FlexK35M} and the *Cdk4*^{L} alleles and their modifications following Cre recombinase mediated genetic recombination. Exons (boxes), wildtype loxP sites (white triangles), mutated loxP sites (grey triangles). The modified exon 2, driving expression for the subsequent K35M mutant protein is indicated (*).

In addition, this experimental *Therapeutic model* allows us to determine potential systemic toxic effects since the elimination of the targets occurs ubiquitously in the whole body of the mice mimicking a pharmacological treatment. To that end, we exposed non-tumor bearing mice (*Kras*$^{+/+}$; *Cdk4*$^{FlexK35M/L}$;*hUBC-CreERT2*$^{+/T}$) to a TX containing diet at 8 months after birth (same time point at which tumor-bearing mice are exposed to TX).

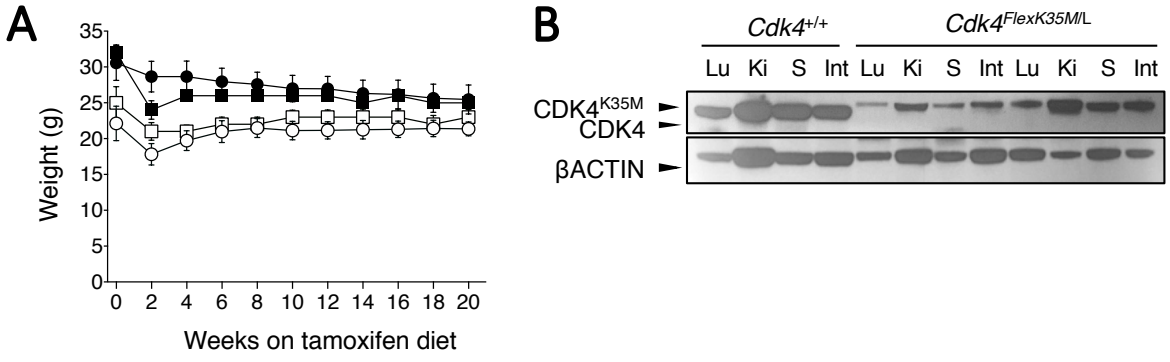

Figure 23: CDK4 systemic catalytic inactivation is not toxic
A) Body weight change in grams (g) of non-tumor-bearing male mice (solid) and female mice (open) exposed to TX for 20 weeks. *Cdk4*$^{+/+}$;*hUBC-CreERT2*$^{+/T}$ (circles) and *Cdk4*$^{FlexK35M/L}$;*hUBC-CreERT2*$^{+/T}$ (squares) mice. n=5 mice/group. Data are shown as means ± SEM. **B)** Western blot analysis of CDK4 expression in tissue lysates from organs of *Cdk4*$^{+/+}$;*hUBC-CreERT2*$^{+/T}$ and *Cdk4*$^{FlexK35M/L}$;*hUBC-CreERT2*$^{+/T}$ mice after 9 weeks of TX exposure. βACTIN was used as loading control. Migration of the above proteins is indicated by arrowheads. Lu: lung; Ki: kidney; S: spleen; Int: intestine.

After analyzing the body weight of these mice compared to the *Cdk4*$^{+/+}$ control strain, we did not observe significant deleterious phenotypes nor changes in the body weight of these mice during 20 weeks, thus indicating that no toxicity is associated to ubiquitous CDK4 KD expression (Figure 23A). Moreover, after 9 weeks in TX diet all adult mouse tissues analyzed exclusively expressed the CDK4^{K35M} isoform as shown by Western blot (Figure 23B).

To further study the therapeutic effect of *Cdk4* inactivation, compound mouse strains were generated by crossing the *Kras*$^{+/FSFG12V}$ allele for lung tumor induction with the *Cdk4*$^{FlexK35M/L}$ and *hUBC-CreERT2* alleles for systemic target inactivation. Of note, this cohort of mice has the *Trp53* tumor suppressor unaltered. Next, we designed an experimental trial with a cohort of 51 individual tumors from 18 *Kras*$^{+/FSFG12V}$*;Cdk4*$^{FlexK35M/L}$*;hUBC-CreERT2*$^{+/T}$ mice from which finally 44 tumors could be followed by CT until the end of the 9-week experiment. In 20% of the cases CDK4 inactivation induces tumor regression with only 9% of these reaching PR (Partial Response) based on RECIST. The rest (80%) of the tumors showed PD (Progressive Disease). However, they grew much slower in comparison with the control group (2.7 % FC *Cdk4*$^{+/+}$ vs. -3.8 % FC *Cdk4*$^{FlexK35M/L}$), being able to delay tumor promotion but not to induce significant regression in already formed tumors (Figure 24A and 24B).

A

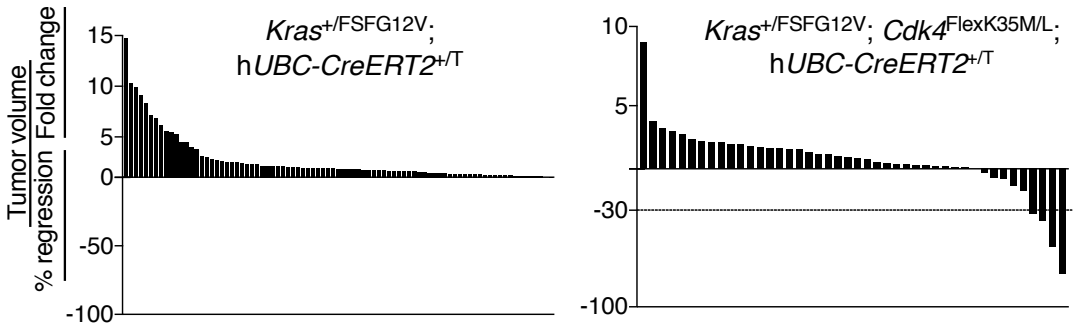

B

Kras$^{+/FSFG12V}$	*Cdk4*$^{+/+}$		*Cdk4*$^{FlexK35M/L}$	
	Number T		Number T	
Final Number T	85		44	
SD	0	0%	5	11%
PR (>30%)	0	0%	4	9%
CR	0	0%	0	0%
PD	0	100%	35	80%

Figure 24: Genetic inhibition of CDK4 kinase activity in established mutant *Kras*^{G12V}-driven tumors induce minimal tumor regression

A) (Left) Waterfall plot representing the tumor volume fold change and the % of regression of individual CT+ lung tumors present in *Kras*$^{+/FSFG12V}$*;hUBC-CreERT2*$^{+/T}$ (n=25mice/85tumors) and **(right)** *Kras*$^{+/FSFG12V}$*;hUBC-CreERT2*$^{+/T}$*;Cdk4*$^{FlexK35M/L}$ (n=18mice/44 tumors) mice exposed to TX for 9 weeks. **B)** Table resuming the data of the above-mentioned waterfall plots representing the number and percentage of tumors (T) that show Partial Response (PR), Complete Response (CR), Progression Disease (PD) and Stable Disease (SD). The changes in tumor volumes depicted (A-B) were calculated for each individual tumor based on CT scans performed at the beginning and at the end of the 9-week-long trial.

To take into account other additional alterations observed in human disease we crossed our strains with *Trp53*$^{F/F}$ alleles since the loss of function of the tumor suppressor *TP53* is a very common event, accounting for 46% of the KRAS human LUAD cases (Chen et al., 2014). In mice p53, loss induces more aggressive adenocarcinomas and prompts more rapid tumor (Jackson et al., 2005; Sanclemente et al., 2018). This approach allowed us to study the effect of CDK4 inactivation in a more aggressive tumor context. From 27 mice carrying *Kras*$^{+/FSFG12V}$;*Trp53*$^{F/F}$;*Cdk4*$^{FlexK35M/L}$;*hUBC-CreERT2*$^{+/T}$ alleles (further referred as: *Cdk4*$^{K35M/L}$) 11% of the tumors regressed, but only 7% of regressors elicited PR after CDK4 inactivation, suggesting that inhibition of CDK4 kinase solely does not impair significantly tumor development (Figure 25A and 25B). This was not due to inefficient target recombination as complete protein excision was detected in almost all the tumors analyzed (n=12 mice; 14 tumors) after 9 weeks of TX diet (Figure 25C).

A

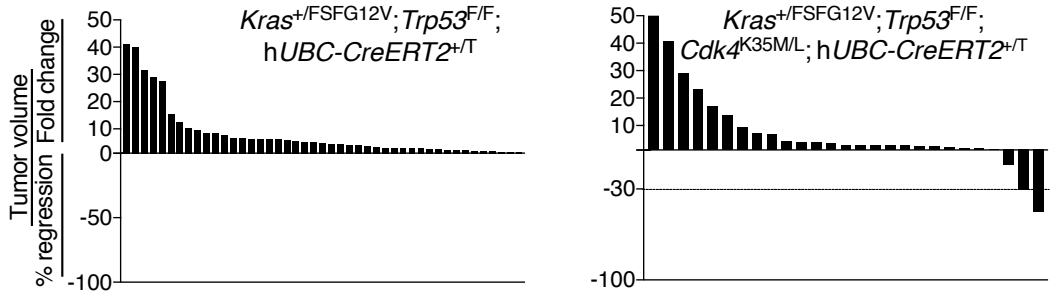

B

Kras$^{+/FSFG12V}$	*Cdk4*$^{+/+}$; *Trp53*$^{F/F}$		*Cdk4*$^{K35M/L}$; *Trp53*$^{F/F}$	
	Number T		Number T	
Final Number T	45		27	
SD	0	0%	1	4%
PR (>30%)	0	0%	2	7%
CR	0	0%	0	0%
PD	0	100%	24	89%

C

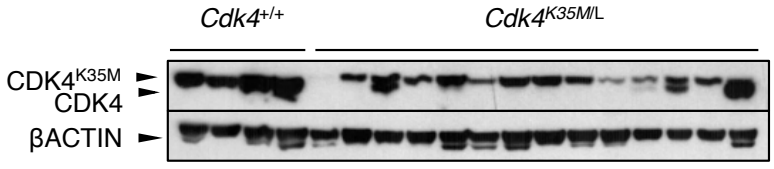

Figure 25: Genetic inhibition of CDK4 kinase activity in established mutant *Kras*^{G12V}-driven, *Trp53* deleted tumors induce minimal tumor regression

A) (Left) Waterfall plot representing the tumor volume fold change and the % of regression of individual CT^{+} lung tumors present in *Cdk4*$^{+/+}$ (n=14mice/45tumors) mice and **(right)** *Cdk4*$^{K35M/L}$ (n=16mice/28tumors) mice exposed to TX for 9 weeks. **B)** Table resuming the data of the above-mentioned waterfall plots representing the number and percentage of tumors (T) that show Partial Response (PR), Complete Response (CR), Progression Disease (PD) and Stable Disease (SD). The changes in tumor volumes depicted (A-B) were calculated for each individual tumor based on CT scans performed at the beginning and at the end of the 9-week-long trial. **C)** Western blot analysis of CDK4 expression in tumor lysates from *Cdk4*$^{+/+}$ and *Cdk4*$^{K35M/L}$ mice after 9 weeks of TX exposure. βACTIN was used as loading control.

2.2. Combinatorial therapies against Kras^{G12V}- driven LUAD: RAF1 protein ablation

CDK4/6 inhibitors (Palbociclib, Abemaciclib and Ribociclib) have been first approved for the treatment of ER-positive breast cancer (Beaver et al., 2015; Corona and Generali, 2018; Tripathy et al., 2018). A phase II clinical trial studied the efficacy of Palbociclib in patients with pre-treated advanced NSCLC. Unfortunately, no tumor regressions were observed albeit 50% of the patients enrolled in the trial showed SD (Gopalan et al., 2018). Monotherapy has demonstrated to not to be to very effective for patients, therefore it is mandatory to find combinatorial therapies in order to potentiate the efficacy and reduce the resistant mechanisms associated to these inhibitors (Goldman et al., 2018; Gopalan et al., 2018; Pacheco and Schenk, 2019). These results are in agreement with our genetically engineered mouse model, where CDK4 inactivation alone is not sufficient to eradicate lung cancer. We hypothesized that the concomitant inactivation of two single targets at different levels could lead to synergistic effects in LUAD. Consequently, searching for additive or synergistic effects we proposed the inhibition of CDK4 combined with RAF1 protein deletion based on (i) their role over cell cycle (ii) their implications in signaling downstream of mutant KRAS, (iii) their nature to become druggable, (iv) their non-essential role in adult homeostasis and (v) their validated therapeutic benefit in LUAD (Blasco et al., 2011; Puyol et al., 2010; Sanclemente et al., 2018).

Unpublished data from our laboratory indicate that RAF1 kinase independent functions are essential in *Kras^{G12V}*driven LUAD. Therefore, we decided to genetically ablate RAF1 protein as it showed a significant regression of LUAD tumors with tolerable toxicities (Sanclemente et al., 2018).

First, we analyzed the possible toxicity issues associated to the concomitant target inhibition. Again, we exposed non-tumor bearing mice *Kras$^{+/+}$;Cdk4$^{FlexK35M/L}$;Raf1$^{L/L}$;hUBC-CreERT2$^{+/T}$* to a TX containing diet at 8 months after birth as this would be approximately the time when a therapeutic approach with CT+ tumors would be initiated. We first analyzed the recombination efficiency by quantifying protein expression levels in several tissues of mice expressing *Cdk4$^{FlexK35M/L}$;Raf1$^{L/L}$* alleles. As shown in the Figure 26A both targets are properly ablated after 9 weeks of TX exposure. To deeper evaluate the status of these two cohorts of mice in a long-term trial, mice were fed on TX-containing diet during 20 weeks. *Cdk4$^{FlexK35M/L}$;Raf1$^{L/L}$* male mice exhibit a slight reduction in body weight (Figure 26B), however the reasons of this reduction in body weight need for further analysis because no histopathological differences were observed between control mice (*Cdk4$^{+/+}$;Raf1$^{+/+}$*) and combined target inactivated mice (*Cdk4$^{FlexK35M/L}$;Raf1$^{L/L}$*) (Figure 26C) when analyzing representative sections of several tissues at the same time of TX exposure normal histopathology in *Cdk4$^{FlexK35M/L}$;Raf1$^{L/L}$* mice comparing with the wildtype cohort (Figure 26D). Thus, CDK4 and RAF1 pharmacological co-targeting should be considered as a putative treatment for LUAD patients since it does not induce undesirable toxicities.

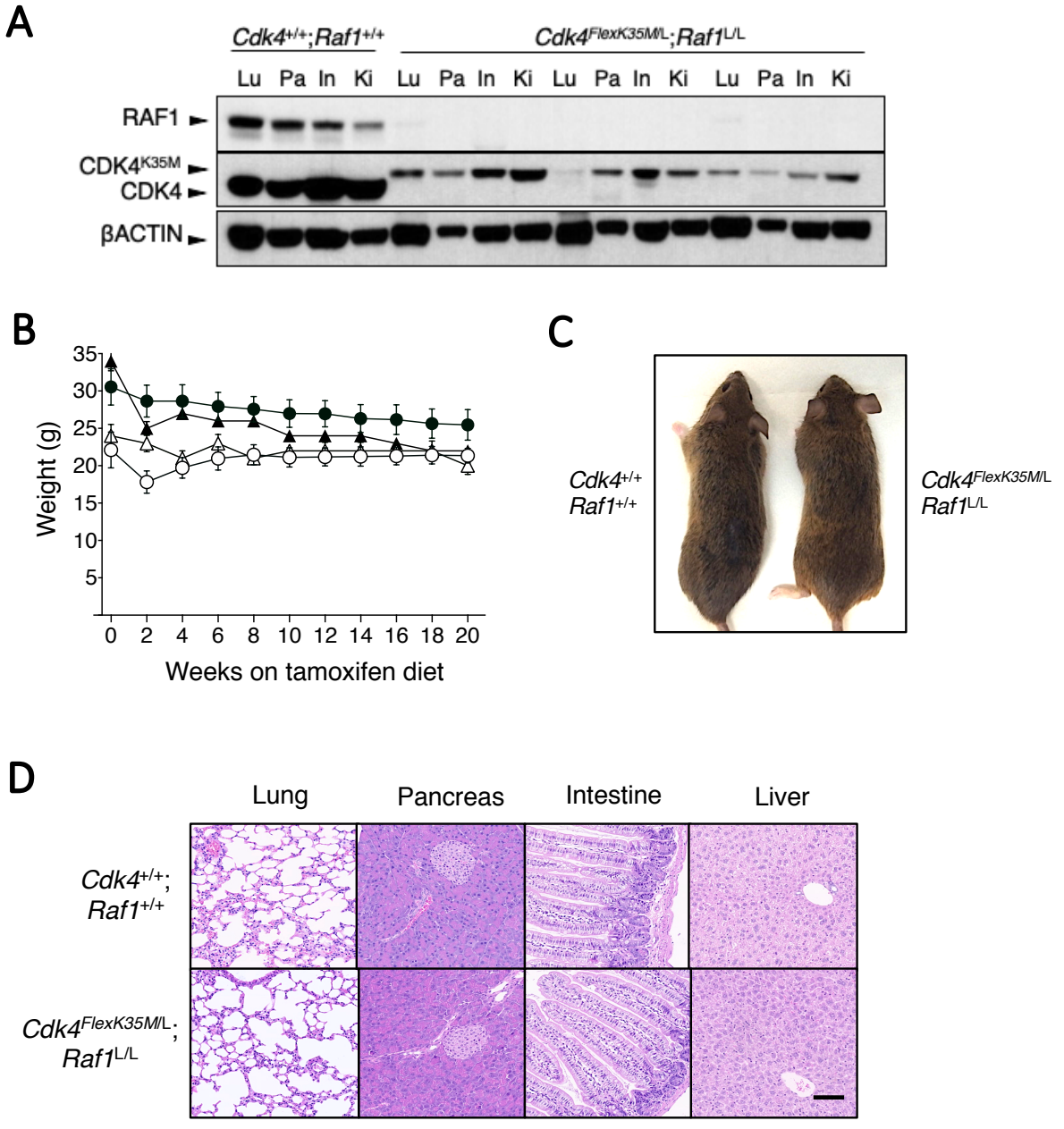

Figure 26: Concomitant genetic inhibition of CDK4 and RAF1 induces tolerable toxicities

A) Western blot analysis of RAF1 and CDK4 expression in tissue lysates from organs of *Cdk4*$^{+/+}$;*Raf1*$^{+/+}$;*hUBC-CreERT2*$^{+/T}$ and *Cdk4*$^{FlexK35M/L}$;*Raf1*$^{L/L}$;*hUBC-CreERT2*$^{+/T}$ after 9 weeks of TX exposure. βACTIN was used as loading control. Migration of the above proteins is indicated by arrowheads. Lu: lung; Pa: pancreas; In: intestine; Ki: kidney. **B)** Body weight change in grams (g) of non-tumor-bearing male mice (solid) and female mice (open) exposed to TX for 20 weeks. *Cdk4*$^{+/+}$;*Raf1*$^{+/+}$;*hUBC-CreERT2*$^{+/T}$ (circles) and *Cdk4*$^{FlexK35M/L}$;*Raf1*$^{L/L}$;*hUBC-CreERT2*$^{+/T}$ (triangles). n=5mice/group. Data are shown as means ± SEM. **C) (Left)** Representative photos of *Cdk4*$^{+/+}$;*Raf1*$^{+/+}$;*hUBC-CreERT2*$^{+/T}$ and **(right)** *Cdk4*$^{FlexK35M/L}$;*Raf1*$^{L/L}$;*hUBC-CreERT2*$^{+/T}$ mice at 20 weeks after continuous exposure to TX. **D) (Upper panel)** Representative pictures of H&E stained histological sections of paraffin embedded organs of *Cdk4*$^{+/+}$;*Raf1*$^{+/+}$;*hUBC-CreERT2*$^{+/T}$ and **(lower panel)** *Cdk4*$^{FlexK35M/L}$;*Raf1*$^{L/L}$;*hUBC-CreERT2*$^{+/T}$ mice at 20 weeks after continuous exposure to TX. Scale bar: 0.1 mm.

To properly compare single from combined target inactivation in a *Trp53* proficient background, 16 *Kras*$^{+/FSFG12V}$;*Raf1*$^{L/L}$;*hUBC-CreERT2*$^{+/T}$ tumor bearing mice were enrolled in the experimental trial. As previously described (Sanclemente et al., 2018) RAF1 ablation provides significant therapeutic benefit as single target. In the current study, 73% of the tumors showed PR (Figure 27A and 26B). Furthermore, RAF1 ablation induces CR in 12% of the cases but still, 6% of the tumors showed SD after 9 weeks of TX exposure. This data suggests that, as for CDK4, RAF1 ablation alone may not be sufficient to completely eradicate LUAD, so combination of both targeted therapies could provide a potential clinical benefit. To further study this, 15 tumor bearing mice carrying *Kras*$^{+/FSFG12V}$;*Cdk4*$^{K35M/L}$;*Raf1*$^{L/L}$;*hUBC-CreERT2*$^{+/T}$ alleles were enrolled in the trial. From them, 100% of the tumors regressed with 26% reaching CR. Furthermore, no detectable PD or even SD tumors were observed (Figure 27A and 27B).

A

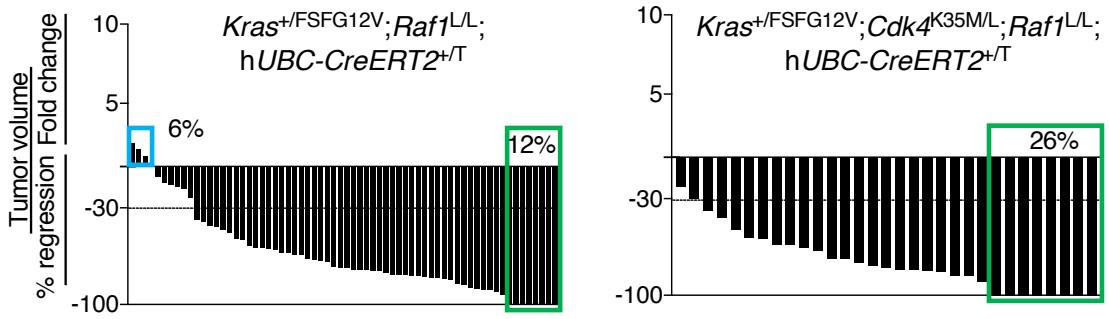

B

Kras$^{+/FSFG12V}$	*Raf1*$^{L/L}$		*Cdk4*$^{K35M/L}$; *Raf1*$^{L/L}$	
	Number T		Number T	
Final Number T	66		31	
SD	6	9%	2	6%
PR (>30%)	48	73%	21	68%
CR	8	12%	8	26%
PD	4	6%	0	0%

Figure 27: Complete regression of *Kras*^{G12V}-driven adenocarcinoma upon combined inhibition of CDK4 and RAF1

A) Waterfall plot representing the tumor volume fold change and the % of regression of individual CT^{+} lung tumors present in *Kras*$^{+/FSFG12V}$;*Raf1*$^{L/L}$;*hUBC-CreERT2*$^{+/T}$ (n=16mice/66tumors) and *Kras*$^{+/FSFG12V}$;*Cdk4*$^{K35M/L}$;*Raf1*$^{L/L}$;*hUBC-CreERT2*$^{+/T}$ (n=15mice/31tumors) exposed to TX for 9 weeks. **B)** Table resuming the data of the above-mentioned waterfall plots representing the number and percentage of tumors (T) that show Partial Response (PR), Complete Response (CR), Progression Disease (PD) and Stable Disease (SD). The changes in tumor volumes depicted (A-B) were calculated for each individual tumor based on CT scans performed at the beginning and at the end of the 9-week trial.

Next, we carried out a therapeutic study in a *Trp53* deficient background. To do so, we decided to generate a new cohort of mice rather than rely in historical data. In our hands, 10% of the tumors completely regressed upon RAF1 ablation in a *Trp53* deficient background. But, from the 12 *Kras*$^{+/FSFG12V}$;*Trp53*$^{F/F}$;*Raf1*$^{L/L}$;*hUBC-CreERT2*$^{+/T}$ tumor bearing mice included in the trial (further referred as: *Raf1*$^{L/L}$) 24% of the lesions showed PD (Figure 28A and 28B). This is in agreement with the results observed by Sanclemente et al. Importantly, from the 19 *Kras*$^{+/FSFG12V}$;*Trp53*$^{F/F}$;*Cdk4*$^{FlexK35M/L}$;*Raf1*$^{L/L}$;*hUBC-CreERT2*$^{+/T}$ mice enrolled in the study (further referred as: *Cdk4*$^{K35M/L}$;*Raf1*$^{L/L}$), 24% of the tumors show CR upon combined inactivation of both targets and outstandingly, no PD neither SD was observed upon target inactivation (Figure 28A and 28B). Moreover, according to RECIST 66% of the tumors diminished their initial size over the 30% established. Of note, including the CR, more than 90% of the tumors regressed over 30% according to the clinical standards.

A

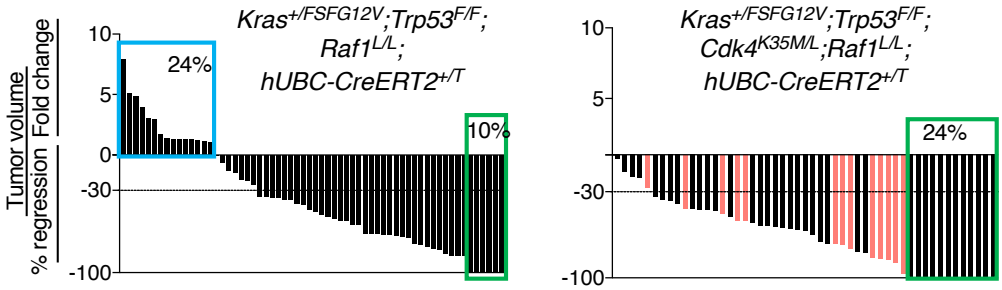

B

Kras$^{+/FSFG12V}$	*Raf1*$^{L/L}$; *Trp53*$^{F/F}$		*Cdk4*$^{K35M/L}$; *Raf1*$^{L/L}$; *Trp53*$^{F/F}$	
	Number T		Number T	
Final Number T	62		51	
SD	7	11%	5	10%
PR (>30%)	34	55%	34	66%
CR	6	10%	12	24%
PD	15	24%	0	0%

Figure 28: Complete regression of *Kras*^{G12V}-driven, *Trp53* deleted tumors upon combined inhibition of CDK4 and RAF1

A) Waterfall plot representing the tumor volume fold change and the % of regression of individual CT^{+} lung tumors present in *Raf1*$^{L/L}$; (n=12mice/62tumors) and *Cdk4*$^{K35M/L}$;*Raf1*$^{L/L}$ (n=19mice/55tumors) mice exposed to TX for 9 weeks. **B)** Table resuming the data of the above-mentioned waterfall plots representing the number and percentage of tumors (T) that show Partial Response (PR), Complete Response (CR) and Progression Disease (PD) and Stable Disease (SD). The changes in tumor volumes depicted (A-B) were calculated for each individual tumor based on CT scans performed at the beginning and at the end of the 9-week-long trial

All together, these data suggest an additive effect of CDK4 and RAF1 inactivation that could lead to a therapeutic benefit for patients suffering KRAS-driven LUAD in both contexts, *Trp53* proficient and deficient backgrounds.

2.3. CDK4 and RAF1 cooperate to reduce tumor proliferation and induce cell death in vivo

In order to evaluate the cooperation between CDK4 and RAF1 at histological levels we first analyzed a subset of residual tumors (Figure 29A, marked as red bars) by laser capture micro-dissection. As shown in Figure 29A both alleles were efficiently recombined in all the residual tumor cells, however, despite the fact of having proper target excision, most of those tumors stayed as stable disease during several weeks (Figure 29B).

A

	Δ *Cdk4* lox	Δ *Cdk4* K35M	Δ *Raf1* lox	Percentage regression
T1	100%	100%	100%	44
T2	79%	96%	0%	83
T3	100%	92%	99%	85
T4	99%	98%	85%	88
T5	100%	90%	99%	26.9
T6	95%	97%	98%	39.9
T7	100%	95%	98%	53.8
T8	100%	85%	100%	72.1
T9	83%	96%	84%	72.2
T10	98%	98%	95%	76.4
T11	99%	95%	95%	79.6
T12	100%	94%	100%	84.5
T13	77%	94%	100%	96.4

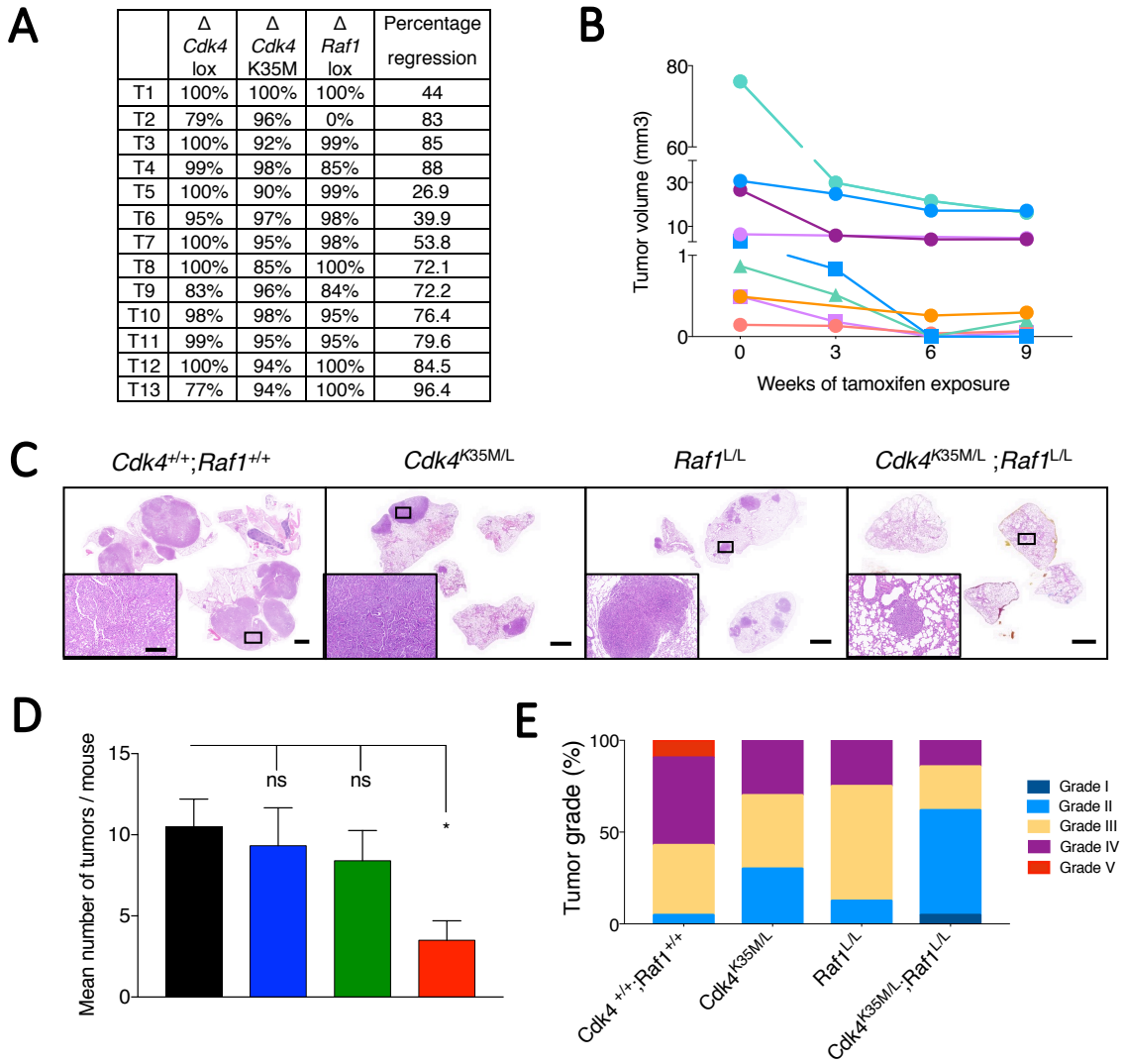

Figure 29: Concomitant inactivation of CDK4 and RAF1 significantly reduces tumor burden

A) Table representing the percentage of *Cdk4* and *Raf1* alleles recombination and tumor regression. **B)** Tumor volume growth curve of residual tumors upon combined inactivation of CDK4 and RAF1 (n=6 mice/10 tumors). **C)** H&E staining of paraffin sections of whole lungs from the indicated genotypes after 9 weeks of TX exposure. Scale bar of panoramic view: 2mm. Scale bar of the magnification: 0.2mm. **D)** Quantification of the mean tumor number per mouse present in $Kras^{+/FSFG12V};Trp53^{F/F};hUBC\text{-}CreERT2^{+/T}$ harboring the following alleles $Cdk4^{+/+};Raf1^{+/+}$ (n=4); (black bars), $Cdk4^{K35M/L}$ (n=6); (blue bars), $Raf1^{L/L}$ (n=10); (green bars) and $Cdk4^{K35M/L};Raf1^{L/L}$ (n=8); (red bars) mice after 9 weeks of TX exposure. *p < 0.05, Mann Whitney test. Data are shown as mean ± SEM. **E)** Percentage of histological grades of tumors present in $Kras^{+/FSFG12V};Trp53^{F/F};hUBC\text{-}CreERT2^{+/T}$ mice harboring the following alleles: $Cdk4^{+/+};Raf1^{+/+}$ (n=4), $Cdk4^{K35M/L}$ (n=3), $Raf1^{L/L}$ (n=10) and $Cdk4^{K35M/L};Raf1^{L/L}$ (n=8) mice after 9 weeks on TX diet.

Histo-pathological analysis of these samples also revealed less tumor numbers in the combined *Cdk4*$^{K35M/L}$;*Raf1*$^{L/L}$ group compared to the single target inhibition (*Cdk4*$^{K35M/L}$ or *Raf1*$^{L/L}$) and the controls (*Cdk4*$^{+/+}$;*Raf1*$^{+/+}$) (Figure 29C and 29D) confirming again the high percentage of complete regressions previously assessed by CT imaging. In addition, the residual tumors analyzed after CDK4 and RAF1 inactivation are less aggressive than the controls and the single targeted ones (Figure 29E) following the grading criteria of Jackson et al., (Jackson et al., 2005).

Moreover, there was an additive effect in terms of proliferation upon concomitant CDK4 and RAF1 inactivation since these tumors proliferated significantly less as it is shown by Ki67 immuno-staining (Figure 30A). As we previously reported (Sanclemente et al., 2018), single RAF1 ablation (*Raf1*$^{L/L}$) induced apoptosis so we were wondering if this effect would be enhanced upon simultaneous inhibition of both targets (*Cdk4*$^{K35M/L}$;*Raf1*$^{L/L}$). As shown in Figure 30A apoptosis was increased in the residual tumors upon CDK4 and RAF1 concomitant inactivation, determined by cleaved Caspase 3 immunohistochemistry.

It was previously described that ablation of CDK4 in *Kras*^{G12V} advanced lung tumors induced cellular senescence in a *Trp53* proficient background (Puyol et al., 2010). So, the next question we raised was if the same effect occurs when expressing the Cdk4K35M KD allele in a *Trp53* deficient background. To do so, we assayed for senescence-associated beta-galactosidase (SA-β-gal) activity and showed that SA-β-gal activity was not significantly induced in none of the 3 groups when compared to control tumors (Figure 30B).

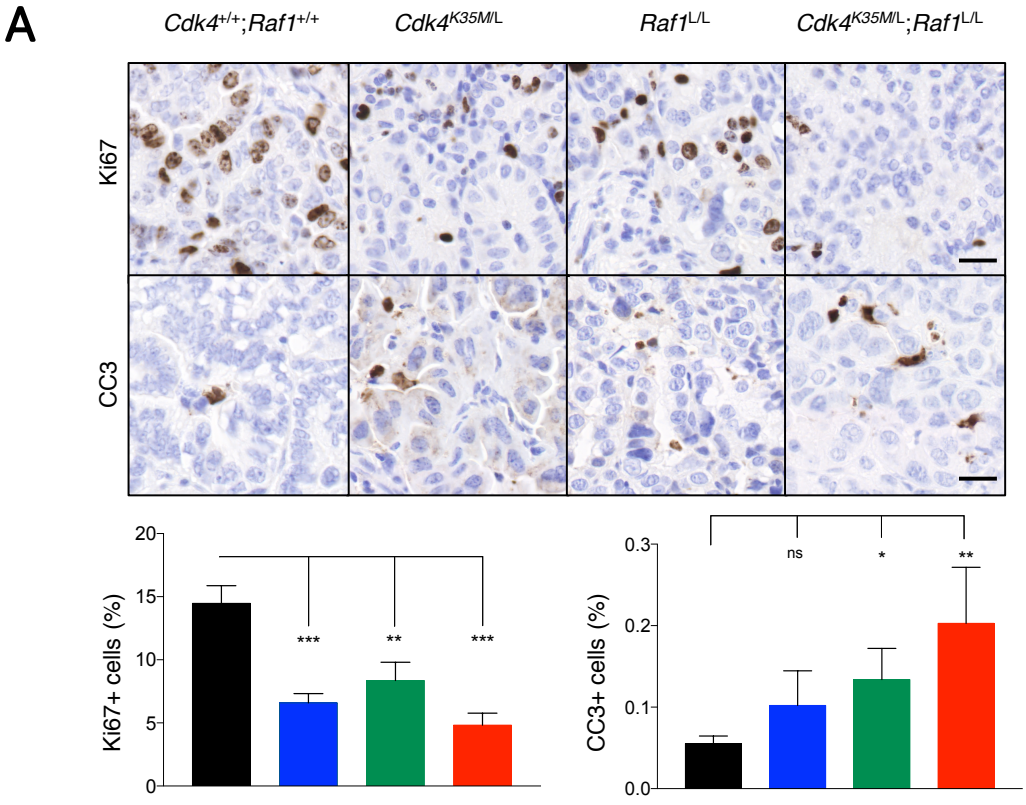

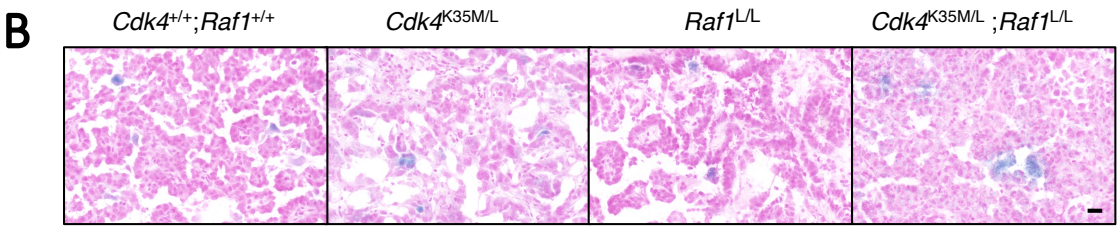

Figure 30: RAF1 and CDK4 cooperate together to reduce tumor proliferation and induce cell death
A) (Upper panels) KI67 and Cleaved Caspase 3 (CC3) staining and **(bottom panels)** quantification in paraffin embedded serial sections of tumors from *Kras*$^{+/FSFG12V}$;*Trp53*$^{F/F}$;*hUBC-CreERT2*$^{+/T}$ mice harboring the following alleles: *Cdk4*$^{+/+}$;*Raf1*$^{+/+}$ (n=3mice/28tumors); (black bars), *Cdk4*$^{K35M/L}$ (n=3/28tumors); (blue bars), *Raf1*$^{L/L}$ (n=3/23tumors); (green bars), *Cdk4*$^{K35M/L}$;*Raf1*$^{L/L}$ (n=8/28tumors); (red bars) after 9 weeks of TX exposure. Scale bar: 0,02mm Scale bar: 0,02mm. ***p < 0.001, **p < 0.01, *p < 0.05, unpaired Student's t test. Data are shown as means ± SEM. **B)** Representative pictures of X-Gal staining in tumors from *Kras*$^{+/FSFG12V}$;*Trp53*$^{F/F}$;*hUBC-CreERT2*$^{+/T}$ mice harboring the following alleles: *Cdk4*$^{+/+}$;*Raf1*$^{+/+}$, *Cdk4*$^{K35M/L}$, *Raf1*$^{L/L}$ *and Cdk4*$^{K35M/L}$;*Raf1*$^{L/L}$ after 9 weeks of TX exposure

Previous studies have shown that recruitment of immune cells plays a role in the regression of lung tumors (DuPage and Jacks, 2013; DuPage et al., 2012). We next interrogated the immune-profile of the lesions from our mice and we saw increased infiltration of CD3$^+$ T lymphocytes (Figure 31A), CD4$^+$ T helper cells (Figure 31B), and CD8$^+$ cytotoxic T cells (Figure 31C), in the *Cdk4*$^{K35M/L}$, *Raf1*$^{L/L}$ and *Cdk4*$^{K35M/L}$;*Raf1*$^{L/L}$ tumors compared to the wildtype controls.

Moreover, in order to analyze other possible cytotoxic lymphocytes in addition to T cells a double GranzymeB/CD8 staining was performed (Figure 31D). Granzymes are dominant constituents of the cytolytic granules expressed by NK cells and cytotoxic T cells (Pardo et al., 2009). Quantification of GranzymeB$^+$ but CD8$^-$ cell population showed an increase of, most likely, NK cells upon CDK4 and RAF1 inactivation when compared to the single target inhibition and the wildtype controls (Figure 31D).

Infiltrating F4/80$^+$ macrophages were slightly reduced when inactivating both targets concomitantly (*Cdk4*$^{K35M/L}$;*Raf1*$^{L/L}$) compared to the control tumors (*Cdk4*$^{+/+}$;*Raf1*$^{+/+}$) but the difference was not significant (Figure 31E). Given the lack of augmentation of the infiltrating immune cells on the combined treatment compared to the single target inactivation in the residual tumors, it remains to be determined to what extent these inflammatory responses contributed to the observed therapeutic response.

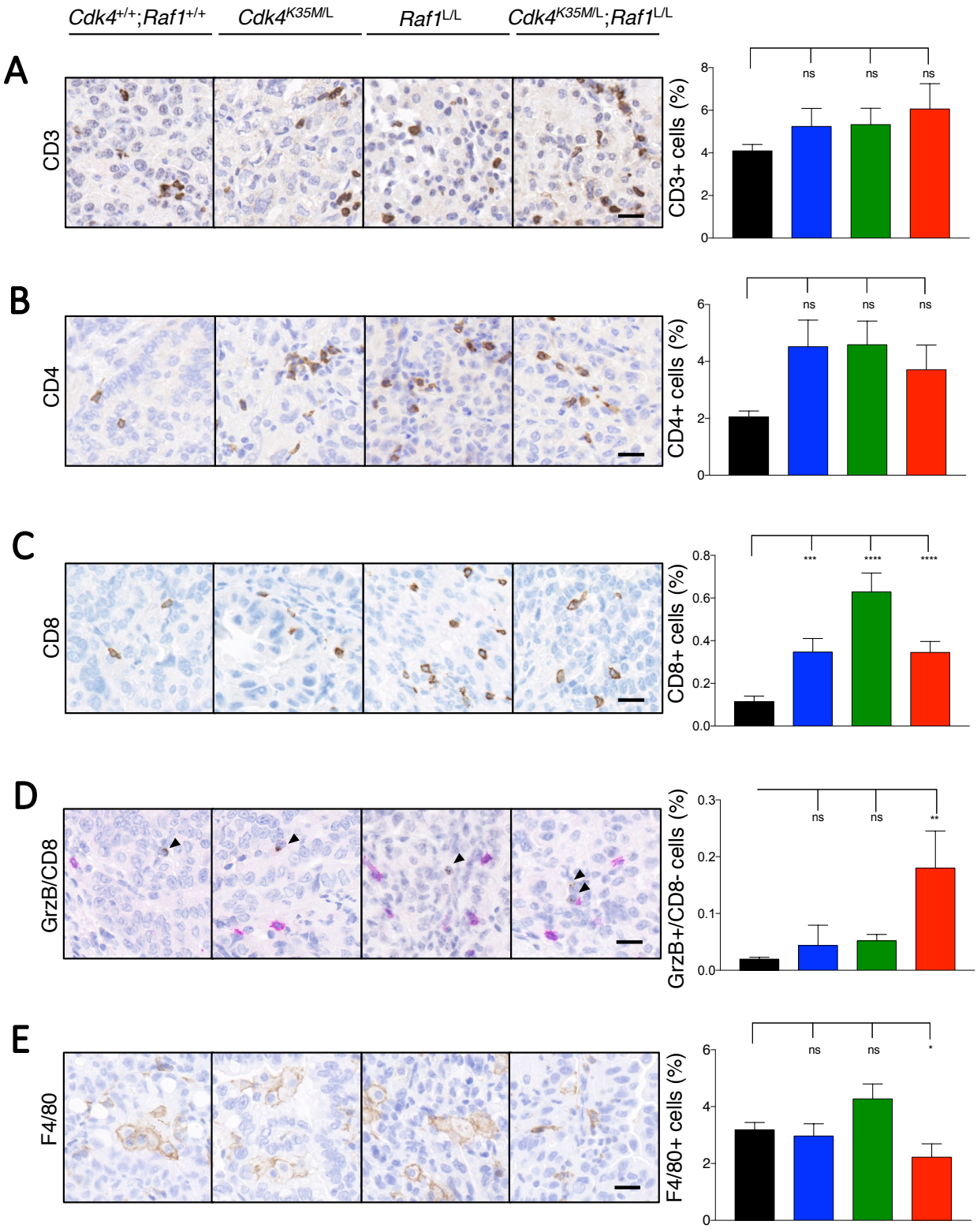

Figure 31: Immune profile of tumors upon CDK4 and RAF1 inactivation

(Left) A) Staining of CD3, **B)** CD4, **C)** CD8, **D)** GranzymeB/CD8 and **E)** F480 and **(right)** quantification from paraffin embedded serial sections of *Cdk4*$^{+/+}$;*Raf1*$^{+/+}$ (n=3/28tumors); (black bars), *Cdk4*$^{K35M/L}$ (n=3/28tumors); (red bars), *Raf1*$^{L/L}$ (n=3/23tumors); (green bars), *Cdk4*$^{K35M/L}$;*Raf1*$^{L/L}$ (n=8/28tumors); (red bars) after 9 weeks of TX exposure. Scale bar: 0,02mm. ***p < 0.001, **p < 0.01, *p < 0.05, ns: not significant, ANOVA test. Data are shown as means ± SEM.

2.4. Concomitant inhibition of CDK4 and RAF1 boosts apoptosis in vitro

To determine the mechanisms by which CDK4 and RAF1 concomitant inhibition lead to tumor regression and due to the limitation of tumor samples as a consequence of the significant tumor regressions in the *in vivo* model, *Kras*$^{+/G12V}$;*Trp53*$^{-/-}$;hUBC-CreERT2$^{+/T}$ cell lines from non-TX exposed advanced lung tumors were established. These cell lines harbored the following conditional alleles: *Cdk4*$^{K35M/L}$, *Raf1*$^{L/L}$ and the combination *Cdk4*$^{K35M/L}$;*Raf1*$^{L/L}$ in which CDK4 and/or RAF1 expression can be inactivated *in vitro* in a Cre-dependent manner.

First, we wanted to see whether inhibition of CDK4 and RAF1 prevented proliferation *in vitro*. To fully achieve complete recombination of the *Cdk4* and *Raf1* loci in the upper mentioned cell lines we used both AdCre infection and TX exposure at the same time (hereafter: AdCre-TX). Single target inhibition *in vitro*, showed a decrease in cell proliferation when compared to cell lines still harboring the functional targets (AdGFP infected controls). However, when combining the inhibition of both targets the reduction in proliferation was enhanced, mimicking the same effect observed *in vivo* (Figure 32A). A 90% reduction in cell growth was observed 10 days after CDK4 and RAF1 concomitant inhibition and only 70% for the single target inactivation.

Further, expression of CDK4^{K35M} and complete elimination of the RAF1 protein was confirmed 4 days after allele recombination was induced by AdCre/TX (Figure 32B). Interestingly, the levels of phospho-ERK were not significantly downregulated upon inactivation of CDK4 and RAF1, either alone or in combination (Figure 22B). Likewise, although showing a reduction in some cell lines RB was still phosphorylated, most likely due to compensatory mechanisms associated to the presence of either CDK6 or CDK2. Interestingly, the expression of these kinases was not affected. However, one of their cognate partners, CYCLIND1, showed a reduction upon combined CDK4 and RAF1 inactivation (Figure 32B).

In addition, we intravenously injected 2 different *Kras*$^{+/G12V}$;*Trp53*$^{-/-}$;*Cdk4*$^{K35M/L}$;*Raf1*$^{L/L}$;hUBC-CreERT2$^{+/T}$ tumor cell lines in immunocompromised nude mice and analyzed the tumor burden variations after 10 days in TX diet (Figure 32C). As shown in the H&E staining, tumor burden was almost completely abolished upon CDK4 and RAF1 inactivation compared to the same cell line not exposed to TX still retaining both targets (Figure 32C). Proliferation index was measured by BrdU incorporation. The results demonstrated that the percentage of BrdU positive cells was reduced upon CDK4 and RAF1 inactivation 10 days after TX exposure (Figure 32C). Furthermore, these results indicate the limited role that the immune system may be playing in mediating tumor regression.

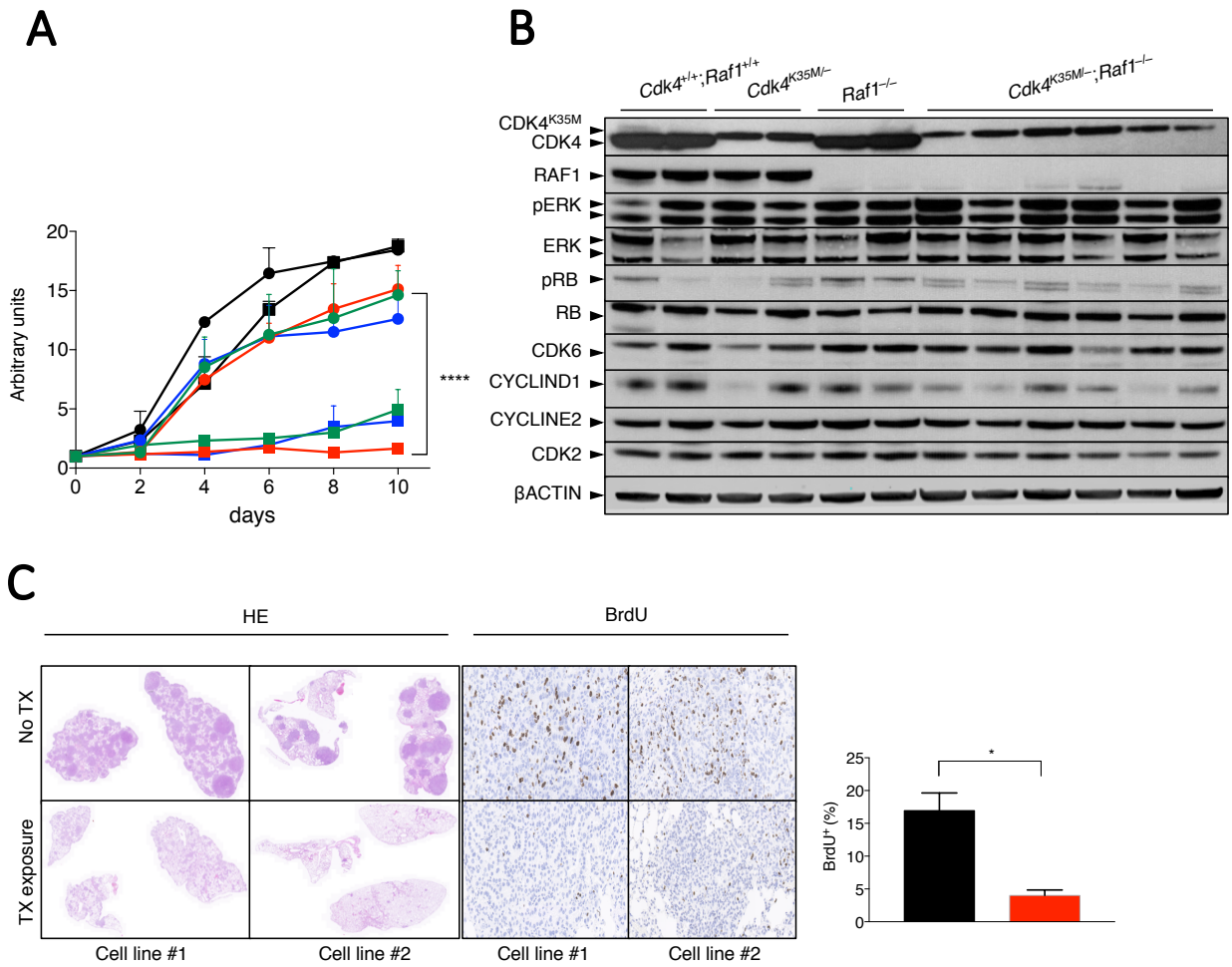

Figure 32: Concomitant inhibition of *Cdk4* and *Raf1* halts proliferation *in vitro* and *in vivo*

A) Proliferation curve of *Kras*$^{+/G12V}$;*Trp53*$^{-/-}$;*hUBC-CreERT2*$^{+/T}$ tumor cell lines harboring the following conditional alleles: *Cdk4*$^{+/+}$;*Raf1*$^{+/+}$ (black), *Cdk4*$^{K35M/L}$ (blue), *Raf1*$^{L/L}$ (green), *Cdk4*$^{K35M/L}$;*Raf1*$^{L/L}$ (red) infected with AdGFP as controls (circles) and exposed to AdCre-TX in order to inactivate the targets (squares). Error bars indicate mean ± SEM. P values were calculated, unpaired Student´s T test. ****p <0.0001. **B)** Western blot analysis of RAF1, CDK4, phospho-ERK (pERK), ERK1/2 (ERK), phospho-RB (pRB), RB, CDK6, CYCLIND1, CYCLINE2 and phospho-CDK2 (pCDK2) expression in lysates from *Kras*$^{+/G12V}$;*Trp53*$^{-/-}$;*hUBC-CreERT2*$^{+/T}$ lung tumor cell lines harboring the following alleles: *Cdk4*$^{+/+}$;*Raf1*$^{+/+}$, *Cdk4*$^{K35M/L}$, *Raf1*$^{L/L}$ and Cdk4$^{K35M/L}$;Raf1$^{L/L}$ 5 days after TX exposure. βACTIN was used as loading control. Migration of the above proteins is indicated by arrowheads. **C) (Left)** H&E and BrdU staining of lung sections of Foxn1$^{nu/nu}$ mice intravenously injected with two different *Kras*$^{+/G12V}$;*Trp53*$^{-/-}$;*Cdk4*$^{K35M/L}$;*Raf1*$^{L/L}$;*hUBC-CreERT2*$^{+/T}$ cell lines 10 days after TX exposure. **(Right)** Quantification of proliferative cells measured by the percentage of positive BrdU cells (BrdU^{+}). ****p <0.0001, unpaired t test. Data are shown as means ± SEM.

Next, in order to gain further insights of how essential *Cdk4* and *Raf1* are in the progression of *Kras*^{G12V}-driven tumors, we decided to analyze the gene expression changes associated to the co-inactivation of both targets. RNA sequencing (RNAseq) analysis of *Kras*^{G12V};*Trp53*$^{-/-}$ mutant lung tumor cells was performed before and after CDK4 and RAF1 inhibition *in vitro*. Single sample Gene Set Enrichment Analysis (ssGSEA) was performed with the purpose of identifying molecular mechanisms related to CDK4 and RAF1 tumor response. In good agreement with the Western blot data, correct

excision of the targets was reconfirmed after the short-reads alignments form the RNAseq data were mapped to the mouse genome (Figure 33A and 32B). The change of a lysine for a methionine (K35M) as point mutation in exon 2 of the *Cdk4* gene was detected (Figure 33A-red line), confirming correct expression of the CDK4 KD allele, and complete deletion of *Raf1* exon 3 was identified (Figure 33B).

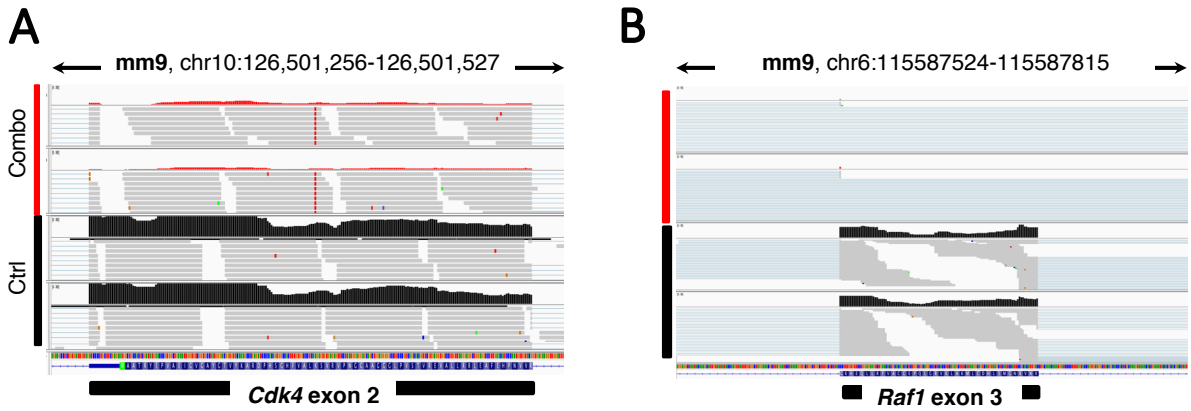

Figure 33: Short-read alignments to validate target excision
A) Short-reads alignments from the RNAseq data mapped to the mouse genome reference (Genome assembly MGSCv37, mm9). *Cdk4* exon 2 was mutated from AAG coding for K35 to ATG coding for M35 (red line) in cells before CDK4 and RAF1 inactivation (Ctrl; black bar) and 4 days after CDK4 and RAF1 inactivation (Combo; red bar). Control cells exposed to AdGFP did not show the mutation. **B)** Short-reads alignments from the RNAseq data mapped to the mouse genome reference (Genome assembly MGSCv37, mm9) in in cells before CDK4 and RAF1 inactivation (Ctrl; black bar) and 4 days after CDK4 and RAF1 inactivation (Combo; red bar). Control cells exposed to AdGFP did not show the mutation. Two samples for each genotype are shown for illustrative purposes. Combo: CDK4/RAF1 combined inactivation. Ctrl: Control.

Bioinformatic analysis revealed that pathways associated with cell cycle progression are downregulated upon CDK4 and RAF1 concomitant inactivation (Figure 34A-Combo) when comparing with cells still harboring both targets (Figure 34A-Ctrl). In the same line, pathways which involve genes that become upregulated upon G1 cell cycle arrest are overexpressed in the combination group (ARF PATHWAY) (Figure 34A-cell cycle).

As demonstrated both *in vivo* and *in vitro*, pathways linked to apoptosis are clearly upregulated (HALLMARK OF APOTOSIS or DEATH PATHWAY) (Figure 34A-apoptosis). In fact, several apoptosis-related genes such as *Bcl2l1*, *Bcl2*, *Bak1 Cdkn1a*, *Gadd45g*, *Sqstm1* and *Fas* appeared significantly differentially expressed when both targets are concomitantly inactivated compared with control samples where the targets are expressed (Figure 34B).

Overall, most oncogenic pathways, including KRAS, PI3K/AKT/mTOR, MYC, WNT, NOTCH or ERBB pathways were downregulated corroborating the fact that combined inhibition of CDK4 and RAF1 leads to a slowdown in oncogene activity as well as an induction of tumor regression mainly driven by apoptotic processes (Figure 34-oncogenic pathways).

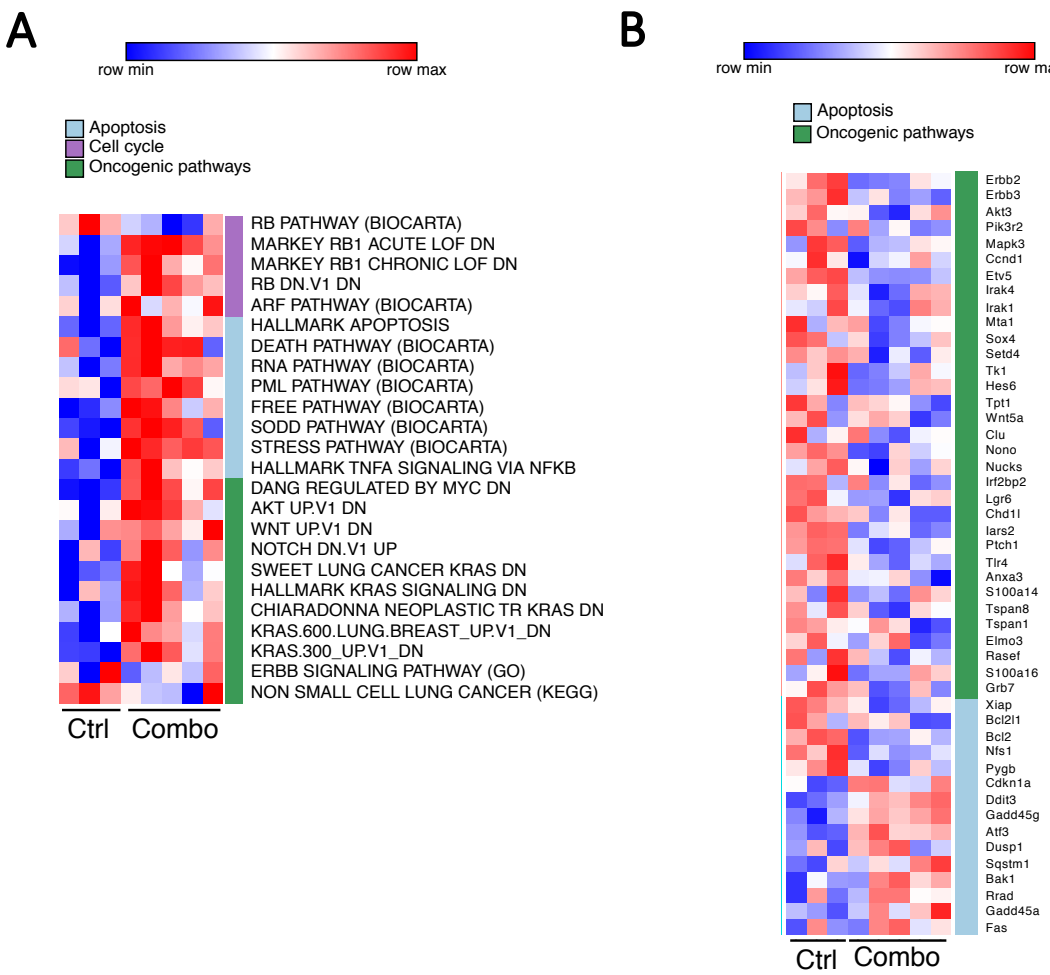

Figure 34: Transcriptomic analysis of CDK4 and RAF1 inactivation
A) Heatmap of ssGSEA normalized enrichment scores (NES) for gene sets related to apoptosis (blue), cell cycle (purple) and oncogenic processes (green). Each column represents individual samples before CDK4 and RAF1 inactivation (Ctrl) and 4 days after CDK4 and RAF1 inactivation (Combo). **B)** 48 differentially expressed genes (adjusted P-value<0.05) between CDK4/RAF1 inactivated (Combo) and control (Ctrl) cells related to cell cycle, apoptosis and oncogenic signaling pathways known to participate in the progression of LUAD are shown in the heatmap, with upregulation shown in red, downregulation shown in blue, and no change shown in white. Combo: CDK4/RAF1 combined inactivation. Ctrl: Control.

To further confirm the cell death tumor regression mechanism, 3D tumoral spheroids were generated since they are an accurate model to mirror *in vivo* conditions (Vinci et al., 2012). As shown in Figure 35A, inactivation of CDK4 activity and RAF1 expression leads to efficient cell death as determined by Topro-3/Hoechst assay in 3D cultures. Cell death is likely to be mediated by an apoptotic mechanism, therefore we checked for this apoptotic marker in monolayer cultures. We observed that combined target inactivation showed the rapid induction of Cleaved Caspase 3 (CC3) expression levels in a time course dependent manner (Figure 35B).

Analysis of β-galactosidase, a well-known senescence marker, failed to reveal significant levels of senescent cells, with only 3% of the cells showing β-galactosidase positivity (SA-β-gal) (Figure 35C).

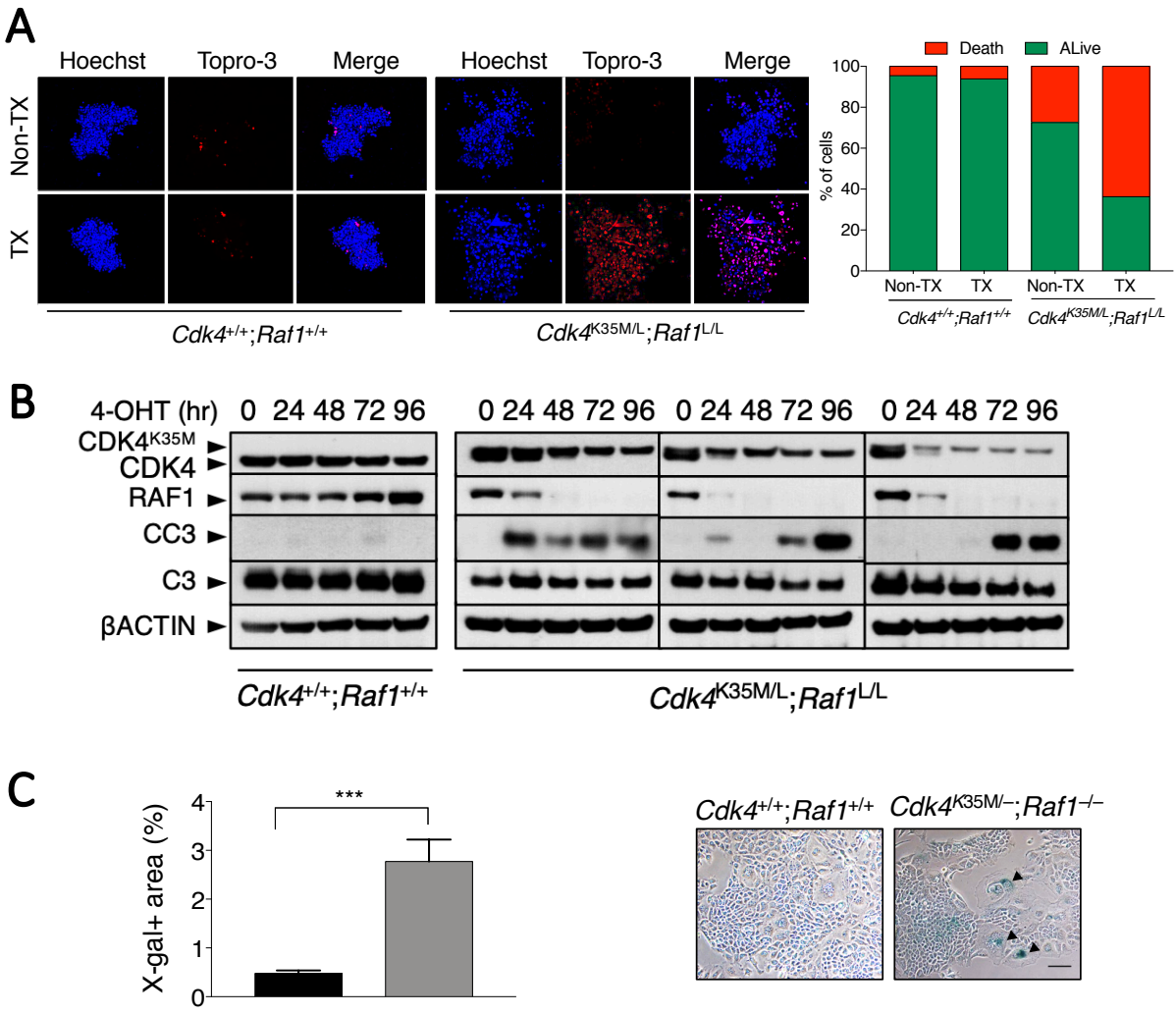

Figure 35: CDK4 and RAF1 inactivation prompts apoptosis *in vitro*

A) (Left) Staining for Topro-3 and Hoechst in *Kras*$^{+/G12V}$;*Trp53*$^{-/-}$;*hUBC-CreERT2*$^{+/T}$ lung tumor cell line 3D spheroids harboring the following alleles: *Cdk4*$^{+/+}$;*Raf1*$^{+/+}$ and *Cdk4*$^{K35M/L}$;*Raf1*$^{L/L}$ **(above)** non-exposed to TX and **(bottom)** exposed to TX. **(Right)** Quantification of death/alive cells; n=3 spheroids/condition. **B)** Western blot analysis of RAF1, CDK4, cleaved Caspase 3 (CC3), Caspase 3 (C3) expression in lysates from *Kras*$^{+/G12V}$;*Trp53*$^{-/-}$;*hUBC-CreERT2*$^{+/T}$ lung tumor cell lines harboring the following alleles: *Cdk4*$^{+/+}$;*Raf1*$^{+/+}$ and *Cdk4*$^{K35M/L}$;*Raf1*$^{L/L}$ maintained in 4OHT-containing media. Samples were harvested at the indicated times in hr. βACTIN was used as loading control. Migration of the above proteins is indicated by arrowheads. **C) (Left)** Quantification of X-gal positive cells in *Kras*$^{+/G12V}$;*Trp53* $^{-/-}$;*hUBC-CreERT2*$^{+/T}$ tumor cell lines harboring the following conditional alleles: *Cdk4*$^{+/+}$;*Raf1*$^{+/+}$ (black) and *Cdk4*$^{K35M/L}$;*Raf1*$^{L/L}$ (grey) exposed to 4-OHT during 72 hours. ***p < 0.001, unpaired Student's t test. Data are shown as mean ± SEM. **(Right)** X-gal stained representative pictures of each mentioned genotypes. Positive cells stained are shown by arrowheads. Original magnification 10x.

These results add further evidence indicating that apoptosis, rather than senescence, is the primary mechanism behind tumor regression upon combined inhibition of CDK4 and RAF1.

2.5. Pharmacological inhibition of CDK4 and RAF1

It stands to reason that genetic inhibition is not the same than pharmacologic treatment. However, in order to corroborate the potential therapeutic activity of the available inhibitors to target both, cell cycle and the MAPK pathway we decided to evaluate a pharmacological approach *in vivo*. Since there are no specific inhibitors targeting CDK4 nor RAF1 we decided to use Abemaciclib (CDK4/6) in combination with LSN3074753 (a panRAF kinase inhibitor) in tumor bearing *Kras*$^{+/FSFG12V}$;*Trp53*$^{F/F}$ mice. The treatment with CDK4/6 inhibitor as single agent had no significant effect on tumor growth (Figure 36A). Although the use of a panRAF inhibitor slowed down the growth, it is not until the combined treatment (Abemaciclib + LSN3074753) when we found cooperativity, having tumors growing significantly less than the vehicle treated controls after 4 weeks of drug treatment. However, only very few regressions, 10%, were observed (Figure 36A). A comparative waterfall plot from the *in vivo* genetic model at the same time (4 weeks of TX exposure) shows that Abemaciclib pharmacological treatment induced fewer regressions compared to CDK4 genetic inactivation by itself (7% vs. 27%) (Figure 36A), suggesting that either CDK6 is not playing a major role in *Kras*-driven LUAD (Puyol et al., 2010) or that Abemaciclib has not met the expectations being clinically inefficient. RAF1 genetically ablation induces by far a significant decrease in tumor burden that is not achieved upon treatment with the panRAF inhibitor (10% vs. 86%) (Figure 36A). In addition, combined inactivation of CDK4 and RAF1 ablation by genetic means leads to a regression of 100% of the tumors as previously mentioned whereas most of the tumors keep growing upon combined pharmacological inhibition (Figure 36A).

In addition, longer treatments up to 10 weeks revealed that tumors far from decreasing their initial size started progressing again, pointing out to resistance as it commonly occurs in patients after treatments (Figure 36B).

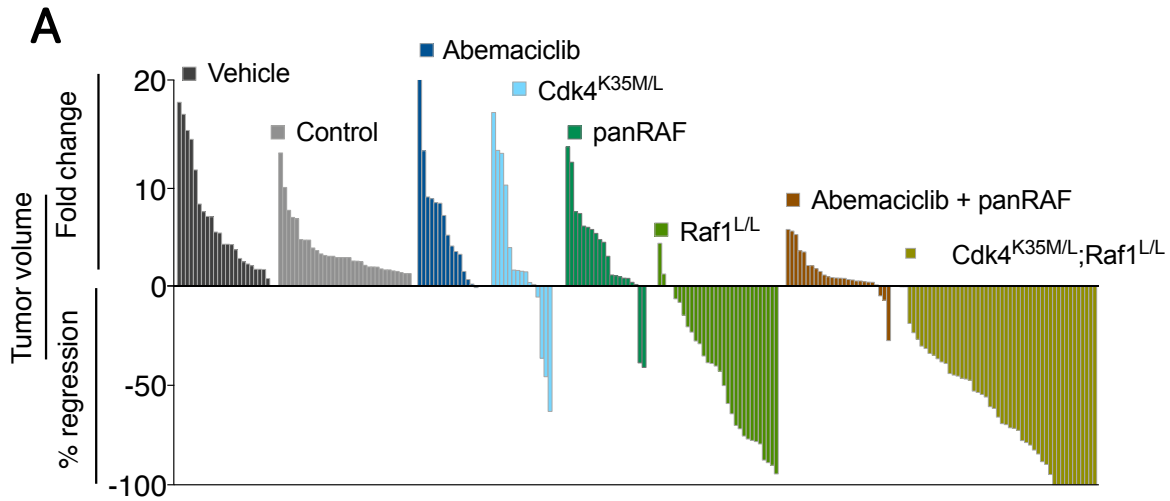

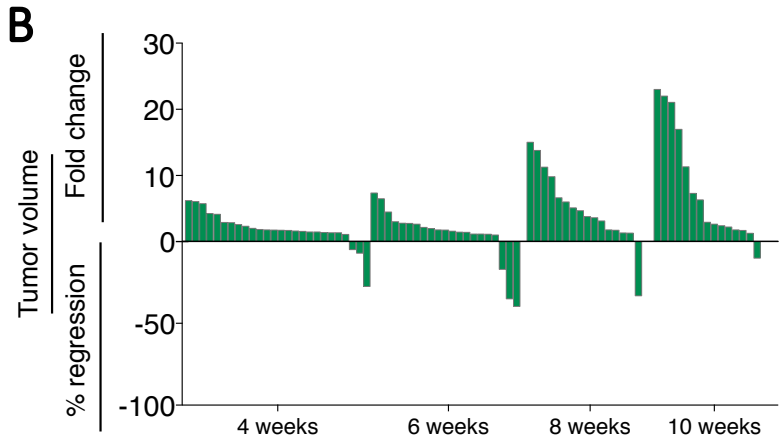

Figure 36: Pharmacologic in *vivo* treatments with CDK4/6 and RAF1 inhibitors
A) Waterfall plot representing the tumor volume fold change and the % of regression of individual CT^{+} lung tumors comparing drug treatments with genetic target inactivation after 2 months of treatment or TX exposure respectively. Vehicle treatment (n=8) or *Cdk4*$^{+/+}$;*Raf1*$^{+/+}$ control (n=14), Abemaciclib treatment (n=8), genetic CDK4 inactivation by TX exposure (n=16), panRAF treatment (n=9), genetic RAF1 ablation by TX exposure (n=7), Abemaciclib + panRAF (n=15) and combined genetic inactivation of CDK4 and RAF1 (n=17). **B)** Waterfall plot representing the tumor volume fold change and the % of regression of individual CT^{+} lung tumors from *Kras*$^{+/FSFG12V}$;*Trp53*$^{F/F}$ mice upon combined Abemaciclib plus panRAF (n=15; Combo) treatment for up to 10 weeks.

2.6. CDK4 and RAF1 concomitant inactivation results in acquired tumor resistance in vitro

Even in the most aggressive lung tumor model, concomitant inactivation of CDK4 and RAF1 resulted in 90% response including the 24% of complete responders (Figure 28A). However, there is a percentage of tumors, 30%, that maintained their size displaying SD between 6 and 9 weeks of TX exposure (Figure 29B). Disease relapse may depend on a small population of "persister" cells that remain in a dormant state for months or even years after the initial response to treatment. This process is difficult to mimic in our *in vivo* model due to the limited mouse lifespan (Hangauer et al., 2017; Ramirez et al., 2016). Still, considering the importance of tumor resistance after most anti-cancer treatments we recapitulated this phenomenon *in vitro*.

To do so, a colony formation assay of *Kras*$^{+/G12V}$;*Trp53*$^{-/-}$;*hUBC-CreERT2*$^{+/T}$;*Cdk4*$^{K35M/L}$;*Raf1*$^{L/L}$ cells was seeded right after the targets were inhibited by AdCre-TX exposure. Interestingly, there were three cell lines that never gave rise to a single colony being complete responders (RP, henceforth), mimicking the complete regressors observed *in vivo*. However, in some other tumoral cell lines, although almost the whole population responded, a small proportion was able to grow, giving rise to resistant clones (RT, henceforth), (Figure 37A). This small percentage of RT cells, that accounts for around 5-10% when compared to controls (Figure 37B) was isolated and expanded in order to check for the recombination of *Cdk4* and *Raf1* loci by the h*UBC-CreERT2* allele. As shown in Figure 37B, in fact, the CDK4 KD isoform

was expressed and RAF1 protein completely ablated in all clones confirming that these cells are able to grow in a CDK4 and RAF1 independent manner.

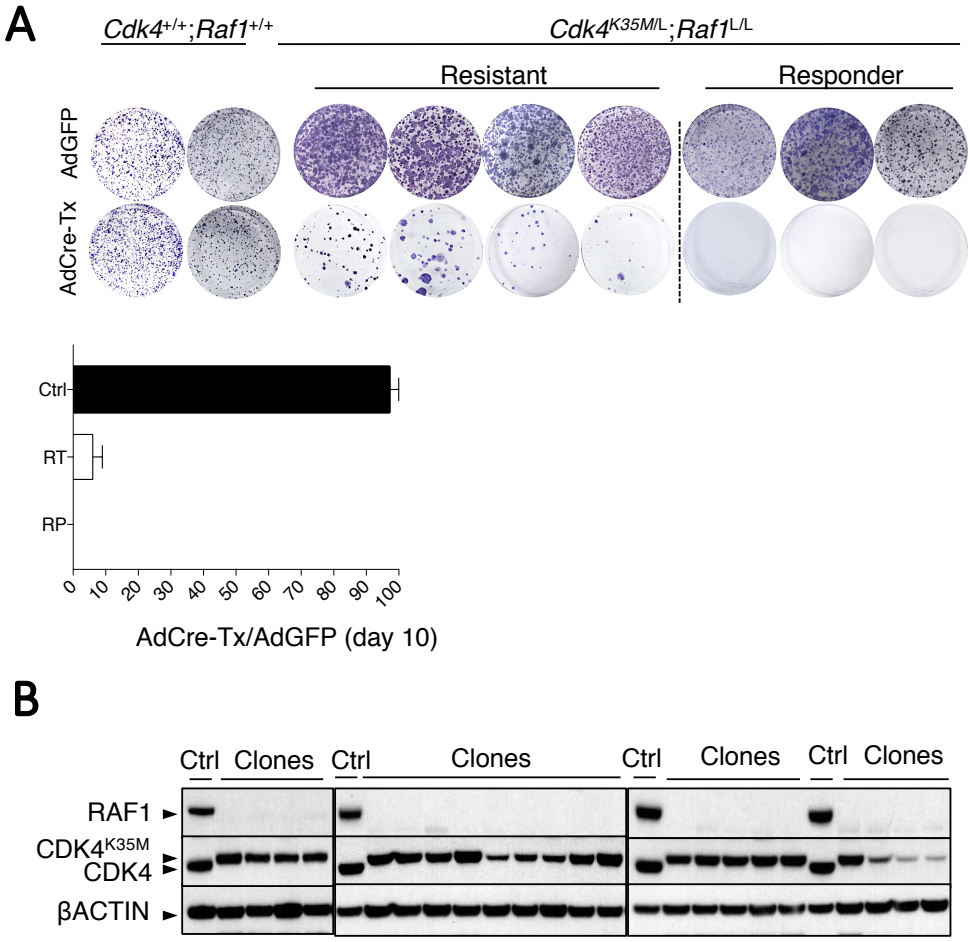

Figure 37: A low percentage of cells are able to grow in a CDK4 and RAF1 independent manner.
A) (Upper panel) Colony formation assay of tumor cell lines derived from non-treated *Cdk4*$^{+/+}$;*Raf1*$^{+/+}$ (n=2; Ctrl) and *Cdk4*$^{K35M/L}$;*Raf1*$^{L/L}$ mice (n=7; RT or RP). Tumor cell lines are classified as RT or RP according to their ability to form colonies after 10 days of AdCre-TX exposure. AdGFP was used as a negative control. (**Bottom panel)** Quantification of the number of colonies that appear upon CDK4 and RAF1 concomitant inhibition upon AdCre-TX exposure expressed as percentage of the colonies observed in their control infected with AdGFP particles. Data are shown as mean ± SEM. **B)** Western blot analysis of Ctrl cells and clones isolated from A. Protein levels of RAF1 and CDK4 are shown. βACTIN served as loading control. Migration of the above proteins is indicated by arrowheads. Ctrl: Control; RT: Resistant; RP: Responder.

2.7. Resistant cells show high levels of heterogeneity among themselves

In order to evaluate the mechanisms underlying the resistance to CDK4 and RAF1 inhibition we submitted to RNAseq analysis the following conditions: cell lines that are able to grow in a CDK4/RAF1 independent manner (Resistant, RT1-RT9), cell lines which are completely dependent on CDK4/RAF1

expression (Responder, RP1-3) and control samples before the targets have been inactivated (Ctrl).

First, we were wondering which genes and pathways differ when comparing RT vs. RP cells and RT vs. Ctrl cells. In general, we identified different clusters in terms of DEGs (Differentially Expressed Genes) as determined by Gene Set Enrichment Analysis (GSEA) among these samples (Figure 38A). But unfortunately, no common significantly up-regulated DEGs resulted from these comparisons could be validated for all RT cells analyzed (Figure 38B). These results made us think that there is a high inter-tumoral heterogeneity between the resistant cells.

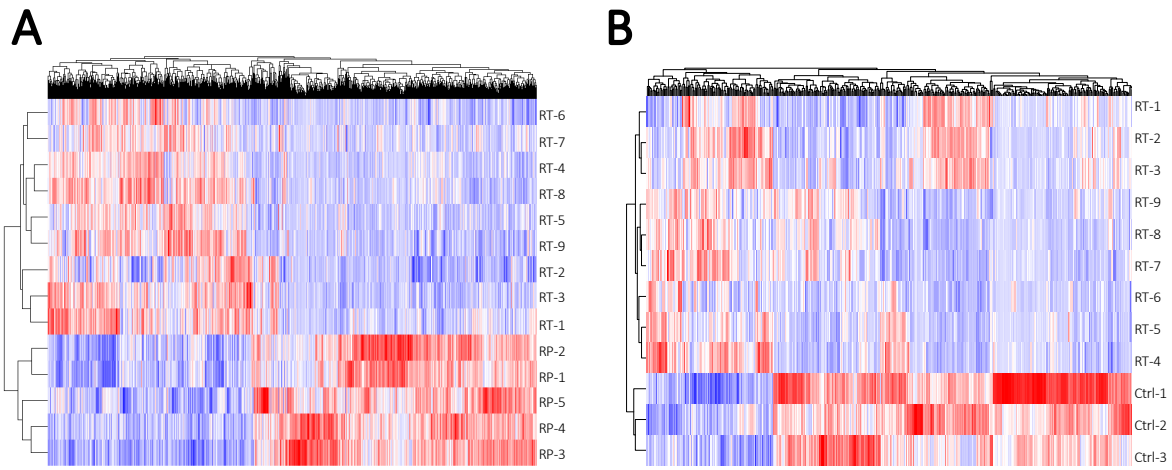

Figure 38: Transcriptome analysis of Resistant (RT), Responder (RP) and Control (Ctrl) cells A) Heatmap representing color-coded expression levels of differentially expressed genes (DEGs) in Responder (RP n=5) and Resistant (RT1-9) cells after CDK4 and RAF1 inactivation. **B)** Heatmap representing color-coded expression levels of differentially expressed genes (DEGs) in Resistant (RT1-9) and Control (Ctrl 1-3) after and before target inactivation respectively.

Given the difficulties found in identifying a common pattern among the resistant cells due to the high heterogeneity, we further compared only the resistant cells among themselves. As illustrated in Figure 38, hierarchical clustering revealed that there are indeed two main groups of resistant cells (RT1-3-black line and RT4-9-white line) clearly demonstrating that there might be different resistance mechanisms.

A significant number of pathways related to energy metabolism and lipid metabolism appeared upregulated in RT1-3 vs. Ctrl compared to RT4-9 vs. Ctrl (Table 7), suggesting that a metabolic adaptation has taken place in order to support cell growth to those cells, but still these assumptions need to be further investigated.

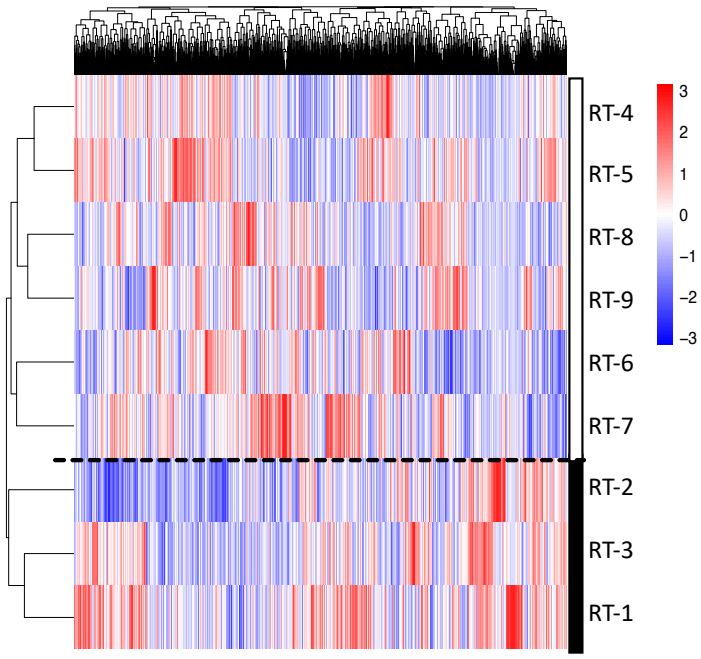

Figure 39: Resistant cells show high levels of heterogeneity among themselves

Heatmap representing color-coded expression levels of differentially expressed genes (DEGs) in Resistant (RT n=9). The white and black bars show 2 different hierarchical clustering's between the RT clones.

Table 7: Metabolism functions related to Resistant 1-3 or 4-9 cells

	PATHWAY NAME	NES
	RT 1-3 VS. CTRL	
1.	REACTOME_RESPIRATORY_ELECTRON_TRANSPORT_ATP_SYNTHESIS _BY_CHEMIOSMOTIC_COUPLING_AND_HEAT_PRODUCTION_BY_UN COUPLING_PROTEINS_	2,59
2.	REACTOME_RESPIRATORY_ELECTRON_TRANSPORT	2,51
3.	HALLMARK_OXIDATIVE_PHOSPHOYLATION	2,46
4.	KEGG_GLYCOLYSIS_GLUCONEOGENESIS	2,43
5.	HALLMARK_FATTY_ACID_METABOLISM	2,42
6.	REACTOME_TCA_CYCLE_AND_RESPIRATORY_ELECTRON_TRANSPORT	2,40
7.	KEGG_OXIDATIVE_PHOSPHOYLATION	2,34
8.	KEGG_HISTIDINE_METABOLISM	2,32
9.	KEGG_FRUCTOSE_AND_MANNOSE_METABOLISM	2,19
10.	KEGG_PENTOSE_PHOSPHATE_PATHWAY	2,20
11.	HALLMARK_MTORC1_SIGNALING	2,24
12.	HALLMARK_CHOLESTEROL_HOMEOSTASIS	2,24
13.	HALLMARK_BILE_ACID_METABOLISM	2,17
14.	KEGG_FATTY_ACID_METABOLISM	2,12
15.	REACTOME_GLYCOLYSIS	2,12
16.	REACTOME_GLUCONEOGENESIS	2,10
17.	REACTOME_GLUCOSE_METABOLISM	2,04
18.	KEGG_BUTANOATE_METABOLISM	1,97
19.	BIOCARTA_GLYCOLYSIS_PATHWAY	1,97
20.	KEGG_STEROID_BIOSYNTHESIS	1,95
21.	REACTOME_TRIGLYCERIDE_BIOSYNTHESIS	1,91
22.	REACTOME_METABOLISM_OF_LIPIDS_AND_LIPOPROTEINS	1,82
23.	KEGG_PYRUVATE_METABOLISM	1,81
24.	REACTOME_FATTY_ACID_TRIACYLGLYCEROL_AND_KETONE_BODY _METABOLISM	1,80
25.	REACTOME_CITRIC_ACID_CYCLE_TCA_CYCLE	1,79
26.	KEGG_CITRATE_CYCLE_TCA_CYCLE	1,74

	PATHWAY NAME	NES
	RT 4-9 VS. CTRL	
1.	REACTOME_PEROXISOMAL_LIPID_METABOLISM	1,93
2.	KEGG_OTHER_GLYCAN_DEGRADATION	1,86
3.	KEGG_OXIDATIVE_PHOSPHOYLATION	1,88
4.	KEGG_FATTY_ACID_METABOLISM	1,84
5.	HALLMARK_OXIDATIVE_PHOSPHOYLATION	1,82
6.	KEGG_HISTIDINE_METABOLISM	1,82

Then, we wanted to know if this RT cells were able to proliferate *in vivo*. To that end, we implanted these cells subcutaneously in immunodeficient Foxn1$^{nu/nu}$ mice and the growth curves revealed: (i) RT cells are able to grow *in vivo*, (ii) the different RT cells show different behaviors that comprise two growth rate curves correlating with the clusters found after computational analysis (Figure 40 and see white and black bars in Figure 39).

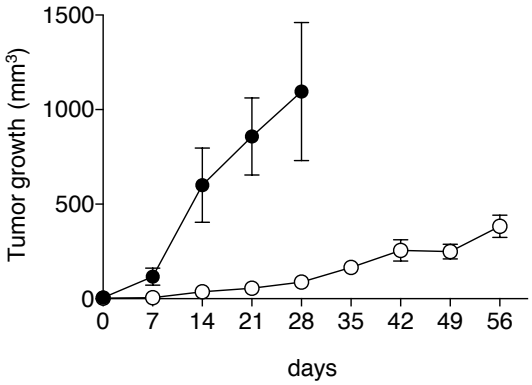

Figure 40: Resistant cells show high levels of heterogeneity among themselves
Tumor growth of the resistant cells after subcutaneous implantation in immunosuppressed Foxn1$^{nu/nu}$ mice during the indicated time. Black circles represent RT 1-3 and white circles represent RT 4-9. Data are shown as mean ± SEM.

2.8. Resistance upon CDK4 and RAF1 inactivation is mediated by diverse mechanisms

Next, we performed GSEA which confirmed two different mechanisms of resistance when comparing cells that are able to grow in a CDK4/RAF1 independent manner (RT) with either cells that respond after CDK4/RAF1 inactivation (RP) or control cells where the targets have not been yet excised (Ctrl).

On one hand, in RT1-3 we saw significantly downregulated genes which correlated with upregulated gene sets after treatment with demethylation agents (Figure 41A). This means, genes that in RT1-3 cells are likely to be silenced due to gene methylation. They are mainly tumor suppressor genes (*Lrig3*; $\log_2$FC=-6.3, *Sirpa* $\log_2$FC=-6.15, *Rspo2*; $\log_2$FC=-4.3, *Fbln2*; $\log_2$FC=-1.6 and *Nrg1*; $\log_2$FC=-1.5) known to undergo promoter methylation.

To assess whether in these cells, demethylation agents could lead to therapeutic benefits, we treated the cells with 5-Azacytidine (5-AZAi), a demethylating agent already in clinical trials. As illustrated in Figure 41B, 5-AZAi demonstrated that RT1-3 cells are significantly sensitive with IC50s raging from 0.7-4 µM compared to the 11 µM of the control cell lines. Based on these results, cell viability curves and colony formation assays were performed with a 2 µM dose of 5-AZAi during 9 days. The results showed that these resistant cells displayed selective sensitivity to this drug compared to the control cell lines (Figure 41C and 41D).

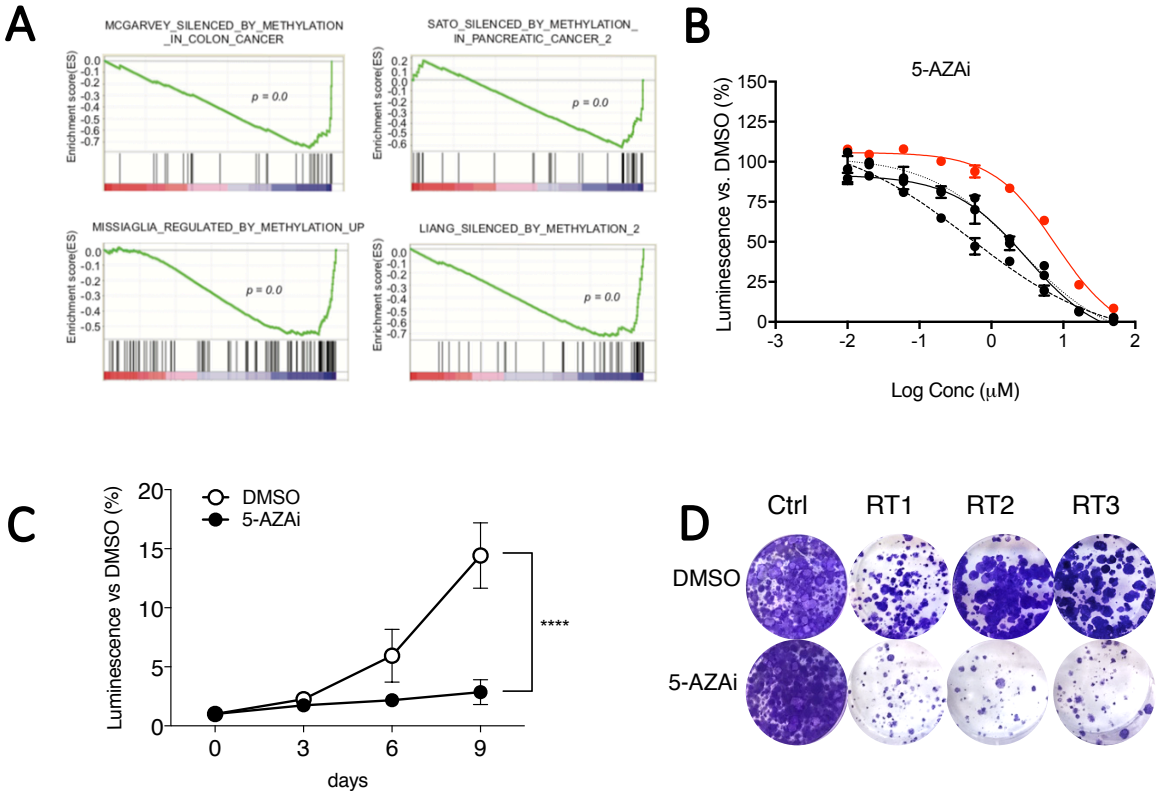

Figure 41: *In vitro* validation of 5-Azacytidine efficacy in lung tumor cell lines

A) Gene set enrichment graphs for DNA methylation pathways comparing **(upper panel)** Resistant (RT1-3) versus Control (Ctrl) cells and **(bottom panel)** Resistant (RT1-3) versus Responder (RP) cells **B)** IC50 estimation of RT1-3 (black) and their control (red) relative to the DMSO treated cells. **C)** Cell viability assays of resistant cells (n=3; RT1-3) treated with DMSO (empty circles) or 2 µM Azacytidine (5-AZAi) (black circles) during 9 days. ***p < 0.001, unpaired Student's t test. Data are shown as mean ± SEM **D)** Colony formation assay of resistant cells (n=3; RT1-3) treated with **(upper panel)** DMSO or **(bottom panel)** with 2 µM of 5-AZAi for 9 days. Cells harboring wild type *Cdk4* and *Raf1* alleles exposed to DMSO and 2 µM of 5-AZAi were used as controls (Ctrl).

On the other hand, the other set of RT cells (RT4-9) have upregulated DEGs enriched in upregulated gene sets related to PI3K activation, both pathways leading to AKT activation (Figure 42A). In order to corroborate the RNAseq results and find out more potential vulnerabilities after CDK4 and RAF1 inactivation in our RT cells, a library of 114 compounds which covers most of the oncogenic-related pathways, was screened (Figure 42B). For the RT4-9, among the 24 compounds that reduce proliferation >75%, 10 were indeed PI3K inhibitors (PI3Ki) (Figure 42C-white bars), whereas in the case of the resistant cells that display a hypermethylated phenotype (RT1-3) only 4 out of the 17 compounds that reduced proliferation >75%, were PI3K inhibitors (Figure 42C-black bars). More importantly, unlike for RT4-9, none of these four compounds inhibited PI3K alone but other targets in combination,

suggesting that single PI3K inhibition would not be sufficient to impair lung proliferation in this set of resistant cells (RT1-3) (Figure 42C).

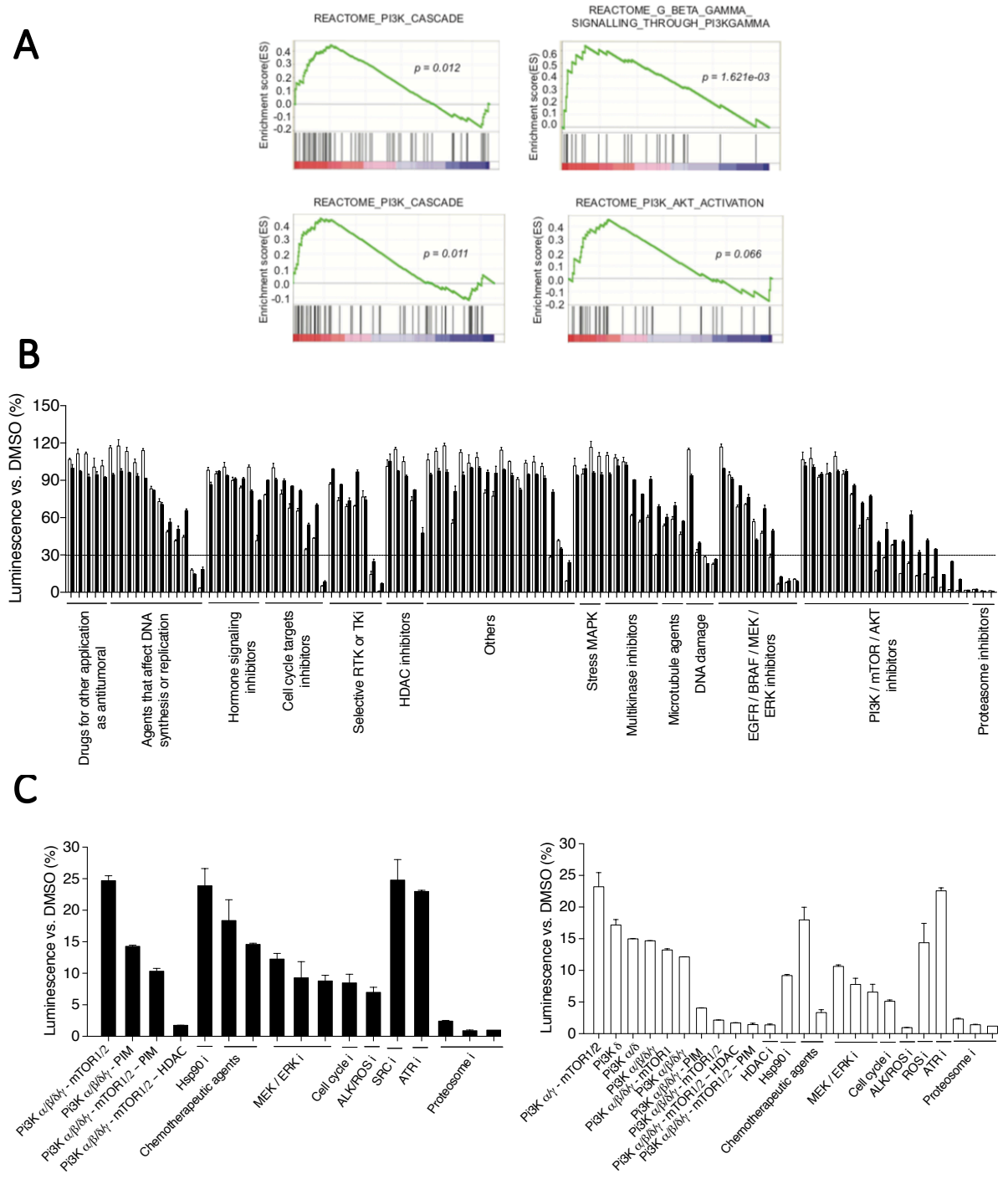

Figure 42: Evidences of PI3K pathway upregulation in Resistant cells (RT4-9)
A) Gene set enrichment graphs for AKT-related pathways activation comparing **(upper panel)** resistant (RT4-9) versus Control (Ctrl) cells and **(bottom panel)** Resistant (RT4-9) versus Responder (RP) cells. **B)** Cell viability assay of resistant cells RT1-3 (black bars) and RT4-9 (white bars) screened with a library of 114 compounds at a unique 5 µM dose during 72h. The library consists of compounds blocking the majority of known cancer related pathways. **C)** Magnification from B, of the data showing the compounds that achieved a cell growth inhibition > 75%. **(Left)** RT1-3 cells. **(Right)** RT4-9 cells.

As a consequence, RT4-9 were treated with a pan-PI3K inhibitor (CNIO-PI3K) (Ortega-Molina et al., 2015). The resistant cells displaying an activated AKT pathway (RT4-9) were at least 100 times more sensitive than their respective control cells (Ctrl), with an average IC50 of 0.3 µM vs. 30 µM, respectively (Figure 43A). Cell viability curves during 9 days of treatment with 1 µM CNIO-PI3Ki demonstrated that RT4-9 cells are significantly more sensitive than the controls (Figure 43B). Moreover, colony formation assays upon CNIO-PI3Ki treatment further confirmed the therapeutic benefit by inhibiting the PI3K pathway in this subset of RT clones (Figure 43C). Western blot analysis revealed the presence of elevated phospho-AKT levels compared to the controls, hence, adding further support to the role of an elevated PI3K pathway in these resistant cells (Figure 43D). In addition, exposure of these cells to the CNIO-PI3K inhibitor for 24 hours decreased the levels of phospho-AKT to those present in control cells. Of note, CDK4 protein levels decreased upon CNIO-PI3Ki treatment, whether PI3K controls the expression and/or stability of CDK4 in this context needs to be further addressed (Figure 43D).

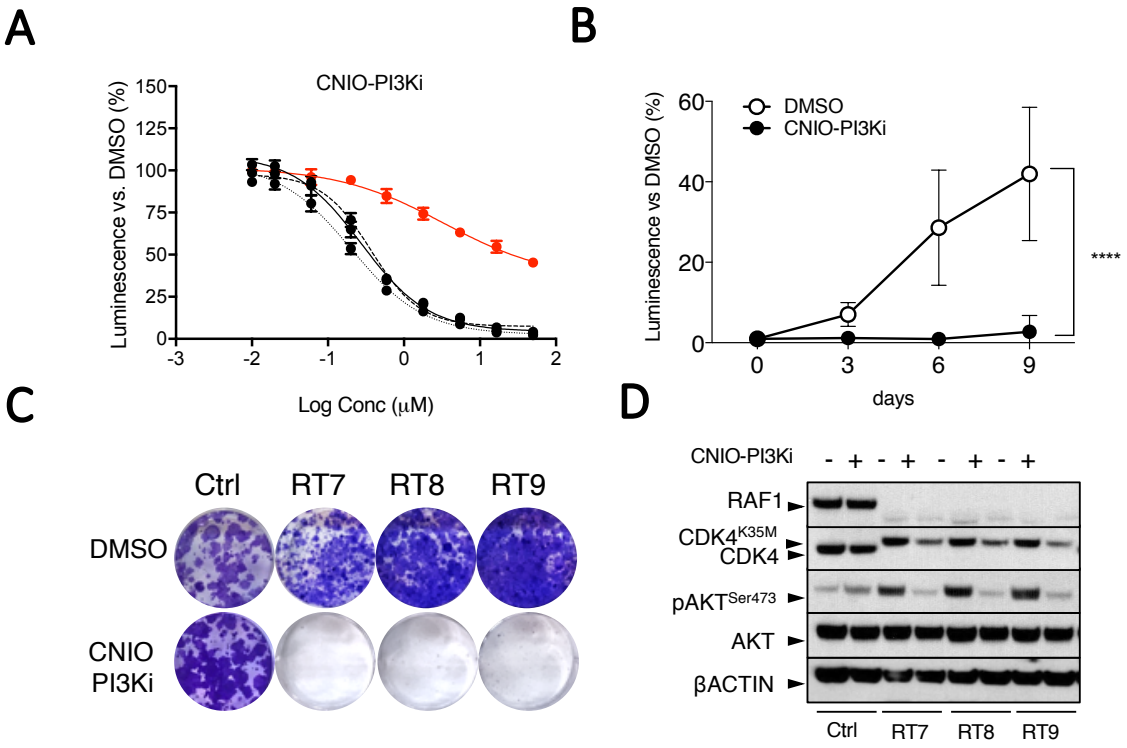

Figure 43: *In vitro* validation of PI3K resistant treatment

A) IC50 estimation of RT7-9 (black) and its control (red) relative to the DMSO treated cells. **B)** Cell viability assays of resistant cells (n=6; RT4-9) treated with DMSO (empty circles) or 1 µM CNIO-PI3Ki (black circles) during 9 days. The compound was administered on days 0, 3, 6 and 9 of the experiment. CNIO-PI3Ki is covered by the patent WO2010/119264. ***p < 0.001, unpaired Student's t test. Data are shown as mean ± SEM. **C)** Colony formation assay of resistant cells (n=3; RT7-9) treated with **(upper panel)** DMSO or **(bottom panel)** 1 µM of CNIO-PI3Ki for 9 days. Cells harboring wild type *Cdk4* and *Raf1* alleles exposed to DMSO or 1 µM CNIO-PI3Ki were used as controls (Ctrl). **D)** Western blot analysis of RAF1, CDK4, phospho-AKT (pAKT), AKT expression after 24hr in the absence or the presence CNIO-PI3Ki in control and resistant cells. βACTIN was used as loading control. Migration of the above proteins is indicated by arrowheads.

To further validate these resistance mechanisms *in vivo,* we subcutaneously implanted control and resistant cells and checked for tumor responses after either 5-Azacytidine (Figure 44A) or CNIO-PI3K treatment (Figure 44B). Recent data obtained from this experiment confirmed that the resistant tumors which have shown to display a hypermethylated phenotype (RT1), upon 21 days of 5-AZA treatment when compared to vehicle treated tumors, halt their proliferation (Figure 44A). In addition, control tumors that still harbor wildtype *Cdk4* and *Raf1* alleles, although showing a slight response to 5-AZA treatment, do not depend so much on this pathway allowing these tumors finally, to overcome this limited proliferation (Figure 44A). Similar results were obtained upon CNIO-PI3K treatments. Despite the fact that these tumors have only been under treatment for 18 days, the preliminary data confirms a specific response for the resistant tumors (RT4) (Figure 44B) and not for the control tumors (Figure 44B).

Together, all these data provide evidences that either epigenetic modifications or activation of PI3K activity are two bona fide mechanisms of resistance for at least a subset of LUAD cell lines lacking CDK4/RAF1 expression.

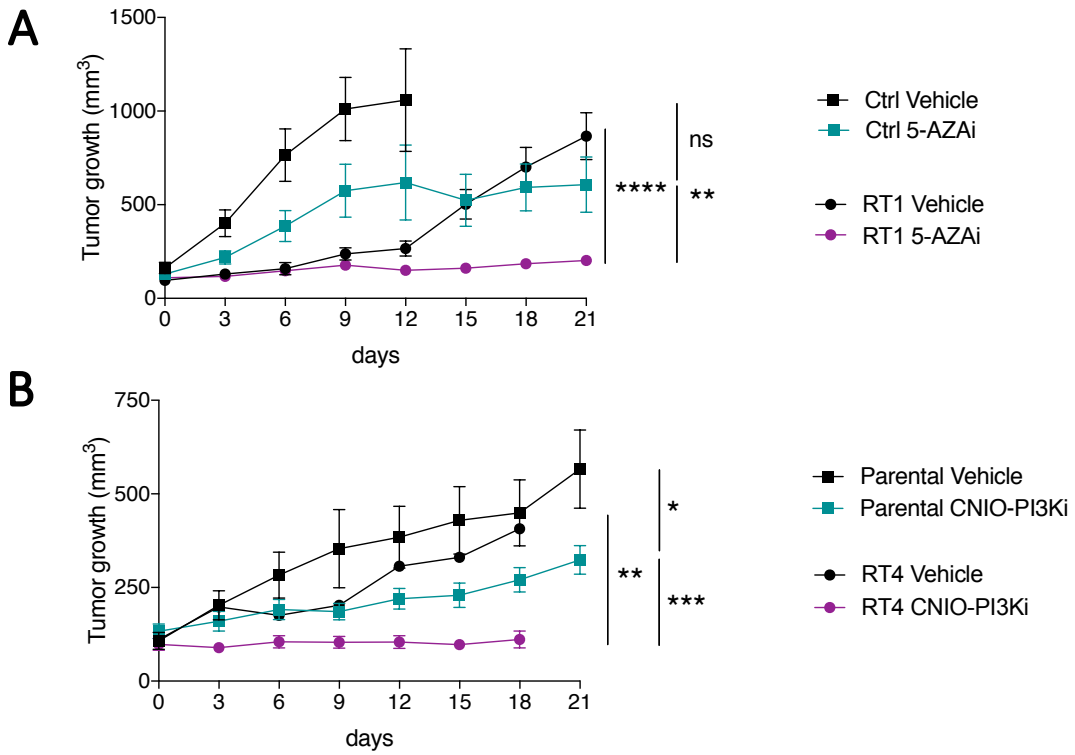

Figure 44: *In vivo* validation of two independent resistant mechanisms

A) Tumor growth of Resistant (RT1) and Control cells (Ctrl) after subcutaneous implantation in immunosuppressed Foxn1$^{nu/nu}$ mice during the indicated time. Black squares represent vehicle treatment of Ctrl tumors, green squares represent 5-Azacytidine treatment (5-AZAi) of Ctrl tumors, black circles represent vehicle treatment of resistant tumors (RT1), and purple circles represent 5-AZAi treatment of resistant tumors (RT1). **B)** Tumor growth of Resistant (RT4) and Control cells (Ctrl) after subcutaneous implantation in immunosuppressed Foxn1$^{nu/nu}$ mice during the indicated time. Black squares represent vehicle treatment of Ctrl tumors, green squares represent PI3K treatment (CNIO-PI3Ki) of Ctrl tumors, black circles represent vehicle treatment of resistant tumors (RT4), and purple circles represent CNIO-PI3Ki treatment of resistant tumors (RT4). ****$p < 0.0001$, ***$p < 0.001$, **$p < 0.01$, *$p < 0.1$, unpaired Student's t test. Data are shown as mean ± SEM.

DISCUSSION

1. Validation of CDK4 kinase activity inactivation in *Kras-driven* LUAD

1.1. The pros and cons of target inactivation in two GEMMs.

During my thesis, we aimed to shed light on the role of CDK4 catalytic inactivation in order to better mimic a pharmacological intervention where the protein of interest is inhibited rather than eliminated. Additionally, we were wondering if the benefit previously described in $Kras^{G12V}$-driven NSCLC (Puyol et al., 2010) fully relied on CDK4 catalytic activity.

In order to approach this question, two different models where the kinase activity of the protein is "dead" were used: (i) mutating the Lys (K) of the ATP-binding pocket by a Methionine (M), K35M, and (ii) mutating the Aspartic acid (D) residue of the DFG which acts as a proton acceptor site by an Alanine (A), D140A. (See Figure 7; Materials and Methods Section 1.3). Although a mutation that impedes the binding of the ATP will confer a kinase dead property to the protein impairing the kinase activity, there are several evidences which demonstrated that mutations in the DFG motif in the catalytic loop of the kinase domain are also efficient because their function is required for chelating Mg^{2+} and stabilizing ATP binding (Dankort et al., 2007; Schnutgen et al., 2003). There are none reported mouse models of CDK4 catalytic inactive mutants. The only work claiming an interruption in the CDK4/RB binding consists of a mutation on an RB docking site preventing CDK4 from binding and phosphorylating RB, therefore enhancing its tumor suppressor activities (Wallace and Ball, 2004).

In both cases the mutant form of CDK4 is expressed from the endogenous promoter, therefore transcriptional regulation is as physiological as possible. For instance, in the case of oncogenic *Kras*, it was reported that high levels of protein expression lead to senescence whereas the expression at physiological levels favors cell proliferation (Tuveson et al., 2004) raising the importance of having appropriate mouse models to study in a more physiological manner the effect of specific modifications.

To our surprise, when we checked for CDK4 protein expression levels in untreated E13.5 MEFs, , no functional protein was detected in none of the two GEMMs. This technical drawback has been already reported in mouse models from our laboratory targeting the *Pi3k* gene (unpublished data) as well as by others when generating conditional alleles for the Huntington's disease gene homolog (*Hdh*) (Dragatsis and Zeitlin, 2001), the 3-phosphoinositide-dependent protein kinase-1 (*Pdk1)* (Bayascas et al., 2006) or the *B-Raf* gene (Dragatsis and Zeitlin, 2001), thus interpretation of possible causes is discussed below.

In the case of the Flex system it is possible that the mutated inverted exon is interfering somehow over the wildtype protein since both are transcribed before Cre-mediated recombination. A putative explanation is that the homology between the loxP sites induces conformational changes increasing the chances of getting secondary structures which will finally block transcription. A possible

way to bypass this pitfall could be to introduce additional polyadenylation transcriptional termination sequences to ablate expression of the mutant protein, in non-Cre-expressing tissues, in a more efficient way (Bayascas et al., 2006).

The "minigene" system utilizes a very different strategy, however we face the same problem as previously described. Although in this case, there is a STOP cassette inserted downstream of the *Cdk4* cDNA in order to prevent transcription read-through into the mutant allele, it could be possible that this halt in transcription did not work properly leading to difficulties or even blocking normal mRNA transcription. Another possibility is that the insertion of a Neo cassette within an intron may randomly result in either unaltered expression, a reduction in the targeted gene expression (hypomorphic allele) or a silent null allele due to complete inactivation of the gene expression (Dragatsis and Zeitlin, 2001). A third possibility is that there could be an interference with splicing signals due to the small size of the *Cdk4* introns which might difficult the location of the loxP sites, since they better need 250 bp from the exon boundaries. The different degrees of protein loss depend on how efficiently the splicing mistakes happens. If still, there is production of the mRNA and it arrives to the cytoplasm the amount of endogenous protein translated will be reduced but if no mRNA levels are produced at all the protein will be completely absence. Unfortunately, in our case no protein was detected assuming that tampering with the *Cdk4* locus interferes somehow with the correct expression of the protein. The problem is solved in the presence of the Cre recombinase, when the Neo cassette and the sequences between the loxP sites are removed allowing the expression of the mutated targeted allele.

Nevertheless, to solve this issue, as it was essential for us to study the role of CDK4 inactivation after LUAD development, we decided to combine a standard *Cdk4* floxed allele (Lagarrigue et al., 2016) and CDK4 inactivation using the Flex system (Schnutgen et al., 2003) resulting in the *Cdk4*$^{FlexK35M/L}$ strain (See Figure 22). Thus, leading to a functional wildtype allele expressed from the endogenous locus before the Cre recombinase is expressed.

1.2. Beyond the catalytic activity of the protein: kinase independent functions

These technical difficulties did not preclude us from studying the overall consequences of CDK4 inactivation during homeostasis. But first, using a baculoviral-expression system we confirmed complete kinase inactivation of both KD models. The baculovirus system is a widely spread system that allows for post-transcriptional modifications (Harashima and Sekine, 2011), however the amount of protein generated is not at physiological levels, therefore we decided to immunoprecipitate CDK4^{WT}, CDK4^{K35M} and CDK4^{D140A} in embryos where other CDKs and CYCLINs such as CDK6 and CYCLIND are present (Figure 12). Despite the fact that the background of the immunoprecipitation did not allow us

to robustly confirm the absence of residual kinase activity, when quantifying the intensity of the RB protein levels phosphorylation in the IP versus MOCK conditions, we concluded that both KD models are not able to phosphorylate its substrate RB. These two results in parallel proved the impairment of $CDK4^{K35M}$ and $CDK4^{D140A}$ catalytic activity, confirming the already published K35M inactivating mutation (Kato et al., 1993) in our GEMM model.

Ideally, identification of putative therapeutic targets that are essential for tumor development but have a non-essential role for normal homeostasis will increase the chances of success in the clinic. This could be the case of CDK4 since we have confirmed that CDK4 kinase inactivation is dispensable during homeostasis as these mice are viable, but it has an important role in lung tumor initiation and progression. Another example for this is CYCLIND1 which is dispensable for the adult mouse homeostasis but required for the mammary gland in a tumor-specific context (Yu et al., 2006). This could be the reason why CDK4/6 inhibitors have got ahead for the treatment of breast cancer (Finn et al., 2009).

First of all, in order to properly compare with the data in the literature (Martin et al., 2003; Padmakumar et al., 2009; Rane et al., 1999; Tsutsui et al., 1999), we decided to generate the KO for *Cdk4* (*Cdk4*$^{-/-}$) in a pure genetic background (C57BL/6) to avoid phenotype penetrance variations. To our surprise, only a very small percentage (1,2%) of *Cdk4*$^{-/-}$ mice survived embryogenesis (Table 5). These results are in disagreement with the ones observed by Tsutsui and colleagues where *Cdk4*$^{-/-}$ mice were viable in the same genetic background (Tsutsui et al., 1999). The reason why this happened is unknown, however the group of Tsutsui *et al*. did not reported to have reached Mendelian ratios in the *Cdk4*$^{-/-}$ mice and claimed some postnatal lethality in 27% of the born homozygous mice. Moreover, two more groups (Martin et al., 2003; Rane et al., 1999) gave rise to the same conclusion of *Cdk4* being dispensable for mouse development using, in this case, a mixed 129/Sv background. Some years later, Padmakumar *et al.* observed that in a mixed C57BL/6:129/Sv genetic background and in a tumor context where p53 is suppressed, *Cdk4*$^{-/-}$;*Trp53*$^{-/-}$ mice are not born (Padmakumar et al., 2009). All this data together, suggest that at least in stringent genetic conditions, *Cdk4* is essential for animal development indicating that, other CDKs cannot compensate for the lack of the protein. The reason why these KO mice are not viable is still under investigation no obvious defects were observed neither in the embryos nor in the few pups that were born. Nevertheless, as the penetrance was 100% in the pure genetic background, we decided to backcross with wildtype 129/Sv mice. These F1 newborns, almost restored to Mendelian ratios the viability of *Cdk4*$^{-/-}$ mice (16,7% over the expected 25%) (Table 5). Special attention to the genetic backgrounds used and the influences they could cause in the mouse phenotype should be taken in consideration when generating GEMMs, in order not to misinterpret information. Therefore, most of the studies made in this thesis were done in mixed genetic backgrounds

in order to compare the effect of CDK4 kinase inhibition with CDK4 complete deletion. Of importance, both KD models are perfectly viable in all genetic backgrounds tested confirming that according to our data, CDK4 catalytic activity is not essential for mouse development.

It was reported and then confirmed in this thesis that CDK4 is essential for the development of specific cellular types such as β-pancreatic cells. Indeed, mice lacking CDK4 developed an insulin-deficient diabetic phenotype at the early age of 2 months (Rane et al., 1999; Tsutsui et al., 1999 and Figure 15). This cell autonomous CDK4 dependent mechanism is related with the fact that other kinases such as CDK6 which normally would compensate CDK4 loss, is not expressed in normal pancreatic cells. The diabetic phenotype was also manifested when mice express both inactivating CDK4 mutations (K35M and D140A), albeit later in time and with limited penetrance as demonstrated by the increase in size and number of the Langerhans islets compared to the *Cdk4* null pancreas, highlighting the relevance of kinase independent mechanisms during homeostasis. The delay in the appearance of diabetes as well as the lower penetrance of the phenotype allow mice carrying the inactivating mutations to increase their lifespan whereas the CDK4 KO mice do not live more than 8 months (in the C57BL/6:129/Sv controlled-mixed genetic background that is the only one where CDK4 KO mice are born). We think the postnatal death is directly related to the diabetic phenotype. This hypothesis is based on our observations that at the moment *Cdk4*$^{-/-}$ mice die, 11 out of 12 animals had already developed diabetes. Instead, Tsutsui *et al.* claimed that is not a direct consequence of the diabetic illness since not all *Cdk4*$^{-/-}$ mice were hyperglycemic before dying and glucosuria did not appear until 5 or 6 weeks (Tsutsui et al., 1999). This, together with the fact that the KO mice are smaller compared to the KD mutant isoforms and the fertility problems of the KO mice that are bypassed in the KD models due to normal prolactin-producing lactotrophs lead us to contemplate the possibility of kinase independent functions related to CDK4 (Figure 14 and Figure 16).

Several studies suggest that lack of CDK4 has a role in delaying cell cycle entry and progression (Martin et al., 2003; Padmakumar et al., 2009; Rane et al., 1999; Tsutsui et al., 1999). In order to study this, we isolated MEFs from the pure genetic background from all different genotypes and we confirmed that CDK4 is not essential for *in vitro* proliferation, neither its kinase activity. However, although not significantly, a slight slowdown in proliferation rate in *Cdk4*$^{-/-}$ MEFs was observed. In addition, the capacity of *Cdk4*$^{-/-}$ MEFs to immortalize was compromised although finally they manage to bypass the crisis phase undergoing continuous cell division (Figure 17). This suggests that ablation of CDK4 induces a limited capacity for proliferation that may be bypassed by other CDKs during *in vitro* cell division. Moreover, this process is kinase independent since CDK4 catalytic inactivation possesses the ability to immortalize after several passages.

The final outcome of this study allows us to speculate about CDK4 pharmacological intervention since this genetic model is a good proof of concept to understand its consequences (feasibility, toxicity, etc.) in physiological conditions, indicating that CDK4 kinase inhibition should be feasible and well tolerated in patients. Whether CDK4 inactivation has a role in tumor development will be further discuss.

In order to decipher whether the contribution of CDK4 to tumor initiation and progression could also rely in part on kinase independent properties we generated i) *Kras*^{G12V} MEFs capable to transform upon Cre-mediated recombination and ii) cells capable to transform upon the expression of a mutant RAS and a dominant negative version of p53 (*Hras*^{G12V}*/DNTrp53*). In these *Kras*-driven contexts, both CDK4 inactivation or the lack of it made cells to reduce their proliferation and their transformation potential compared to CDK4^{WT} cells. Nevertheless, this effect was enhanced in the CDK4^{KO} context (Puyol et al., 2010). Among the KD mutants, mainly CDK4^{K35M} cells were not able to proliferate or transform in a *Kras*-dependent manner (Figure 18). Probably, a more stringent context where low serum conditions are present in these cultures may allow us to better see the effect for CDK4 target ablation versus inactivation. Nevertheless, this data suggests that CDK4 kinase inactivation has a limited role in *Kras-driven* tumor cell proliferation. In fact, we confirmed these results in an *in vivo* model where lung tumors were induced by the *Kras*^{G12V} oncogene along with the expression of two CDK4 KD isoforms from the germline of the mouse (K35M or D140A). Again, the reduction in tumor burden was enhanced upon CDK4 ablation, implying most likely kinase independent functions (Figure 19). However, this model might not be suitable predicting the therapeutic value related to CDK4 inhibition in adult tumor-bearing mice since CDK4 is already inactivated at embryonic developmental stages. Hence, the *Therapeutic Model* had been designed in order to decipher all these questions.

The phenotypic and mechanistic differences found, both in homeostasis and tumor initiation, between the inactivation of the catalytic activity of CDK4 and its protein ablation pointed out to kinase independent functions. It is already known that CDK4/6-CYCLIND complexes have mainly two ways to regulate cell cycle progression: one catalytic function responsible of RB and other targets, e.g. Smads, phosphorylation and another related to its different titration rates accomplished by the CIP/KIP inhibitors driven by non-catalytic functions. In normal conditions, CIP/KIP inhibitors have a dual role apart of their inhibiting properties, these proteins favor the assembly and stabilization of CDK4/6-CYCLIND complexes. Therefore, CDK2 is inhibitor-free leading to cell cycle progression (Sherr and Roberts, 1999). On the contrary, upon CDK4 depletion, *p27*^{Kip1} is free to bind and inhibit CDK2-CYCLINE complexes halting S-phase entry (Tsutsui et al., 1999). In *p27*$^{-/-}$ cells, the levels of CDK2-CYCLINE complexes formation are reduced, and only upon *p27*^{Kip1} reintroduction the assembly is rescued. The question is then: are catalytic inactive CDK4 mutants titrating more of this CIP/KIP inhibitors leading to

CDK2 indirect compensatory mechanisms? In other words, is CDK2 being less inhibited by the CIP/KIP proteins when a CDK4 KD is present compared to the complete ablation of the CDK4 protein? Is this titration key?

To answer these questions, the CDK2 protein was immunoprecipitated in MEF extracts where the *Kras*^{G12V} oncogene can be activated upon Cre-mediated recombination in the different conditions (CDK4^{WT}, CDK4^{D140A}, CDK4^{K35M} and CDK4^{KO}, Figure 21). We confirmed that CIP/KIP inhibitors bind more extensively in the absence of CDK4 (e.g.. p27/CDK2: 3,4) and this binding is reduced in the presence of CDK4 K35M or D140A mutants (e.g. p27/CDK2: 2,1 and p27/CDK2: 1,4 respectively).This data suggests that this partial binding of the CIP/KIP inhibitors to CDK2 when CDK4 is inactivated finally allows some cells to enter in S-phase by CDK2 compensatory mechanisms (See proposed working model below, Figure 45). Still, there is an additional possibility that CDK4 has, like CDK6 (Kollmann et al., 2013), kinase independent functions beyond direct or indirect cell cycle control that have not been reported yet.

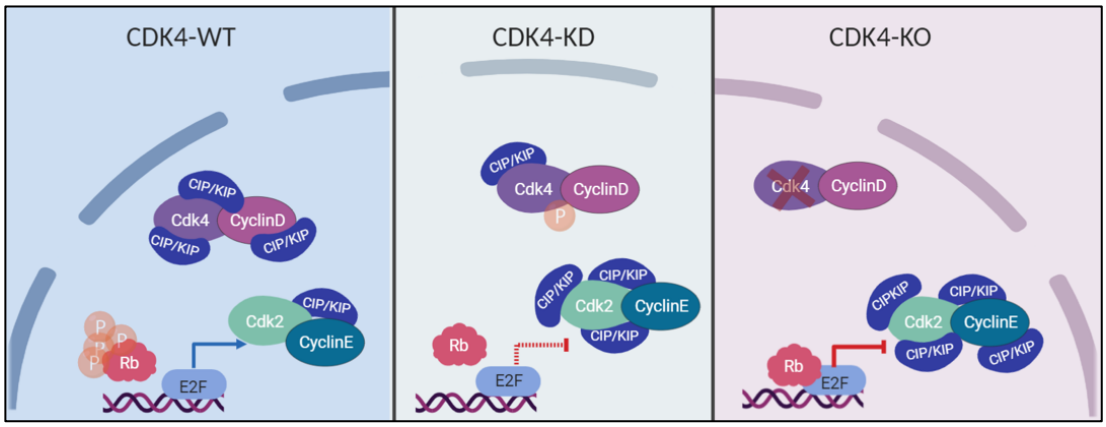

Figure 45: Hypothetical model for CDK4 kinase independent functions in different contexts.

2. Study of the effect of concomitant inactivation of CDK4 and RAF1 in *Kras-driven* lung adenocarcinoma

Identifying the molecular mechanisms responsible of sustaining cell growth in an aberrant manner has been one of the biggest challenges for researchers and clinicians during the past 30 years. As time passes, we have learned that the accumulation of mutations in the genome, among others, are responsible of rapid tumor initiation and growth. Based on these discoveries, nowadays, the scientific community has turned its attention into finding candidates for cancer-specific activities that consists of inhibiting the defective proteins produced by these altered genes. However, although many efforts have been employed until now, it has not been a complete successful path. Still, these targeted therapies are not approved for the treatment for *Kras*-driven LUAD patients, and for other types of tumors they mostly result in the appearance of tumor recurrence after favorable tumor response.

2.1. CDK4 and RAF1 inhibition: an ideal combinatory therapy

Targeting CDK4 has already demonstrated a specific therapeutic benefit in preventing mutant *Kras-driven* LUAD progression in a mouse model (Puyol et al., 2010). Yet, only less aggressive tumors with a functional *Trp53* tumor suppressor were studied. In the present thesis we have confirmed the previous results and added more value to that study: i) CDK4 catalytic activity inactivation has been assessed in both *Trp53* deficient and proficient backgrounds and ii) an efficient dual Cre recombinase system that allows for spatial and temporal analysis of lung tumor regression upon CDK4 inactivation once a tumor is established has been used *(Therapeutic Model).* Unfortunately, catalytic inactivation of CDK4 albeit having an important role in delaying tumor initiation, does not induce a significant regression of established tumors (Figure 24 and Figure 25), highlighting the importance of finding combinatorial options for the treatment of *Kras-driven* LUAD.

However, our findings demonstrated no toxic side effects associated to CDK4 kinase systemic inactivation in the mice (Figure 23). This correlates with the previous study in our laboratory where it was demonstrated that CDK4 is dispensable for normal mouse tissues, including normal lung development (Puyol et al., 2010). Therefore, other therapies combined with CDK4 inhibition can be made without increasing additional toxicity, a very sought-after feature in the field of drug development since in the clinic monotherapy has demonstrated to result insufficient.

Now, the question would be: which is the best additional candidate to add synergism to CDK4 inactivation? There are several preclinical and clinical attempts co-targeting the MEK kinases (Lee et al., 2016; Posch et al., 2018; Ruscetti et al., 2018; Tao et al., 2016; Teh et al., 2018; Zhou et al., 2017), yet it is already known that genetic elimination of both kinases ERK1/ERK2 or MEK1/MEK2, although efficiently block LUAD initiation, it is extremely toxic being incompatible with adult life (Blasco et al., 2011). Of course, it is unlikely that drug treatments are as efficient as genetic intervention but data from our laboratory and others suggest that the inhibition of these kinases will not be well tolerated. In words of R. Marais, this idea “need to be borne in mind in the clinical setting” (Rebocho and Marais, 2011). However, only if very low doses of the compounds are given, the therapeutic window to avoid these toxic effects could be bypassed with the major risk of not reaching complete pathway inhibition. With this aim, two clinical trials (NCT02022982 and NCT02703571) are nowadays recruiting patients for the treatment of solid tumors combining MEK + CDK4/6 inhibitors.

Anyhow, giving the importance of the MAPK pathway, one target that has already demonstrated to be tolerable upon its depletion in adult mice and induce important therapeutic benefits in LUAD is *Raf1* (Blasco et al., 2011; Lee et al., 2019; Sanclemente et al., 2018). Therefore, as mentioned in the introduction (See sections 3.1 and 3.4), due to its direct implications in cell cycle and its kinase independent antiapoptotic functions, one of the most important objectives of this thesis was

to study the role of RAF1 ablation in combination with CDK4 inactivation in LUAD progression. Over all, 100% of the tumors regressed upon CDK4 and RAF1 inactivation irrespectively of the p53 status. More importantly, 24% of those tumors were no longer detectable by CT suggesting complete regression (Figure 27 and Figure 28). The *in vivo* results obtained claim there are no precedents achieving this important tumor regression in other preclinical assays for the treatment of LUAD apart from immunotherapy (Forde et al., 2018).

How these cells respond to concomitant inactivation is a matter of debate, *in vitro* we have demonstrated that most of them die trough a programmed cell death mechanism via cleavage of Caspase-3 (CC3). To asses for apoptosis *in vivo* we have performed CC3 immunohistochemistry 9 weeks after TX exposure (Figure 30), and in fact there is a significantly increase in CC3+ cells (1,5 FC) when comparing with RAF1 ablation alone which has already demonstrated to induce apoptosis (Sanclemente et al., 2018). Ideally, this experiment, should be done at earlier time points, in order to catch the first induction of cell death. However, due to technical difficulties, this approach cannot be performed since there is no complete excision of the targets before 9 weeks of TX exposure (data not shown). Surprisingly, and in contrast to our previous results in $Kras^{G12V}$-driven LUAD (Puyol et al., 2010), *in vitro* but specially *in vivo* no clear senescence phenotype was observed as assessed by the senescence-associated β -galactosidase (SA-β-gal) activity assay (Figure 30). Whether this is p53 depletion-related should be further analyzed. However, others have demonstrated that treating LUAD bearing $Kras^{G12D}$ and *Trp53* mutations (KP model) with Palbociclib (CDK4/6) + Trametinib (MEK) inhibitors drive tumor cells towards senescence (Ruscetti et al., 2018). Nevertheless, they reported no apoptotic phenotype induced but instead an immune system clearance of senescent cells. Whether this effect is MEK and CDK6 dependent / RAF1 independent will need further studies. In addition, it is already known that the specificity of drug treatments is not as high as genetic inhibition, having other off-target effects rather than the above-mentioned ones. Moreover, it has been shown that CDK4/6 counteract the induction of senescence by phosphorylating the Forkhead Box M1 (FOXM1) gene, a transcription activator opposite to the tumor suppressor RB (Anders et al., 2011; Wang et al., 2005). Whether CDK6 can be inhibiting senescence since in our model we only target CDK4 should be further assessed too by checking FOXM1 phosphorylation levels.

In order to mechanistically characterize what is essential for CDK4 and RAF1 to sustain *Kras*-driven tumor progression, cell lines derived from tumors not exposed to TX were generated. Of note, a reduction of $pRB^{Ser807-811}$ was found by Western blot although not complete loss (Figure 32). This lack of complete reduction is somehow expected, as we already saw that CDK4 has kinase independent functions in our previous models, where $p21^{Cip1}$ and $p27^{Kip1}$ are less bound to CDK2 when the KD isoforms are expressed. But also, our laboratory reported that $Cdk4^{-/-};Cdk2^{-/-}$ embryonic fibroblast

displayed robust pRB$^{Ser807\text{-}811}$ despite the fact of lacking these two CDKs (Barrière et al., 2007). Other suggested that p38 can phosphorylate pRB$^{Ser807\text{-}811}$ in response to stress signals (Faust et al., 2012). On the other hand, in 2014 Narasimha *et al*. separated for the first time, all RB isoforms by two-dimensional gel electrophoresis and studied deeply the different phosphorylation states through G1 to S-phase. Moreover, upon DNA damage, cells arrested in G1 phase have constitutive CDK4/6-CYCLIND activity, loss of CDK2/CYCLINE activity and mono-phosphorylated RB (Narasimha et al., 2014). And interestingly, they proved that commercial antibodies to detect specific phospho-sites, including the one used in this thesis (Cell Signaling-9308) recognize the mono-phosphorylated RB isoforms from early G1 arrested cells. Therefore, suggesting that RB phosphorylation is compatible with G1 arrested cells. Together, these observations demonstrated that in response to DNA damage, cells select for mono-phosphorylated RB by activating CDK4/6-CYCLIND complexes and that could be the reason why still, we do see RB phosphorylation. Still, more experiments to rule out DNA damage responses should be done since in our model, H2AX or pCHK1 markers were not differentially expressed upon combined inhibition of CDK4/RAF1 compared to the controls.

Moreover, although most of the previous studies have focused on the role of RB in the nucleus, it is also known that it can be present in the cytoplasm, and afterwards translocated to the mitochondria suggesting a role of RB in apoptosis (Roth et al., 2009). Phosphorylation at the Ser^{567} favors cell death (Ma et al., 2003). Additionally, phosphorylation at Ser$^{807\text{-}811}$, the main sites of RB activation which prime other RB phosphorylation sites, promotes apoptosis when located in the mitochondria in a BAX dependent manner, indicating that RB can have transcriptional-independent functions (Hilgendorf et al., 2013). In fact, some years before it was already reported that pRB can activate transcription of several apoptotic genes (Ianari et al., 2009). This group reported a tumor suppressor role of RB in the mitochondria in a *p16^{INK4a}* knock-down context in MEFs (Hilgendorf et al., 2013). Similarly, Roscovitine inhibition, which induces cell death in human colorectal cancer cells, targets the RB at Ser^{795}, but not Ser$^{807\text{-}811}$ although here it could be argued that other CDKs and other targets rather than pRB may be playing a role when drug administration (De Leon et al., 2010). Whether this is the case in our *Kras^{G12V};Trp53$^{-/-}$;Cdk4$^{K35M/-}$;Raf1$^{-/-}$* lung tumor cells still need further characterization; as a first step a cellular fractionation experiment in order to localize RB should be performed.

Similarly, pERK protein levels remained unaltered (Figure 32), demonstrating that in this context, RAF1 elimination does not modify its downstream effectors linking the apoptotic function of RAF1 ablation to MAPK independent functions (Figure 32 and Sanclemente et al., 2018). According to this, evidences of Sorafenib impairing cell growth in a RAF-independent-ERK activation manner have been disclosed in *Kras* mutant NSCLC cell lines (Takezawa et al., 2009).

In addition, bioinformatic analysis show a downregulation in most oncogenic pathways when inactivating both targets concomitantly, such as KRAS, ERBB, PI3K/AKT/mTOR, MYC, WNT or NOTCH signaling, leading to a remarkable switch off of the oncogenic machinery (Figure 34). This suggests that combined inhibition of CDK4 and RAF1 leads to a synergistic effect that triggers a slow-down in tumor proliferation and the inactivation of anti-apoptotic activities from which these targets may be responsible.

2.2. Consequences of combined Cdk4 and Raf1 inactivation in adult homeostasis

Minimizing pharmacologic treatment-derived toxicities is of high priority right now in the clinic. One of the ways to reduce the side effects is to rationally schedule timing and doses of drug treatments. For instance, CDK4/6 inhibitors arrest cells in G1 phase, therefore they should not be used in combination with chemotherapy, since the cells would be insensitive to chemotherapeutics, as they specifically kill actively dividing cells. For that reason, combination of CDK4/6 inhibitors with targeted therapies could be a good option rather than with chemotherapy. As an example, CDK4/6 inhibitors have been recently combined with anti-estrogen therapy (Malorni et al., 2018).

One of the main advantages of our mouse models is that the toxicity related to target inhibition can be assessed in non-tumor bearing mice before continuing with the efficacy studies. For this purpose, it is only needed the presence of a conditional allele which simplifies the model. This is accomplished thanks to an inducible hUBC-CreERT2 allele, that as its name indicates it induces the recombination ubiquitously in all the cells, mimicking a human treatment where drug delivery is also systemic. This approach is followed when *Cdk4*$^{FlexK35M/L}$;*Raf1*$^{L/L}$ mice are 8 months of age, the same time when tumor-bearing mice would enter in a TX-containing diet after CT+ detection. Therefore, combination of the widespread loss of RAF1 expression (Sanclemente et al., 2018), the old age of the mice and the continuous exposure to tamoxifen diet, lead to some toxicity as observed by the body weight loss during the 5 months mice were maintained (Figure 26). Yet, several histological analyses of the tissues did not reveal any obvious defect thereby suggesting that concomitant inhibition of CDK4 and RAF1 is well tolerated (Figure 26). Alternatives to reduce the toxicity associated to the age and the tamoxifen-containing diet could be either to develop reversible and inducible alleles to turn ON and OFF the selected target when desired (Soucek et al., 2008), as is the case of pharmacological treatments in the clinic where compounds are not given during some days, or to completely remove the tamoxifen once we are sure correct excision has occurred, although genetic manipulation would be irreversible in this case. To demonstrate the importance of correct treatment appliance, a deep study about different timing protocols of CDK4/6 and MEK inhibitors had been performed, giving rise to the conclusion that

the better responses are achieved upon continuous MEK and discontinuous CDK4/6 inhibition (Teh et al., 2018).

2.3. What does not kill you makes you stronger: when cells become resistant to a therapy

As mentioned before (Introduction Section 2.6) there are several pathways a cell can find in order to overcome tumor growth inhibition. An interesting view of cancer recurrence came out in 2016 when it was suggested that resistant cells may give rise from a small cluster of "persister" cells that stay dormant acting as a reservoir until finally evolve to the bona fide drug-resistance heterogenous mechanism (Hangauer et al., 2017; Ramirez et al., 2016). Hightroughput screening from persister cultures rising from a single cell, identified diverse resistance mechanisms including those commonly found in the clinic during drug treatments (Ramirez et al., 2016). This is suggesting that this reservoir of latent cells is not reducing the high variability of resistant mechanisms. However, trying to find and target the vulnerabilities of this small population of persister cells before they sustain disease relapse, would be a promising strategy for the treatment or even for the prevention of resistance.

This seemed to be the case in our study, since isolation of a small percentage of single cell colonies (~10%) demonstrated the capability to revive and spawn new cancer growth in a CDK4 and RAF1 independent manner. As demonstrated by the RNAseq data, among the 9 resistant established cells lines, expanded from 9 different single colonies, from different original cell lines, it was not feasible to find a common upregulated gene or pathway shared among all of them (Figure 38). Only once we assumed that heterogenous resistant mechanisms were implicit in the way cells escape CDK4 and RAF1 inhibition, and analyzed the resistant cell lines as independents, we identified specific vulnerabilities for two different sets of resistant cells: RT1-3 and RT4-9 (Figure 39); this time indicating the existence of inter-tumor heterogeneity.

On one hand, epigenetic changes are one of the main causes leading to tumor resistance (Acevedo et al., 2016; Guler et al., 2017; Knoechel et al., 2014). In fact, it was described that upon CDK4/6 inhibition, DNA methyltransferase (DNMT) mRNA levels are reduced leading to $p21^{Cip1}$ demethylation, therefore favoring cell cycle arrest (Goel et al., 2018). According to the bioinformatic analysis, among others, $p21^{Cip1}$ gene was methylated (-1,25 log2FC) when comparing resistant cells with responder cells in 3 out of 9 cell lines analyzed. Indicating that the methylation of tumor suppressor genes or cell cycle inhibitors allow the cells to evade therapeutic treatments. As a consequence, a set of resistant cells significantly responded to 5-Azacytidine treatment, a DNA methylation inhibitor (Figure 41). In agreement with this, it was recently found, that in 50% of the melanoma cases where B-RAF is mutated increases their chances to respond to HDACs inhibitors, since it was reported an

increase expression of the protein histone deacetylase 8 (HDAC 8) in melanoma B-RAF/MEK resistant cells (Emmons et al., 2019).

On the other hand, there was another set of cells, 6 out of 9, that developed resistance by activation of PI3K pathway (Figure 42). It was previously described by Vora and colleagues that persistent CDK4 protein levels leads to acquired resistance to PI3K inhibitors, indicating that the combination of CDK4/6 + PI3K inhibition sensitizes breast cancer cell lines (Vora et al., 2014). In addition, a pre-existing mutation in PI3K (PIK3CAE545K) conferred resistance to CDK4/6 + MEK inhibition in *Nras* mutant melanoma (Romano et al., 2018). Therefore, inhibition of PI3K pathway resulted in efficacious resistance impairment as we demonstrated (Figure 43).

In addition, resistant cells became more metabolically active (Table 7). As already described, RT1-3 (the group that grew faster when subcutaneously injected) are much more active in terms of energy and lipid metabolism. In fact, they seem to be more dependent on oxidative phosphorylation than RT4-9. In order to assess the importance of upregulating metabolic pathways, inhibitors of the electron transport chain such as metformin, would make cells become energetically inefficient, reducing glucose uptake and presumably leading to tumor growth inhibition. As a consequence, those cells more vulnerable to glucose metabolism will be significantly affected. Moreover, a ketogenic diet consisting on a high-fat-carbohydrate-restricted regime would therefore, shed light on this aspect and could help us to understand the metabolic role these cells may be playing during resistance.

Of course, many other mechanisms of resistance may be responsible of CDK4/RAF1 independent cell growth. In this behalf, the application of individual personalized medicine to identify genetic susceptibilities would help to diminish, or at least delay, the appearance of tumor relapses. Importantly, the identification of biomarkers that can predict tumor responses will definitely help to counteract tumor resistance.

3. Future perspectives for the clinic

3.1. More specific and potent inhibitors should be design

Although more conservative studies support the idea of CDK4 and CDK6 being functionally redundant (Malumbres et al., 2004), it has been previously described that CDK4 and CDK6 have tissue-specific functions (Tsutsui et al., 1999), different phosphorylated residues for their activation (Bockstaele et al., 2009) or kinase independent functions (for CDK6) to induce tumor proliferation and angiogenesis (Kollmann et al., 2013). In addition, most of the side effects caused by the available CDK4/6 compounds such as neutropenia are due to CDK6 inhibition, since its genetic inhibition is known to induce important hematopoietic defects (Malumbres et al., 2004). Therefore, in order to develop

better inhibitors and reduce toxicities, the industry is trying to selectively inhibit CDK4, although it has become a difficult challenge due to the high homology of the two cell cycle kinases. Nevertheless, overexpression of *CDK4*, and not *CDK6*, has been reported in the context of lung cancer (Dobashi et al., 2004; Wikman et al., 2005). In fact, *CDK4* amplification is more frequently found in LUADs; among 230 human samples 7% have *CDK4* amplified, whereas only 2.6% have *CDK6* amplification (Figure 46). According to the TCGA database, *CDK4* amplification co-occur with *Kras* in 43% (7 out of 16) of the cases, whereas no CDK6 amplifications are detected together with the *KRAS* oncogene (Figure 46). In addition, it was demonstrated that CDK6 is irrelevant for *Kras*-driven LUAD progression in mice (Puyol et al., 2010). Moreover, Abemaciclib inhibition in endogenous LUAD (Figure 36) does not mimic the effect of CDK4 catalytic inactivation by genetic means nor induces lung tumor regressions indicating that more potent anti CDK4 compounds will be required.

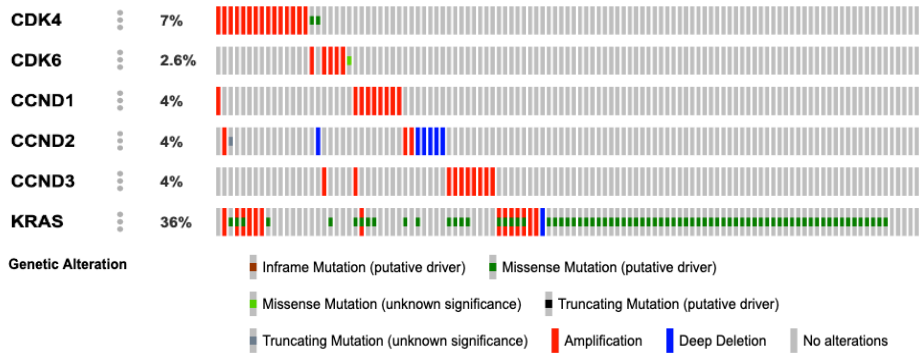

Figure 46: Alterations (mutations, amplifications or deletions) in CDK4, CDK6, CCND1, CCND2 and CCND3 in human Lung Adenocarcinoma (TCGA; http://bit.ly/2K0Ls1c).

3.2. A novel approach for targeted therapy: degron chemistry

Nowadays, as previously mentioned, there are no specific drugs against CDK4 nor RAF1. In contrast those inhibitors are designed against either CDK4/6 or against all RAF family members due to the high homology of the kinase domain shared among them.

In addition, it was demonstrated that combined ablation of B-RAF and RAF1 (C-RAF) leads to unacceptable toxicities (Sanclemente et al., 2018). Other drugs such as Dabrafenib or Vemurafenib were designed as potent B-RAF^{V600E} inhibitors (Gibney and Zager, 2013; Tsai et al., 2008), demonstrating a potent clinical benefit to melanoma patients expressing this specific mutation (Flaherty et al., 2010). However, one of the biggest drawbacks of these compounds is that they paradoxically activate the MAPK pathway in B-RAF wildtype cells, accelerating tumor growth by inducing B-RAF/RAF1 heterodimers (Hatzivassiliou et al., 2010; Heidorn et al., 2010). As a consequence, second-generation RAF inhibitors were developed. They rise as “paradox breakers” since they are not supposed to activate

the MAPK pathway when RAS is mutated. Instead, they block RAF when in dimers (Peng et al., 2015). These "paradox breakers" (PLX7904 and PLX8394), have shown potent B-RAF^{V600E} inhibition without inducing MAPK activation (Tutuka et al., 2017), hence PLX8394 is currently in phase II clinical trials for the treatment of solid tumors.

In our hands, the use of panRAF inhibitors until the moment has not achieved the same therapeutic benefit as complete genetic RAF1 protein elimination for the treatment of *Kras*^{G12V}-driven LUAD (Figure 36). As mentioned before, on one hand therapeutic intervention is not as precise as genetic allele elimination; but on the other, the pharmacological industry is targeting the catalytic activity of the protein. Therefore, only if that target has important kinase independent functions, as is the case for RAF1, degradation of the protein should be a better drug-design approach. Our laboratory has sufficient evidences to confirm that the therapeutic effect of RAF1 ablation in LUAD is mainly due to RAF1 kinase independent functions. Two different *Raf1* KD models, one mutating the ATP binding site (K375M) and another mutating the proton acceptor (D468A) of the protein, do not recapitulate the effect on tumor regression seen when the protein was completely abrogated (Blasco et al., 2011; Sanclemente et al., 2018 and this thesis). Although these experiments are still ongoing, the catalytic inactivation of RAF1 seems to be not essential for *Kras*^{G12V}-driven, p53 deleted lung tumor induction (unpublished data).

Likewise, in the present thesis, we have demonstrated that specific CDK4 complete protein ablation leads to an increased reduction in lung tumor initiation compared to the expression of two KD isoforms, one mutating the ATP binding site (K35M) and another mutating the proton acceptor (D140A) (Figure 19).

Many kinase independent functions have been identified after drug treatments therefore the available kinase inhibitors may not be as useful as expected. As a consequence, a new field is emerging with the aim of prompting those putative targets to the proteasome to be degraded (Nabet et al., 2018). For this purpose, a new technique to experimentally validate protein degradation, called dTAG (degradation tag) is being used: the drug binds to an E3 ubiquitin ligase and at the same time, to the protein of interest fused to a FKBP12^{mut} protein that triggers polyubiquitination and proteasome-mediated degradation. In addition, this effect can be reversible when the drug is removed, minimizing the toxicities related to long-term protein elimination. One of the main drawbacks of this technique, is the large size of these molecules, hence, drug delivery is a concern. Once bioavailability of these compounds will be solved, the PROTAC (proteolic-targeting chimeras) technology seems to be a potent and promising strategy to improve the current drug designs when the catalytic activities of the protein are not the only responsible of tumor progression. Consequently, the idea is that inhibitors should

target both CDK4 and RAF1 therefore, closely recapitulating genetic ablation with pharmacological approaches.

The hypothetical model shown below, depicted a complete global picture of the results obtained from the present thesis (Figure 47).

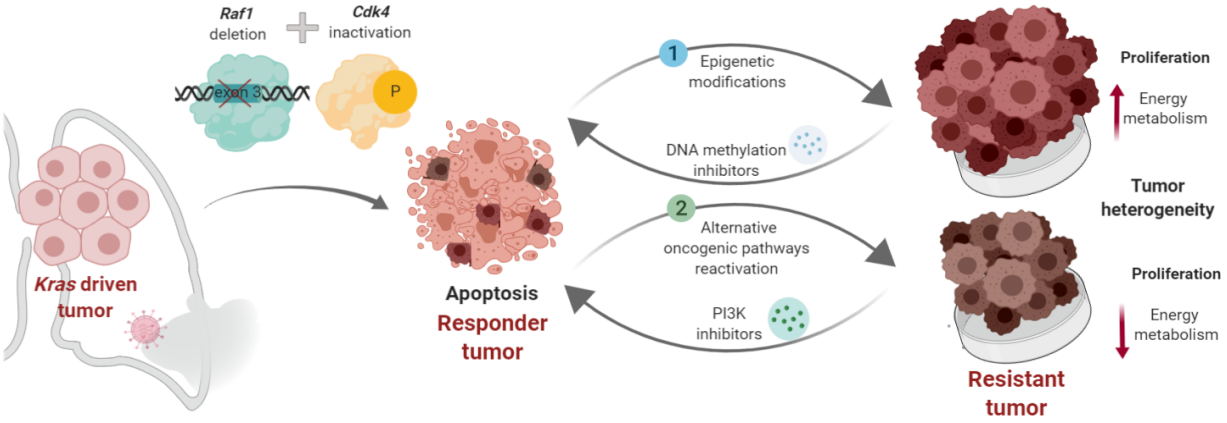

Figure 47: Hypothetical model for CDK4 and RAF1 inactivation in *Kras*-driven, *Trp53* deficient lung tumors.

Lots of questions need still to be answered. The complexity of the oncogenic KRAS signaling and its link with cell cycle progression needs deeper genetic and biochemical analysis. Both the cellular context as well as the crosstalk between pathways have demonstrated to play an essential role in LUAD progression. Full understanding of the whole picture in the oncogenic puzzle will help to better design selective and efficient inhibitors.

CONCLUSIONS

The conclusions obtained in this thesis were the following:

1. CDK4 catalytic activity is dispensable for life. Expression of K35M and D140A catalytic inactive mutants during embryonic development is associated with smaller weight and size as well as the development of insulin-deficient diabetes due to defects in the β-pancreatic cells; recapitulating the CDK4 null phenotype but later in time and with less penetrance.

2. The elimination of CDK4 kinase activity impairs lung tumor formation driven by the *Kras*^{G12V} oncogene although to a lesser extent than the *Cdk4* null allele, suggesting the existence of CDK4 kinase independent functions in this tumor context. These, could be in part due to the sequestration of CIP/KIP inhibitors by the CDK4 protein that might facilitate CDK2 compensatory activity.

3. Expression of kinase inactive CDK4^{K35M} isoform results in a limited therapeutic effect when induced in already established tumors, either in a *Trp53* proficient or deficient backgrounds.

4. Concomitant CDK4 and RAF1 inactivation results in a significant therapeutic benefit in 100% of the *Kras*^{G12V}-driven LUADs irrespectively of the *Trp53* status. CDK4 and RAF1 synergistically cooperate to increase apoptotic-related genes and decrease oncogenic activity.

1. *In vitro* CDK4 and RAF1 independent cell growth appears in a small population of cells by either epigenetic modifications or activation of alternative pathways, such as PI3K. Yet, these cells display high degree of tumoral heterogeneity, therefore further research is required in order understand other putative resistant mechanisms that may be playing a role.

Las conclusiones obtenidas en la presente tesis son las siguientes:

1. La eliminación de la actividad quinasa de CDK4 es dispensable para la vida. La expresión de dos mutantes catalíticamente inactivos, K35M y D140A, está asociada con una reducción del peso y el tamaño de los ratones, así como al desarrollo de diabetes debido a un defecto en las células β–pancreáticas del ratón; recapitulando así el fenotipo de la eliminación de CDK4, pero con mayor latencia y menor penetrancia.

2. La eliminación de la actividad catalítica de CDK4 retarda la formación de tumores dirigidos por el oncogén *Kras*^{G12V}, aunque en menor medida que la eliminación de CDK4, sugiriendo la existencia de funciones catalíticamente independientes en este contexto tumoral. Se podría deber, en parte, a la capacidad de CDK4 de secuestrar los inhibidores CIP/KIP lo que facilitaría un mecanismo compensatorio por parte de CDK2.

3. La inactivación de CDK4^{K35M} tiene un efecto terapéutico limitado cuando es inactivado en tumores ya establecidos, tanto en ausencia como en presencia del tumor supresor *Trp53*.

4. La inhibición conjunta de CDK4 y RAF1 da lugar a un claro beneficio terapéutico ya que el 100% de los adenocarcinomas de pulmón dirigidos por el oncogén *Kras*^{G12V} paralizan su desarrollo tanto en ausencia como en presencia del tumor supresor *Trp53.* CDK4 y RAF1 cooperan de manera sinergística para incrementar genes relacionados con la apoptosis y disminuir la señalización oncogénica.

5. La inactivación de CDK4 y RAF1 *in vitro* resulta en un crecimiento independiente a estos genes al inducir cambios epigenéticos o la reactivación de vías alternativas, como PI3K. Sin embargo, estas células muestran un alto grado de heterogeneidad tumoral, por lo tanto, se requiere más investigación para comprender otros posibles mecanismos de resistencia que podrían estar también desempeñando un papel importante.

BIBLIOGRAPHY

Abella, A., Dubus, P., Malumbres, M., Rane, S. G., Kiyokawa, H., Sicard, A., Vignon, F., Langin, D., Barbacid, M., and Fajas, L. (2005). Cdk4 promotes adipogenesis through PPARgamma activation. Cell Metab *2*, 239-249.

Acevedo, M., Vernier, M., Mignacca, L., Lessard, F., Huot, G., Moiseeva, O., Bourdeau, V., and Ferbeyre, G. (2016). A CDK4/6-Dependent Epigenetic Mechanism Protects Cancer Cells from PML-induced Senescence. Cancer Res *76*, 3252-3264.

Aggarwal, P., Vaites, L. P., Kim, J. K., Mellert, H., Gurung, B., Nakagawa, H., Herlyn, M., Hua, X., Rustgi, A. K., McMahon, S. B., and Diehl, J. A. (2010). Nuclear cyclin D1/CDK4 kinase regulates CUL4 expression and triggers neoplastic growth via activation of the PRMT5 methyltransferase. Cancer Cell *18*, 329-340.

Alagesan, B., Contino, G., Guimaraes, A. R., Corcoran, R. B., Deshpande, V., Wojtkiewicz, G. R., Hezel, A. F., Wong, K.-K., Loda, M., Weissleder, R.*, et al.* (2015). Combined MEK and PI3K inhibition in a mouse model of pancreatic cancer. Clinical cancer research : an official journal of the American Association for Cancer Research *21*, 396-404.

Albers, M. W., Williams, R. T., Brown, E. J., Tanaka, A., Hall, F. L., and Schreiber, S. L. (1993). FKBP-rapamycin inhibits a cyclin-dependent kinase activity and a cyclin D1-Cdk association in early G1 of an osteosarcoma cell line. J Biol Chem *268*, 22825-22829.

Aleem, E., Kiyokawa, H., and Kaldis, P. (2005). Cdc2-cyclin E complexes regulate the G1/S phase transition. Nat Cell Biol *7*, 831-836.

Alexander, M., Wolfe, R., Ball, D., Conron, M., Stirling, R. G., Solomon, B., MacManus, M., Officer, A., Karnam, S., Burbury, K., and Evans, S. M. (2017). Lung cancer prognostic index: a risk score to predict overall survival after the diagnosis of non-small-cell lung cancer. British Journal Of Cancer *117*, 744.

An, H. X., Beckmann, M. W., Reifenberger, G., Bender, H. G., and Niederacher, D. (1999). Gene amplification and overexpression of CDK4 in sporadic breast carcinomas is associated with high tumor cell proliferation. Am J Pathol *154*, 113-118.

Anders, L., Ke, N., Hydbring, P., Choi, Y. J., Widlund, H. R., Chick, J. M., Zhai, H., Vidal, M., Gygi, S. P., Braun, P., and Sicinski, P. (2011). A systematic screen for CDK4/6 substrates links FOXM1 phosphorylation to senescence suppression in cancer cells. Cancer Cell *20*, 620-634.

Andrews, S. (2010). FastQC. Available at: http://www.bioinformatics. babraham.ac.uk/projects/fastqc/.

Annicotte, J. S., Blanchet, E., Chavey, C., Iankova, I., Costes, S., Assou, S., Teyssier, J., Dalle, S., Sardet, C., and Fajas, L. (2009). The CDK4-pRB-E2F1 pathway controls insulin secretion. Nat Cell Biol *11*, 1017-1023.

Aprelikova, O., Xiong, Y., and Liu, E. T. (1995). Both p16 and p21 families of cyclin-dependent kinase (CDK) inhibitors block the phosphorylation of cyclin-dependent kinases by the CDK-activating kinase. J Biol Chem *270*, 18195-18197.

Asghar, U., Witkiewicz, A. K., Turner, N. C., and Knudsen, E. S. (2015). The history and future of targeting cyclin-dependent kinases in cancer therapy. Nat Rev Drug Discov *14*, 130-146.

Avruch, J. (1998). Insulin signal transduction through protein kinase cascades. Mol Cell Biochem *182*, 31-48.

Avruch, J., Khokhlatchev, A., Kyriakis, J. M., Luo, Z., Tzivion, G., Vavvas, D., and Zhang, X. F. (2001). Ras activation of the Raf kinase: tyrosine kinase recruitment of the MAP kinase cascade. Recent Prog Horm Res *56*, 127-155.

Baccarini, M. (2005). Second nature: biological functions of the Raf-1 "kinase". FEBS Lett *579*, 3271-3277.

Barbie, D. A., Tamayo, P., Boehm, J. S., Kim, S. Y., Moody, S. E., Dunn, I. F., Schinzel, A. C., Sandy, P., Meylan, E., Scholl, C.*, et al.* (2009). Systematic RNA interference reveals that oncogenic KRAS-driven cancers require TBK1. Nature *462*, 108-112.

Barrière, C., Santamaría, D., Cerqueira, A., Galán, J., Martín, A., Ortega, S., Malumbres, M., Dubus, P., and Barbacid, M. (2007). Mice thrive without Cdk4 and Cdk2. Mol Oncol *1*, 72-83.

Bauer, C. A., Kim, E. Y., Marangoni, F., Carrizosa, E., Claudio, N. M., and Mempel, T. R. (2014). Dynamic Treg interactions with intratumoral APCs promote local CTL dysfunction. The Journal of clinical investigation *124*, 2425-2440.

Bayascas, J. R., Sakamoto, K., Armit, L., Arthur, J. S., and Alessi, D. R. (2006). Evaluation of approaches to generation of tissue-specific knock-in mice. J Biol Chem *281*, 28772-28781.

Beach, D., Durkacz, B., and Nurse, P. (1982). Functionally homologous cell cycle control genes in budding and fission yeast. Nature *300*, 706-709.

Beaver, J. A., Amiri-Kordestani, L., Charlab, R., Chen, W., Palmby, T., Tilley, A., Zirkelbach, J. F., Yu, J., Liu, Q., Zhao, L.*, et al.* (2015). FDA Approval: Palbociclib for the Treatment of Postmenopausal Patients with Estrogen Receptor-Positive, HER2-Negative Metastatic Breast Cancer. Clin Cancer Res *21*, 4760-4766.

Beroukhim, R., Mermel, C. H., Porter, D., Wei, G., Raychaudhuri, S., Donovan, J., Barretina, J., Boehm, J. S., Dobson, J., Urashima, M.*, et al.* (2010). The landscape of somatic copy-number alteration across human cancers. Nature *463*, 899-905.

Berthet, C., Aleem, E., Coppola, V., Tessarollo, L., and Kaldis, P. (2003). Cdk2 knockout mice are viable. Curr Biol *13*, 1775-1785.

Berthet, C., Klarmann, K. D., Hilton, M. B., Suh, H. C., Keller, J. R., Kiyokawa, H., and Kaldis, P. (2006). Combined loss of Cdk2 and Cdk4 results in embryonic lethality and Rb hypophosphorylation. Dev Cell *10*, 563-573.

Bisi, J. E., Sorrentino, J. A., Jordan, J. L., Darr, D. D., Roberts, P. J., Tavares, F. X., and Strum, J. C. (2017). Preclinical development of G1T38: A novel, potent and selective inhibitor of cyclin dependent kinases 4/6 for use as an oral antineoplastic in patients with CDK4/6 sensitive tumors. Oncotarget *8*, 42343-42358.

Bisteau, X., Paternot, S., Colleoni, B., Ecker, K., Coulonval, K., De Groote, P., Declercq, W., Hengst, L., and Roger, P. P. (2013). CDK4 T172 Phosphorylation Is Central in a CDK7-Dependent Bidirectional CDK4/CDK2 Interplay Mediated by p21 Phosphorylation at the Restriction Point. PLOS Genetics *9*, e1003546.

Blain, S. (2008). Switching cyclin D-Cdk4 kinase activity on and off. Cell Cycle *7*, 892-898.

Blasco, M. T., Navas, C., Martin-Serrano, G., Grana-Castro, O., Lechuga, C. G., Martin-Diaz, L., Djurec, M., Li, J., Morales-Cacho, L., Esteban-Burgos, L.*, et al.* (2019). Complete Regression of Advanced Pancreatic Ductal Adenocarcinomas upon Combined Inhibition of EGFR and C-RAF. Cancer Cell *35*, 573-587 e576.

Blasco, R. B., Francoz, S., Santamaria, D., Canamero, M., Dubus, P., Charron, J., Baccarini, M., and Barbacid, M. (2011). c-Raf, but not B-Raf, is essential for development of K-Ras oncogene-driven non-small cell lung carcinoma. Cancer Cell *19*, 652-663.

Blumenschein, G. R., Jr., Smit, E. F., Planchard, D., Kim, D. W., Cadranel, J., De Pas, T., Dunphy, F., Udud, K., Ahn, M. J., Hanna, N. H.*, et al.* (2015). A randomized phase II study of the MEK1/MEK2 inhibitor trametinib (GSK1120212) compared with docetaxel in KRAS-mutant advanced non-small-cell lung cancer (NSCLC)dagger. Ann Oncol *26*, 894-901.

Bockstaele, L., Bisteau, X., Paternot, S., and Roger, P. P. (2009). Differential regulation of cyclin-dependent kinase 4 (CDK4) and CDK6, evidence that CDK4 might not be activated by CDK7, and design of a CDK6 activating mutation. Mol Cell Biol *29*, 4188-4200.

Bonelli, M. A., Digiacomo, G., Fumarola, C., Alfieri, R., Quaini, F., Falco, A., Madeddu, D., La Monica, S., Cretella, D., Ravelli, A.*, et al.* (2017). Combined Inhibition of CDK4/6 and PI3K/AKT/mTOR Pathways Induces a Synergistic Anti-Tumor Effect in Malignant Pleural Mesothelioma Cells. Neoplasia *19*, 637-648.

Bourdeau, V., and Ferbeyre, G. (2016). CDK4-CDK6 inhibitors induce autophagy-mediated degradation of DNMT1 and facilitate the senescence antitumor response. Autophagy *12*, 1965-1966.

Bray, F., Ferlay, J., Soerjomataram, I., Siegel, R. L., Torre, L. A., and Jemal, A. (2018). Global cancer statistics 2018: GLOBOCAN estimates of incidence and mortality worldwide for 36 cancers in 185 countries. CA Cancer J Clin *68*, 394-424.

Cekanova, M., Majidy, M., Masi, T., Al-Wadei, H. A., and Schuller, H. M. (2007). Overexpressed Raf-1 and phosphorylated cyclic adenosine 3'-5'-monophosphatate response element-binding protein are early markers for lung adenocarcinoma. Cancer *109*, 1164-1173.

Cen, L., Carlson, B. L., Schroeder, M. A., Ostrem, J. L., Kitange, G. J., Mladek, A. C., Fink, S. R., Decker, P. A., Wu, W., Kim, J. S.*, et al.* (2012). p16-Cdk4-Rb axis controls sensitivity to a cyclin-dependent kinase inhibitor PD0332991 in glioblastoma xenograft cells. Neuro Oncol *14*, 870-881.

Cerqueira, A., Martín, A., Symonds, C. E., Odajima, J., Dubus, P., Barbacid, M., and Santamaría, D. (2014). Genetic characterization of the role of the Cip/Kip family of proteins as cyclin-dependent kinase inhibitors and assembly factors. Molecular and cellular biology *34*, 1452-1459.

Chen, J., Fujii, K., Zhang, L., Roberts, T., and Fu, H. (2001). Raf-1 promotes cell survival by antagonizing apoptosis signal-regulating kinase 1 through a MEK-ERK independent mechanism. Proc Natl Acad Sci U S A *98*, 7783-7788.

Chen, Z., Fillmore, C. M., Hammerman, P. S., Kim, C. F., and Wong, K.-K. (2014). Non-small-cell lung cancers: a heterogeneous set of diseases. Nature reviews Cancer *14*, 535-546.

Cheung, T. H., Yu, M. M., Lo, K. W., Yim, S. F., Chung, T. K., and Wong, Y. F. (2001). Alteration of cyclin D1 and CDK4 gene in carcinoma of uterine cervix. Cancer Lett *166*, 199-206.

Chow, Y. H., Zhu, X. D., Liu, L., Schwartz, B. R., Huang, X. Z., Harlan, J. M., and Schnapp, L. M. (2010). Role of Cdk4 in lymphocyte function and allergen response. Cell Cycle *9*, 4922-4930.

Coley, W. B. (1991). The treatment of malignant tumors by repeated inoculations of erysipelas. With a report of ten original cases. 1893. Clin Orthop Relat Res, 3-11.

Corona, S. P., and Generali, D. (2018). Abemaciclib: a CDK4/6 inhibitor for the treatment of HR+/HER2- advanced breast cancer. Drug Des Devel Ther *12*, 321-330.

Curran, W. J., Jr., Paulus, R., Langer, C. J., Komaki, R., Lee, J. S., Hauser, S., Movsas, B., Wasserman, T., Rosenthal, S. A., Gore, E.*, et al.* (2011). Sequential vs. concurrent chemoradiation for stage III non-small cell lung cancer: randomized phase III trial RTOG 9410. J Natl Cancer Inst *103*, 1452-1460.

Dankort, D., Filenova, E., Collado, M., Serrano, M., Jones, K., and McMahon, M. (2007). A new mouse model to explore the initiation, progression, and therapy of BRAFV600E-induced lung tumors. Genes Dev *21*, 379-384.

Dasgupta, P., Rastogi, S., Pillai, S., Ordonez-Ercan, D., Morris, M., Haura, E., and Chellappan, S. (2006). Nicotine induces cell proliferation by beta-arrestin-mediated activation of Src and Rb-Raf-1 pathways. J Clin Invest *116*, 2208-2217.

Davidson, M. R., Gazdar, A. F., and Clarke, B. E. (2013). The pivotal role of pathology in the management of lung cancer. J Thorac Dis *5 Suppl 5*, S463-478.

De Leon, G., Cavino, M., D'Angelo, M., and Krucher, N. A. (2010). PNUTS knockdown potentiates the apoptotic effect of Roscovitine in breast and colon cancer cells. Int J Oncol *36*, 1269-1275.

Deng, J., Wang, E. S., Jenkins, R. W., Li, S., Dries, R., Yates, K., Chhabra, S., Huang, W., Liu, H., Aref, A. R.*, et al.* (2018). CDK4/6 Inhibition Augments Antitumor Immunity by Enhancing T-cell Activation. Cancer Discov *8*, 216-233.

Desai, T. J., Brownfield, D. G., and Krasnow, M. A. (2014). Alveolar progenitor and stem cells in lung development, renewal and cancer. Nature *507*, 190-194.

Dickler, M. N., Tolaney, S. M., Rugo, H. S., Cortes, J., Dieras, V., Patt, D., Wildiers, H., Hudis, C. A., O'Shaughnessy, J., Zamora, E.*, et al.* (2017). MONARCH 1, A Phase II Study of Abemaciclib, a CDK4 and CDK6 Inhibitor, as a Single Agent, in Patients with Refractory HR(+)/HER2(-) Metastatic Breast Cancer. Clin Cancer Res *23*, 5218-5224.

Dobashi, Y., Goto, A., Fukayama, M., Abe, A., and Ooi, A. (2004). Overexpression of cdk4/cyclin D1, a possible mediator of apoptosis and an indicator of prognosis in human primary lung carcinoma. Int J Cancer *110*, 532-541.

Dobin, A., Davis, C. A., Schlesinger, F., Drenkow, J., Zaleski, C., Jha, S., Batut, P., Chaisson, M., and Gingeras, T. R. (2013). STAR: ultrafast universal RNA-seq aligner. Bioinformatics *29*, 15-21.

Douillard, J. Y., Ostoros, G., Cobo, M., Ciuleanu, T., McCormack, R., Webster, A., and Milenkova, T. (2013). First-line gefitinib in Caucasian EGFR mutation-positive NSCLC patients: a phase-IV, open-label, single-arm study. British Journal Of Cancer *110*, 55.

Dragatsis, I., and Zeitlin, S. (2001). A method for the generation of conditional gene repair mutations in mice. Nucleic acids research *29*, E10-E10.

Drosten, M., Lechuga, C. G., and Barbacid, M. (2014). Ras in epidermal proliferation. Oncotarget *5*, 5194-5195.

DuPage, M., and Jacks, T. (2013). Genetically engineered mouse models of cancer reveal new insights about the antitumor immune response. Curr Opin Immunol *25*, 192-199.

DuPage, M., Mazumdar, C., Schmidt, L. M., Cheung, A. F., and Jacks, T. (2012). Expression of tumour-specific antigens underlies cancer immunoediting. Nature *482*, 405-409.

Dyson, N. (1998). The regulation of E2F by pRB-family proteins. Genes Dev *12*, 2245-2262.

Ehrenreiter, K., Kern, F., Velamoor, V., Meissl, K., Galabova-Kovacs, G., Sibilia, M., and Baccarini, M. (2009). Raf-1 addiction in Ras-induced skin carcinogenesis. Cancer Cell *16*, 149-160.

Ehrenreiter, K., Piazzolla, D., Velamoor, V., Sobczak, I., Small, J. V., Takeda, J., Leung, T., and Baccarini, M. (2005). Raf-1 regulates Rho signaling and cell migration. J Cell Biol *168*, 955-964.

Emmons, M. F., Faiao-Flores, F., Sharma, R., Thapa, R., Messina, J. L., Becker, J. C., Schadendorf, D., Seto, E., Sondak, V. K., Koomen, J. M.*, et al.* (2019). HDAC8 Regulates a Stress Response Pathway in Melanoma to Mediate Escape from BRAF Inhibitor Therapy. Cancer Res *79*, 2947-2961.

Faust, D., Schmitt, C., Oesch, F., Oesch-Bartlomowicz, B., Schreck, I., Weiss, C., and Dietrich, C. (2012). Differential p38-dependent signalling in response to cellular stress and mitogenic stimulation in fibroblasts. Cell communication and signaling : CCS *10*, 6-6.

Finn, R. S., Aleshin, A., and Slamon, D. J. (2016). Targeting the cyclin-dependent kinases (CDK) 4/6 in estrogen receptor-positive breast cancers. Breast Cancer Res *18*, 17.

Finn, R. S., Crown, J. P., Lang, I., Boer, K., Bondarenko, I. M., Kulyk, S. O., Ettl, J., Patel, R., Pinter, T., Schmidt, M.*, et al.* (2015). The cyclin-dependent kinase 4/6 inhibitor palbociclib in combination with letrozole versus letrozole alone as first-line treatment of oestrogen receptor-positive, HER2-negative, advanced breast cancer (PALOMA-1/TRIO-18): a randomised phase 2 study. Lancet Oncol *16*, 25-35.

Finn, R. S., Dering, J., Conklin, D., Kalous, O., Cohen, D. J., Desai, A. J., Ginther, C., Atefi, M., Chen, I., Fowst, C.*, et al.* (2009). PD 0332991, a selective cyclin D kinase 4/6 inhibitor, preferentially inhibits proliferation of luminal estrogen receptor-positive human breast cancer cell lines in vitro. Breast Cancer Res *11*, R77.

Fisher, R. P. (2005). Secrets of a double agent: CDK7 in cell-cycle control and transcription. J Cell Sci *118*, 5171-5180.

Flaherty, K. T., Puzanov, I., Kim, K. B., Ribas, A., McArthur, G. A., Sosman, J. A., O'Dwyer, P. J., Lee, R. J., Grippo, J. F., Nolop, K., and Chapman, P. B. (2010). Inhibition of mutated, activated BRAF in metastatic melanoma. N Engl J Med *363*, 809-819.

Flaherty, K. T., Robert, C., Hersey, P., Nathan, P., Garbe, C., Milhem, M., Demidov, L. V., Hassel, J. C., Rutkowski, P., Mohr, P.*, et al.* (2012). Improved survival with MEK inhibition in BRAF-mutated melanoma. N Engl J Med *367*, 107-114.

Forde, P. M., Chaft, J. E., Smith, K. N., Anagnostou, V., Cottrell, T. R., Hellmann, M. D., Zahurak, M., Yang, S. C., Jones, D. R., Broderick, S.*, et al.* (2018). Neoadjuvant PD-1 Blockade in Resectable Lung Cancer. N Engl J Med *378*, 1976-1986.

Fu, M., Rao, M., Bouras, T., Wang, C., Wu, K., Zhang, X., Li, Z., Yao, T. P., and Pestell, R. G. (2005). Cyclin D1 inhibits peroxisome proliferator-activated receptor gamma-mediated adipogenesis through histone deacetylase recruitment. J Biol Chem *280*, 16934-16941.

Gacche, R. N., and Assaraf, Y. G. (2018). Redundant angiogenic signaling and tumor drug resistance. Drug Resist Updat *36*, 47-76.

Galaktionov, K., Jessus, C., and Beach, D. (1995). Raf1 interaction with Cdc25 phosphatase ties mitogenic signal transduction to cell cycle activation. Genes Dev *9*, 1046-1058.

Gan, L., Liu, P., Lu, H., Chen, S., Yang, J., McCarthy, J. B., Knudsen, K. E., and Huang, H. (2009). Cyclin D1 promotes anchorage-independent cell survival by inhibiting FOXO-mediated anoikis. Cell Death Differ *16*, 1408-1417.

Gandhi, L., Rodriguez-Abreu, D., Gadgeel, S., Esteban, E., Felip, E., De Angelis, F., Domine, M., Clingan, P., Hochmair, M. J., Powell, S. F.*, et al.* (2018). Pembrolizumab plus Chemotherapy in Metastatic Non-Small-Cell Lung Cancer. N Engl J Med *378*, 2078-2092.

Ganuza, M., Saiz-Ladera, C., Canamero, M., Gomez, G., Schneider, R., Blasco, M. A., Pisano, D., Paramio, J. M., Santamaria, D., and Barbacid, M. (2012). Genetic inactivation of Cdk7 leads to cell cycle arrest and induces premature aging due to adult stem cell exhaustion. EMBO J *31*, 2498-2510.

Geng, Y., Whoriskey, W., Park, M. Y., Bronson, R. T., Medema, R. H., Li, T., Weinberg, R. A., and Sicinski, P. (1999). Rescue of cyclin D1 deficiency by knockin cyclin E. Cell *97*, 767-777.

Gibney, G. T., and Zager, J. S. (2013). Clinical development of dabrafenib in BRAF mutant melanoma and other malignancies. Expert Opin Drug Metab Toxicol *9*, 893-899.

Goel, S., DeCristo, M. J., McAllister, S. S., and Zhao, J. J. (2018). CDK4/6 Inhibition in Cancer: Beyond Cell Cycle Arrest. Trends Cell Biol *28*, 911-925.

Goel, S., DeCristo, M. J., Watt, A. C., BrinJones, H., Sceneay, J., Li, B. B., Khan, N., Ubellacker, J. M., Xie, S., Metzger-Filho, O.*, et al.* (2017). CDK4/6 inhibition triggers anti-tumour immunity. Nature *548*, 471-475.

Goel, S., Wang, Q., Watt, A. C., Tolaney, S. M., Dillon, D. A., Li, W., Ramm, S., Palmer, A. C., Yuzugullu, H., Varadan, V.*, et al.* (2016). Overcoming Therapeutic Resistance in HER2-Positive Breast Cancers with CDK4/6 Inhibitors. Cancer Cell *29*, 255-269.

Goldman, J. W., Mazieres, J., Barlesi, F., Koczywas, M., Dragnev, K. H., Göksel, T., Cortot, A. B., Girard, N., Wesseler, C., Bischoff, H.*, et al.* (2018). A randomized phase 3 study of abemaciclib versus erlotinib in previously treated patients with stage IV NSCLC with KRAS mutation: JUNIPER. Journal of Clinical Oncology *36*, 9025-9025.

Gong, X., Litchfield, L. M., Webster, Y., Chio, L. C., Wong, S. S., Stewart, T. R., Dowless, M., Dempsey, J., Zeng, Y., Torres, R.*, et al.* (2017). Genomic Aberrations that Activate D-type Cyclins Are Associated with Enhanced Sensitivity to the CDK4 and CDK6 Inhibitor Abemaciclib. Cancer Cell *32*, 761-776 e766.

Gopalan, P. K., Villegas, A. G., Cao, C., Pinder-Schenck, M., Chiappori, A., Hou, W., Zajac-Kaye, M., Ivey, A. M., and Kaye, F. J. (2018). CDK4/6 inhibition stabilizes disease in patients with p16-null non-small cell lung cancer and is synergistic with mTOR inhibition. Oncotarget *9*, 37352-37366.

Guerra, C., Mijimolle, N., Dhawahir, A., Dubus, P., Barradas, M., Serrano, M., Campuzano, V., and Barbacid, M. (2003). Tumor induction by an endogenous K-ras oncogene is highly dependent on cellular context. Cancer Cell *4*, 111-120.

Guler, G. D., Tindell, C. A., Pitti, R., Wilson, C., Nichols, K., KaiWai Cheung, T., Kim, H. J., Wongchenko, M., Yan, Y., Haley, B.*, et al.* (2017). Repression of Stress-Induced LINE-1 Expression Protects Cancer Cell Subpopulations from Lethal Drug Exposure. Cancer Cell *32*, 221-237.e213.

Hainsworth, J. D., Cebotaru, C. L., Kanarev, V., Ciuleanu, T. E., Damyanov, D., Stella, P., Ganchev, H., Pover, G., Morris, C., and Tzekova, V. (2010). A phase II, open-label, randomized study to assess the efficacy and safety of AZD6244 (ARRY-142886) versus pemetrexed in patients with non-small cell lung cancer who have failed one or two prior chemotherapeutic regimens. J Thorac Oncol *5*, 1630-1636.

Hanahan, D., and Weinberg, R. A. (2011). Hallmarks of cancer: the next generation. Cell *144*, 646-674.

Hangauer, M. J., Viswanathan, V. S., Ryan, M. J., Bole, D., Eaton, J. K., Matov, A., Galeas, J., Dhruv, H. D., Berens, M. E., Schreiber, S. L.*, et al.* (2017). Drug-tolerant persister cancer cells are vulnerable to GPX4 inhibition. Nature *551*, 247-250.

Harashima, H., and Sekine, M. (2011). Measurement of plant cyclin-dependent kinase activity using immunoprecipitation-coupled and affinity purification-based kinase assays and the baculovirus expression system. Methods Mol Biol *779*, 65-78.

Hatzivassiliou, G., Song, K., Yen, I., Brandhuber, B. J., Anderson, D. J., Alvarado, R., Ludlam, M. J., Stokoe, D., Gloor, S. L., Vigers, G.*, et al.* (2010). RAF inhibitors prime wild-type RAF to activate the MAPK pathway and enhance growth. Nature *464*, 431-435.

Heidorn, S. J., Milagre, C., Whittaker, S., Nourry, A., Niculescu-Duvas, I., Dhomen, N., Hussain, J., Reis-Filho, J. S., Springer, C. J., Pritchard, C., and Marais, R. (2010). Kinase-dead BRAF and oncogenic RAS cooperate to drive tumor progression through CRAF. Cell *140*, 209-221.

Heilmann, A. M., Perera, R. M., Ecker, V., Nicolay, B. N., Bardeesy, N., Benes, C. H., and Dyson, N. J. (2014). CDK4/6 and IGF1 receptor inhibitors synergize to suppress the growth of p16INK4A-deficient pancreatic cancers. Cancer Res *74*, 3947-3958.

Heist, R. S., Sequist, L. V., and Engelman, J. A. (2012). Genetic changes in squamous cell lung cancer: a review. J Thorac Oncol *7*, 924-933.

Herrera-Abreu, M. T., Palafox, M., Asghar, U., Rivas, M. A., Cutts, R. J., Garcia-Murillas, I., Pearson, A., Guzman, M., Rodriguez, O., Grueso, J.*, et al.* (2016). Early Adaptation and Acquired Resistance to CDK4/6 Inhibition in Estrogen Receptor-Positive Breast Cancer. Cancer Res *76*, 2301-2313.

Hilgendorf, K. I., Leshchiner, E. S., Nedelcu, S., Maynard, M. A., Calo, E., Ianari, A., Walensky, L. D., and Lees, J. A. (2013). The retinoblastoma protein induces apoptosis directly at the mitochondria. Genes & development *27*, 1003-1015.

Hindley, A., and Kolch, W. (2007). Raf-1 and B-Raf promote protein kinase C theta interaction with BAD. Cell Signal *19*, 547-555.

Hirashita, Y., Tsukamoto, Y., Yanagihara, K., Fumoto, S., Hijiya, N., Nakada, C., Uchida, T., Matsuura, K., Kodama, M., Okimoto, T.*, et al.* (2016). Reduced phosphorylation of ribosomal protein S6 is associated with sensitivity to MEK inhibition in gastric cancer cells. Cancer Sci *107*, 1919-1928.

Hirsch, F. R., Scagliotti, G. V., Mulshine, J. L., Kwon, R., Curran, W. J., Jr., Wu, Y. L., and Paz-Ares, L. (2017). Lung cancer: current therapies and new targeted treatments. Lancet *389*, 299-311.

Hortobagyi, G. N., Stemmer, S. M., Burris, H. A., Yap, Y. S., Sonke, G. S., Paluch-Shimon, S., Campone, M., Blackwell, K. L., Andre, F., Winer, E. P.*, et al.* (2016). Ribociclib as First-Line Therapy for HR-Positive, Advanced Breast Cancer. N Engl J Med *375*, 1738-1748.

Hu, M. G., Deshpande, A., Schlichting, N., Hinds, E. A., Mao, C., Dose, M., Hu, G. F., Van Etten, R. A., Gounari, F., and Hinds, P. W. (2011). CDK6 kinase activity is required for thymocyte development. Blood *117*, 6120-6131.

Huang, Z. Y., Baldwin, R. L., Hedrick, N. M., and Gutmann, D. H. (2002). Astrocyte-specific expression of CDK4 is not sufficient for tumor formation, but cooperates with p53 heterozygosity to provide a growth advantage for astrocytes in vivo. Oncogene *21*, 1325-1334.

Hüser, M., Luckett, J., Chiloeches, A., Mercer, K., Iwobi, M., Giblett, S., Sun, X. M., Brown, J., Marais, R., and Pritchard, C. (2001). MEK kinase activity is not necessary for Raf-1 function. The EMBO journal *20*, 1940-1951.

Hwang, S. J., Cheng, L. S., Lozano, G., Amos, C. I., Gu, X., and Strong, L. C. (2003). Lung cancer risk in germline p53 mutation carriers: association between an inherited cancer predisposition, cigarette smoking, and cancer risk. Hum Genet *113*, 238-243.

Hydbring, P., Malumbres, M., and Sicinski, P. (2016). Non-canonical functions of cell cycle cyclins and cyclin-dependent kinases. Nat Rev Mol Cell Biol *17*, 280-292.

Ianari, A., Natale, T., Calo, E., Ferretti, E., Alesse, E., Screpanti, I., Haigis, K., Gulino, A., and Lees, J. A. (2009). Proapoptotic function of the retinoblastoma tumor suppressor protein. Cancer Cell *15*, 184-194.

Inamura, K. (2017). Lung Cancer: Understanding Its Molecular Pathology and the 2015 WHO Classification. Front Oncol *7*, 193.

Iorns, E., Turner, N. C., Elliott, R., Syed, N., Garrone, O., Gasco, M., Tutt, A. N., Crook, T., Lord, C. J., and Ashworth, A. (2008). Identification of CDK10 as an important determinant of resistance to endocrine therapy for breast cancer. Cancer Cell *13*, 91-104.

Jablonska, B., Aguirre, A., Vandenbosch, R., Belachew, S., Berthet, C., Kaldis, P., and Gallo, V. (2007). Cdk2 is critical for proliferation and self-renewal of neural progenitor cells in the adult subventricular zone. J Cell Biol *179*, 1231-1245.

Jackson, E. L., Olive, K. P., Tuveson, D. A., Bronson, R., Crowley, D., Brown, M., and Jacks, T. (2005). The differential effects of mutant p53 alleles on advanced murine lung cancer. Cancer Res *65*, 10280-10288.

Janes, M. R., Zhang, J., Li, L. S., Hansen, R., Peters, U., Guo, X., Chen, Y., Babbar, A., Firdaus, S. J., Darjania, L.*, et al.* (2018). Targeting KRAS Mutant Cancers with a Covalent G12C-Specific Inhibitor. Cell *172*, 578-589.e517.

Janne, P. A., van den Heuvel, M. M., Barlesi, F., Cobo, M., Mazieres, J., Crino, L., Orlov, S., Blackhall, F., Wolf, J., Garrido, P.*, et al.* (2017). Selumetinib Plus Docetaxel Compared With Docetaxel Alone and Progression-Free Survival in Patients With KRAS-Mutant Advanced Non-Small Cell Lung Cancer: The SELECT-1 Randomized Clinical Trial. JAMA *317*, 1844-1853.

Janne, P. A., Yang, J. C., Kim, D. W., Planchard, D., Ohe, Y., Ramalingam, S. S., Ahn, M. J., Kim, S. W., Su, W. C., Horn, L.*, et al.* (2015). AZD9291 in EGFR inhibitor-resistant non-small-cell lung cancer. N Engl J Med *372*, 1689-1699.

Jesenberger, V., Procyk, K. J., Rüth, J., Schreiber, M., Theussl, H. C., Wagner, E. F., and Baccarini, M. (2001). Protective role of Raf-1 in Salmonella-induced macrophage apoptosis. J Exp Med *193*, 353-364.

Joshi, M., Rice, S. J., Liu, X., Miller, B., and Belani, C. P. (2015). Trametinib with or without vemurafenib in BRAF mutated non-small cell lung cancer. PLoS One *10*, e0118210.

Karreth, F. A., Frese, K. K., DeNicola, G. M., Baccarini, M., and Tuveson, D. A. (2011). C-Raf is required for the initiation of lung cancer by K-Ras(G12D). Cancer discovery *1*, 128-136.

Kato, J., Matsushime, H., Hiebert, S. W., Ewen, M. E., and Sherr, C. J. (1993). Direct binding of cyclin D to the retinoblastoma gene product (pRb) and pRb phosphorylation by the cyclin D-dependent kinase CDK4. Genes Dev *7*, 331-342.

Kenfield, S. A., Wei, E. K., Stampfer, M. J., Rosner, B. A., and Colditz, G. A. (2008). Comparison of aspects of smoking among the four histological types of lung cancer. Tob Control *17*, 198-204.

Kerkhoff, E., and Rapp, U. R. (1997). Induction of cell proliferation in quiescent NIH 3T3 cells by oncogenic c-Raf-1. Molecular and cellular biology *17*, 2576-2586.

Khatib, Z. A., Matsushime, H., Valentine, M., Shapiro, D. N., Sherr, C. J., and Look, A. T. (1993). Coamplification of the CDK4 gene with MDM2 and GLI in human sarcomas. Cancer Res *53*, 5535-5541.

Kim, C. F., Jackson, E. L., Woolfenden, A. E., Lawrence, S., Babar, I., Vogel, S., Crowley, D., Bronson, R. T., and Jacks, T. (2005). Identification of bronchioalveolar stem cells in normal lung and lung cancer. Cell *121*, 823-835.

Knoechel, B., Roderick, J. E., Williamson, K. E., Zhu, J., Lohr, J. G., Cotton, M. J., Gillespie, S. M., Fernandez, D., Ku, M., Wang, H.*, et al.* (2014). An epigenetic mechanism of resistance to targeted therapy in T cell acute lymphoblastic leukemia. Nat Genet *46*, 364-370.

Knudsen, E. S., Hutcheson, J., Vail, P., and Witkiewicz, A. K. (2017). Biological specificity of CDK4/6 inhibitors: dose response relationship, in vivo signaling, and composite response signature. Oncotarget *8*, 43678-43691.

Kohler, J., Catalano, M., and Ambrogio, C. (2018). Back to the Bench? MEK and ERK Inhibitors for the Treatment of KRAS Mutant Lung Adenocarcinoma. Curr Med Chem *25*, 558-574.

Kollmann, K., Heller, G., Schneckenleithner, C., Warsch, W., Scheicher, R., Ott, R. G., Schafer, M., Fajmann, S., Schlederer, M., Schiefer, A. I.*, et al.* (2013). A kinase-independent function of CDK6 links the cell cycle to tumor angiogenesis. Cancer Cell *24*, 167-181.

Lagarrigue, S., Lopez-Mejia, I. C., Denechaud, P.-D., Escoté, X., Castillo-Armengol, J., Jimenez, V., Chavey, C., Giralt, A., Lai, Q., Zhang, L.*, et al.* (2016). CDK4 is an essential insulin effector in adipocytes. The Journal of clinical investigation *126*, 335-348.

Lakso, M., Pichel, J. G., Gorman, J. R., Sauer, B., Okamoto, Y., Lee, E., Alt, F. W., and Westphal, H. (1996). Efficient in vivo manipulation of mouse genomic sequences at the zygote stage. Proc Natl Acad Sci U S A *93*, 5860-5865.

Lange, C., Huttner, W. B., and Calegari, F. (2009). Cdk4/cyclinD1 overexpression in neural stem cells shortens G1, delays neurogenesis, and promotes the generation and expansion of basal progenitors. Cell Stem Cell *5*, 320-331.

Lavoie, H., Thevakumaran, N., Gavory, G., Li, J. J., Padeganeh, A., Guiral, S., Duchaine, J., Mao, D. Y. L., Bouvier, M., Sicheri, F., and Therrien, M. (2013). Inhibitors that stabilize a closed RAF kinase domain conformation induce dimerization. Nature chemical biology *9*, 428-436.

Le Mellay, V., Troppmair, J., Benz, R., and Rapp, U. R. (2002). Negative regulation of mitochondrial VDAC channels by C-Raf kinase. BMC Cell Biol *3*, 14-14.

Lee, C. L., Moding, E. J., Huang, X., Li, Y., Woodlief, L. Z., Rodrigues, R. C., Ma, Y., and Kirsch, D. G. (2012). Generation of primary tumors with Flp recombinase in FRT-flanked p53 mice. Dis Model Mech *5*, 397-402.

Lee, C. S., Lee, L. C., Yuan, T. L., Chakka, S., Fellmann, C., Lowe, S. W., Caplen, N. J., McCormick, F., and Luo, J. (2019). MAP kinase and autophagy pathways cooperate to maintain RAS mutant cancer cell survival. Proc Natl Acad Sci U S A.

Lee, M. S., Helms, T. L., Feng, N., Gay, J., Chang, Q. E., Tian, F., Wu, J. Y., Toniatti, C., Heffernan, T. P., Powis, G.*, et al.* (2016). Efficacy of the combination of MEK and CDK4/6 inhibitors in vitro and in vivo in KRAS mutant colorectal cancer models. Oncotarget *7*, 39595-39608.

Lee, Y., Dominy, J. E., Choi, Y. J., Jurczak, M., Tolliday, N., Camporez, J. P., Chim, H., Lim, J. H., Ruan, H. B., Yang, X.*, et al.* (2014). Cyclin D1-Cdk4 controls glucose metabolism independently of cell cycle progression. Nature *510*, 547-551.

Leicht, D. T., Balan, V., Kaplun, A., Singh-Gupta, V., Kaplun, L., Dobson, M., and Tzivion, G. (2007). Raf kinases: function, regulation and role in human cancer. Biochim Biophys Acta *1773*, 1196-1212.

Li, B., and Dewey, C. N. (2011). RSEM: accurate transcript quantification from RNA-Seq data with or without a reference genome. BMC Bioinformatics *12*, 323.

Lim, S., and Kaldis, P. (2012). Loss of Cdk2 and Cdk4 induces a switch from proliferation to differentiation in neural stem cells. Stem Cells *30*, 1509-1520.

Lim, S., and Kaldis, P. (2013). Cdks, cyclins and CKIs: roles beyond cell cycle regulation. Development *140*, 3079-3093.

Liu, F., and Korc, M. (2012). Cdk4/6 inhibition induces epithelial-mesenchymal transition and enhances invasiveness in pancreatic cancer cells. Mol Cancer Ther *11*, 2138-2148.

Lopez-Mejia, I. C., Lagarrigue, S., Giralt, A., Martinez-Carreres, L., Zanou, N., Denechaud, P. D., Castillo-Armengol, J., Chavey, C., Orpinell, M., Delacuisine, B.*, et al.* (2017). CDK4 Phosphorylates AMPKalpha2 to Inhibit Its Activity and Repress Fatty Acid Oxidation. Mol Cell *68*, 336-349.e336.

Love, M. I., Huber, W., and Anders, S. (2014). Moderated estimation of fold change and dispersion for RNA-seq data with DESeq2. Genome Biol *15*, 550.

Ma, D., Zhou, P., and Harbour, J. W. (2003). Distinct mechanisms for regulating the tumor suppressor and antiapoptotic functions of Rb. J Biol Chem *278*, 19358-19366.

Ma, L., Chen, Z., Erdjument-Bromage, H., Tempst, P., and Pandolfi, P. P. (2005). Phosphorylation and functional inactivation of TSC2 by Erk implications for tuberous sclerosis and cancer pathogenesis. Cell *121*, 179-193.

Mainardi, S., Mijimolle, N., Francoz, S., Vicente-Duenas, C., Sanchez-Garcia, I., and Barbacid, M. (2014). Identification of cancer initiating cells in K-Ras driven lung adenocarcinoma. Proc Natl Acad Sci U S A *111*, 255-260.

Majem, M., Juan, O., Insa, A., Reguart, N., Trigo, J. M., Carcereny, E., García-Campelo, R., García, Y., Guirado, M., and Provencio, M. (2019). SEOM clinical guidelines for the treatment of non-small cell lung cancer (2018). Clin Transl Oncol *21*, 3-17.

Malorni, L., Curigliano, G., Minisini, A. M., Cinieri, S., Tondini, C. A., D'Hollander, K., Arpino, G., Bernardo, A., Martignetti, A., Criscitiello, C.*, et al.* (2018). Palbociclib as single agent or in combination with the endocrine therapy received before disease progression for estrogen receptor-positive, HER2-negative metastatic breast cancer: TREnd trial. Ann Oncol *29*, 1748-1754.

Malumbres, M., and Barbacid, M. (2001). To cycle or not to cycle: a critical decision in cancer. Nat Rev Cancer *1*, 222-231.

Malumbres, M., and Barbacid, M. (2009). Cell cycle, CDKs and cancer: a changing paradigm. Nat Rev Cancer *9*, 153-166.

Malumbres, M., Harlow, E., Hunt, T., Hunter, T., Lahti, J. M., Manning, G., Morgan, D. O., Tsai, L. H., and Wolgemuth, D. J. (2009). Cyclin-dependent kinases: a family portrait. Nat Cell Biol *11*, 1275-1276.

Malumbres, M., Sotillo, R., Santamaria, D., Galan, J., Cerezo, A., Ortega, S., Dubus, P., and Barbacid, M. (2004). Mammalian cells cycle without the D-type cyclin-dependent kinases Cdk4 and Cdk6. Cell *118*, 493-504.

Marchetti, A., Doglioni, C., Barbareschi, M., Buttitta, F., Pellegrini, S., Gaeta, P., La Rocca, R., Merlo, G., Chella, A., Angeletti, C. A.*, et al.* (1998). Cyclin D1 and retinoblastoma susceptibility gene alterations in non-small cell lung cancer. Int J Cancer *75*, 187-192.

Marshall, C. (1999). How do small GTPase signal transduction pathways regulate cell cycle entry? Curr Opin Cell Biol *11*, 732-736.

Martin, J., Hunt, S. L., Dubus, P., Sotillo, R., Nehme-Pelluard, F., Magnuson, M. A., Parlow, A. F., Malumbres, M., Ortega, S., and Barbacid, M. (2003). Genetic rescue of Cdk4 null mice restores pancreatic beta-cell proliferation but not homeostatic cell number. Oncogene *22*, 5261-5269.

Matallanas, D., Birtwistle, M., Romano, D., Zebisch, A., Rauch, J., von Kriegsheim, A., and Kolch, W. (2011). Raf family kinases: old dogs have learned new tricks. Genes Cancer *2*, 232-260.

Matallanas, D., Romano, D., Yee, K., Meissl, K., Kucerova, L., Piazzolla, D., Baccarini, M., Vass, J. K., Kolch, W., and O'Neill, E. (2007). RASSF1A elicits apoptosis through an MST2 pathway directing proapoptotic transcription by the p73 tumor suppressor protein. Mol Cell *27*, 962-975.

McFarlin, D. R., and Gould, M. N. (2003). Rat mammary carcinogenesis induced by in situ expression of constitutive Raf kinase activity is prevented by tethering Raf to the plasma membrane. Carcinogenesis *24*, 1149-1153.

Meyer, C. A., Jacobs, H. W., Datar, S. A., Du, W., Edgar, B. A., and Lehner, C. F. (2000). Drosophila Cdk4 is required for normal growth and is dispensable for cell cycle progression. The EMBO journal *19*, 4533-4542.

Mielgo, A., Seguin, L., Huang, M., Camargo, M. F., Anand, S., Franovic, A., Weis, S. M., Advani, S. J., Murphy, E. A., and Cheresh, D. A. (2011). A MEK-independent role for CRAF in mitosis and tumor progression. Nat Med *17*, 1641-1645.

Mikula, M., Schreiber, M., Husak, Z., Kucerova, L., Ruth, J., Wieser, R., Zatloukal, K., Beug, H., Wagner, E. F., and Baccarini, M. (2001). Embryonic lethality and fetal liver apoptosis in mice lacking the c-raf-1 gene. Embo j *20*, 1952-1962.

Miliani de Marval, P. L., Macias, E., Rounbehler, R., Sicinski, P., Kiyokawa, H., Johnson, D. G., Conti, C. J., and Rodriguez-Puebla, M. L. (2004). Lack of cyclin-dependent kinase 4 inhibits c-myc tumorigenic activities in epithelial tissues. Mol Cell Biol *24*, 7538-7547.

Moons, D. S., Jirawatnotai, S., Tsutsui, T., Franks, R., Parlow, A. F., Hales, D. B., Gibori, G., Fazleabas, A. T., and Kiyokawa, H. (2002). Intact follicular maturation and defective luteal function in mice deficient for cyclin- dependent kinase-4. Endocrinology *143*, 647-654.

Morgan, D. O. (1997). Cyclin-dependent kinases: engines, clocks, and microprocessors. Annu Rev Cell Dev Biol *13*, 261-291.

Nabet, B., Roberts, J. M., Buckley, D. L., Paulk, J., Dastjerdi, S., Yang, A., Leggett, A. L., Erb, M. A., Lawlor, M. A., Souza, A*., et al.* (2018). The dTAG system for immediate and target-specific protein degradation. Nat Chem Biol *14*, 431-441.

Narasimha, A. M., Kaulich, M., Shapiro, G. S., Choi, Y. J., Sicinski, P., and Dowdy, S. F. (2014). Cyclin D activates the Rb tumor suppressor by mono-phosphorylation. eLife *3*, e02872.

Nieto, P., Ambrogio, C., Esteban-Burgos, L., Gomez-Lopez, G., Blasco, M. T., Yao, Z., Marais, R., Rosen, N., Chiarle, R., Pisano, D. G*., et al.* (2017). A Braf kinase-inactive mutant induces lung adenocarcinoma. Nature *548*, 239-243.

Niihori, T., Nagai, K., Fujita, A., Ohashi, H., Okamoto, N., Okada, S., Harada, A., Kihara, H., Arbogast, T., Funayama, R*., et al.* (2019). Germline-Activating RRAS2 Mutations Cause Noonan Syndrome. Am J Hum Genet *104*, 1233-1240.

O'Leary, B., Finn, R. S., and Turner, N. C. (2016). Treating cancer with selective CDK4/6 inhibitors. Nat Rev Clin Oncol *13*, 417-430.

O'Neill, E., and Kolch, W. (2005). Taming the Hippo: Raf-1 controls apoptosis by suppressing MST2/Hippo. Cell Cycle *4*, 365-367.

Odogwu, L., Mathieu, L., Blumenthal, G., Larkins, E., Goldberg, K. B., Griffin, N., Bijwaard, K., Lee, E. Y., Philip, R., Jiang, X.*, et al.* (2018). FDA Approval Summary: Dabrafenib and Trametinib for the Treatment of Metastatic Non-Small Cell Lung Cancers Harboring BRAF V600E Mutations. Oncologist *23*, 740-745.

Ortega, S., Malumbres, M., and Barbacid, M. (2002). Cyclin D-dependent kinases, INK4 inhibitors and cancer. Biochim Biophys Acta *1602*, 73-87.

Ortega, S., Prieto, I., Odajima, J., Martin, A., Dubus, P., Sotillo, R., Barbero, J. L., Malumbres, M., and Barbacid, M. (2003). Cyclin-dependent kinase 2 is essential for meiosis but not for mitotic cell division in mice. Nat Genet *35*, 25-31.

Ortega-Molina, A., Lopez-Guadamillas, E., Mattison, J. A., Mitchell, S. J., Munoz-Martin, M., Iglesias, G., Gutierrez, V. M., Vaughan, K. L., Szarowicz, M. D., Gonzalez-Garcia, I.*, et al.* (2015). Pharmacological inhibition of PI3K reduces adiposity and metabolic syndrome in obese mice and rhesus monkeys. Cell Metab *21*, 558-570.

Pacheco, J., and Schenk, E. (2019). CDK4/6 inhibition alone and in combination for non-small cell lung cancer. Oncotarget *10*, 618-619.

Padmakumar, V. C., Aleem, E., Berthet, C., Hilton, M. B., and Kaldis, P. (2009). Cdk2 and Cdk4 activities are dispensable for tumorigenesis caused by the loss of p53. Molecular and cellular biology *29*, 2582-2593.

Pandey, K., An, H. J., Kim, S. K., Lee, S. A., Kim, S., Lim, S. M., Kim, G. M., Sohn, J., and Moon, Y. W. (2019). Molecular mechanisms of resistance to CDK4/6 inhibitors in breast cancer: A review. Int J Cancer *145*, 1179-1188.

Pardee, A. B. (1974). A restriction point for control of normal animal cell proliferation. Proc Natl Acad Sci U S A *71*, 1286-1290.

Pardo, J., Aguilo, J. I., Anel, A., Martin, P., Joeckel, L., Borner, C., Wallich, R., Mullbacher, A., Froelich, C. J., and Simon, M. M. (2009). The biology of cytotoxic cell granule exocytosis pathway: granzymes have evolved to induce cell death and inflammation. Microbes Infect *11*, 452-459.

Peng, S. B., Henry, J. R., Kaufman, M. D., Lu, W. P., Smith, B. D., Vogeti, S., Rutkoski, T. J., Wise, S., Chun, L., Zhang, Y.*, et al.* (2015). Inhibition of RAF Isoforms and Active Dimers by LY3009120 Leads to Anti-tumor Activities in RAS or BRAF Mutant Cancers. Cancer Cell *28*, 384-398.

Petersen, B. O., Lukas, J., Sorensen, C. S., Bartek, J., and Helin, K. (1999). Phosphorylation of mammalian CDC6 by cyclin A/CDK2 regulates its subcellular localization. Embo j *18*, 396-410.

Phillips, A. C., Ernst, M. K., Bates, S., Rice, N. R., and Vousden, K. H. (1999). E2F-1 potentiates cell death by blocking antiapoptotic signaling pathways. Mol Cell *4*, 771-781.

Piazzolla, D., Meissl, K., Kucerova, L., Rubiolo, C., and Baccarini, M. (2005). Raf-1 sets the threshold of Fas sensitivity by modulating Rok-alpha signaling. J Cell Biol *171*, 1013-1022.

Pikor, L. A., Ramnarine, V. R., Lam, S., and Lam, W. L. (2013). Genetic alterations defining NSCLC subtypes and their therapeutic implications. Lung Cancer *82*, 179-189.

Posch, C., Sanlorenzo, M., Ma, J., Kim, S. T., Zekhtser, M., and Ortiz-Urda, S. (2018). MEK/CDK4,6 co-targeting is effective in a subset of NRAS, BRAF and 'wild type' melanomas. Oncotarget *9*, 34990-34995.

Puyol, M., Martin, A., Dubus, P., Mulero, F., Pizcueta, P., Khan, G., Guerra, C., Santamaria, D., and Barbacid, M. (2010). A synthetic lethal interaction between K-Ras oncogenes and Cdk4 unveils a therapeutic strategy for non-small cell lung carcinoma. Cancer Cell *18*, 63-73.

Qureshi, S. A., Joseph, C. K., Hendrickson, M., Song, J., Gupta, R., Bruder, J., Rapp, U., and Foster, D. A. (1993). A dominant negative Raf-1 mutant prevents v-Src-induced transformation. Biochem Biophys Res Commun *192*, 969-975.

Ramirez, M., Rajaram, S., Steininger, R. J., Osipchuk, D., Roth, M. A., Morinishi, L. S., Evans, L., Ji, W., Hsu, C.-H., Thurley, K.*, et al.* (2016). Diverse drug-resistance mechanisms can emerge from drug-tolerant cancer persister cells. Nature Communications *7*, 10690.

Rane, S. G., Cosenza, S. C., Mettus, R. V., and Reddy, E. P. (2002). Germ line transmission of the Cdk4(R24C) mutation facilitates tumorigenesis and escape from cellular senescence. Mol Cell Biol *22*, 644-656.

Rane, S. G., Dubus, P., Mettus, R. V., Galbreath, E. J., Boden, G., Reddy, E. P., and Barbacid, M. (1999). Loss of Cdk4 expression causes insulin-deficient diabetes and Cdk4 activation results in beta-islet cell hyperplasia. Nat Genet *22*, 44-52.

Raub, T. J., Wishart, G. N., Kulanthaivel, P., Staton, B. A., Ajamie, R. T., Sawada, G. A., Gelbert, L. M., Shannon, H. E., Sanchez-Martinez, C., and De Dios, A. (2015). Brain Exposure of Two Selective Dual CDK4 and CDK6 Inhibitors and the Antitumor Activity of CDK4 and CDK6 Inhibition in Combination with Temozolomide in an Intracranial Glioblastoma Xenograft. Drug Metab Dispos *43*, 1360-1371.

Rebocho, A. P., and Marais, R. (2011). New insight puts CRAF in sight as a therapeutic target. Cancer Discov *1*, 98-99.

Reck, M., Heigener, D. F., Mok, T., Soria, J. C., and Rabe, K. F. (2013). Management of non-small-cell lung cancer: recent developments. Lancet *382*, 709-719.

Riabowol, K., Draetta, G., Brizuela, L., Vandre, D., and Beach, D. (1989). The cdc2 kinase is a nuclear protein that is essential for mitosis in mammalian cells. Cell *57*, 393-401.

Rizvi, N. A., Hellmann, M. D., Snyder, A., Kvistborg, P., Makarov, V., Havel, J. J., Lee, W., Yuan, J., Wong, P., Ho, T. S.*, et al.* (2015). Cancer immunology. Mutational landscape determines sensitivity to PD-1 blockade in non-small cell lung cancer. Science (New York, NY) *348*, 124-128.

Rodríguez-Puebla (2002). cdk4 Deficiency Inhibits Skin Tumor Development but Does Not Affect Normal Keratinocyte Proliferation
.

Romano, G., Chen, P. L., Song, P., McQuade, J. L., Liang, R. J., Liu, M., Roh, W., Duose, D. Y., Carapeto, F. C. L., Li, J.*, et al.* (2018). A Preexisting Rare PIK3CA(E545K) Subpopulation Confers Clinical Resistance to MEK plus CDK4/6 Inhibition in NRAS Melanoma and Is Dependent on S6K1 Signaling. Cancer Discov *8*, 556-567.

Roth, D. M., Harper, I., Pouton, C. W., and Jans, D. A. (2009). Modulation of nucleocytoplasmic trafficking by retention in cytoplasm or nucleus. J Cell Biochem *107*, 1160-1167.

Ruscetti, M., Leibold, J., Bott, M. J., Fennell, M., Kulick, A., Salgado, N. R., Chen, C. C., Ho, Y. J., Sanchez-Rivera, F. J., Feucht, J*., et al.* (2018). NK cell-mediated cytotoxicity contributes to tumor control by a cytostatic drug combination. Science *362*, 1416-1422.

Rushworth, L. K., Hindley, A. D., O'Neill, E., and Kolch, W. (2006). Regulation and role of Raf-1/B-Raf heterodimerization. Mol Cell Biol *26*, 2262-2272.

Samatar, A. A., and Poulikakos, P. I. (2014). Targeting RAS-ERK signalling in cancer: promises and challenges. Nat Rev Drug Discov *13*, 928-942.

Sanclemente, M., Francoz, S., Esteban-Burgos, L., Bousquet-Mur, E., Djurec, M., Lopez-Casas, P. P., Hidalgo, M., Guerra, C., Drosten, M., Musteanu, M., and Barbacid, M. (2018). c-RAF Ablation Induces Regression of Advanced Kras/Trp53 Mutant Lung Adenocarcinomas by a Mechanism Independent of MAPK Signaling. Cancer Cell *33*, 217-228 e214.

Santamaria, D., Barriere, C., Cerqueira, A., Hunt, S., Tardy, C., Newton, K., Caceres, J. F., Dubus, P., Malumbres, M., and Barbacid, M. (2007). Cdk1 is sufficient to drive the mammalian cell cycle. Nature *448*, 811-815.

Schaer, D. A., Beckmann, R. P., Dempsey, J. A., Huber, L., Forest, A., Amaladas, N., Li, Y., Wang, Y. C., Rasmussen, E. R., Chin, D*., et al.* (2018). The CDK4/6 Inhibitor Abemaciclib Induces a T Cell Inflamed Tumor Microenvironment and Enhances the Efficacy of PD-L1 Checkpoint Blockade. Cell Rep *22*, 2978-2994.

Schmidt, E. E., Ichimura, K., Reifenberger, G., and Collins, V. P. (1994). CDKN2 (p16/MTS1) gene deletion or CDK4 amplification occurs in the majority of glioblastomas. Cancer Res *54*, 6321-6324.

Schnutgen, F., Doerflinger, N., Calleja, C., Wendling, O., Chambon, P., and Ghyselinck, N. B. (2003). A directional strategy for monitoring Cre-mediated recombination at the cellular level in the mouse. Nat Biotechnol *21*, 562-565.

Scott, L. J. (2019). Larotrectinib: First Global Approval. Drugs *79*, 201-206.

Sewing, A., Wiseman, B., Lloyd, A. C., and Land, H. (1997). High-intensity Raf signal causes cell cycle arrest mediated by p21Cip1. Molecular and cellular biology *17*, 5588-5597.

Shaw, A. T., Solomon, B. J., Besse, B., Bauer, T. M., Lin, C. C., Soo, R. A., Riely, G. J., Ou, S. I., Clancy, J. S., Li, S*., et al.* (2019). ALK Resistance Mutations and Efficacy of Lorlatinib in Advanced Anaplastic Lymphoma Kinase-Positive Non-Small-Cell Lung Cancer. J Clin Oncol *37*, 1370-1379.

Sherr, C. J., and Roberts, J. M. (1999). CDK inhibitors: positive and negative regulators of G1-phase progression. Genes Dev *13*, 1501-1512.

Sherr, C. J., and Roberts, J. M. (2004). Living with or without cyclins and cyclin-dependent kinases. Genes Dev *18*, 2699-2711.

Siegel, R. L., Miller, K. D., and Jemal, A. (2019). Cancer statistics, 2019. CA Cancer J Clin *69*, 7-34.

Song, Y., Li, Z., Xue, W., and Zhang, M. (2019). Predictive biomarkers for PD-1 and PD-L1 immune checkpoint blockade therapy. Immunotherapy *11*, 515-529.

Soria, J. C., Shepherd, F. A., Douillard, J. Y., Wolf, J., Giaccone, G., Crino, L., Cappuzzo, F., Sharma, S., Gross, S. H., Dimitrijevic, S*., et al.* (2009). Efficacy of everolimus (RAD001) in patients with advanced NSCLC previously treated with chemotherapy alone or with chemotherapy and EGFR inhibitors. Ann Oncol *20*, 1674-1681.

Sotillo, R., Dubus, P., Martín, J., de la Cueva, E., Ortega, S., Malumbres, M., and Barbacid, M. (2001). Wide spectrum of tumors in knock-in mice carrying a Cdk4 protein insensitive to INK4 inhibitors. The EMBO journal *20*, 6637-6647.

Soucek, L., Whitfield, J., Martins, C. P., Finch, A. J., Murphy, D. J., Sodir, N. M., Karnezis, A. N., Swigart, L. B., Nasi, S., and Evan, G. I. (2008). Modelling Myc inhibition as a cancer therapy. Nature *455*, 679-683.

Subramanian, A., Tamayo, P., Mootha, V. K., Mukherjee, S., Ebert, B. L., Gillette, M. A., Paulovich, A., Pomeroy, S. L., Golub, T. R., Lander, E. S., and Mesirov, J. P. (2005). Gene set enrichment analysis: a knowledge-based approach for interpreting genome-wide expression profiles. Proc Natl Acad Sci U S A *102*, 15545-15550.

Sun, C., Wang, L., Huang, S., Heynen, G. J., Prahallad, A., Robert, C., Haanen, J., Blank, C., Wesseling, J., Willems, S. M*., et al.* (2014). Reversible and adaptive resistance to BRAF(V600E) inhibition in melanoma. Nature *508*, 118-122.

Sun, J.-M., Hwang, D. W., Ahn, J. S., Ahn, M.-J., and Park, K. (2013). Prognostic and predictive value of KRAS mutations in advanced non-small cell lung cancer. PLoS One *8*, e64816-e64816.

Suzuki, A., Ito, T., Kawano, H., Hayashida, M., Hayasaki, Y., Tsutomi, Y., Akahane, K., Nakano, T., Miura, M., and Shiraki, K. (2000). Survivin initiates procaspase 3/p21 complex formation as a result of interaction with Cdk4 to resist Fas-mediated cell death. Oncogene *19*, 1346-1353.

Swanton, C., and Govindan, R. (2016). Clinical Implications of Genomic Discoveries in Lung Cancer. N Engl J Med *374*, 1864-1873.

Takezawa, K., Okamoto, I., Yonesaka, K., Hatashita, E., Yamada, Y., Fukuoka, M., and Nakagawa, K. (2009). Sorafenib inhibits non-small cell lung cancer cell growth by targeting B-RAF in KRAS wild-type cells and C-RAF in KRAS mutant cells. Cancer Res *69*, 6515-6521.

Tao, Z., Le Blanc, J. M., Wang, C., Zhan, T., Zhuang, H., Wang, P., Yuan, Z., and Lu, B. (2016). Coadministration of Trametinib and Palbociclib Radiosensitizes KRAS-Mutant Non-Small Cell Lung Cancers In Vitro and In Vivo. Clin Cancer Res *22*, 122-133.

Teh, J. L. F., Cheng, P. F., Purwin, T. J., Nikbakht, N., Patel, P., Chervoneva, I., Ertel, A., Fortina, P. M., Kleiber, I., HooKim, K*., et al.* (2018). In Vivo E2F Reporting Reveals Efficacious Schedules of MEK1/2-CDK4/6 Targeting and mTOR-S6 Resistance Mechanisms. Cancer Discov *8*, 568-581.

Teo, Z. L., Versaci, S., Dushyanthen, S., Caramia, F., Savas, P., Mintoff, C. P., Zethoven, M., Virassamy, B., Luen, S. J., McArthur, G. A*., et al.* (2017). Combined CDK4/6 and PI3Kalpha Inhibition Is Synergistic and Immunogenic in Triple-Negative Breast Cancer. Cancer Res *77*, 6340-6352.

Tetsu, O., and McCormick, F. (2003). Proliferation of cancer cells despite CDK2 inhibition. Cancer Cell *3*, 233-245.

Thatcher, N., Hirsch, F. R., Luft, A. V., Szczesna, A., Ciuleanu, T. E., Dediu, M., Ramlau, R., Galiulin, R. K., Balint, B., Losonczy, G.*, et al.* (2015). Necitumumab plus gemcitabine and cisplatin versus gemcitabine and cisplatin alone as first-line therapy in patients with stage IV squamous non-small-cell lung cancer (SQUIRE): an open-label, randomised, controlled phase 3 trial. Lancet Oncol *16*, 763-774.

Thorgeirsson, T. E., Geller, F., Sulem, P., Rafnar, T., Wiste, A., Magnusson, K. P., Manolescu, A., Thorleifsson, G., Stefansson, H., Ingason, A.*, et al.* (2008). A variant associated with nicotine dependence, lung cancer and peripheral arterial disease. Nature *452*, 638-642.

Todaro, G. J., and Green, H. (1963). Quantitative studies of the growth of mouse embryo cells in culture and their development into established lines. J Cell Biol *17*, 299-313.

Toyoshima, H., and Hunter, T. (1994). p27, a novel inhibitor of G1 cyclin-Cdk protein kinase activity, is related to p21. Cell *78*, 67-74.

Treviño, J. G., Verma, M., Singh, S., Pillai, S., Zhang, D., Pernazza, D., Sebti, S. M., Lawrence, N. J., Centeno, B. A., and Chellappan, S. P. (2013). Selective disruption of rb-raf-1 kinase interaction inhibits pancreatic adenocarcinoma growth irrespective of gemcitabine sensitivity. Molecular cancer therapeutics *12*, 2722-2734.

Tripathy, D., Im, S. A., Colleoni, M., Franke, F., Bardia, A., Harbeck, N., Hurvitz, S. A., Chow, L., Sohn, J., Lee, K. S.*, et al.* (2018). Ribociclib plus endocrine therapy for premenopausal women with hormone-receptor-positive, advanced breast cancer (MONALEESA-7): a randomised phase 3 trial. Lancet Oncol *19*, 904-915.

Truett, G. E., Heeger, P., Mynatt, R. L., Truett, A. A., Walker, J. A., and Warman, M. L. (2000). Preparation of PCR-quality mouse genomic DNA with hot sodium hydroxide and tris (HotSHOT). Biotechniques *29*, 52, 54.

Tsai, J., Lee, J. T., Wang, W., Zhang, J., Cho, H., Mamo, S., Bremer, R., Gillette, S., Kong, J., Haass, N. K.*, et al.* (2008). Discovery of a selective inhibitor of oncogenic B-Raf kinase with potent antimelanoma activity. Proc Natl Acad Sci U S A *105*, 3041-3046.

Tsutsui, T., Hesabi, B., Moons, D. S., Pandolfi, P. P., Hansel, K. S., Koff, A., and Kiyokawa, H. (1999). Targeted disruption of CDK4 delays cell cycle entry with enhanced p27(Kip1) activity. Mol Cell Biol *19*, 7011-7019.

Tutuka, C. S. A., Andrews, M. C., Mariadason, J. M., Ioannidis, P., Hudson, C., Cebon, J., and Behren, A. (2017). PLX8394, a new generation BRAF inhibitor, selectively inhibits BRAF in colonic adenocarcinoma cells and prevents paradoxical MAPK pathway activation. Mol Cancer *16*, 112.

Tuveson, D. A., Shaw, A. T., Willis, N. A., Silver, D. P., Jackson, E. L., Chang, S., Mercer, K. L., Grochow, R., Hock, H., Crowley, D.*, et al.* (2004). Endogenous oncogenic K-ras(G12D) stimulates proliferation and widespread neoplastic and developmental defects. Cancer Cell *5*, 375-387.

Tyagi, P., and Santiago, C. (2018). New features in MEK retinopathy. BMC Ophthalmol *18*, 221.

Vermeulen, K., Van Bockstaele, D. R., and Berneman, Z. N. (2003). The cell cycle: a review of regulation, deregulation and therapeutic targets in cancer. Cell Prolif *36*, 131-149.

Vinci, M., Gowan, S., Boxall, F., Patterson, L., Zimmermann, M., Court, W., Lomas, C., Mendiola, M., Hardisson, D., and Eccles, S. A. (2012). Advances in establishment and analysis of three-dimensional tumor spheroid-based functional assays for target validation and drug evaluation. BMC Biol *10*, 29.

Visvader, J. E. (2011). Cells of origin in cancer. Nature *469*, 314-322.

Vora, S. R., Juric, D., Kim, N., Mino-Kenudson, M., Huynh, T., Costa, C., Lockerman, E. L., Pollack, S. F., Liu, M., Li, X.*, et al.* (2014). CDK 4/6 inhibitors sensitize PIK3CA mutant breast cancer to PI3K inhibitors. Cancer Cell *26*, 136-149.

Wallace, M., and Ball, K. L. (2004). Docking-dependent regulation of the Rb tumor suppressor protein by Cdk4. Mol Cell Biol *24*, 5606-5619.

Wang, I. C., Chen, Y. J., Hughes, D., Petrovic, V., Major, M. L., Park, H. J., Tan, Y., Ackerson, T., and Costa, R. H. (2005). Forkhead box M1 regulates the transcriptional network of genes essential for mitotic progression and genes encoding the SCF (Skp2-Cks1) ubiquitin ligase. Mol Cell Biol *25*, 10875-10894.

Wang, S., Ghosh, R. N., and Chellappan, S. P. (1998). Raf-1 physically interacts with Rb and regulates its function: a link between mitogenic signaling and cell cycle regulation. Mol Cell Biol *18*, 7487-7498.

Wee, S., Jagani, Z., Xiang, K. X., Loo, A., Dorsch, M., Yao, Y. M., Sellers, W. R., Lengauer, C., and Stegmeier, F. (2009). PI3K pathway activation mediates resistance to MEK inhibitors in KRAS mutant cancers. Cancer Res *69*, 4286-4293.

Weinberg, R. A. (1995). The retinoblastoma protein and cell cycle control. Cell *81*, 323-330.

Wellbrock, C., Karasarides, M., and Marais, R. (2004). The RAF proteins take centre stage. Nat Rev Mol Cell Biol *5*, 875-885.

Welsh, S. J., and Corrie, P. G. (2015). Management of BRAF and MEK inhibitor toxicities in patients with metastatic melanoma. Ther Adv Med Oncol *7*, 122-136.

Wikman, H., Nymark, P., Vayrynen, A., Jarmalaite, S., Kallioniemi, A., Salmenkivi, K., Vainio-Siukola, K., Husgafvel-Pursiainen, K., Knuutila, S., Wolf, M., and Anttila, S. (2005). CDK4 is a probable target gene in a novel amplicon at 12q13.3-q14.1 in lung cancer. Genes Chromosomes Cancer *42*, 193-199.

Wojnowski, L., Stancato, L. F., Zimmer, A. M., Hahn, H., Beck, T. W., Larner, A. C., Rapp, U. R., and Zimmer, A. (1998). Craf-1 protein kinase is essential for mouse development. Mech Dev *76*, 141-149.

Wolfel, T., Hauer, M., Schneider, J., Serrano, M., Wolfel, C., Klehmann-Hieb, E., De Plaen, E., Hankeln, T., Meyer zum Buschenfelde, K. H., and Beach, D. (1995). A p16INK4a-insensitive CDK4 mutant targeted by cytolytic T lymphocytes in a human melanoma. Science *269*, 1281-1284.

Xu, X., Rock, J. R., Lu, Y., Futtner, C., Schwab, B., Guinney, J., Hogan, B. L., and Onaitis, M. W. (2012). Evidence for type II cells as cells of origin of K-Ras-induced distal lung adenocarcinoma. Proc Natl Acad Sci U S A *109*, 4910-4915.

Yamaguchi, O., Watanabe, T., Nishida, K., Kashiwase, K., Higuchi, Y., Takeda, T., Hikoso, S., Hirotani, S., Asahi, M., Taniike, M.*, et al.* (2004). Cardiac-specific disruption of the c-raf-1 gene induces cardiac dysfunction and apoptosis. J Clin Invest *114*, 937-943.

Yang, J., Nie, J., Ma, X., Wei, Y., Peng, Y., and Wei, X. (2019). Targeting PI3K in cancer: mechanisms and advances in clinical trials. Mol Cancer *18*, 26-26.

Ye, X., Zhu, C., and Harper, J. W. (2001). A premature-termination mutation in the Mus musculus cyclin-dependent kinase 3 gene. Proc Natl Acad Sci U S A *98*, 1682-1686.

Yu, Q., Sicinska, E., Geng, Y., Ahnstrom, M., Zagozdzon, A., Kong, Y., Gardner, H., Kiyokawa, H., Harris, L. N., Stal, O., and Sicinski, P. (2006). Requirement for CDK4 kinase function in breast cancer. Cancer Cell *9*, 23-32.

Zappa, C., and Mousa, S. A. (2016). Non-small cell lung cancer: current treatment and future advances. Transl Lung Cancer Res *5*, 288-300.

Zhang, J., Bu, X., Wang, H., Zhu, Y., Geng, Y., Nihira, N. T., Tan, Y., Ci, Y., Wu, F., Dai, X*., et al.* (2018). Cyclin D-CDK4 kinase destabilizes PD-L1 via cullin 3-SPOP to control cancer immune surveillance. Nature *553*, 91-95.

Zheng, L., and Lee, W. H. (2001). The retinoblastoma gene: a prototypic and multifunctional tumor suppressor. Exp Cell Res *264*, 2-18.

Zhou, J., Zhang, S., Chen, X., Zheng, X., Yao, Y., Lu, G., and Zhou, J. (2017). Palbociclib, a selective CDK4/6 inhibitor, enhances the effect of selumetinib in RAS-driven non-small cell lung cancer. Cancer Lett *408*, 130-137.

Zimmermann, S., and Moelling, K. (1999). Phosphorylation and regulation of Raf by Akt (protein kinase B). Science *286*, 1741-1744.

Zou, X., Ray, D., Aziyu, A., Christov, K., Boiko, A. D., Gudkov, A. V., and Kiyokawa, H. (2002). Cdk4 disruption renders primary mouse cells resistant to oncogenic transformation, leading to Arf/p53-independent senescence. Genes Dev *16*, 2923-2934.

PUBLICATIONS

I. Nieto, P., Ambrogio, C., **Esteban-Burgos, L.**, Gomez-Lopez, G., Blasco, M. T., Yao, Z., Marais, R., Rosen, N., Chiarle, R., Pisano, D. G.*, et al.* (2017). A Braf kinase-inactive mutant induces lung adenocarcinoma. Nature *548*, 239-243.

II. Sanclemente, M., Francoz, S., **Esteban-Burgos, L.**, Bousquet-Mur, E., Djurec, M., Lopez-Casas, P. P., Hidalgo, M., Guerra, C., Drosten, M., Musteanu, M., and Barbacid, M. (2018). c-RAF Ablation Induces Regression of Advanced Kras/Trp53 Mutant Lung Adenocarcinomas by a Mechanism Independent of MAPK Signaling. Cancer Cell *33*, 217-228 e214.

III. Blasco, M. T., Navas, C., Martin-Serrano, G., Grana-Castro, O., Lechuga, C. G., Martin-Diaz, L., Djurec, M., Li, J., Morales-Cacho, L., **Esteban-Burgos, L.***, et al.* (2019). Complete Regression of Advanced Pancreatic Ductal Adenocarcinomas upon Combined Inhibition of EGFR and C-RAF. Cancer Cell *35*, 573-587 e576.